# A STUDY OF THE ENERGY BALANCE IN THE ATMOSPHERES OF THE MAJOR PLANETS

Thesis by
Laurence Munro Trafton

In Partial Fulfillment of the Requirements
For the Degree of
Doctor of Philosophy

California Institute of Technology
Pasadena, California
1965
(Submitted March 19, 1965)

# ACKNOWLEDGEMENTS

It is with great pleasure that I thank Dr. G. Münch for originally suggesting the topic of this thesis, which has engrossed me in two stimulating years of study. Thanks are also due to Dr. Münch for critical advice and encouragement throughout the work on this thesis. I wish to thank Dr. D. Mihalas for permitting me to use sections of his stellar atmospheres program and to Mr. W. T. Lungershausen, Jr. for making available the IBJOB version of this program. I wish to thank Dr. J. Greenstein for his generous allotment of computing funds, without which this thesis could not have been accomplished.

As a graduate student, I have received financial support from the National Science Foundation, the Institute, the Dobbins fund, the Anthony fund and finally, the Van Maanen fund. To each of these donors I express my appreciation.

# ABSTRACT

The monochromatic absorption of infrared and microwave radiation due to pressure-induced rotational and translational transitions in $H_2$ gas and gaseous mixtures of $H_2$ and He is investigated quantitatively. Existing laboratory data are used to obtain semi-empirical absorption coefficients of the rotational transitions as a function of frequency. A quantum mechanical calculation is carried out to obtain the translational absorption coefficient as a function of frequency for a diatomic gas, mixtures of diatomic and monatomic gases and mixtures of monatomic gases. The resulting expressions are used to compute the translational absorption coefficient for $H_2$ and the enhancement in $H_2$-He mixtures using a 6 - 12 Lennard-Jones potential for the molecular interaction and the EXP-4 model for the expectation value of the induced dipole moment over the ground electronic and vibrational states. A numerical method is devised for the efficient computation of the translational absorption and the results of the computations are given. The infrared opacity of $NH_3$ is also considered. With certain assumptions, existing laboratory data are used to obtain approximate, semi-empirical mean transmissions over the rotation structure of $NH_3$ as a function of frequency.

Several non-gray model atmospheres are constructed for Jupiter, Saturn, Uranus and Neptune for various effective temperatures and He-$H_2$ ratios taking the opacity due to $H_2$ and He into account. The effect of adding the opacity due to $NH_3$ is considered. The models are examined for self consistency and characteristic phenomena. They are then compared with the observations.

The observations are used to restrict the range of the free parameters of the models. It is found that models of Jupiter and Neptune for which only the thermal opacity of $H_2$ and $NH_3$ is taken into account are incompatible with the observations. The presence of He is strongly indicated in the atmospheres of Jupiter, Uranus and Neptune. In the case of Jupiter, a rather large $N(He)/N(H_2)$ value is implied if there is no internal heat source. However, the observations indicate a preference for $N(He)/N(H_2)$ less than 2 and thus imply the existence of a small internal heat source greater than one-tenth of the incident solar flux. The effect of $NH_3$ on the thermal equilibrium of the major planets is negligible except possibly in the case of Jupiter. However, its presence in the Jovian atmosphere does not alter the above conclusions.

# TABLE OF CONTENTS

# PART I

# THE COMPUTATION OF THE THERMAL OPACITIES

## I-1. INTRODUCTION

Molecular hydrogen, methane and ammonia have been detected in the atmospheres of the major planets and the presence of helium is strongly suspected, as well. Methane bands are quite visible in the spectra of all the major planets and are very strong in Uranus and Neptune. The $\lambda 6460$ ammonia band is easily seen on Jupiter but is not visible on Saturn. No ammonia has been detected on Uranus or Neptune either. Since molecular hydrogen quadrupole lines are visible on Jupiter, Saturn and Uranus and the pressure-induced dipole lines are detectable on Uranus and Neptune, all of the major planets contain molecular hydrogen in their atmospheres. The presence of helium on Jupiter is suggested by the mean molecular weight of 3.3, derived from the occultation of $\sigma$-Arietis (Baum and Code 1953), and the low ammonia and methane abundance relative to hydrogen (Kuiper 1952; Zabriskie 1962; Spinrad and Trafton 1963; and Foltz and Rank 1963). The presence of helium on Uranus and Neptune is indicated, according to Hertzberg (1952), by its effect of inhibiting the double transitions in the spectra of the pressure-induced (3, 0) lines, but blending due to methane makes it difficult to ascertain the relative helium abundance in these cases.

This thesis investigates the role played by these molecules, with particular reference to hydrogen and helium, in determining

the physical structure of these atmospheres. We observe that the solar and thermal spectra of the major planets must overlap negligibly in frequency. For the greenhouse mechanism to be operative in this case, it is sufficient that the bulk of the solar radiation be absorbed below a layer which is optically deep at thermal frequencies. This condition is satisfied when the atmosphere is composed of molecular hydrogen or mixtures of molecular hydrogen and helium. This is because these molecules have a pressure-induced rotational-translational absorption lying between 10 $cm^{-1}$ and 1400 $cm^{-1}$ or in the thermal region of the spectrum. The small value of the absorption coefficient is more than compensated by the long path lengths of hydrogen available in the atmospheres of the major planets and the fact that the absorption increases as the square of the density (Trafton 1964). This motivates us to study this pressure-induced absorption.

Ammonia also absorbs in the infrared, but at cold planetary temperatures, it will be saturated and the vapor pressure then decreases very rapidly with temperature. Only in the deeper and warmer part of Jupiter's atmosphere is ammonia apt to affect the radiative equilibrium.

Methane is a non-polar molecule and does not give rise to marked absorption in the frequencies of the planetary thermal spectra longwards of 1200 $cm^{-1}$ (Opik 1962; Gross and Rasool 1964). For this reason, we ignore its opacity contribution. We assume that the major opacities are due to molecular hydrogen, helium and perhaps ammonia and construct model atmospheres of the major planets on this basis. With this in mind, we turn to the investigation of these opacities.

## I-2. EMPIRICAL LINE SHAPES OF THE PRESSURE-INDUCED ROTATIONAL SPECTRUM

The pressure induced absorption can be divided into contributions from three physical processes. The first, called quadrupolar induction, arises from the permanent quadrupole moment of the hydrogen molecule. Its field induces a dipole moment in its partner by virtue of that partner's polarizability. Molecular hydrogen has no permanent dipole moment and hence, no permitted dipole spectrum. However, the dipole moment which is induced in a neighboring molecule is modulated by the rotation and relative motion of the hydrogen molecule, resulting in absorption. That is, the system absorbs a photon and undergoes a change of translational and possibly an accompanying change of rotational state. Furthermore, if that partner has an anisotropic polarizability, as well as a set of rotational energy levels, the induced dipole will also be modulated by the latter molecule's rotation, permitting transitions between its energy levels and permitting "simultaneous" transitions where a single photon causes a change of state in both molecules as well as changing the relative kinetic energy.

The second process, due to overlap forces, arises from the asymmetry of the electric cloud distortion when the hydrogen molecule is in close proximity to another molecule or atom. Due to lack of symmetry, a dipole moment is formed by this distortion during collision. This moment is modulated by the rotation and translation of the $H_2$ molecule relative to its partner and hence, contributes to the rotational-translational spectrum.

The third process, termed "apparent absorption" by Van Kranendonk, is negligible except at extremely high densities. It results from the long range dipole-dipole interaction between the molecules. Classically, it results from the interaction of one molecule with the wavelets emitted by the dipole moments set up by the radiation field in the other molecules. It is an internal field effect and is not due to any intrinsic change in the properties of the molecules themselves. In the worst case delt with by Kiss, Gush and Welsh (1959), who worked with pressures higher than 100 atm, this correction amounted to less than one percent. We ignore this process in the treatment of planetary atmospheres.

Laboratory measurements of the absorption as a function of frequency have been made at several temperatures for pure hydrogen and hydrogen-helium mixtures using a variety of pressures. Unfortunately, the laboratory measurements are confined to frequencies greater than 300 $cm^{-1}$ as the window of the high-pressure cell becomes opaque at lesser frequencies. For this reason, much of the translational profile was not measured although most of the rotational profile was (Kiss, Gush and Welsh 1959; Colpa and Ketelaar 1958). The first group found that the integrated absorption coefficient, integrated between 300 $cm^{-1}$ and 1400 $cm^{-1}$, varied quite accurately as the square of the density for pure hydrogen and as the product of the densities of hydrogen and helium for the enhancement in hydrogen-helium mixtures. This implies that over a large range of densities ( 0 to 120 Amagats), binary collisions are the dominant sources of absorption rather than collisions between three or more molecules. The absorption $C_v$ per cm is defined as

$$C_v = \frac{1}{L} \ln \frac{I_{vo}}{I_v} \qquad (I\text{-}1)$$

where L is the path length of the absorption cell, $I_{vo}$ the measured intensity at frequency V with the cell empty and $I_v$ the corresponding intensity with the cell charged. For binary collisions,

$$C_v = A_v n^2 + B_v n n' \qquad (I\text{-}2)$$

where $A_v$ and $B_v$ are called the binary absorption coefficients. We define $A_v$ as that due to hydrogen alone and $B_v$ as the enhancement in mixtures of hydrogen and helium. n and n' are the number densities of hydrogen and helium, respectively. When these coefficients are integrated over wave number dV, the corresponding equation for the integrated binary absorption coefficients B and C is

$$C = A n^2 + B n n' . \qquad (I\text{-}3)$$

The optical depth is then

$$\tau_v = \tau_{vo} + \int_{L_o}^{L} C_v dx . \qquad (I\text{-}4)$$

The quantities $A_v$ and $B_v$ depend on the temperature in a way which reflects the Boltzmann distribution of the rotational and translational energy states. As the temperature is lowered, the smaller-J rotational lines become stronger at the expense of the other lines and the maximum of the translational profile shifts towards longer wave lengths. The half-widths of the rotational and

translational profiles also decrease and the profiles become more asymmetrical. Figure 1 shows the experimental profiles at three temperatures. The Raman frequencies of the four lowest rotational absorption lines, S(0), S(1), S(2) and S(3) are 354.4, 587.1, 814.4 and 1034.7 $cm^{-1}$, respectively. Note that the continuity of the profile is due to the large half-widths. The latter is a consequence of the uncertainty principle. The fact that absorption can take place only during collisions instead of anytime between collisions severely limits the uncertainty in the time that a transition occurs, resulting in a large uncertainty in the energy (Heastie and Martin 1962). At the same time, the Raman and quadrupole lines remain quite sharp, even at very high pressures. Therefore, the energy levels themselves are not significantly perturbed. The shape of the rotational profiles results from the coupling between the rotational and translational energies. That is, when a photon is absorbed, part of its energy may cause the S(0) transition while the difference appears in the relative kinetic energy. The asymmetry of the rotational profile is explained by the fact that as the energy of the absorbed photon becomes weaker (i.e. as its frequency becomes smaller), the kinetic energy available to make up the difference between the photon's energy and the rotation-energy falls off exponentially. If the observed profile is divided by V, the profile which results is proportional to the probability that a photon of energy hcV is absorbed. If we then localize a rotational line at a low enough temperature such that the translational contribution is negligible and compute the ratio at various frequency intervals $\Delta V$ above $V_o$ to $\Delta V$ below $V_o$, we find that this ratio varies as $\exp(hc\Delta V/kT)$ with only an $8^o$ error at 85 $^oK$ using the wings of the

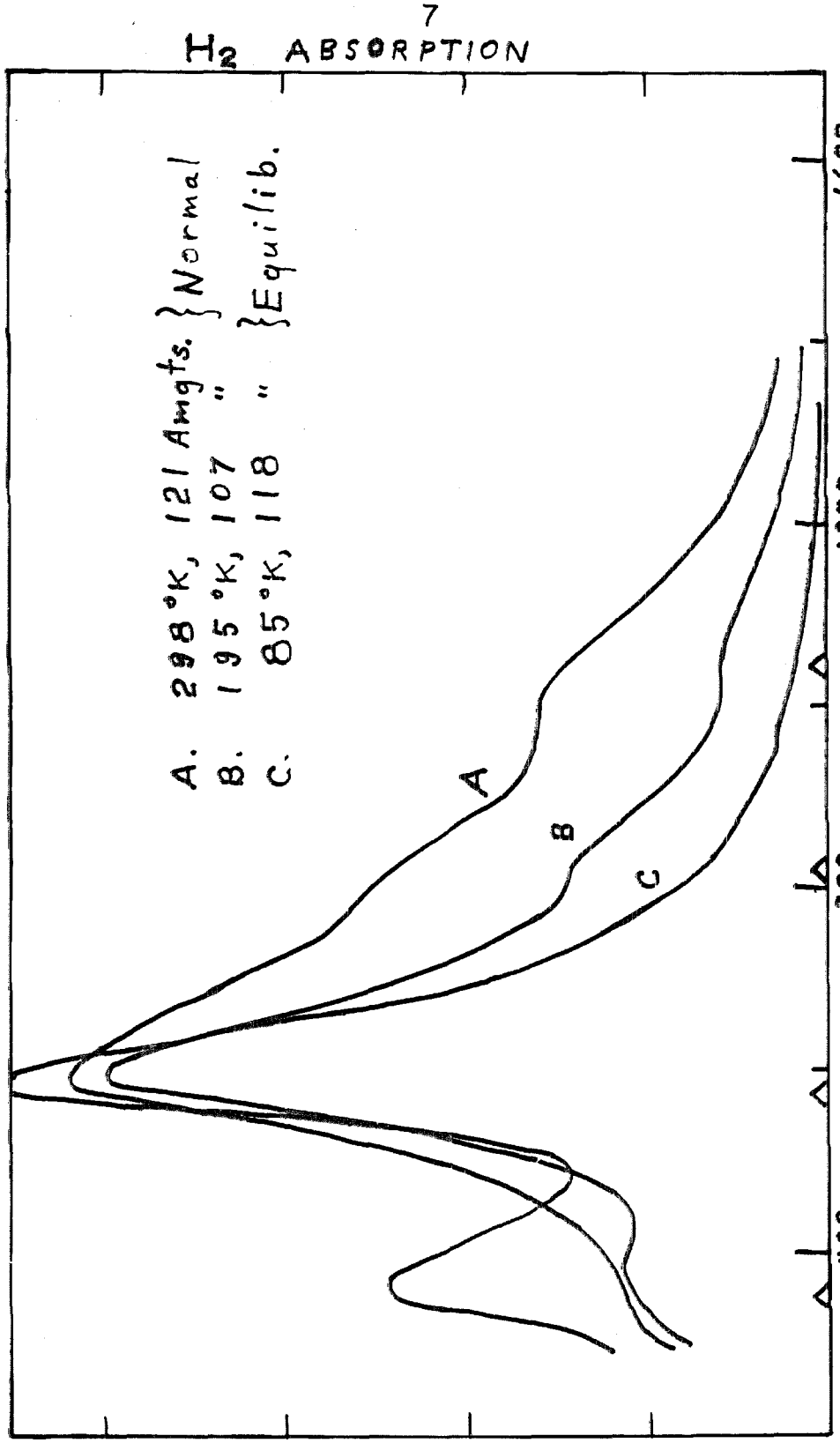
$H_2$ ABSORPTION
A. 298°K, 121 Amgts. } Normal
B. 195°K, 107 " }
C. 85°K, 118 " } Equilib.
A
B
C
400
800
1200
1600
Experimental Profiles V cm⁻¹

FIG. 1

S(1) line (Kiss and Welsh 1959). These profiles thus have the intensity distribution of a continuous distribution of summation and difference translational tones with the rotational frequency. That is, for a rotational transition at $V_o$, the simultaneous translational transition and its inverse occur at equal frequency intervals on opposite sides of $V_o$. The relative transition probabilities at these two frequencies is given solely by the translational Boltzmann factor $\exp(hc\Delta V/kT)$. This appears to be the case for both equilibrium and normal hydrogen (where normal hydrogen has an ortho to para ratio determined by equilibrium at room temperature).

Kiss and Welsh also find that the high frequency wing of the rotational probability curve can be fitted with a Lorentz profile with a half-width $2\delta$ where $\delta$ is equal to $9.1\ T^{1/2}\ cm^{-1}$ and T is the temperature. This is in agreement with the uncertainty principle since $T^{1/2}$ is inversely proportional to the duration of the collision. We do not expect the Lorentz profile to fit exactly, because the line is also broadened by translational processes. In fact, the Lorentz profile is observed to be too large in the tail. The low frequency wing is given quite accurately by the product of the Lorentz profile and the Boltzmann factor, $\exp(-hc\Delta V/kT)$.

In their discussion of the profiles of the vibrational fundamental Hunt and Welsh (1964) obtain $\delta$ about equal to $8\ T^{1/2}\ cm^{-1}$. They also mention that their value $9.1\ T^{1/2}$ for the rotational profile was rough. I found that $\delta$ should be $8.1\ T^{1/2}$ for the rotational profile if the Lorentz profiles are truncated at $(V-V_o)/\delta = 14$ in normalizing by comparing empirical and experimental laboratory integrated absorption. This appeared to give a better fit. The

equations for a single rotational probability line profile are

$$\frac{S(J)}{(V-V_o)^2/\delta^2 + 1} \qquad \text{if } V \geq V_o$$

$$\frac{S(J)}{(V-V_o)^2/\delta^2 + 1} \exp(-hc(V_o-V)/kT) \quad \text{if } V < V_o \qquad \text{(I-5)}$$

$$\delta = 8.1\sqrt{T}\ \text{cm}^{-1}$$

where $V_o$ is the Raman frequency of the line in wave numbers and the S(J) are the normalization factors determined by integrating these expressions from V = 0 to V = $14\delta + V_o$ and comparing them with the corresponding theoretical expression derived in the next section. To get the final rotational absorption profile, we sum over all four rotational lines and multiply by V if V is less than V' = $589 + 2.5\delta$ or by V' if V is greater than V'. The latter improves the fit with the experimental data by causing the Lorentz profile to fall off faster in its high frequency tail. The errors in this correction are not critical for application to planetary atmospheres.

While not strictly true, we assume that $\delta$ is the same for $H_2$-He collisions as for $H_2$-$H_2$ collisions. The error is about 12 per cent and since the $H_2$-He rotational absorption is several times weaker than that for $H_2$-$H_2$, we neglect the error. We now have determined all of the parameters of the empirical fit to the observed rotational profile except the normalization factors, S(J) for $H_2$-$H_2$ and for $H_2$-He collisions. To evaluate these, it is necessary to go into the theory of the integrated absorption coefficient and this is the subject of the next section.

## I-3. THE ROTATIONAL NORMALIZATION FACTORS S(J)

### I-3.a. Assumptions of the Theory.

We neglect the apparent absorption mentioned in section 2 on the grounds that this correction is very small at planetary densities.

We assume that the absorption of the rotational lines results only from binary collisions, on the grounds that the absorption varies quite accurately as the product of the partial densities up to densities over a hundred Amagats, both for pure $H_2$ and for $H_2$-He enhancement in mixtures.

We assume that the expectation value of the induced dipole moment over the ground electronic and vibrational states is given sufficiently accurately by the EXP-4 model used by Van Kranendonk and Kiss (1959). This model approximates the induced moment by its shortest and longest range components. The quadrupolar induction moment is taken to vary as the inverse fourth power of the separation of the molecules and the overlap induction moment is taken to vary exponentially with this separation. The intermediate terms are ignored. No adequate theory exists for the overlap proportionality and scale constants and so these quantities must be evaluated by laboratory experiments. The induced moment is expanded in spherical harmonics and the $i^{th}$ coefficient of the overlap component is $\lambda_i \exp(-r/\rho)$ where $\lambda_i$ and $\rho$ are overlap parameters.

We make the assumption that the intermolecular potential U is a function of the separation r but not of the angular orientation of either molecule. In the expressions for the integrated absorption coefficient, only the pair distribution function is affected by this assumption.

We further assume that U(r) is given adequately by the 6-12 Lennard-Jones potential

$$U(r) = 4\epsilon \left[ \left(\frac{\sigma}{r}\right)^{12} - \left(\frac{\sigma}{r}\right)^{6} \right] \qquad \text{(I-6)}$$

where $\epsilon$ and $\sigma$ are the Lennard-Jones parameters. Objections to this potential have been raised because it does not increase fast enough to explain experiments at high temperatures. However, we are encouraged to use it in planetary atmospheres because it has been quite successful in helping to explain the low temperature experiments on the second virial coefficients of the equation of state.

We assume that the temperature is high enough so that we may use a quasi-classical pair distribution function involving the classical expression with the first and second quantum corrections:

$$g(x) = \exp(-U(x)/kT) \left[ 1 + \hbar^2 a(x) + \hbar^4 b(x) + 0(\hbar^6) \right] \qquad \text{(I-7)}$$

where x is equal to $r/\sigma$. We make use of results tabulated by Van Kranendonk and Kiss (1959) containing this correction and find that the error is not more than 7 per cent at 40 $^{o}$K for pure $H_2$ according to the alternating nature of the correction terms. For $H_2$-He mixtures, we get the corresponding accuracy at about 60 $^{o}$K. At these low temperatures, the Planck curve is shifted into the translational domain where the back-warming is due almost entirely to the translational absorption, and the errors in the rotational profile may be quite large without affecting the thermal equilibrium. Therefore, the errors after the quantum corrections are not critical to our ultimate problem.

We assume that the dipole approximation suffices since the wave length of the absorbed radiation is large compared to the effective range of the intermolecular forces.

Following Van Kranendonk and Kiss (1959), we assume that for unlike collision partners, the Lennard-Jones parameters are given by the arithmetical mean of the $\sigma$ and the geometrical mean of the $\epsilon$. For want of experimental data, we assume that $\sigma/\rho$ is the same for $H_2$-$H_2$ and $H_2$-He enhancement. The $\lambda_i$ are obtained empirically by fitting the theoretical absorption to the laboratory data.

I-3. b. The Theoretical Expressions For The Integrated Rotational Absorption.

If the respective coefficients for the transition probability of the $J^{th}$ rotational line in units of $sec^{-1}$ $cm^6$ are defined by

$$\overline{A}(J) = c \int_0^\infty A_V(J) \frac{dV}{V}$$

$$\overline{B}(J) = c \int_0^\infty B_V(J) \frac{dV}{V} \qquad \text{(I-8)}$$

where c is the speed of light, $A_V(J)$ is the contribution of the $J^{th}$ rotational line to $A_V$ and $B_V(J)$ is that to $B_V$, then the normalization factors are

$$S(J) = \begin{cases} \dfrac{\overline{A}(J)}{B} & \text{for } H_2\text{-}H_2 \\ \dfrac{\overline{B}(J)}{B} & \text{for } H_2\text{-He enhancement} \end{cases} \qquad \text{(I-9)}$$

where $\mathbb{P}$ is the integral of the empirical profile for the case $S(J) = 1$.

I-3. b. 1. The $H_2$-$H_2$ Case.

Van Kranendonk and Kiss (1959) give for this case

$$A(J) = L(J)\left[\left(\lambda_o^2 + 2\lambda_1^2\right)I + \mu^2 J' + \mu\left(\lambda_o - \frac{2}{\sqrt{3}}\lambda_1\right)K\right] p + L(J)L'\mu'^2 J' p \quad \text{(I-10)}$$

where $\mu = \alpha Q/e\sigma^5$, $\mu' = \sqrt{88/225}\,\gamma Q/e\sigma^5$, e is the cgs unit of charge, Q is the expectation value of the quadrupole moment over the ground vibrational state and equals $0.49ea_o^2$ where $a_o$ is the Bohr radius, $p = 4\pi^2 e^2 \sigma^5/3\hbar$, $\alpha$ is the mean polarizability of the $H_2$ molecule $(2\alpha_\perp + \alpha_{11})/3$ and $\gamma$ is the anisotropy of the polarizability of the hydrogen molecule $\alpha_{11} - \alpha_\perp$,

$$L(J) = \frac{3(J+1)(J+2)}{2(2J+3)}\left[P(J) - P(J+2)\right] \quad \text{(I-11)}$$

$$L' = \sum_J \frac{J(J+1)(2J+1)}{(2J-1)(2J+3)} P(J), \quad \text{(I-12)}$$

$P(J)$ is the Boltzmann factor normalized so that $\sum_J (2J+1)P(J) = 1$. For equilibrium hydrogen,

$$P(J) = g_J \exp(-E(J)/kT)/Z$$

$$g_J = \begin{cases} 1 & \text{if } J \text{ is even} \\ 3 & \text{if } J \text{ is odd} \end{cases} \quad \text{(I-13)}$$

and the partition function Z is given by

$$Z = \sum_J g_J(2J+1)\exp(-E(J)/kT) \qquad \text{(I-14)}$$

where E(J) is the energy of the $J^{th}$ rotational level. Also, we have

$$\begin{aligned} I &= 4\pi \int_o^\infty \exp(-2(x-1)\sigma/\rho)g(x)x^2dx \\ J' &= 12\pi \int_o^\infty x^{-8}g(x)x^2dx \\ K &= \frac{24\pi}{\sqrt{5}} \int_o^\infty x^{-4}\exp(-(x-1)\sigma/\rho)g(x)x^2dx \end{aligned} \qquad \text{(I-15)}$$

where the pair distribution function g(x) is derived in Appendix B. The result for the $H_2$-$H_2$ case is, including the first quantum correction,

$$g(x) = \exp(-U(x)/kT)\left[1 + \frac{417}{T^2x^8}\left\{\frac{444}{Tx^6}\left(\frac{4}{x^{12}} - \frac{4}{x^6} + 1\right) - \frac{22}{x^6} + 5\right\}\right] \qquad \text{(I-16)}$$

which is good down to a temperature of about 180 $^oK$. In evaluating equation (I-10) we ignore the $\lambda^2$ and $\mu^2$ terms, giving

$$\bar{A}(J) = L(J)\,[\mu^2 J' + \mu\lambda K]\,p \qquad \text{(I-17)}$$

where $\lambda = \lambda_o - \lambda_1 2/\sqrt{3} = 0.8 \times 10^{-4}$ by empirical fit, $\epsilon/K = 37.0\,^oK$, $\sigma = 2.93 \times 10^{-8}$cm, $\rho/\sigma = 0.126$, $\alpha = 5.7a_o^3$, $\mu = 5.126 \times 10^{-4}$, $\gamma = 1.6a_o^3$ and $p = 4.63 \times 10^{-29}$cgs. Summing over J gives

$$\bar{A} = L\,(1.21\,J' + 0.19\,K) \times 10^{-35}\ \mathrm{sec}^{-1}\ \mathrm{cm}^{6} \qquad \text{(I-18)}$$

where L as a function of temperature plotted in Figure 2 and $\bar{A}$ is tabulated in Table I-1. The normalization factor is given by

$$S(J) = \frac{L(J)}{\sum L}\,\bar{A} \qquad \text{(I-19)}$$

for pure hydrogen, where $\bar{A}(T)$ is computed once and for all.

I-3. b. 2. The $H_2$-He Enhancement Case.

The corresponding expression is

$$\bar{B}(J) = L(J)\,(\mu^2\,J' + \mu\lambda\,K)\,p \qquad \text{(I-20)}$$

where only the L(J) remain unchanged. Therefore, the distribution among the rotational lines is the same for helium enhancement as for pure hydrogen. Van Kranendonk and Kiss (1959) quote this expression with a factor of 1/2 out in front, in disagreement with Colpa and Ketelaar (1958). Our own derivation of this result is in agreement with the latter indicating that the former is erroneous.

Note that the terms involving the anisotropy of the polarizability do not occur. Also, note that the angle-independent term in the dipole moment expansion is now permitted, but does not contribute to the rotational absorption since it is not modulated by rotation. The Lennard-Jones parameters for this case are $\sigma = 2.74 \times 10^{-8}$ cm and $\epsilon/k = 19.4\ ^{o}$K. They are averaged using the values for helium obtained from the second virial coefficient (Michels and Wouters 1941). The numerical values of the other

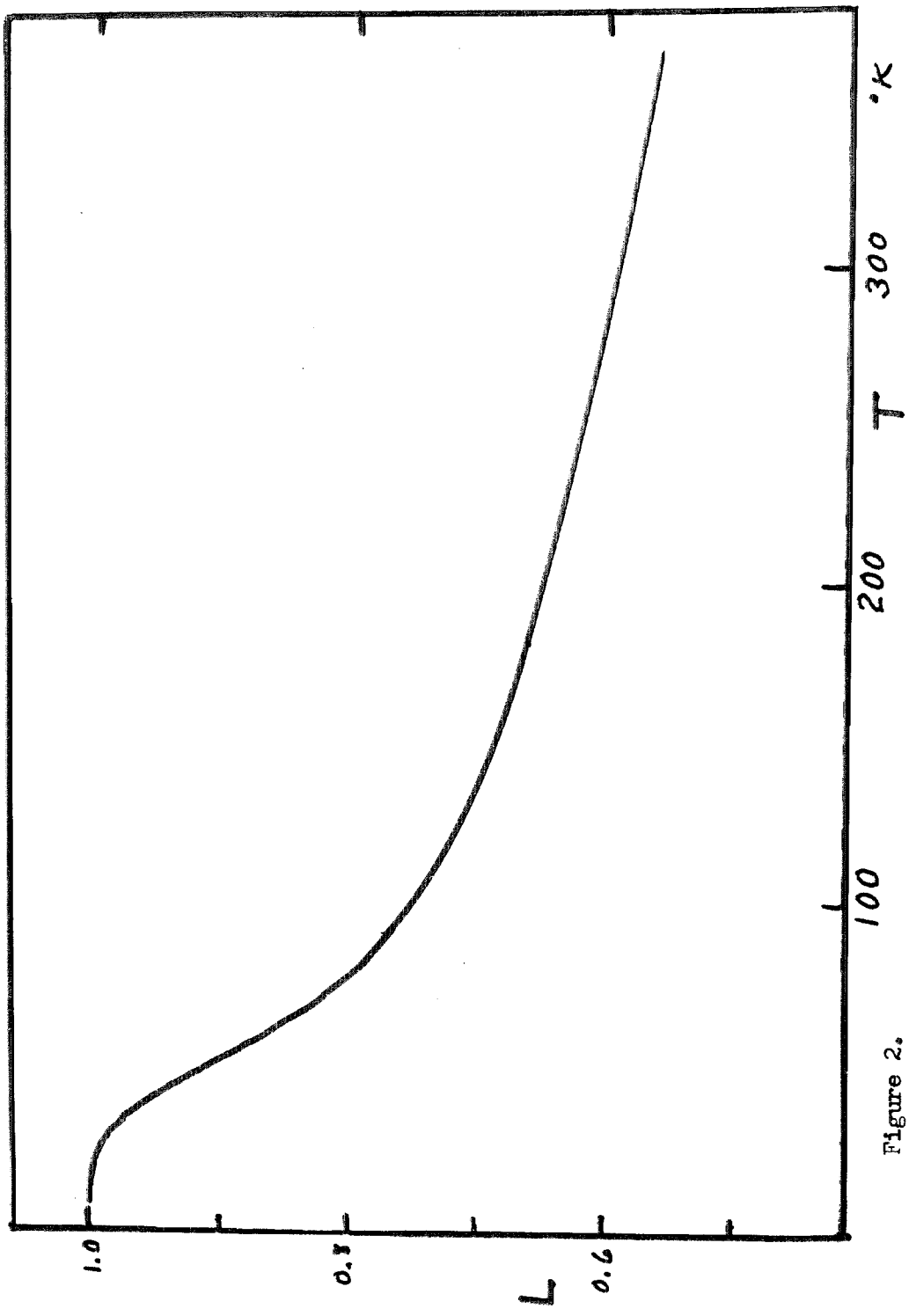


Figure 2.

Table I-1

The Rotational Binary Absorption Coefficients

| T | $\bar{A}$ | $\bar{B}$ |
|---|---|---|
| 0 | $1.72 \times 10^{-34}$ $sec^{-1}$ $cm^6$ | $0.325 \times 10^{-34}$ $sec^{-1}$ $cm^6$ |
| 10 | 1.72 | 0.264 |
| 20 | 1.72 | 0.211 |
| 30 | 1.69 | 0.169 |
| 40 | 1.645 | 0.145 |
| 50 | 1.580 | $0.132_6$ |
| 60 | 1.492 | $0.126_2$ |
| 70 | 1.422 | $0.122_0$ |
| 80 | 1.371 | $0.118_8$ |
| 90 | 1.325 | $0.117_9$ |
| 100 | 1.288 | $0.117_1$ |
| 110 | 1.267 | $0.116_9$ |
| 120 | 1.254 | $0.117_1$ |
| 130 | 1.242 | $0.117_5$ |
| 140 | 1.232 | $0.118_0$ |
| 160 | 1.218 | $0.118_5$ |
| 180 | 1.210 | $0.119_8$ |
| 220 | 1.202 | $0.121_2$ |
| 260 | 1.193 | $0.122_7$ |
| 300 | 1.180 | $0.122_8$ |
| 380 | 1.168 | $0.123_1$ |
| 500 | $1.145 \times 10^{-34}$ | $0.116_7 \times 10^{-34}$ |

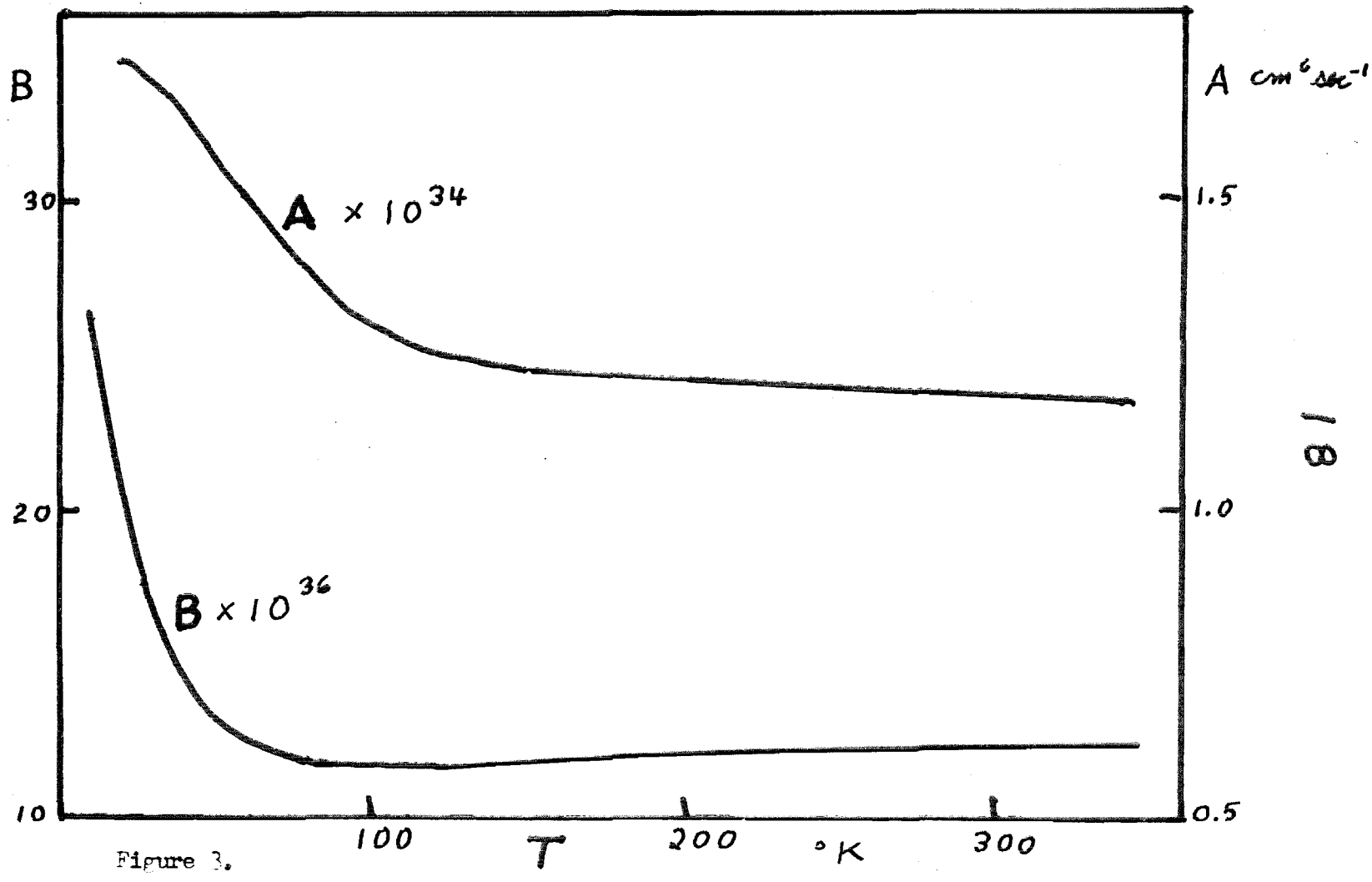


Figure 3.

quantities in equation (I-20) are $p = 3.33_5 \times 10^{-29} \text{sec}^{-1}\text{cm}^6$, $\rho/\sigma = 0.126$ (approximately), $\alpha = 1.4a_o^2 = 2.02 \times 10^{-25}\text{cm}^3$, $Q = 0.49\, ea_o^2$, $\lambda = 0.5 \times 10^{-4}$, $\mu = \alpha Q/e\sigma^5 = 1.84_3 \times 10^{-4}$ and the integrals J' and K are functionally the same as equations (I-15) but with a different g(x), given by

$$g(x) = \exp(-U(x)/kT)\left\{1 + \frac{188}{T^2x^8}\left[\frac{233}{Tx^6}\left(\frac{4}{x^{12}} - \frac{4}{x^6} + 1\right) - \frac{22}{x^6} + 5\right]\right\} \tag{I-21}$$

according to the derivation in Appendix B giving the first quantum correction term. The summation over all the rotational lines gives

$$\bar{B} = L\,(1.13_3\, J' + 0.307\, K) \times 10^{-36}\ \text{sec}^{-1}\ \text{cm}^6 \tag{I-22}$$

and is tabulated in Table I-1. The normalization factor for the $H_2$-He enhancement is given by

$$S(J) = \frac{L(J)}{\sum L}\,\bar{B}\,. \tag{I-23}$$

## I-4. THE THEORETICAL FORMULAE FOR THE INTEGRATED TRANSLATIONAL ABSORPTION

Because the translational profile has not been measured below 300 $\text{cm}^{-1}$, it will be necessary for us to compute this profile theoretically. In order to provide an independent check on our calculation, we first give the expression for the integrated translational absorption, obtained by trace methods, which is due to Poll and Van Kranendonk (1961). We also find it useful to quote

these expressions in checking the self-consistency of the theory and the observations and in evaluating the assumptions of the theory. Both the rotational and translational absorption formulae depend upon overlap parameters, which must be evaluated by fit to the observations. As the same parameters often appear in both expressions, they must be fitted simultaneously. The $\lambda_i$ which we have quoted are those given by the authors of these formulae. We postpone to section I-5 the evaluation of the assumptions of the theory.

I-4.a. The $H_2$-$H_2$ Case.

Poll and Van Kranendonk (1961) give for the integrated translational binary absorption coefficient in the units $sec^{-1}\ cm^5$,

$$a_1 = c \int_0^\infty a_\nu d\nu \qquad \text{(I-24)}$$

where $a_\nu$ is the translational contribution to $A_\nu$, the expression

$$a_1 = \mathcal{L}(T)(\lambda_1^2 I_1 + \lambda_3^2 I_3 + \mu^2 J' + \mu\lambda_3 K)\, p \qquad \text{(I-25)}$$

where the numerical quantities used are $p = 1.2093 \times 10^{-28}$ cgs, $\mu = 5.1260 \times 10^{-4}$, $\lambda_1 = 1.0 \times 10^{-4}$, $\lambda_3 = 0.6 \times 10^{-4}$, $\sigma/\rho = 7.937$, $\sigma = 2.93 \times 10^{-8}$ cm, $\epsilon/k = 37.0\ ^oK$, $\alpha = 5.44 a_o^3$, $Q = 0.49 e a_o^2$, $c = 2.9979 \times 10^{-10}$ cm/sec, e = the esu unit of charge, $\mu'$ = the reduced mass of $H_2$ in grams, and the functional quantities are

$$p = \pi e^2 \sigma^3 / 3\mu' c$$

$$\mu = \alpha Q / e\sigma^5$$

$$I_L = 4\pi \int_0^\infty \exp(-\frac{2\sigma}{\rho}(x-1)) ((\frac{\sigma}{\rho})^2 + \frac{L(L+1)}{X^2}) g(x) x^2 dx \qquad (I-26)$$

$$J' = 336\pi \int_0^\infty x^{-8} g(x) dx$$

$$K = 32\pi/3 \int_0^\infty \exp(-\frac{\sigma}{\rho}(x-1)) (\frac{\sigma}{\rho} + \frac{3}{x}) g(x) x^{-3} dx$$

where only the first few terms of the dipole moment expansion in spherical components have been used. g(x) is the pair distribution function and is given by equation (I-16). Numerically, we find

$$a_1 = (1.00\, I_1 + 0.36\, I_2 + 26.28\, J' + 3.08\, K) \mathcal{L}(T) \times 1.209 \times 10^{-36} \qquad (I-27)$$

in units of $\sec^{-1}\ \mathrm{cm}^5$. $\mathcal{L}(T)$ is the factor which accounts for the distribution of the $H_2$ molecules over their rotational states. For equilibrium hydrogen, it is given by

$$\mathcal{L}(T) = \sum_J g_J \frac{J(J+1)\ (2J+1)}{(2J-1)\ (2J+3)} \exp(-\beta E(J))/Z \qquad (I-28)$$

where $g_J$ and Z are given by equations (I-13) and (I-14), respectively, and $\beta = 1/kT$ so that

$$\beta E(J) = J(J+1)\ [\,85.3768 - 0.06618\, J(J+1) + .000075\, J^2 (J+1)^2\,]/T \qquad (I-29)$$

where the coefficients are taken from the data of Stoicheff (1957) and therefore, may differ somewhat from those actually used by Poll and Van Kranendonk. The summation in equation (I-28) is carried out over both even and odd J.

I-4. b. The $H_2$-He Enhancement Case.

Poll and Van Kranendonk (1961) give the corresponding formula:

$$b_1 = (\lambda^2 I_1 + \mu^2 J' \mathcal{L}(T)) p \qquad \text{(I-30)}$$

where

$$b_1 = c \int_0^\infty b_v dV \ \text{sec}^{-1} \ \text{cm}^5 \qquad \text{(I-31)}$$

and where $b_v$ is the translational contribution to $B_v$.

The first term of equation (I-30) is 97 per cent of the contribution because $\lambda$ is the angle-independent overlap parameter which did not arise in the rotational spectra and it is more than an order of magnitude larger than the first angle-dependent terms. It appears here because its corresponding term is modulated by the relative translational motion. Poll and Van Kranendonk do not quote a value for $\lambda$. We determined the value of $\lambda$ by comparing the results of the calculation of the frequency-dependent translational profile given in sections I-6 and I-7 and the fit to the rotational profile with the observations at room temperature. The calculation of the frequency-dependent translational profile was checked by using an arbitrary $\lambda$ and comparing the integral

with equation (I-30) using this same arbitrary $\lambda$. The numerical values used are $p = 7.44 \times 10^{-29}$ cgs, $\sigma = 2.74 \times 10^{-8}$, $\epsilon/k = 19.4\ ^{o}K$, $\rho/\sigma = 0.126$, $\alpha = 2.02 \times 10^{-25}\ cm^3$, $Q = 0.49ea_o^2$, $\mu = 1.84_3 \times 10^{-4}$, $\lambda = 8.8 \times 10^{-4}$, $\mu' = 2.226 \times 10^{-24}$ gm and the functional quantities are the same as given by equations (I-26) except that the pair distribution function is given by equation (I-21).

## I-5. THE EXPERIMENTAL EVALUATION OF THE U(r) ASSUMPTION

The experimental profiles of Kiss, Gush and Welsh (1959) and Kiss and Welsh (1959) are plotted at various pressures for 300, 195 and 85 $^{o}K$. While the integrated absorption between 300 $cm^{-1}$ and 1400 $cm^{-1}$ increases quite accurately with the product of the densities of the colliding components, the frequency-dependence of the profiles is not quite independent of these densities at a fixed temperature. We conclude that the absorption is due entirely to binary collisions but that there is a coupling between the rotational and translational wave functions. In other words, U is a function of the angular variables as well as a function of r. We now investigate the error made with the U(r) assumption.

I-5.a. For the rotational lines, the theory (equation (I-10) ) gives $\bar{A}(0)/\bar{A}(1) = 1.38$ for the ratio of the strengths of the S(0) and S(1) lines. If the profiles have the same half-width and are otherwise similar, apart from a proportionality factor, this implies that the maxima also have the same ratio. When the corresponding experimental ratio is formed by taking the observed profile at 85 $^{o}K$

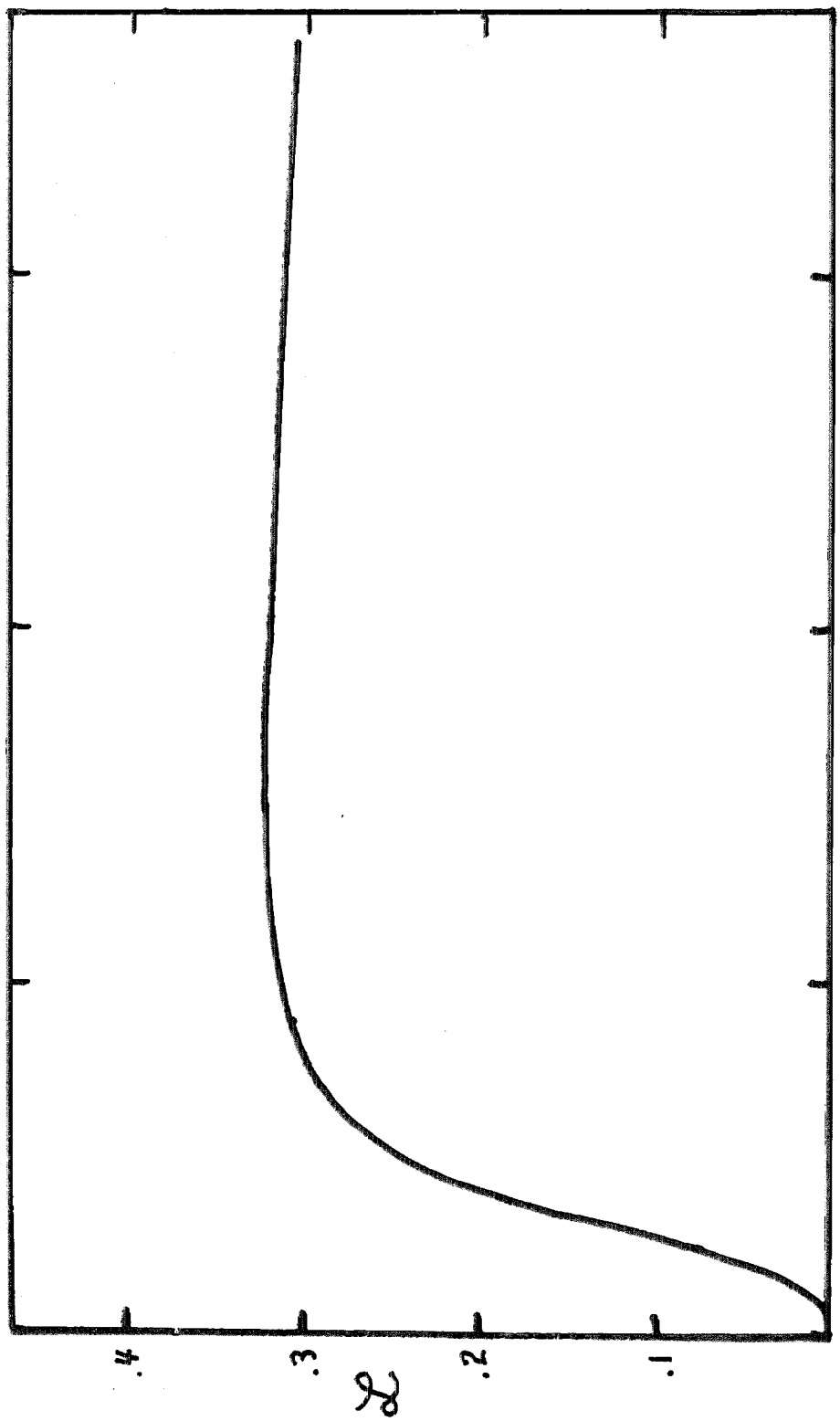


Figure 4.

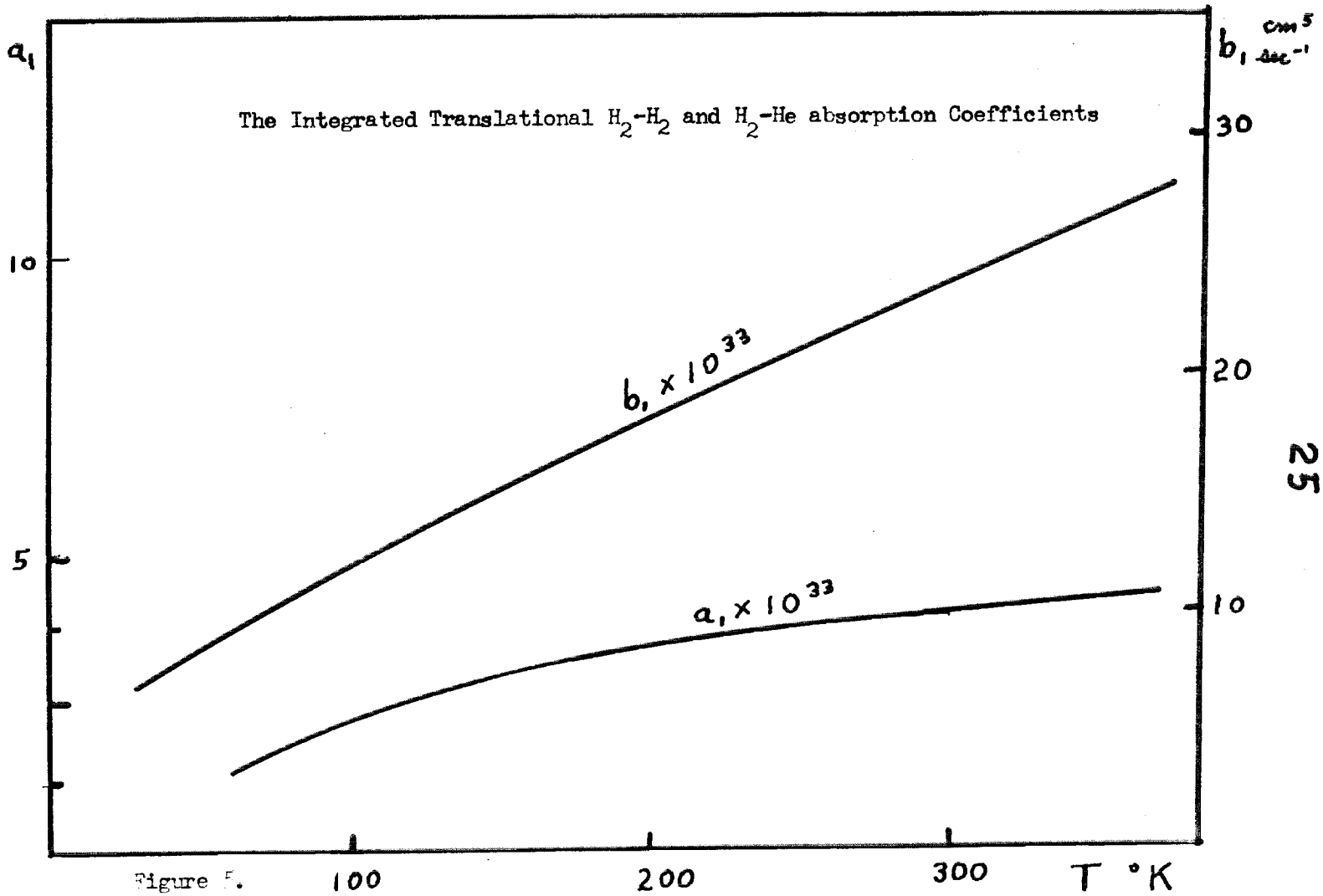
The Integrated Translational $H_2$-$H_2$ and $H_2$-He absorption Coefficients
$a_1$
$b_1$ cm$^5$ sec$^{-1}$
30
20
10
10
5
$b_1 \times 10^{33}$
$a_1 \times 10^{33}$
100
200
300
T °K

Figure 5.

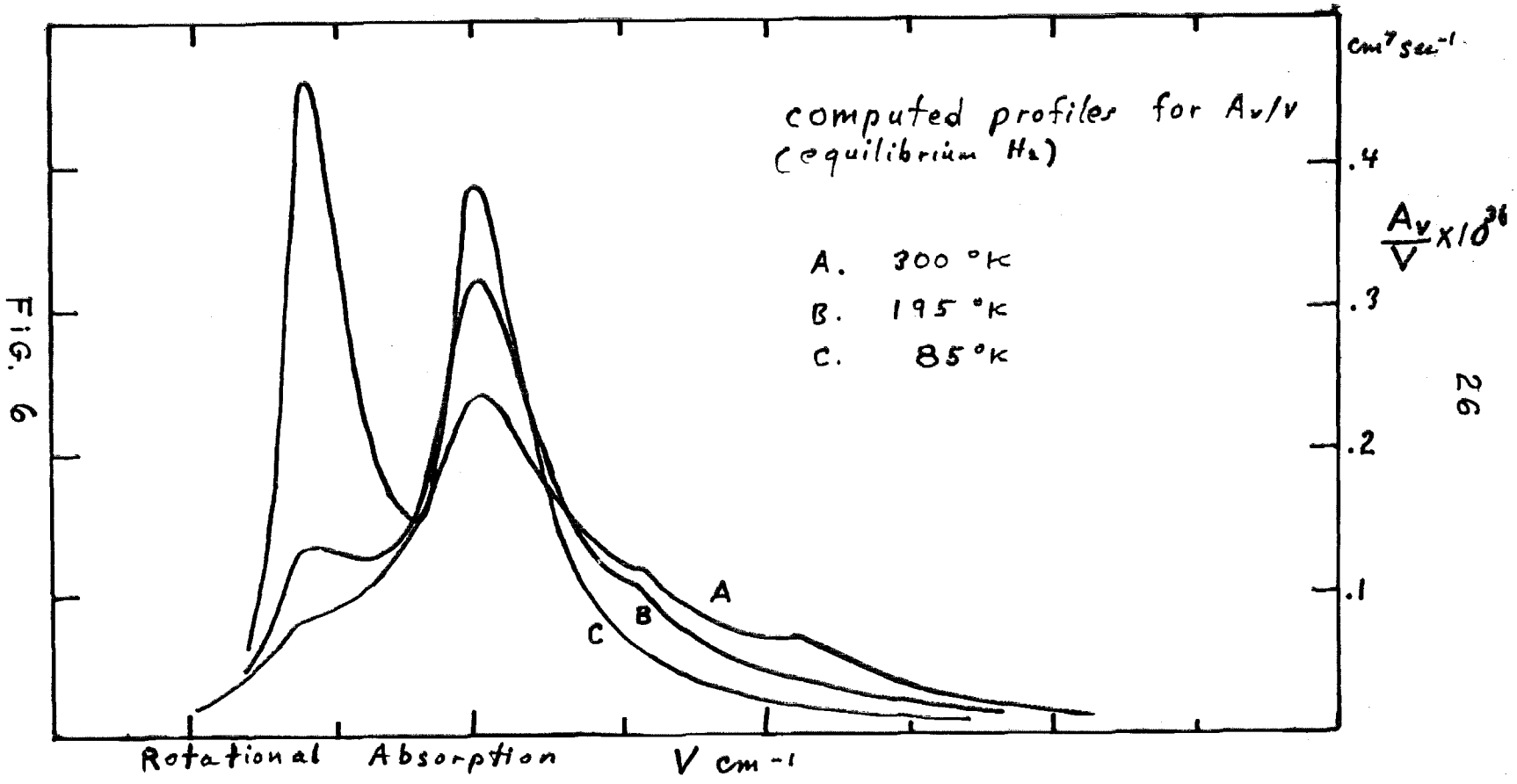
computed profiles for Av/v
(equilibrium H2)
A. 300 °K
B. 195 °K
C. 85 °K
A
B
C
cm² sec⁻¹
.4
.3
.2
.1
Av/v x10³⁶
Rotational Absorption
V cm⁻¹

Fig. 6

and 118 Amagat units of density, dividing by the frequency and taking the ratio of the maxima of the S(0) and S(1) lines, the result is 1.06. The tail of the translational profile is weak at this low temperature and its presence only reduces this experimental value still further. However, when we form this ratio for the lower density profiles, the gap between the theoretical and experimental ratio diminishes. The lowest density profile given for $H_2$-$H_2$ by Kiss and Welsh (1959) is for 48 Amagats where this ratio becomes 1.16. Since we want the absorption for densities less than 5 Amagats in planetary atmospheres, this gap may be unimportant if it continues to monotonically decrease with the density. In the experimental range, the errors due to the U(r) assumption increase monotonically with the density.

I-5.b. When the experimental S(1) profile was fitted using the Boltzmann asymmetry factor $\exp(-hc\Delta V/kT)$ at 85 $^{o}$K, it was found that the fit was best for T = 93 $^{o}$K. At 93 $^{o}$K, the gap between the S(0)/S(1) ratios mentioned in section I-5.a. becomes small, but this is probably a coincidence. The fit of this Boltzmann relation is not perfect, so that the 93 $^{o}$K may not be significant. The effect of the presence of the translational profile would be to give a higher fitting temperature. However, the imperfect fit could simply reflect the complications not accounted for in the idealized model.

I-5.c. The overlap parameters $\lambda_i$ contribute to both the translational and rotational absorption. Because the coordinate frame is different in these two cases, the numerical values of the $\lambda_i$ will be different for the two cases but related by a linear

transformation. Only the simplest angle-dependent terms are ever considered in the dipole moment expansion, the rest being negligible. No successful theoretical calculation of these parameters has been made. As a result, they must be inferred from the comparison of the expressions for the integrated absorption coefficient with the laboratory data. With the exception of the $H_2$-He translational spectrum, which is due almost entirely to the overlap contribution, the overlap terms give less than 20 per cent of the absorption. As a consequence, these parameters are not well determined but suffice for purposes of expressing the net strength of the absorption with fair accuracy.

Using equation (I-10) for the distribution of the line strengths for the individual rotational transitions, Kiss and Welsh obtained an empirical profile for the translational spectrum for V greater than 300 $cm^{-1}$ at room temperature, assuming that it was monotonically decreasing in this range. They did this by subtracting the calculated rotational profiles from the observed profile under the assumption that all the rotational lines have the same shape apart from a scale factor in the ordinate. Using the shape determined from S(1), they were able to get a unique profile for the translational tail and derive $\lambda = 0.8 \times 10^{-4}$ for equation (I-17). Poll and Van Kranendonk (1961) then transformed this into the corresponding parameters in the translational frame, $\lambda_1 = 10^{-4}$ and $\lambda_3 = 0.6 \times 10^{-4}$ for use in equation (I-25). However, when we compared the integrated translational absorption computed from equation (I-25) with the corresponding experimental quantity for the tail (V greater than 300 $cm^{-1}$), we found it to be <u>less</u> than this tail. When the frequency-dependent profile was computed, the

portion for V greater than 300 $cm^{-1}$ at room temperature was divided by V and integrated giving $0.45 \times 10^{-35}$ $sec^{-1}$ $cm^{6}$ compared with the derived experimental value of Kiss and Welsh (1959) for the corresponding quantity, $1.80 \times 10^{-35}$ $sec^{-1}$ $cm^{6}$. This is a factor of four discrepancy. Also, the ordinates at 300 $cm^{-1}$ of the respective profiles are in disagreement by a factor of three.

At first, we thought that the discrepancy could be entirely explained by correcting the $\lambda$'s. One easily sees that the overlap parameters are going to affect the rotational and translational profiles simultaneously, and can only be properly evaluated by fitting the sum of these profiles to the experimental data. However, no $\lambda$ gave a fit better than 5 per cent on the average over the entire range of temperatures for $H_2$-$H_2$ absorption at high densities. However, comparing the fit of the final profiles at lower densities was more encouraging. Again, the gap declines with the density. At low densities, the above quoted values of the $\lambda_i$ should be adequate. The fit is best at low densities and low temperatures, precisely the case for application to the atmospheres of the major planets. Figure 6 shows the comparison with the computed and measured profiles for pure $H_2$.

I-5.d. For the $H_2$-He enhancement case, the molecular constants are less well known and less experimental data is available. The rotational $\lambda = 0.5 \times 10^{-4}$ was obtained by Van Kranendonk and Kiss (1959) at 300 $^{o}K$ by the usual method, although the rotational spectrum is quite weak in this case. The translational $\lambda = 8.75 \times 10^{-4}$ is an order of magnitude greater

and gives rise to most of the translational spectrum. We evaluated this parameter by comparing the ordinate of the translational profile, computed theoretically with $\lambda$ as a free parameter, with the semi-empirical curve obtained by Kiss and Welsh (1959). The error is small in this case because of the dominance of the translational spectrum. However, the shapes of the two profiles do not closely agree, the empirical one falling off slower than the theoretical one. In fact, the empirical profile mimics the shape of the theoretical one at a higher temperature. In the $H_2$-He case, the Lennard-Jones and EXP-4 parameters are not known as well as for the $H_2$-$H_2$ case and this may be mainly responsible for the lack of close agreement.

Insufficient laboratory data are available to determine whether the theoretical and experimental fit improves at low densities for the $H_2$-He case. However, laboratory data at 300 $^{o}$K exist for the translational absorption in mixtures of noble gases in the region V greater than 300 $cm^{-1}$. Because of the symmetry, we expect the U(r) assumption to hold for mixtures of noble gases. Neglecting the difference in the matrix elements, we deduce a $\lambda$ for He-Ne mixtures approximately equal to $9 \times 10^{-4}$ from fitting equation (I-30), using the dominant contribution of the $H_2$-He matrix elements and the He-Ne constants, to the observed profile for He-Ne mixtures at 300 $^{o}$K. This value is in close agreement with the $H_2$-He case where the dominant contribution is from the angle-independent term of the induced dipole moment. In addition, the experimental value for He-Ne mixture falls off faster than for the $H_2$-He enhancement case, leaving the theoretical

$H_2$-He case intermediate between the experimental He-Ne and $H_2$-$H_2$ curves. We must be satisfied with this fit until further experimental data are available.

At least for the $H_2$-$H_2$ case, the pressure-induced absorption coefficient is known to about 6 per cent accuracy on the average. For the $H_2$-He case, the error is greater, because the molecular constants are not known as well. That is, applying nearly the same theory to the $H_2$-He enhancement case as was applied to the $H_2$-$H_2$ case, one expects to obtain results of comparable validity. It does not appear that our assumptions will prevent the construction of meaningful models of the atmospheres of the major planets.

## I-6. THE QUANTUM MECHANICAL CALCULATION OF THE TRANSLATIONAL ABSORPTION COEFFICIENT

It is necessary to calculate the translational absorption profile as most of it lies below the range of experimental observation and in the region of the Planck curve's maximum at planetary temperatures. It will play an important role in the energy balance of the major planets.

We approach the problem from a somewhat general viewpoint. We consider a closed system of N molecules interacting with each other and the radiation field. The eigenvalues and eigenstates are for the whole system of N particles with the absorption computed in the dipole approximation. By means of the Ursell cluster expansions, the absorption coefficient is expanded in powers of the density. The U(r) assumption is

employed with the EXP-4 model for the induced dipole moment to derive the final binary absorption coefficient. At 20 $^{o}$K, Boltzmann statistics govern the relative coordinate distributions of $H_2$ provided the density is less than 11 Amagats. We may therefore use Boltzmann statistics for the energy levels and relative velocities in planetary atmospheres. However, the discrete nature of the angular momenta requires that the rest of the problem be treated quantum mechanically.

Consider a medium of volume v containing a gas of molecules. Let $a_v$ be the translational absorption coefficient at the frequency V, measured in wave numbers. It is defined by the expression

$$a_v = \frac{1}{L} \ln \frac{I_{vo}}{I_v} \tag{I-32}$$

where L is the path length and $I_v$ is the light absorbed only by the translational processes. The corresponding integrated translational absorption coefficient is

$$a = c \int_0^\infty a_v \, dv \, . \tag{I-33}$$

Poll and Van Kranendonk (1961) give

$$a = kv^{-1} \sum_{i<f} (P_i - P_f) |\underline{u}_{if}|^2 \, hcV_{if} \tag{I-34}$$

where $k = 8\pi^3/3h^2c$, h is Planck's constant, $P_i$ are the normalized Boltzmann factors of the state i, i and f are the initial and final

stationary states of the system (eigenstates of the Hamiltonian), $\underline{u}$ is the expectation value of the total dipole moment operator of the gas over the ground vibrational and electronic state, $\underline{u}_{if}$ is the matrix element of $\underline{u}$ between i and f, $hcV_{if} = E_f - E_i$ where E is an eigenvalue of the Hamiltonian, H; and the sum runs over all pairs of states for which $E_i$ is less than $E_f$. Note that the $P_f$ term takes the stimulated emission into account. Also, note that $\underline{u}$ is a function of the nuclear configuration of the gas. The dimensions of a are $sec^{-1}\ cm^5$.

Using the Hermitian property of $\underline{u}_{if}$, equation (I-34) can be written in the form of a trace (see the derivation in Appendix C) which is invariant with respect to the states. The result is

$$a = kv^{-1}\ \mathrm{Tr}\ \left\{ \bar{P}\,\underline{u} \cdot [H, \underline{u}] \right\} \qquad \text{(I-35)}$$

where Tr denotes the trace, $[H, \underline{u}]$ is the commutator of $\underline{u}$ with the Hamiltonian, and $\bar{P}$ is the operator which, when acting on state i, gives rise to the normalized Boltzmann factor as an eigenvalue.

$$\bar{P} = \exp(-\beta H)/Z \qquad \text{(I-36)}$$

where $\beta = 1/kT$ and k is the Boltzmann constant (in this relation) and the partition function Z is

$$Z = \mathrm{Tr}\ \left\{ \exp(-\beta H) \right\} = \sum_J \exp(-\beta E_J) \qquad \text{(I-37)}$$

where the summation is over all the possible states of the gas. Notice that whatever the form of the potential likely to occur in the Hamiltonian, it will commute with $\underline{u}$ giving

$$a = kv^{-1} \, Tr \left\{ \overline{P} \, \underline{u} \cdot [K, \underline{u}] \right\} \tag{I-38}$$

where K are the kinetic terms of H. These terms are independent of each other.

I-6.a. The Cluster Expansion of the Absorption Coefficient Into a Power Series In the Density.

Equation (I-38) is the expectation value of $kv^{-1} \, \overline{Q}$ where the operator $\overline{Q}$ is

$$\overline{Q} = \underline{u} \cdot [K, \underline{u}] \tag{I-39}$$

If the volume v contains N molecules, then

$$\begin{aligned} \overline{Q} &= \overline{Q}(1 \ldots N) \\ \underline{u} &= \underline{u}(1 \ldots N) \\ \overline{P} &= \overline{P}(1 \ldots N) \\ K &= K(1) + K(2) + \ldots + K(N) \end{aligned}$$

are functions of the N sets of coordinates; $1, 2, \ldots, N$. Each set includes all the coordinates of a single one of the molecules. In this gas each molecule exerts its own effective force field out to a volume which may or may not inclose several neighbors, depending on the range of this force field and the density. Such

an association is called a cluster. Each cluster may give rise to absorption since a significent dipole moment is induced. The wavelength of the absorbed light is much greater than the effective range of the intermolecular force field so that the cluster behaves like a quasi-molecule for purposes of absorption and the dipole approximation will suffice. From the classical viewpoint, the cluster rather than the collision concept appears to more adequately describe the processes taking place during absorption. This is no doubt due to the slow speeds of these heavy particles at low temperatures and to the diffuse nature of the collision due to the somewhat diffuse character of the effective range of the intermolecular forces.

Because of the short range of these intermolecular forces, clusters with large populations will be extremely rare and we may approximate the absorption by that due to the lowest populated clusters. This is the basis for the expansion of the absorption coefficient in powers of the density. For molecular hydrogen and mixtures with helium, the laboratory data indicate that we may ignore all but the two-body clusters. However, for mixtures of hydrogen and xenon, we must take the three-body clusters into account at higher densities. We will develop the cluster expansion as far as the three-body case in order to illustrate the expansion and to provide a term for evaluating the error of taking only the two-body clusters into account.

### I-6. a. 1. The Diatomic Gas Case

We begin the derivation of the absorption coefficient for a diatomic gas by considering the Ursell cluster expansion for the

induced dipole moment. Consider a single component diatomic gas of N molecules in a volume v. Let $\underline{u}(\ldots n)$ be the dipole moment induced in the cluster of n molecules when they alone are present in v. We let i stand for the set of coordinates of the $i^{th}$ molecule. The cluster functions $\underline{U}(1\ldots n)$ are defined by

$$\begin{aligned} \underline{u}(12) &= \underline{U}(12) \\ \underline{u}(123) &= \underline{U}(12) + \underline{U}(13) + \underline{U}(23) + \underline{U}(123) \\ \underline{u}(1\ldots N) &= \sum_{i<j} \underline{U}(ij) + \sum_{i<j<k} \underline{U}(ijk) + \ldots \end{aligned} \tag{I-40}$$

These cluster functions are completely defined and can be solved for in terms of the $\underline{u}$'s by successive substitution. We strongly emphasize the fact that these cluster functions have the desired property of being zero unless all of the molecules of the cluster are close enough to induce a non-negligible moment. When the $\underline{U}$'s are substituted into the last of the above equations, we obtain the cluster expansion of $\underline{u}(1\ldots N)$. That we are doing this for a diatomic gas is manifested in the fact that each molecule can give rise to absorption and each can induce a moment in the other. Thus, Poll and Van Kranendonk (1961) obtain the above form of the cluster expansion.

Equation (I-38) may be written in the equivalent form for N molecules in the volume v:

$$a = kv^{-1} \int_v \sum_s \Phi_s^*(1\ldots N)\, \bar{P}(1\ldots N)\, \bar{Q}(1\ldots N)\, \Phi_s(1\ldots N) d1\ldots dN \tag{I-41}$$

In order to obtain the expansion of a in powers of the density, we consider the cluster expansion of the above integrand. We do this by first considering the expansion of $\bar{Q}(1\ldots N)$ using equation (I-39) and the above cluster expansion for the $\underline{u}(1\ldots N)$. In this connection, we note that $[K(1\ldots N),\ \underline{U}(i\ldots j)] = [K(i\ldots j),\ \underline{U}(i\ldots j)]$ and obtain $\bar{Q}(1\ldots N)$ as the sum of cross product terms between K and $\underline{U}$.

Let $\bar{Q}_m(i\ldots j)$ denote the terms in the expansion of $\bar{Q}(1\ldots N)$ involving the m molecules, i...j. Now because the remaining factor in equation (I-41) is symmetric with respect to permutation of 1...N, we may re-label the molecules so that i...j becomes 1, 2...m. There are (N-1)N/2 terms of the form $\underline{U}(ij)\cdot[K(ij),\ \underline{U}(ij)]$ in the expansion of $\bar{Q}(1\ldots N)$ that involve just two molecules, (N+1)N(N-2) terms of the form $\underline{U}(ij)\cdot[K(ik),\ \underline{U}(ik)]$, N(N+1)(N+2)/2 terms of the form $\underline{U}(ijk)\cdot[K(ij),\ \underline{U}(ij)]$ or $\underline{U}(ij)\cdot[K(ijk),\ \underline{U}(ijk)]$, N(N+1)(N+2)/6 terms of the form $\underline{U}(ijk)\cdot[K(ijk),\ \underline{U}(ijk)]$ which involve exactly three molecules and so on for the terms which involve more than three molecules. The terms of the same form give the same contribution to the absorption. We may therefore write equation (I-41) as the sum of contributions from the terms of different form, each weighted by the number of terms having the same form.

Let us now consider the contribution from an arbitrary one of these terms. We define

$$R_m(m\ldots N) = \sum_S \Phi_S^*(1\ldots N)\ \bar{P}(1\ldots N)\ \bar{Q}_m(1\ldots m)\ \Phi_S(1\ldots N) \qquad \text{(I-42)}$$

for $m = 1, 2, \ldots, N$ and $\bar{Q}_1 = 1$. Let the molecules 1...m remain fixed in the cluster. Treat their coordinates as that for a single

molecule with 3m degrees of freedom. Hence, m is to be considered as the set of coordinates for a single particle in the following equations. We now make the corresponding cluster expansion, which is motivated by the fact that $R_m(N)$ breaks up into independent factors in the limit of weak interaction. We obtain

$$
\begin{aligned}
R_m(m) &= S(m) \\
R_m(mk) &= S(mk) + S(m)S(k) \qquad \text{(I-43)} \\
R_m(mkp) &= S(mkp) + S(mk)S(p) + S(kp)S(m) + S(mp)S(k) + S(m)S(p)S(k) \\
&\;\;\vdots
\end{aligned}
$$

where $m = 1, \ldots, N$. Notice that $R_1(1) = 1$ and that this expansion is quantum mechanically valid. The S functions may be solved for explicitly in terms of the $R_m$ for $m = 1, \ldots, N$ by successive substitution. These S functions vanish if any member of the corresponding cluster gets lost. The indices in the arguments of S and $R_m$ denote which molecules are present in the corresponding cluster or volume v, respectively. The quantities $R_m(m \ldots n)$ are the values that equation (I-42) would take on if there were only particles $m \ldots n$ present in v. The particle labeled m corresponds to the fixed m particles and the other labels refer to the other individual particles.

Expressing $R_m(m \ldots N)$ in a form where we distinguish between clusters containing and not containing the "molecule" m, De Boer (1949) gives

$$R_m(m\ldots N) = S(m)R_1(m+1\ldots N) + \sum_k{}' S(mk)R_1(M+2\ldots N) + \sum_{k,p}{}' S(mkp)R_1(M+3\ldots N) + \ldots \quad \text{(I-44)}$$

where the summations are over all the possible ways of forming a cluster containing the particles mkp... by choosing the particles kp... from the available N-m particles and adding to them the original m particles. The number of terms which result is just the number of permutations of N-m quantities taken n at a time where n is the number of particles kp.... This value is

$$\frac{(N-m)!}{n!\,(N-m-n)!} \quad \text{(I-45)}$$

We note that $\mathrm{Tr}\left\{ \bar{P} \right\}$ must be unity and this implies that

$$\int_v R_1(m+n\ldots N)d(m+n)\ldots dN = 1 \quad \text{(I-46)}$$

so that the integral over $d(m+1)\ldots dN$ of equation (I-44) becomes, with the aid of equations (I-43 and 45),

$$\bar{R}_m(N) = R_m(m) + (N-m)b_2(m) + (1/2)(N-m)(N-m-1)b_3(m) + \ldots \quad \text{(I-47)}$$

which defines $\bar{R}_m(N)$, and

$$b_2(m) = \int_v S(mk)dk$$
$$b_3(m) = \int_v S(mkp)\,dkdp \quad \text{(I-48)}$$

We now argue that the $b_n(m)$ are proportional to $v^{-(m+n-1)}$. By virtue of the cluster properties of the S functions, the integrand of $b_n(m)$ vanishes whenever any of the molecules involved becomes far removed from any other. Therefore, the above integration over the coordinates of the n-1 molecules is independent of the volume so long as it is large. However, the S contain a normalization factor $v^{-(m+n-1)}$ arising from the contribution of the partition function for the continuous states of m+n-1 particles in the quantity $\bar{P}(m+n-1)$. We therefore have

$$\bar{R}_m(N) = R_m(m) + \frac{N-m}{v} \frac{B_2(m)}{v^m} + \frac{1}{2} \frac{N-m}{v} \frac{N-m-1}{v} \frac{B_3(m)}{v^m} + \ldots \quad \text{(I-49)}$$

where

$$B_n(m) = v^{(m+n-1)} b_n(m) \quad \text{(I-50)}$$

are independent of v, so long as it is large. Now the contributions from the terms of larger m will be negligible if the density is small enough and the effective range of the intermolecular forces is short enough. In this case we may take N to be much greater than m and obtain the density expansion

$$\bar{R}_m(N) = R_m(m) + n \frac{B_2(m)}{v^m} + \frac{1}{2} n^2 \frac{B_3(m)}{v^m} + \ldots \quad \text{(I-51)}$$

where n is the number density, N/v and

$$B_2(m) = v^{m+1} \int_v [R_m(mk) - R_m(m)R_1(k)]\, dk$$

$$B_2(m) = v^{m+1} \left[ \int_v R_m(mk)dk - R_m(m) \right] \qquad \text{(I-52)}$$

$$B_3(m) = v^{m+2} \int_v S(mkp)dk\, dp \quad .$$

When we integrate equation (I-51) over dm, we obtain its contribution to the absorption coefficient. A factor of v arises when this integration is effected and a factor $N^m$ (in the large N approximation) from the summation over terms of given m so that we obtain a contribution proportional to

$$kv^{-1} \left\{ n^m \int_v v^m R_m(m)dm + n^{m+1} \int_v B_2(m)dm \right.$$

$$\left. + \frac{1}{2} n^{m+2} \int_v B_3(m)dm \right\} + \ldots \qquad \text{(I-53)}$$

We now sum the terms of lowest m (for m greater than 1) and collect terms with the same power of the density to obtain the density expansion of the integrated absorption coefficient. Notice that $v^m R_m(m)$ does not depend upon the volume.

$$a = \frac{1}{2} kv^{-1} n^2 \int_v v^2 R_2(2)d2 + \frac{1}{2} kv^{-1} n^3 \left[ \int_v B_2(2)d2 + \int_v v^3 R_3(3)d3 \right]$$

$$+ 0(n^4) \qquad \text{(I-54)}$$

where $0(n^4)$ means "terms of the order of $n^4$ + etc.". Note that the subscripts 2 and 3 on R and B indicate that the integration is to be performed over m = 2 and 3 particle-space, respectively, rather than over the single particle-space d2 or d3. Letting the density expansion be written in the form

$$a = a_1 n^2 + a_2 n^3 + \dots , \tag{I-55}$$

we have

$$a_1 = \frac{1}{2} kv \, \mathrm{Tr} \left\{ \bar{P}(12) \underline{u}(12) \cdot [K(12), \underline{u}(12)] \right\} \tag{I-56}$$

and

$$\begin{aligned} a_2 = {} & kv^2 \, \mathrm{Tr} \left\{ \bar{P}(123) \underline{u}(12) \cdot [K(13), \underline{u}(13)] \right\} \\ & + \frac{1}{2} kv^2 \, \mathrm{Tr} \left\{ \bar{P}(123) [\underline{U}(123) \cdot [K(12), \underline{U}(12)] + \underline{U}(12) \cdot [K(123), \underline{U}(123)] \right. \\ & \left. + \frac{1}{3} \underline{U}(123) \cdot [K(123), U(123)] \right\} + \frac{1}{2} kv^2 \, [\mathrm{Tr} \left\{ \bar{P}(123) \, \bar{0}(12) \right\} \\ & - \mathrm{Tr} \left\{ \bar{P}(12) \, \bar{0}(12) \right\}] \end{aligned} \tag{I-57}$$

where $\bar{0}(12) = \underline{u}(12) \cdot [K(12), \underline{u}(12)]$. Equation (I-56) gives the integrated translational binary absorption coefficient and equation (I-57) gives the corresponding ternary absorption coefficient.

We have illustrated the technique for obtaining the density expansion of the pressure-induced integrated translational absorption coefficient for any diatomic gas. From this point on, we will consider only the low density limit ($a_1$) and obtain an explicit evaluation of equation (I-56).

We let coordinates 1 refer to the center of mass of the pair of molecules and 2 to the relative coordinates in the center of mass frame. Taking the trace over the center of mass introduces a factor of unity, leaving

$$a_1 = \frac{k}{2} v \, \mathrm{Tr} \left\{ \bar{P} \, \underline{u} \cdot [K, \underline{u}] \right\} \tag{I-58}$$

where the trace is now over only relative coordinates. Equations (I-36 and 37) and give

$$Z = Z^2(\mathrm{rot}) \, Z(\mathrm{trans}), \tag{I-59}$$

where Z(rot) is the rotational partition function of the diatomic molecule and Z (trans) is the translational partition function given by

$$Z(\mathrm{trans}) = \int_{p=0}^{\infty} \int_{V} 4\pi p^2 \, dp \, d\tau \, h^{-3} \exp(-\beta p^2/2\mu). \tag{I-60}$$

This is found to be

$$Z(\mathrm{trans}) = v \, \lambda^{-3},$$

where (I-61)

$$\lambda^2 = h^2/(2\pi\mu \underline{k} T)$$

and $\mu$ is the reduced mass of the two molecules. We finally have

$$a_1 = \frac{k}{2} \frac{\lambda^3}{Z^2} (\mathrm{rot}) \, \mathrm{Tr} \left\{ \exp(-\beta H) \, \underline{u} \cdot [H, \underline{u}] \right\} . \tag{I-62}$$

This is in agreement with the corresponding expression given by Poll and Van Kranendonk in their treatment of the integrated translational absorption.

I-6. a. 2. Monatomic Gas Mixtures and Mixtures of a Monatomic and a Diatomic Gas

We here consider the absorption arising from the dipole moment induced between molecules of different species. No absorption takes place between like monatomic molecules because no net dipole moment is induced due to the symmetry present in this case.

Consider one molecule of species A in the volume v with N-1 monatomic molecules of species B. In this cluster all the molecules of species B will contribute to the net moment induced in A. Denote the coordinate of A by 1 if it is monatomic and by 1' if it is diatomic and denote the coordinates of B by 2...N. $i = \underline{R}_i$ are the coordinates of the center of mass of the monatomic molecule labeled i and $i' = (\underline{R}_i, \underline{w}_i)$ is the corresponding quantity for the diatomic molecule if $\underline{w}_i$ are the angular coordinates of the internuclear axis in an inertial frame.

If $\underline{u}(1...n)$ is the net moment induced in a cluster of n molecules alone in the volume v, the cluster expansion for mixtures of monatomic gases is

$$\begin{aligned} \underline{u}(12) &= \underline{U}(12) \\ \underline{u}(123) &= \underline{U}(12) + \underline{U}(13) + \underline{U}(123) \\ \underline{u}(1...N) &= \sum_{i=2}^{N} \underline{U}(1i) + \sum_{i<j=3}^{N} \underline{U}(1ij) \ . \end{aligned} \tag{I-63}$$

For a diatomic-monatomic gas mixture, the cluster expansion is the same as equation (I-63) except that the label 1 is replaced by 1'.

Again, the $\underline{U}(1\ldots n)$'s all have the property that they vanish if any member $1\ldots n$ is far removed from any other member. Successive substitution allows us to solve for the $\underline{U}$ in terms of the $\underline{u}$.

The operator $\bar{Q}(1\ldots m)$ is expanded as before in terms of the $\underline{U}$ functions and inserted in the cluster expansion of the trace of $\bar{Q}$ for the N-1 molecules of type B and M molecules of type A. We do this for M = 1 and multiply the result by M since the absorption is simply proportional to M in this case. Substituting $\underline{u}(1\ldots N)$, we get cross terms of the type $\bar{Q}_2(1i) = \underline{u}(1i)\cdot[K(1i), \underline{u}(1i)]$ where only a pair is involved, plus higher order terms. There are N-1 such terms so the integrated translational absorption b for mixtures of monatomic gases is

$$b/M = kv^{-1}\,(N-1)\,\mathrm{Tr}\left\{\bar{P}(12)\;\bar{Q}(12)\right\} \tag{I-64}$$

$$b = n_A\, n_B\, kv\,\mathrm{Tr}\left\{\bar{P}(12)\;\bar{Q}(12)\right\} \tag{I-65}$$

Taking the trace over the center of mass, we get

$$b = n_A\, n_B\, kv\,\mathrm{Tr}\left\{\bar{P}\;\bar{Q}\right\} \tag{I-66}$$

where only relative coordinates appear. An analogous expression for diatomic-monatomic mixtures is obtained for the corresponding absorption b' by replacing 1 by 1'. We finally obtain the binary absorption coefficients

$$b_1' = k \frac{\lambda^3}{Z(rot)} \; Tr \left\{ \exp(-\beta H) \, \underline{u}(1'2) \cdot [K(1'2), \underline{u}(1'2)] \right\} \tag{I-67}$$

$$b_1 = k \lambda^3 \; Tr \left\{ \exp(-\beta H) \, \underline{u}(12) \cdot [K(12), \underline{U}(12)] \right\} \tag{I-68}$$

where

$$\begin{aligned} b' &= b_1' n_1 n_2 + \cdots \\ b &= b_1 n_1 n_2 + \cdots \end{aligned} \tag{I-69}$$

are the absorption enhancement in diatomic-monatomic gas mixtures and the absorption in monatomic-monatomic gas mixtures, respectively. Also, we have the relations

$\lambda^2 = h^2/(2\pi\mu \underline{k} T)$

$k = 8\pi^3/(3h^2 c)$

$\beta = 1/\underline{k}T$

$n_i$ = the number density of species i

H = the Hamiltonian operator for the system

$\underline{k}$ is Boltzmann's constant and is not to be confused with k. We mention at this point that we do not make an attempt to calculate the ternary absorption coefficient for gas mixtures.

The outline of the above calculations is due to Poll and Van Kranendonk (1961) and our results agree with theirs. However, they do not give their calculations in detail nor do they give the explicit expression for the ternary absorption coefficient as we

have done. The method is quite general and fairly powerful. We therefore decided to include it in this thesis. We will next make use of the results for the binary case to find the frequency dependence of the absorption coefficients. As this has not been done before, it will be an original contribution.

## I-6. b. The Frequency Dependence of the Translational Absorption Coefficient

Up to now, we have followed the procedures set up by Poll and Van Kranendonk in obtaining the density expansion of the integrated translational absorption coefficient. Since we desire the frequency dependence, we must depart from their discussion at this point. We now propose the following derivation to obtain the hitherto unavailable expression for the frequency-dependent pressure-induced translational absorption coefficient.

The trace is a sum of probabilities that a transition takes place starting from a specified level and terminating on any of the possible remaining levels. We must therefore transform the trace to another expression in order to obtain the frequency dependence. We use the procedure given in Appendix C in reverse to transform the trace back to a summation whose initial energy levels lie below the final ones. To do this, $\Phi_s$ must be the energy eigen-functions. Designating the three cases by A, B and C, we obtain

$$\text{A.} \quad a_1 = \frac{k}{2} \frac{\lambda^3}{Z^2} \sum_{i<f} (B_i - B_f) \, |\underline{u}_{if}|^2 \, hcV_{if}$$

$$\text{B.} \quad b_1' = k \frac{\lambda^3}{Z} \sum_{i<f} (B_i - B_f) \, |\underline{u}_{if}|^2 \, hcV_{if} \qquad \text{(I-70)}$$

$$\text{C.} \quad b_1 = k \, \lambda^3 \sum_{i<f} (B_i - B_f) \, |\underline{u}_{if}|^2 \, hcV_{if}$$

where Z is now the rotational partition function given by equation (I-14) for the case of an equilibrium mixture of $H_2$ and $B_i$ is $\exp(-\beta E(i))$, the Boltzmann factor for state i. Equations (I-70) are the two-particle analogues of equation (I-34). In the equations to follow, A stands for the diatomic case, B stands for the diatomic-monatomic case and C stands for the monatomic-monatomic mixture case.

Let v go to infinity, so that we have essentially a continuum of translational energy states. Let the labels i and f define a two dimensional energy space for the systems A, B and C. That is, let i and f be directly proportional to the energy of the corresponding translational level where the discrete rotational states are held fixed. Then, as i or f changes, only the translational state is understood to change. The summation of the translational states in equations (I-70) will then become a double integral

$$\int_{f=o}^{\infty} \int_{i=o}^{f} (B_i - B_f) \, |\underline{u}_{if}|^2 \, hcV_{if} \, g(i)g(f)di \, df \qquad \text{(I-71)}$$

where g(i) and g(f) are the densities of the initial and final translational states, respectively. We now wish to transform to

the situation where we first integrate over E(i) for constant hcV = E(f) - E(i) = E(w) and then integrate over E(w) (c. f. Figure 7). The Jacobian for this transformation is 1 so that di df = di dw and we find that

$$\int_{w=0}^{\infty} \int_{i=0}^{\infty} (B_i - B_f) \left|\underline{u}_{if}\right|^2 hcV_{if}\, g(i)g(i+w)di\, dw \qquad \text{(I-72)}$$

is equivalent to equation (I-71).

We now recognize the integrand of the dw integral to be proportional to the probability that a translational transition of a given frequency will take place. Therefore, this integrand must be the frequency-dependent translational absorption coefficient. These quantities become for our three cases in the limit as v goes to infinity

$$\text{A.}\quad a_v = \frac{k}{2}\frac{\lambda^3}{Z^2} \int_{i=0}^{\infty} \sum (B_i - B_{i+w}) \left|\underline{u}_{i,\,i+w}\right|^2 h^2c^2 V g(i)g(i+w)di$$

$$\text{B.}\quad b'_v = k\frac{\lambda^3}{Z} \int_{i=0}^{\infty} \sum (B_i - B_{i+w}) \left|\underline{u}_{i,\,i+w}\right|^2 h^2c^2 V g(i)g(i+w)di \qquad \text{(I-73)}$$

$$\text{C.}\quad b_v = k\,\lambda^3 \int_{i=0}^{\infty} \sum (B_i - B_{i+w}) \left|\underline{u}_{i,\,i+w}\right|^2 h^2c^2 V g(i)g(i+w)di$$

where we have used the fact that dw stands for dE(w) = hc dV. The summations are over all the discrete states for which the total energy does not change during a translational absorption.

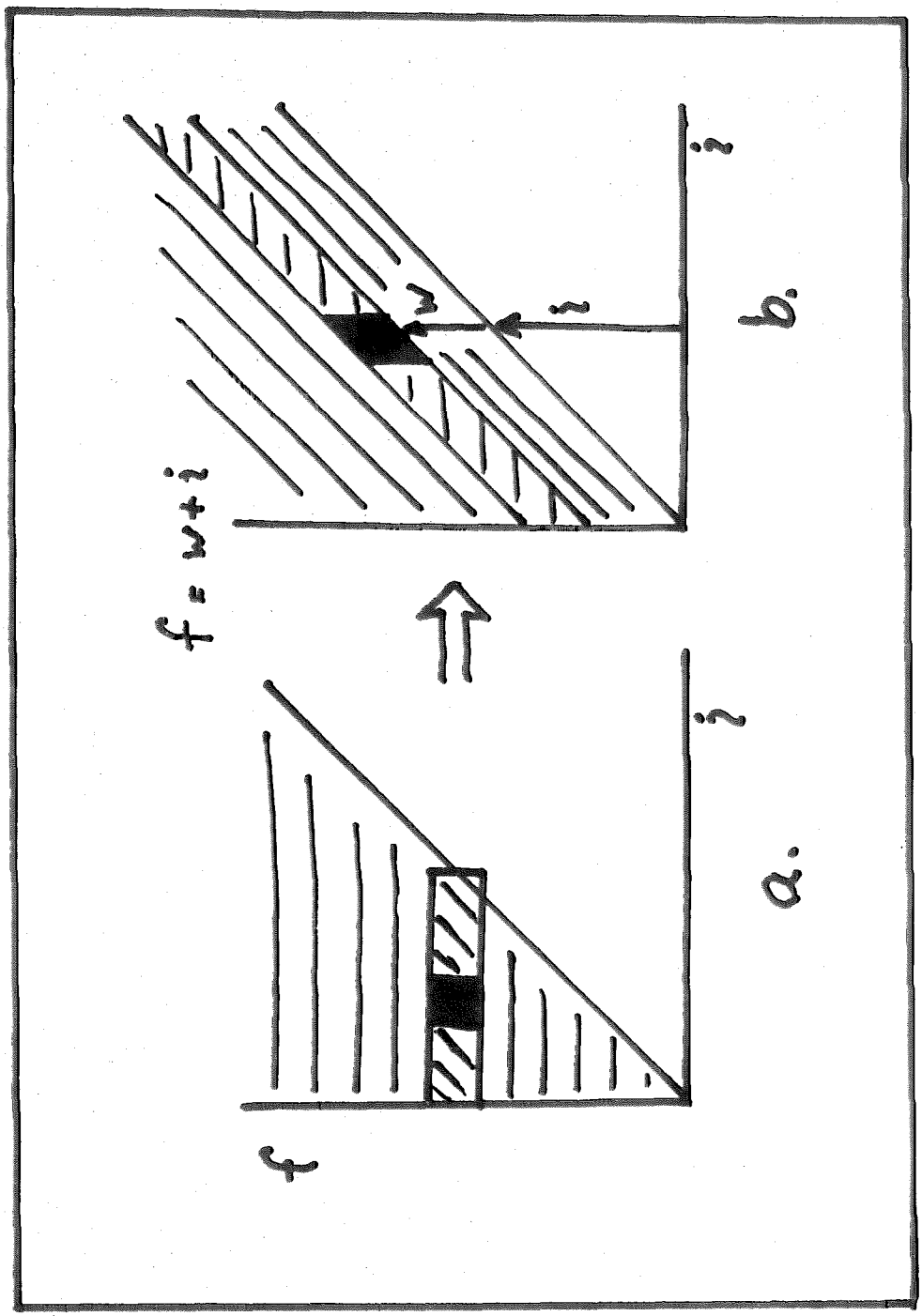


Figure 7. The Equivalence of the i-f and i-w integrations.

Now $B_i = \exp(-\beta E(i)) = \exp(-\beta E_t(i))\exp(-\beta E_r(i))$ where $E_r(i) = E_r(f)$. Then $B_i - B_f = \exp(-\beta E_t(i))(1 - \exp(-\beta E(w)))$ $\exp(-\beta E_r(i)) = B_i(\text{trans})B(\text{rot})(1 - \exp(-\beta hcV))$, giving rise to the familiar stimulated emission factor.

$$\text{A.} \quad B_i - B_f = \exp(-k^2/k_o^2)\, B(\text{rot})(1 - \exp(-\beta hcV))$$

$$\text{B.} \quad B_i - B_f = \exp(-k^2/k_o^2)\, B'(\text{rot})(1 - \exp(-\beta hcV)) \qquad \text{(I-74)}$$

$$\text{C.} \quad B_i - B_f = \exp(-k^2/k_o^2)\, (1 - \exp(-\beta hcV))$$

where $k = p/\hbar$, $k_o^2 = 8\pi^2 \mu kT/h^2$, $B(\text{rot}) = \exp(-\beta E(1)-\beta E(2))$ and $B'(\text{rot}) = \exp(-\beta E(1))$ where $E(i)$ now is the energy state of the $i^{th}$ diatomic molecule.

For the evaluation of $g(i)g(i+w)di$, it is convenient to transform from energy to momentum, or rather, wave number (k) space. Morse and Feshbach (1953) quote the expression for the total number of eigenvalues dn between k and k+dk in the case of the general Lioville equation:

$$dn \cong dk \left[ \frac{1}{\pi} \int_a^b \sqrt{\frac{r(z)}{p(z)}}\, dz \right] \qquad \text{(I-75)}$$

where a and b delineate the range of z and

$$\frac{d}{dz}\left(p(z)\, \frac{d\psi}{dz}\right) + \left\{k^2 r(z) + q(z)\right\} \psi = 0 \qquad \text{(I-76)}$$

is the corresponding Lioville equation. Applying equation (I-75) to the three-dimensional radial Schroedinger equation, we find $dn = dk\, R/\pi$ for $a = 0$ and $b = R$ as R goes to infinity. Now $g(i)di = di(dn/di) = dk(i)dn/dk(i) = dk(i)R/\pi$ so that

$$g(i)di = R\, dk(i)/\pi \tag{I-77}$$

and therefore

$$g(i+w) = \frac{R}{\pi}\, dk(i+w)/d(i+w) \quad . \tag{I-78}$$

Because

$$E = h^2k^2/8\pi^2\mu \, , \tag{I-79}$$

we have

$$g(i+w) = R\, 4\pi\mu/k(i+w) \, . \tag{I-80}$$

Using $E(i+w) = E(i) + E(w)$, we obtain

$$k(i+w) = \sqrt{k^2(i) + 8\pi^2\mu cV/h} \tag{I-81}$$

and finally

$$g(i)g(i+w)di = R^2\, \frac{1}{\pi h}\, \sqrt{\frac{2\mu}{hcV}}\, \frac{dk(i)}{\sqrt{1 + hk^2(i)/8\pi^2\mu cV}} \tag{I-82}$$

Inserting equations (I-74 and 82) in equations (I-73), we obtain

A. $$a_v = \frac{k'}{2}\, (1 - \exp(-\beta hcV))\, \sqrt{V}\ S_1(V, T)$$

$$B. \quad b'_\nu = k'(1 - \exp(-\beta hcV)) \sqrt{V}\ S_2(V, T)$$

$$C. \quad b_\nu = k'(1 - \exp(-\beta hcV)) \sqrt{V}\ S_3(V, T) \tag{I-83}$$

where

$$S_j(V, T) = \int_{k=o}^{\infty} \exp(-k^2/k_o^2) \left\{ \sum_{\substack{\text{ang.} \\ \text{mom.} \\ V, L'}} |Ru^{(j)}_{k, L}|^2 P^{(j)} \right\} \frac{dk}{\sqrt{1 + hk^2/8\pi^2 \mu cV}} \tag{I-84}$$

and

$$k' = 4\sqrt{\pi c}\, (h/\underline{k}T)^{3/2}/3\mu$$

and

$$P^{(i)}(j) = \begin{cases} Z^{-2} \exp(-\beta(E(j_1) + E(j_2))) & i = 1 \\ Z^{-1} \exp(-\beta E(j)) & i = 2 \\ 1 & i = 3 \end{cases} \tag{I-85}$$

where $E(j_i)$ is the $j^{th}$ rotational energy level of molecule i. The factor $1 - \exp(-\beta hcV)$ accounts for stimulated emission.

T is the local temperature, $\mu$ the reduced mass, c the speed of light, h Planck's constant, $\underline{k}$ Boltzmann's constant, Z the rotational partition function, V the frequency in wave numbers and the summation is carried out over all of the angular momentum states compatible with translational absorption. It remains to evaluate this sum in each case.

Because of the large amount of symbolism, we shall explain the matrix element expression. First of all, the wave functions $\Phi_s$ are normalized to unity in the volume v as it goes to infinity. This follows from the fact that the trace of $\bar{P}$ must be unity (where $\bar{P}$ is $\exp(-\beta H)/Z$). For central forces, $\Phi_s$ breaks up into the product of a radial and an angular eigenfunction. The radial eigenfunction is $X(r)/r$, where $X(r)$ is the solution of the one-dimentional Schroedinger equation

$$X''(r) + [k^2 - 2\mu U(r)/\hbar^2 - L(L+1)/r^2]X(r) = 0 \qquad \text{(I-86)}$$

where $k^2 = 2\mu E/\hbar^2$, E being the relative energy. The boundary conditions on X are that

$$\begin{aligned} X(0) &= 0 \\ X'(0) &= \text{is finite} \end{aligned} \qquad \text{(I-87)}$$

and $X(r)$ cannot increase faster than linearly with r as r goes to infinity. The asymptotic form of $X(r)$ for large R and r is

$$X_{kL} \to \sqrt{2/R}\ \sin(kr + \delta_L(k)) \qquad \text{(I-88)}$$

where $\delta_L(k)$ is the phase shift. The factor $R^{-1}$ arising in the corresponding matrix element cancels the factor of R in equation (I-84) so that we might as well have written this equation without this factor, if it is understood that the amplitude of the radial eigenfunction is to be normalized to $\sqrt{2}$ as r goes to infinity. This is the method we use to normalize the numerical solution for $X(r)$.

If we denote the angular eigenfunctions by $\psi$, the total wave function is

$$\Phi = \psi(\underline{\Omega})\, X(r)/r \tag{I-89}$$

where $\underline{\Omega}$ is the set of angular variables. In the Dirac notation,

$$|\underline{u}_{if}^{(j)}|^2 = |\langle f|\underline{u}^{(j)}|i\rangle|^2 \tag{I-90}$$

where the matrix element is given by

$$\langle f|\underline{u}^{(j)}|i\rangle = \int \psi^* \left[\int_{r=o}^{\infty} X^*_{k'L'}\, \underline{u}^{(j)} X_{kL}\, dr\right] \psi\, d\underline{\Omega} \tag{I-91}$$

where the limit as R goes to infinity has been taken.

We note the identity

$$|\langle f|\underline{u}|i\rangle|^2 = |\langle f|u_1|i\rangle|^2 + |\langle f|u_{-1}|i\rangle|^2 + |\langle f|u_o|i\rangle|^2 \tag{I-92}$$

where

$$\begin{aligned} u_1 &= (u_x + iu_y)/\sqrt{2} \\ u_{-1} &= (u_x - iu_y)/\sqrt{2} \\ u_o &= u_z \end{aligned} \tag{I-93}$$

are the spherical components of $\underline{u}$ and they form an irreducible tensor operator of rank one. The Wigner-Eckart theorem assures

us that the sum over the angular momentum states of equation (I-90) using equation (I-92) will take a particularly simple form.

In evaluating this sum, we expand the spherical components of $\underline{u}$, denoted by $u_v$, in terms of the complete set of angular eigenfunctions, $\psi(\underline{\Omega})$. For the case of diatomic molecules, it is necessary to couple three angular momenta. We do this by first coupling the two rotational angular momenta, denoted by the quantum numbers $J_1$ and $J_2$ to give $J_{12}$ and then couple $J_{12}$ with the orbital angular momentum L to give the total angular momentum J. The corresponding projections are $m_1$, $m_2$, $M_{12}$, $m_L$ and M, respectively. The $\psi$ are then related to the spherical harmonics Y(jm) by the following formula:

$$\psi(J_1J_2LJ_{12}JM) = \sum_{\substack{m_1m_2 \\ M_{12}m_L}} Y(J_1m_1)Y(J_2m_2)Y(Lm_L)\, C(J_1J_2J_{12};m_1m_2M_{12}) \cdot C(J_{12}LJ;M_{12}m_LM) \qquad \text{(I-94)}$$

where the C's are Clebsch-Gordan coefficients, described in Appendix D and the spherical harmonics are normalized such that

$$Y(jm;\theta,\Phi) = i^{|m|-m}\sqrt{\frac{(2j+1)}{4\pi}\frac{(j-|m|)!}{(j+|m|)!}}\, P_j^m(\cos\theta)\exp(im\theta) \qquad \text{(I-95)}$$

This is orthonormal with respect to both j and m.

At this point, we should point out the fact that because $H_2$ contains an even number of Fermions, the wave function $\psi$ should be symmetrical with respect to the interchange of the $H_2$ nuclei. This causes the normalization factor of $\psi$ to depend on the angular

momentum quantum numbers. For example, in the case of the He-He wave function, this factor vanishes when L is odd (Beth and Uhlenbeck 1937). We have ignored the symmetry properties of $\psi$ and have simply defined it by equation (I-94). We do this on the basis that the quantities that we are ultimately interested in are the summations over the angular momentum states of the square of the matrix elements, while at planetary temperatures, the L-dependence of these matrix elements for the important values of L is slowly varying (c.f. Figures 9-13). A rough estimate of the error may be obtained by summing over the even values of L, multiplying the result by two and comparing with the summation over all values of L. The slower the variation of the summands, the smaller the error and the closer the quasi-classical case. For $H_2$-He enhancement, we are less concerned with symmetry properties because the molecules involved are less similar and the mean molecular weight is greater. Therefore, the pseudo-classical approximation is better in this case.

We expand $u_v$ according to

$$u_v = \sqrt{\frac{64\pi^3}{3}} \sum_{y_1 y_2 WL} A(y_1 y_2 WL;r)\psi(y_1 y_2 LW1v) \qquad \text{(I-96)}$$

where the A's are fixed by the specific model for the induced dipole moment and will be discussed later.

We define

$$\langle A \rangle = \langle k'L' | A(y_1 y_2 WL'') | kL \rangle = \lim_{R\to\infty} \int_0^R RX^*_{k'L'}(r) \cdot A(y_1 y_2 WL'';r) X_{kL}(r) dr \; . \qquad \text{(I-97)}$$

We now take the matrix elements of equation (I-96), square and analytically sum over the initial and final angular momentum states with the Boltzmann weighting factor for the rotational states. In the course of this, the selection rules will be determined. We treat the general case of the diatomic molecule first and then simplify the results to apply to the cases of the diatomic-monatomic enhancement and the mixture of different monatomic gases. If these are designated cases A, B and C, respectively, then the reduction to case B is effected by setting $J_2 = 0$, $J_{12} = J_1$, $M_{12} = m_1$, $y_2 = 0$ and $W = y_1$. To reduce to case C, we also set $J_1 = m_1 = y_1 = 0$, $J = L$ and $M = m_L$.

Equations (I-94 and 96) are inserted in equation (I-91). The result is squared, weighted by the rotational Boltzmann factors and summed over all initial and final angular momentum states. The integrals over the spherical harmonics are evaluated analytically. This calculation is done in detail in Appendix E, giving

$$\sum_{k'L'} |R\, \underline{u}_{k\ L}|^2 P = \sum_{y_1 y_2 W L'' L L'} L_{L''}(L', L)\, |\langle k'L'|A(y_1 y_2 W L'')|kL\rangle|^2 \cdot \sum_{J_1 J_1' J_2 J_2'} P(J_1) P(J_2) L_{y_1}(J_1', J_1) L_{y_2}(J_2', J_2) \tag{I-98}$$

where the Racah coefficient $L_y(j', j) = (2j+1)\, |C(j, y, j'; 000)|^2$ is symmetric in j and j' and P(j) is the rotational Boltzmann factor.

At this point, it is necessary to distinguish between the three cases A, B and C in an important way. In case A, a double

rotational transition, where the rotational energy of the colliding diatomic molecules changes by equal but opposite amounts, contributes to the translational absorption. Therefore, translational absorption results only if there are no rotational transitions at all or a double transition occurs for which the initial level of one molecule is the final level of the other and no net change of rotational energy has occurred. The quantity on the left hand side of equation (I-98) then becomes:

$$\sum_{y_1 y_2 WL''LL'} L_{L''}(L', L)\,|\langle k'L'|A(y_1 y_2 WL'')|kL\rangle|^2 \cdot \sum_{J_1 J_2} P(J_1)P(J_2) \cdot \left\{L_{y_1}(J_1, J_1)L_{y_2}(J_2, J_2) + L_{y_1}(J_2, J_1)L_{y_2}(J_1, J_2)\right\} . \tag{I-99}$$

We follow Poll and Van Kranendonk (1961) by making use of the EXP-4 model for the induced dipole moment. They give the symmetry relations that $y_1 + y_2 + L + 1$ must be even and the triangular relations, $\Delta(y_1 y_2 W)$ and $\Delta(WL1)$ must hold. Also, if the colliding molecules are identical, we have the further symmetry relation that $A(y_1 y_2 WL) = (-1)^{W+1} A(y_2 y_1 WL)$. These relations give rise to the selection rules. We retain only the first few terms in the dipole moment expansion as the rest of them are negligible in comparison. For homopolar diatomic molecules, we retain the expressions (containing the constants for $H_2$):

$$A(2021) = -A(0221) = 0.820 \exp(-7.94\,x) \text{ e-Angstroms}$$
$$A(2023) = -A(0223) = 0.00260(189.2\exp(-7.94\,x) + 1.00/x^4) \text{ e-Angstroms} \tag{I-100}$$

where $x = r/\sigma$, e is the esu unit of charge. We insert these values and make use of the relations

$$\sum_{j'} L_y(j', j) = 2j + 1 \tag{I-101}$$

Note that $L_o(J_2, J_2) = 2J_2 + 1$ and $L_o(J_1, J_1) = 2J_1 + 1$, so we have

$$\sum_{J} P(J)\, L_o(J, J) = 1 \tag{I-102}$$

Summing over the J-states, we have

$$\mathcal{L}(T) \sum_{L\ L'} 2\left\{L_1(L', L)\,|\,\langle A(2021)\rangle\,|^2 + L_3(L', L)\,|\,\langle A(2023)\rangle\,|^2\right\}. \tag{I-103}$$

Where

$$\mathcal{L}(T) = \sum_{J} P(J) L_2(J, J) \tag{I-104}$$

and $L_2(J, J) = J(J+1)(2J+1)/(2J-1)(2J+3)$ so that $\mathcal{L}(T)$ is the same as given by equation (I-28). The selection rules are given by the factors $L_1(L', L)$ and $L_3(L', L)$ which are zero unless $L' = L \pm 1, \pm 3$. From the definition of $L_y$, we find the values of the statistical weights:

$$
\begin{aligned}
L_1(L+1, L) &= L+1 \\
L_1(L-1, L) &= L \\
L_3(L+3, L) &= \frac{5(L+1)(L+2)(L+3)}{2(2L+3)(2L+5)} \\
L_3(L+1, L) &= \frac{3L(L+1)(L+2)}{2(2L-1)(2L+5)} \\
L_3(L-1, L) &= \frac{3(L-1)L(L+1)}{2(2L-3)(2L+3)} \\
L_3(L-3, L) &= \frac{5(L-2)(L-1)L}{2(2L-3)(2L-1)} \quad .
\end{aligned}
\tag{I-105}
$$

Letting $B_i(kL;k'L') = |\langle k'L'|A(202i)|kL\rangle|^2$, we finally obtain

$$
\begin{aligned}
\sum_{k'L'} |R\, \underline{u}_{k\,L}|^2 P = 2\mathscr{L}(T) \sum_{L=o}^{\infty} \Big\{ & L\, B_1(kL;k', L-1) + (L+1)B_1(kL;k', L+1) \\
& + L_3(L-3, L)B_3(kL;k', L-3) + L_3(L-1, L)B_3(kL;k', L-1) \\
& + L_3(L+1, L)B_3(kL;k', L+1) + L_3(L+3, L)B_3(kL;k', L+3)\Big\}
\end{aligned}
\tag{I-106}
$$

(case A)

The value of k' is fixed by k and V. The above expression is for case A. To reduce to case B, we notice that for purely translational absorption, no rotational transitions at all are permitted in this case. Therefore, $J_2' = J_2$ and $J_1' = J_1$ must hold in equation (I-98). Noting that $L_o(0, 0) = 1$ and $P(J_2) = 1$ in this case we reduce equation (I-98) to

$$
\sum_{\substack{y \\ L\,L'}} \sum_{L''} L_{L''}(L', L) |\langle kL|A(y0yL'')|k'L'\rangle|^2 \sum_{J} P(J)\, L_y(J, J)
\tag{I-107}
$$

Introducing the EXP-4 model, the A(0001) term is now permitted since non-identical molecules are involved in the collision. Poll and Van Kranendonk (1961) then neglect the angle-dependent part of the overlap moment and take care of the quadrupolar induction by A(2023) = $\sqrt{3}\, Q_1\, \alpha_2\, r^{-4}$. Therefore, we obtain

$$\sum_{L,\,L'} \Big[ L_1(L', L)\, \bar{B}_1(kL;k'L') \cdot \sum_J P(J)(2J+1) + L_3(L', L)\, \bar{B}_3(kL;k'L') \cdot \sum_J P(J)\, L_2(J, J) \Big] \qquad \text{(I-108)}$$

where $\bar{B}_y$ corresponds to $B_y$ except that the A's for case B are used. Making use of equations (I-102 and 104), we obtain for case B:

$$\sum_{k'L'} |R\, \underline{u}_{k\,L}|^2 P = \sum_{L=0}^{\infty} \Big\{ L\, \bar{B}_1(kL;k', L-1) + (L+1)\, \bar{B}_1(kL;k', L+1) + \mathcal{L}(T) \big[ L_3(L-3, L)\bar{B}_3(kL;k', L-3) + L_3(L-1, L)\bar{B}_3(kL;k', L-1) + L_3(L+1, L)\bar{B}_3(kL;k', L+1) + L_3(L+3, L)\bar{B}_3(kL;k', L+3) \big] \Big\} . \qquad \text{(I-109)}$$

(case B)

In this case, A(0001) = $\xi_1 \exp(-x\sigma/\rho)$ and A(2023) is given above. Notice that $\mathcal{L}(T)$ does not affect the A(0001) term.

In the simplification to case C, the only non-vanishing coefficient is A(0001) = $\xi_2 \exp(-x\sigma/\rho)$. We set y = 0, L'' = 1 and J = 0 in equation (I-107) to obtain

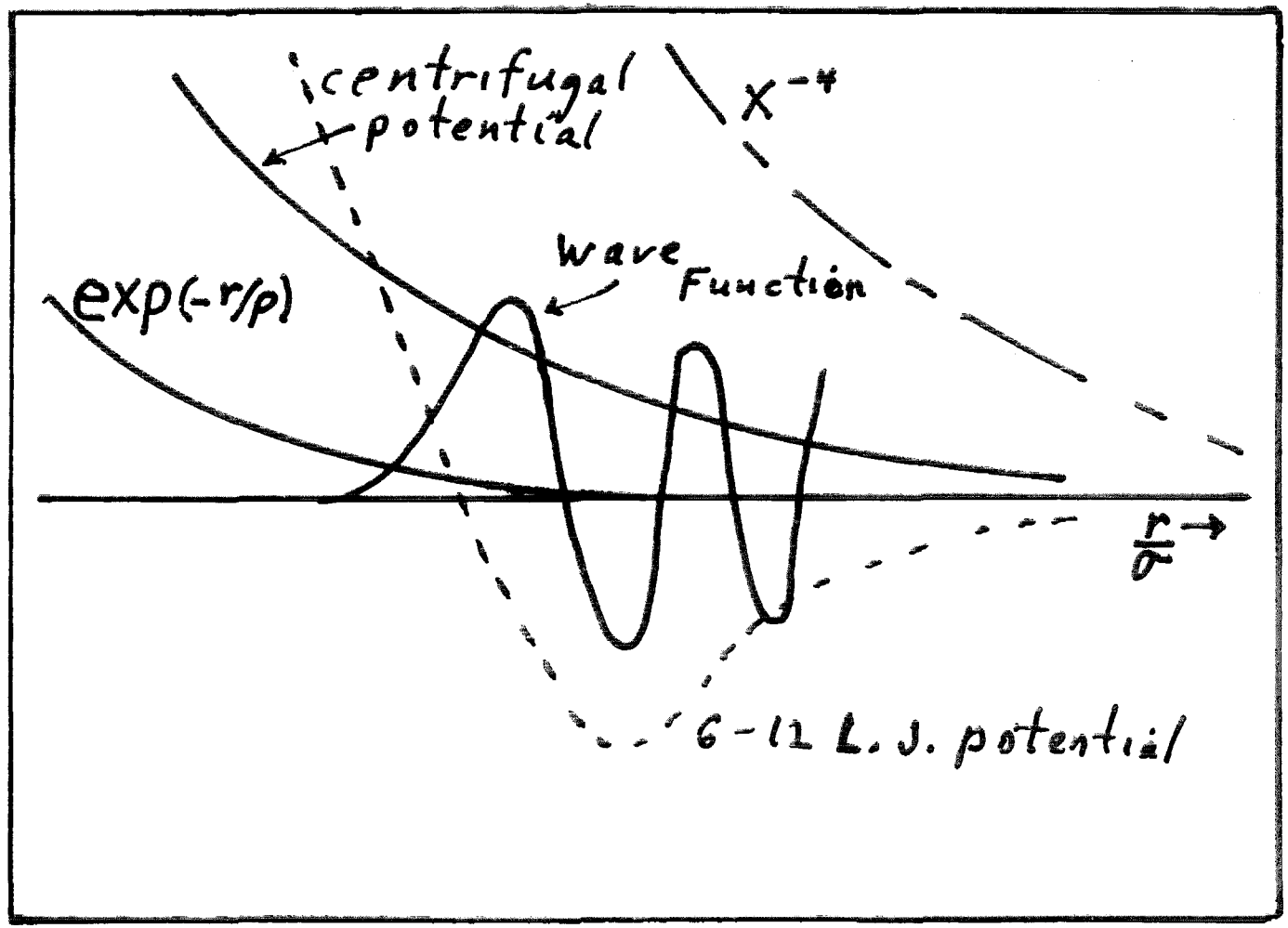


Figure 8. A schematic diagram showing the wave function and other fuctions to be considered in computing the matrix elements.

$$\sum_{L\,L'} L_1(L', L)\,|\,\langle kL|A(0001)|k'L'\rangle\,|^2 \qquad \text{(I-110)}$$

and this becomes

$$\sum_{L=o}^{\infty} [L|\,\langle kL|\,A(0001)|\,k', L-1\rangle\,|^2$$

$$\text{(case C)} \qquad + (L+1)|\,\langle kL|\,A(0001)|\,k', L+1\rangle\,|^2] \; . \qquad \text{(I-111)}$$

This expression is independent of the temperature. The actual temperature dependence of the absorption coefficient enters when we integrate over the translational states. The Boltzmann factor, $\exp(k^2/k_o^2)$, then governs the temperature dependence. Again, the value of k' is fixed by k and the frequency $V(cm^{-1})$.

This completes the analytical formulation of the problem. To obtain the translational absorption, it is necessary to numerically compute the radial matrix elements $B_y$ and $\bar{B}_y$. We then use equations (I-106, 109 or 111) with equations (I-83 and 84). The next section deals with the problem of the numerical computation of equations (I-106, 109 and 111).

## I-7. THE NUMERICAL COMPUTATION OF THE TRANSLATIONAL TRANSITION PROBABILITIES

This section explains the methods by which the translational matrix elements were numerically computed for the cases of $H_2$-$H_2$ and $H_2$-He pairs. Because of the large number of matrix elements needed, it was necessary to use efficient and sometimes original numerical techniques. As a result, a complicated but numerically fast IBM 7090-7094 electronic computer program was developed for accurately computing the summation over the orbital angular momentum states of the squares of the translational matrix elements.

### I-7. a. Starting the Solution of the Radial Schroedinger Equation

When we let $x = r/\sigma$, $t = \sigma k$ and denote the unnormalized form of $X(r)$ by $S(x)$, the one dimensional radial Schroedinger equation takes the dimensionless form

$$d^2S/dx^2 + [t^2 - a(x^{-12} - x^{-6}) - L(L+1)/x^2]\, S = 0 \qquad \text{(I-112)}$$

where we note that the origin is an irregular singular point and

$$a = 8\mu\epsilon\sigma^2/\hbar^2 \qquad \text{(I-113)}$$

and equals 52.73 for the $H_2$-$H_2$ case and 32.1 for the $H_2$-He case. $\epsilon$ and $\sigma$ are the Lennard-Jones parameters and $\mu$ is the reduced mass. The WKB solutions for small x are

$$S(1) = \frac{x^3}{a^{1/4}} \exp(-a^{1/2}/5x^5) \qquad \text{(I-114)}$$

$$S(2) = \frac{x^3}{a^{1/4}} \exp(+a^{1/2}/5x^5) \qquad \text{(I-115)}$$

and only the first one satisfies the boundary conditions.

Notice that we should not start the numerical solution at the origin because lnS and lnS' diverge to $-\infty$ there. Instead, we start the solution in the region x greater than 0.5 using the approximate WKB solutions for the initial values and the Runge-Kutta technique for the continuation. If the initial value of x is not too large, the error in S due to the approximate initial conditions will be rapidly damped out as we integrate in the direction of larger x in the non-oscillatory region. The reason for this is as follows: The approximate solution at the initial value of x is a linear combination of solutions which behave like S(1) and S(2). The coefficient of the latter must be very small since this solution goes very rapidly to infinity as x goes to zero. As x increases from this initial value, this latter solution decreases to the order of magnitude of the former so that the term containing this former solution is practically the entire contribution of the numerical solution. It was found by comparing numerical solutions of specific k and L values but different initial x values that the relative error in S and S' is less than $10^{-5}$ if we start the integration at a point for which S is less than $10^{-4}$ times its maximum value, or is less than $10^{-6}$ if S is less than $10^{-5}$ times its maximum value. At either point, the contribution of smaller x to the matrix elements is negligible.

We now explain how the initial value of x and the initial step size H was determined as a function of t and L for a tolerance of $10^{-5}$ in S and S'. Let

$$D(x) = t^2 - L(L+1)/x^2 - a(x^{-12} - x^{-6}) \ . \qquad \text{(I-116)}$$

When t or L is large enough so that the "a" term is negligible, the solution of the radial equation is approximated by the spherical Bessel function. This, in turn, is approximated by Carlini as (Watson 1944)

$$S(z) \sim \sqrt{\pi vz/2}\ |J_v(vz)| \leq \frac{z^{v+1}\exp(v\sqrt{1-z})/2}{(1-z^2)^{1/4}(1+\sqrt{1-z^2})^v} \qquad \text{(I-117)}$$

where z is less than 1. This is more accurate than the WKB approximation. We set this expression equal to $10^{-5}$ and solve for z by iteraction using Newton's method, z equals tx/v, where we approximated v by $\sqrt{L(L+1)}$ for convenience. This procedure is quite successful for producing the initial x when the Bessel approximation applies.

The initial step size need be found only roughly since the step size is tested during the Runge-Kutta integration. Nevertheless, Carlini's approximation is too crude to give an estimate of the step size in the Bessel case. From empirical calculations, it was found that the initial step size was given with sufficient accuracy for the Bessel approximation by

$$H = 0.291\, x/v - 0.086/t\,. \qquad \text{(I-118)}$$

This was obtained by fitting a linear curve in z to the empirical step sizes plotted as a function of z.

In the non-Bessel case, the Lennard-Jones term of equation (I-116) dominates. We distinguish two cases in this event: One is where the $ax^{-12}$ term dominates and the other is the transition case where it does not. We consider the former case and modify it later to accommodate the transition region. We use the WKB approximation to get

$$\frac{S(x)}{S(x_o)} \approx \left[\frac{x}{x_o}\right]^3 \exp\left[\frac{-a^{1/2}}{5}\,(x^{-5} - x_o^{-5})\right] \qquad \text{(I-119)}$$

where we let $x_o$ be the smallest root of $D(x) = 0$. Our criterion requires that this be set equal to $10^{-5}$. We then solve the resulting transcendental equation for x by iteration, giving

$$x = x_o\,[1 + x_o^{5}\, 5a^{-1/2}\,(3{\cdot}1\ln(x/x_o) + 11.5)]^{-1/5}. \qquad \text{(I-120)}$$

This converges without difficulty. In the transition region we find that the following expression fits:

$$x = x_o\,[1 + 5a^{-1/2}\,(3{\cdot}1\ln(x/x_o) + 12.4)]^{-1/5}\,. \qquad \text{(I-121)}$$

These expressions suffice except that for low t and L, it is necessary to change the constant 11.5 in equation (I-120) to 15.

The number of additional computations is not large in this case since the step size is large. For t less than 3, we use the initial values for t = 3. We obtain $x_o$ by Newton's method starting from $x_o = v/t$.

The step size for the first non-Bessel case, where the $ax^{-12}$ term dominates in D(x), is given by the criterion

$$\delta S/S \sim \text{constant} \tag{I-122}$$

where the variation is with respect to x. In other words,

$$H \propto S/S' \tag{I-123}$$

We compute S and S' from the WKB approximations and determine the constant of proportionality empirically. Thus,

$$H = 0.066x/(3 + 7.25/x^5) \tag{I-124}$$

where x is the initial value of x. This suffices for the desired accuracy of a factor of two or four in H. For the other non-Bessel case (the transition case) the Bessel step size suffices.

The second order differential equation for S may be written as a system of two simultaneous first order differential equations:

$$\begin{aligned} dW/dx + D(x)\, S &= 0 \\ dS/dx - W &= 0 \end{aligned} \tag{I-125}$$

where D(x) is given by equation (I-116). Once the initial values are known, we integrate this system by a modified Runge-Kutta scheme of order four. The general Runge-Kutta scheme, such as provided by Library routines, is numerically inefficient. An important simplification of the Runge-Kutta method occurs for the case

$$y'' = G(x, y, y') \tag{I-126}$$

and another simplification occurs when G is independent of y' (Hildebrand 1956). Such is our case. We find

$$\begin{aligned} S(n+1) &= S(n) + H\,W(n) + \frac{H}{6}\,(m(0) + (m(1)+m(2))) \\ W(n+1) &= W(n) + \frac{1}{6}\,(m(0) + 2(m(1)+m(2)) + m(3)) \end{aligned} \tag{I-127}$$

where

$$\begin{aligned} m(0) &= -H\,D(x)S(n) \\ m(1) &= -H\,D(x + H/2)(S(n) + \tfrac{1}{2}H\,W(n)) \\ m(2) &= -H\,D(x + H/2)(S(n) + \tfrac{1}{2}H\,W(n) + \tfrac{1}{4}H\,m(0)) \\ m(3) &= -H\,D(x + H)\,(S(n) + H\,W(n) + \tfrac{1}{2}H\,m(1))\ . \end{aligned} \tag{I-128}$$

This scheme was tested for the case where a = 0 in D(x). The resulting numerical solutions were compared with tables of spherical Bessel functions where these tables also provided the initial values. The agreement of these solutions with these

tables at all of the values of x, L and t examined, indicated that the program was correct. Replacing the correct value of "a" in D(x) then gave us the correct program for S(x).

After integrating six steps, the last values of S and W computed are recomputed using a double step. If the relative errors are both less than a tolerance of $10^{-6}$, then the step size is automatically doubled and the integration is continued. If not, then the last point is recomputed using a half-step with two cycles from the previous point. If any difference is greater than the tolerance, the step size is halved and the integration is continued. Otherwise, the same step size is used. The tolerance $10^{-6}$ controls the cumulative error accumulating over the 50 to about 300 steps to the matching point. The induced moment falls off as $x^{-4}$ so that the contribution to the error in the matrix element decreased as x increases beyond a certain point. The dominant error in S appears in the phase rather than the normalization so that the matching point may be at quite large x before the values of the matrix elements are affected significantly.

We compute the initial and final states simultaneously, so that the abscissa will match, making interpolation unnecessary in the matrix element integrations. The step size is fixed by the final solutions since they oscillate more rapidly. In general, there are four possible final states for each initial state. Simpson's rule is used to effect the integration of each of these matrix elements as soon as the ordinates have been computed by the Runge-Kutta scheme. We found that empirical calculations using just the $x^{-4}$ term of the induced moment (which always has a truncation error greater than the exp(-7.9x) term when Simpson's rule is used) that

a Simpson's rule step four times that of the Runge-Kutta step gave results similar to those when a Simpson's rule step equal to that of the Runge-Kutta integration was used. In this case, the integration error in a fixed interval is proportional to the fourth power of the step size. This indicates that the Simpson's rule step is not too large. To be safe, especially at low t, we used a step three times the size of the Runge-Kutta step. This amounts to about six intervals per semicycle of oscillation. The error is greatest for the low t and low $\Delta t$ solutions. Comparing the matrix elements with those calculated for a Runge-Kutta tolerance of $10^{-7}$ per step (instead of $10^{-6}$, which is the adopted value), we found a relative difference of less than $0.5 \times 10^{-4}$.

I-7. b. The Solution of the Radial Equation in the Oscillatory Region

If we were to simply integrate the wave functions by the Runge-Kutta method out to the point where the Bessel function approximation was valid, normalize and continue analytically, too many calculations would have to be made. The computing time would be prohibitively long and expensive and the accumulating round-off error makes the results only approximate. The reason for this is that the step size of the Runge-Kutta integration is restricted by the variation of S in the oscillatory region so that there are about 20 steps per semicycle for a relative error of $10^{-6}$ per step. The higher the value of t, the higher the frequency of oscillation of S in a given x interval and the smaller the step size. Only for the lowest t is the above scheme practical.

For these reasons, it was decided to use an entirely different method for solving the radial equation in the oscillatory region.

Since the amplitude of S is a much more slowly varying function of x than is S, we let the amplitude and the phase be the dependent variables. In this way, the oscillatory behavior is factored out as

$$S(x) = A(x) \exp\left[ i \int_a^x p(x)dx \right] \tag{I-129}$$

where A(x) is the amplitude and the integral is the phase difference between a and x. D(x) is positive in the oscillatory region. When we substitute this expression into the radial equation for S and separate the real and imaginary parts, we obtain

$$\begin{aligned} A'' - p^2 A + D\,A &= 0 \\ 2pA' + p'A &= 0 \end{aligned} \tag{I-130}$$

The last equation is separable and may be integrated directly, giving

$$p(x) = K/A^2(x) \tag{I-131}$$

where K is the constant of integration. We emphasize the fact that the phase is an integral function of the amplitude only. When equation (I-131) is substituted into the first of equations (I-130), we obtain the "amplitude equation":

$$A'' + D\,A - K^2/A^3 = 0 \tag{I-132}$$

which is a non-linear differential equation involving only the amplitude as the unknown and differing from the radial equation by the $K^2/A^3$ term. The above derivation was found in Modern Computing Methods (Teddington 1958).

Examining the amplitude of the WKB solution for large x, we note the boundary conditions:

$$\begin{aligned} A(\infty) &= \sqrt{2} \\ A'(\infty) &= 0 \end{aligned} \tag{I-133}$$

to give the proper normalization. Also, $A''(\infty) = 0$ asymptotically and D goes to $t^2$ so that the constant k is found to be

$$k = 2t \tag{I-134}$$

for positive phases. We thus obtain the explicit equations

$$S(x) = A(x) \sin\left[2t \int_c^x \frac{dx}{A^2(x)} + P(c)\right] \tag{I-135}$$

for x greater than c, where c is an arbitrary point on the x axis in the oscillatory region and P(c) is the phase at that point. The amplitude A(x) is the solution of

$$A''(x) + D(x)A(x) - 4t^2/A^3(x) = 0 \tag{I-136}$$

for which A' and A'' go to zero as x goes to infinity. It should be noted that equations (I-135) and (I-136) are valid for D(x) containing

potential functions different from the Lennard-Jones. We will postpone to later the discussion of a stable method for solving the tricky amplitude equation and now discuss the matching and normalization of the solutions.

Let x = c be the matching point. The integration up to c is accomplished by the Runge-Kutta technique described above. Then the solution in the oscillatory region is fixed by the boundary conditions at infinity and extended analytically by a power series solution of the amplitude equation down to a value of $x = x_f$ where the series begins to fail and is extended from $x_f$ to c by a numerical solution of equation (I-136). At the matching point c, the unknown constants P(c) and the normalization factor of S, which we denote by F, are evaluated by imposing the conditions of the continuity of the wave function and its slope at the matching point. When this is done, we find, at x = c;

$$P(c) = \tan^{-1}\left[\frac{2t}{(A^2)'/2 + A^2 W/S}\right] \qquad \text{(I-137)}$$

where we carefully note that the derivative $(A^2)'$ is with respect to d(-x) since we are proceding from infinity to x = c. To resolve the ambiguity of the branch of the $\tan^{-1}$, we note

$$\begin{aligned} 0 \leq P(c) \leq \pi \qquad & \text{if } S(c) \geq 0 \\ \pi < P(c) < 2\pi \qquad & \text{if } S(c) < 0 \end{aligned} \qquad \text{(I-138)}$$

and finally, at c,

$$F = S/A \sin P(c) . \qquad \text{(I-139)}$$

F loses some figures of accuracy if S is close to zero at the matching point. This can be avoided by not matching near a zero of S.

We now look at the asymptotic solutions of the amplitude equation. The first is the WKB solution, for which $A''(x) = 0$. This leads to

$$A(x) \tilde{=} [\, 4t^2 / D(x) \,]^{1/4} \qquad \text{(I-140)}$$

which is pretty good for larger t or x sufficiently larger than the zeros of D(x). However, the error is difficult to pin down quantitatively. For this reason, we constructed a power series expansion in $x^{-2}$ for A(x). This expansion is done for the case of the 6-12 Lennard-Jones potential in D(x). If $E = L(L+1)$ and M = the value of "a" of equation (I-113), we have

$$A(x) = \sqrt{2}\,[1 + a/x^2 + b/x^4 + c/x^6 + d/x^8 + \ldots] \qquad \text{(I-141)}$$

where

$$\begin{aligned} a &= E/K^2 \\ b &= E(5E - 12)/2K^4 \\ c &= (15\,E^3 - 148\,E^2 + 240\,E)/2K^6 - M/K^2 \\ d &= (42 - 5E)M/K^4 + (135E^4/4 - 656\,E^3 + 3969\,E^2 \\ &\quad - 5040\,E)/K^8 - (75E^4/8 - 45\,E^3 + 54\,E^2)/K^{10} \end{aligned} \qquad \text{(I-142)}$$

and for the phase, we find

$$P(x) = \int_{x_f}^{x} \frac{K}{A^2}\, dx + P(x_f) \tag{I-143}$$

so that

$$P(x) = P(x_f) + \frac{K}{2}\left[x - \alpha/x - \beta/3x^3 - \gamma/5x^5 - \delta/7x^7 - \ldots\right]\Big|_{x_f}^{x} \tag{I-144}$$

where

$$\begin{aligned}
\alpha &= -2E/K^2 \\
\beta &= 2E(6 - E)/K^4 \\
\gamma &= 2M/K^2 - 4(E^3 - 28\,E^2 + 60\,E)/K^6 \\
\delta &= 4M(E - 21)/K^4 + (-95\,E^4/4 + 850\,E^3 - 2868\,E^2 \\
&\quad + 10080\,E)/K^8 - (75\,E^4/4 - 90\,E^3 + 108\,E^2)/K^{10}.
\end{aligned} \tag{I-145}$$

We find $x = x_f$ by requiring the last term of the A(x) expansion to be equal to the desired error, which we took as $10^{-5}$.

At this point, we discuss the numerical solution of equation (I-136) in the range from $x_f$ to c. The boundary conditions are established at the point $x = x_f$ by means of the power series expansion for A(x).

If we try to solve the amplitude equation by the Runge-Kutta technique, the solution blows up no matter what the direction of integration. This is partially because an extraneous oscillatory solution exists with a very short period for high t requiring a

very small step size and partially because A'' is a fairly small quantity and is the difference of two large quantities which are nearly equal. Consequently, many significant figures are lost in computing A'' and the solution is unstable for any step size. Transforming equation (I-136) to an integral equation will get rid of the former difficulty because the boundary conditions are "built in", but we could find no way of efficiently coping with the latter difficulty by this approach. We finally found an iterative technique involving correction terms to the WKB solution which gives a rapid and satisfactory convergence. Because of the originality and utility of this method, we will derive it below:

Multiplying equation (I-136) through by 2A', we obtain

$$2A'A'' + 2AA'D - K^2 2A'/A^3 = 0 \qquad \text{(I-146)}$$

where K = 2t. This is

$$(A'^2)' + (A^2)'D + K^2(A^{-2})' = 0 \qquad \text{(I-147)}$$

or

$$\left[\frac{A^2A'^2 + K^2}{A^2}\right]' + A^{2'}D = 0 \qquad \text{(I-148)}$$

or

$$\left[\frac{(A^{2'}/2K)^2 + 1}{A^2}\right] + A^{2'}\,D/K^2 = 0 \qquad \text{(I-149)}$$

Letting

$$y = A^2$$
$$s = (y'/2K)^2 \qquad \text{(I-150)}$$
$$B = D/K^2$$

then

$$\left(\frac{1+s}{y}\right)' + y'B = 0. \qquad \text{(I-151)}$$

When s(x) is zero (identically), the WKB solution is obtained: $y = B^{-1/2}$. With this in mind, we carry out the differentiation of the left hand term and rearrange the terms and find that

$$\frac{1+s}{y^2} = B + 2\,\frac{s'}{(y^2)'} \qquad \text{(I-152)}$$

or

$$y = +\sqrt{\frac{1+s}{B + 2\,s'/(y^2)'}}\ . \qquad \text{(I-153)}$$

We now introduce the quantity

$$f = y\sqrt{B} \qquad \text{(I-154)}$$

which is 1 in the WKB approximation and is slowly varying in actuality, as long as x is significantly greater than the largest zero of B. Introducing the definition of s in equation (I-153), we have

$$y = \sqrt{\frac{1 + (y'/2K)^2}{B + y''/2K^2 y}} \tag{I-155}$$

where we could solve for y by iteration. However, we work with the better-behaved f:

$$\begin{aligned} y' &= f'/B^{1/2} - (f/2)B'/B^{3/2} \\ y'' &= f''/B^{1/2} - f'B'/B^{3/2} + (3B'^2/4B^2 - B''/2B)f/B^{1/2} \end{aligned} \tag{I-156}$$

and

$$f = \sqrt{\frac{1 + (y'/2K)^2}{1 + y''/2K^2 f B^{1/2}}} \tag{I-157}$$

Inserting equations (I-156) in (I-157), we obtain the iteration formula for f. We note that as f goes to 1, both f' and f'' go to zero. In the WKB approximation,

$$B'' = \frac{5\,B'^2}{4\,B} \quad \text{(WKB)} \tag{I-158}$$

and we make use of this relation to check that the denominator of equation (I-157) equals the numerator in the WKB case, so that f goes to 1 as it should.

Letting

$$R = B'/B = D'/D \tag{I-159}$$

we finally obtain the desired equation:

$$f = \left[ \frac{1 + (f' - fR/2)^2/4D}{1 + (2f''/f - 2Rf'/f + 3R^2/2 - D''/D)/4D} \right]^{1/2} \qquad \text{(I-160)}$$

which also holds for any likely intermolecular potential, U(r).

If we choose the WKB solution as the starting point of the iteration, the initial value of the function f(x) is then given by

$$f_i = \left[ \frac{1 + R^2/16D}{1 + (6R^2 - 4D''/D)/16D} \right]^{1/2} . \qquad \text{(I-161)}$$

Using equation (I-161), we compute f' and f'' by three point formulae:

$$f_1' = \frac{1}{2h}(f_{-1} - 4f_o + 3f_1) + \frac{h^2}{3} f'''(\xi)$$

$$f_1'' = \frac{1}{h^2}(f_{-1} - 2f_o + f_1) + h\, f'''(\xi) \qquad \text{(I-162)}$$

We then substitute these results in equation (I-160) to obtain the result for the first iteration. We do this for each point on a grid of equally spaced points between c and $x_f$, comparing the result with the previous result. If the difference is less than $10^{-5}$, the iteration is assumed to be complete at that point. The largest-x points are always the first to converge. The interval under treatment thus shrinks with each iteration cycle giving a rapid convergence with a minimum of unnecessary calculations. In our application, equation (I-161) is already so accurate that it gives the correct values of f to within this tolerance for about 80 per cent of the interval. More than two iterations are seldom required. The

last point to converge is the matching point, c. The number of iterations depends on the value of c. The matching point must be chosen at a value of x for which the wave function has already made several oscillations so that the third and fifth derivatives of f are not so large that the error terms in the numerical differentiation formulae are too big. For a fixed step size, equations (I-162) are the greatest source of error. Their error contribution exceeds that of matching (c. f. equation (I-163)) or of the Simpson's rule for the phase integrations. If c is too small, f may give the appearance of converging whereas the result may be in error by more than the desired tolerance. On the other hand, after several oscillations of the wave function, one iteration cycle usually suffices to obtain A(x) within the desired accuracy.

In matching, we make use of a five point formula for f':

$$f'_2 = \frac{1}{12h}(3f_{-2} - 16f_{-1} + 36f_o - 48f_1 + 25f_2) + \frac{h^4}{5} f^V(\xi) \qquad \text{(I-163)}$$

where h is the grid interval and $\xi$ lies in the corresponding interval. In general, we require that the error terms be limited and h large enough so that the amplitude method is more efficient than the Runge-Kutta scheme. This puts an upper limit on the derivatives of f and hence, a lower limit on the value of the matching point. We found no way of estimating the values of f''' and $f^V$ except by numerical differencing techniques on solutions computed for various matching points. This, in effect, is the basis of our error determination and quoted tolerances.

I-7. c. Integration Schemes For the Matrix Element Computation

We now discuss the computation of the matrix elements. The dipole moment consists of two functional parts. The quadrupolar induction part behaves like $x^{-4}$ while the overlap part varies like exp(-7. 94x). As soon as both the initial and final states take on significant values, the computation of the matrix elements begins. The corresponding analytic expressions are

$$\int_{x'}^{c} S(t', L')\exp(-7.94x)S(t, L)dx$$

$$\int_{x'}^{c} S(t', L')\, x^{-4}\, S(t, L)dx \qquad \text{(I-164)}$$

where x' is the value of x where we may no longer neglect the contribution to the matrix element. t' and L' are the final states and t and L are the initial states. These integrals are computed in this fashion by Simpson's rule up to the matching point. They are normalized after the matching has been accomplished. The constants of proportionality are not added until the summation over L has been effected.

In order to save computing time, it is necessary to stop the relatively inefficient Runge-Kutta process as soon as possible and transfer to the amplitude-phase iteration procedure. However, it was decided to continue the Runge-Kutta process until the contributions to the overlap matrix element became negligible. For safety, this was taken to be the point x = 2. 2. If the matching point c was greater than this value, the Runge-Kutta process was

continued to x = c. Because the $x^{-4}$ integrands fall off slowly, we must take the higher-x contributions into account. Because the amplitude varies more slowly than the wave function, the numerical solution of the amplitude can take place at a much larger step size for the higher t. However, the matrix elements involve the rapidly oscillating wave functions so the advantage is lost unless a method more suitable than direct quadrature is employed for the integration. We now introduce such a method:

In the amplitude-phase region, the relevant matrix element contribution is

$$M = \int_c^{x_f} S' \, x^{-4} \, S \, dx \qquad \text{(I-165)}$$

where S' denotes the final state wave function. This expression becomes

$$M = \int_c^{x_f} \frac{dx}{X^4} AA' \sin P \sin P' \qquad \text{(I-166)}$$

where P and P' are the phases. The rapid variation comes from the sinP sinP' factor. From a trigonometric identity, we obtain

$$M = 1/2 \int_c^{x_f} dx \, x^{-4} \, AA' \cos(P-P') - 1/2 \int_c^{x_f} dx \, x^{-4} \, AA' \cos(P+P') \qquad \text{(I-167)}$$

The first integral now has a more slowly oscillating integrand and may be integrated by Simpson's rule with little error except when $|P-P'|$ is large. The second integral has an even faster oscillating integrand. We propose the following evaluation of this

integral: (1) Let $z = P+P'$ be the independent variable. (2) Fit a quadratic polynomial in z to $AA'x^{-4}dx/dz$ in each pair of unequally spaced intervals of z into which $(z(c), z(x_f))$ is divided. (3) Integrate analytically

$$\int_{z_1}^{z_2} z^n \cos(z)dz \qquad n = 0, 1, 2. \tag{I-168}$$

(4) Finally, evaluate the coefficients of the integrals in equation (I-168) in terms of A, A' and x. We find that

$$dx/dz = K/A^2(z) + K'/A'^2(z) \tag{I-169}$$

Let the two integrals in equation (I-167) be denoted by Q and R, respectively. Let $\Delta R$ be the contribution to R of a pair of equally spaced intervals in x. If these corresponding intervals in z are called $h_1$ and $h_2$ so that

$$\begin{aligned} h_1 &= z_o - z_{-1} \\ h_2 &= z_1 - z_o \end{aligned} \tag{I-170}$$

for $z_1$ greater than $z_o$ and $z_o$ greater than $z_{-1}$, we have

$$\Delta R = 2a\,[h_2 \cos z_1 - \sin z_1 + h_1 \cos z_{-1} + \sin z_{-1} + 0.5(h_2^2 \sin z_1 - h_1^2 \sin z_{-1})] + b\,[\cos z_1 + h_2 \sin z_1 - \cos z_{-1} + h_1 \sin z_{-1}] + c\,[\sin z_1 - \sin z_{-1}] \tag{I-171}$$

where

$$a = \frac{E_1 + E_2}{h_1 + h_2}$$

$$b = \frac{h_1 E_1 + h_2 E_2}{h_1 + h_2} \qquad \text{(I-172)}$$

$$c = P_o$$

and where

$$E_1 = (P_1 - P_o)/h_2$$

$$E_2 = (P_o - P_{-1})/h_1 \qquad \text{(I-173)}$$

and

$$P(z) = \frac{A\,A'}{2x^{-4}(K/A^2 + K'/A'^2)} \qquad \text{(I-174)}$$

is computed numerically. This scheme was checked by planimeter.

In fitting the parabola to equation (I-174), the error is, after integrating, like that for Simpson's rule. For a tolerance of $10^{-6}$, this implied a step size roughly like $0.1\,x^{8/5}$. For safety, we used

$$h = .037\,x^{8/5} \qquad \text{(I-175)}$$

and when this exceeded an even multiple of the grid step size, the step for the quadrature of Q and R was increased accordingly. We add up all the $\Delta R$ to get R and then compute

$$M = Q - R. \tag{I-176}$$

From empirical calculations, we found an approximate formula for the grid step size containing the adjustable parameter p:

$$h = p \times (2tx/L)^{0.4} \tag{I-177}$$

where p varies between 0.01 and 0.07 depending on t and the matching point. The ultimate check in the step sizes is the separate computation of matrix elements, varying the step sizes and comparing the results. The error of a given step size or set of parameters is determined by comparing its result with the asymptotic results of the smaller step sizes. This is a successful procedure provided that the step sizes are not so small that the round-off error begins to dominate.

We finally explain the calculation of the contribution of the values of x between $x_f$ and $\infty$ to the matrix element. The integrand is known analytically in this region but there is no simple expression for the integral. We therefore make an asymptotic expansion, starting from equation (I-167). The power series expansion of the phase is used to compute P-P' as a function of x. The terms of order $x^{-5}$ in this expansion are neglected. This is the criterion for fixing the position of $x_f$. The cos(P-P') term is expanded as

$$\cos(P-P') = \cos\alpha \cos y - \sin\alpha \sin y \tag{I-178}$$

where $\alpha$ contains only positive powers of x and y contains only negative powers. Cos y and sin y are expanded as far as $0(x^8)$. $AA'/2x^4$ also is expanded in powers of $x^{-2}$ and is multiplied by the cos(P-P') series. We then get

$$Q = \int_{x_f}^{\infty} (1/x^4 - G_6/x^6 + G_8/x^8 + \ldots)\cos\alpha(x)dx$$
$$- \int_{x_f}^{\infty} (G_5/x^5 - G_7/x^7 + G_9/x^9 + \ldots)\sin\alpha(x)dx \ . \qquad \text{(I-179)}$$

The odd powers of 1/x are eliminated by integrating by parts and the even powers are evaluated by a fairly rapid asymptotic expansion derived by us in Appendix F and based on an idea obtained from G. Blanch's fast asymptotic expansion for the exponential integrals (1946).

In the R integral, we set $z = \Delta(P+P')/(t+t')$ as the independent variable, where $\Delta(P+P')$ is the phase difference between $x_f$ and x. This z series is inverted to give x(z). The quantity dx/dz is found by directly differentiating the x(z) series term by term. We then obtain the z-series for $(AA'/x^{-4}(z))(dx/dz)$. The result is that we obtain an expression of the form

$$R = \int_{z(x_f)}^{\infty} (1/z^4 + H_1/z^6 + H_2/z^8 + \ldots)\cos(az + b)\, dz \qquad \text{(I-180)}$$

which we evaluate by the same asymptotic expansion used for the Q integral. The final contribution is

$$T = Q - R \qquad \text{(I-181)}$$

The value of R must be less than $2/3(x_f)^3$.

Several matrix elements were computed varying the value of $x_f$ in each. The results appeared to be independent of the value of $x_f$ so long as it was above its minimum allowed value and not so large that round-off error was important. This is our final check on this part of the program.

I-7. d. The Summation Over the Orbital Angular Momentum States

As the initial orbital angular momentum of a matrix element of fixed t and t' is varied, the matrix element typically goes through a maximum and then begins to decrease more and more exponentially, giving a straight line on a semi-log plot of the high L values (see Figures 9 to 13). For this reason, after each matrix element is calculated (taking about a quarter of a second execution time), the value of the next one is predicted by extrapolation in the logarithm. Also, the present value is compared with the previous prediction. If the error is less than $5 \times 10^{-4}$, the step in L is doubled and the omitted matrix elements are computed by logarithmic interpolation. In this way, much computing time is saved, especially in the cases where the sum extends up to L over 100. In addition, the summation is halted whenever the contribution becomes negligible with respect to the current value of the sum.

We emphasize that these summations are molecular quantities and are computed once and for all for the adopted grid of parameters and tolerance. As far as the numerical accuracy goes, they should be accurate to about a tenth of a percent or better.

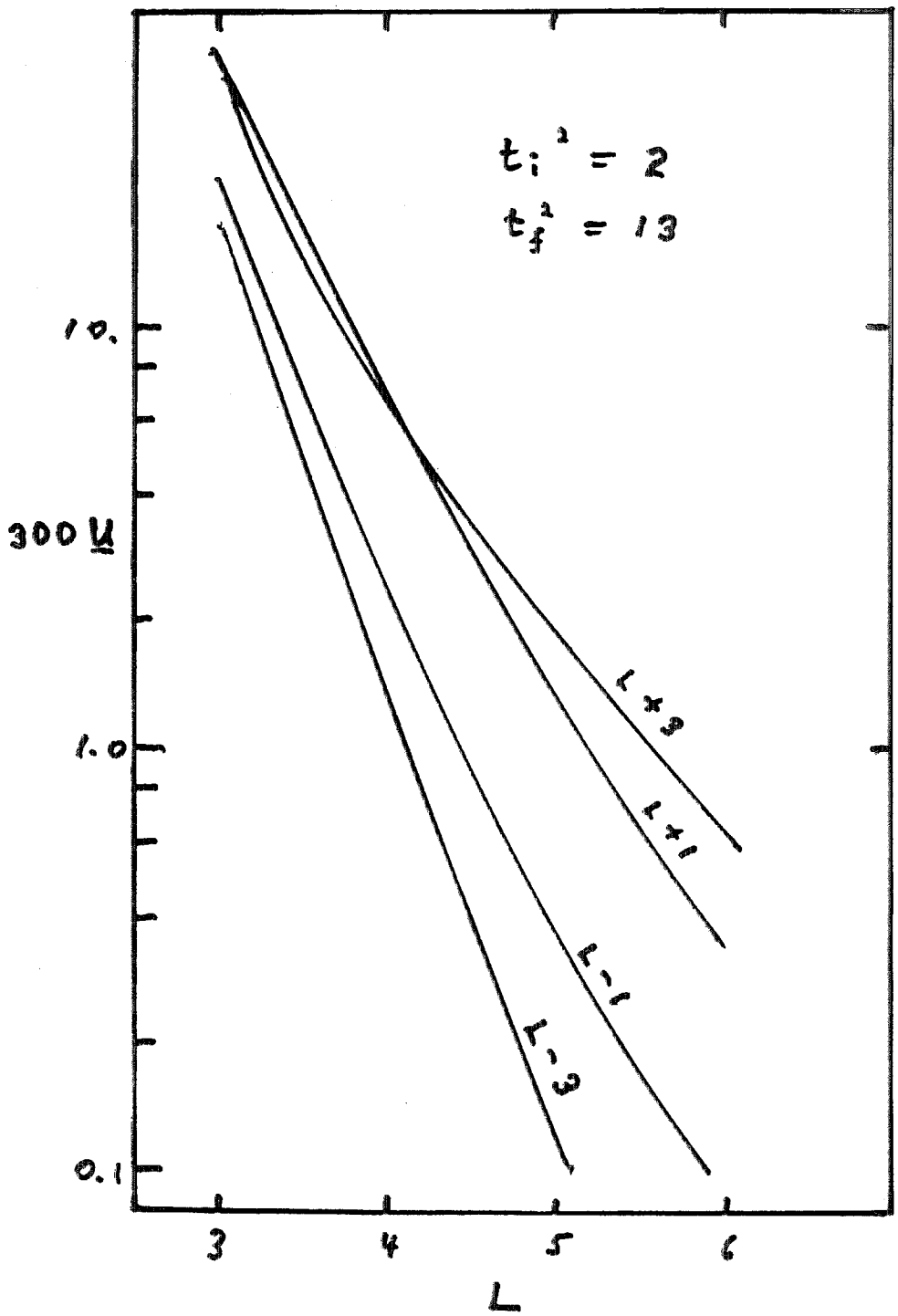


FIG. 9

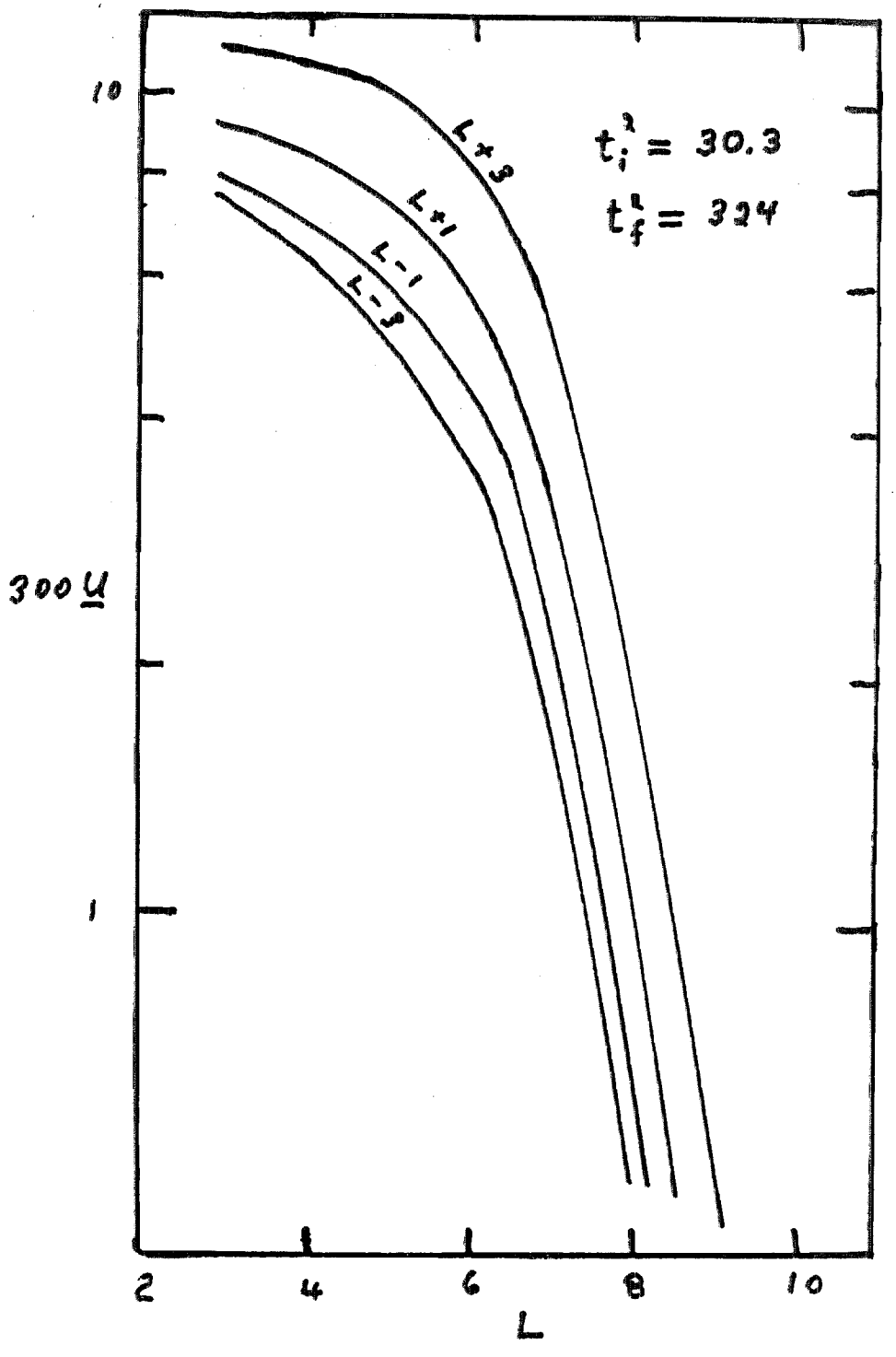


FIG. 10

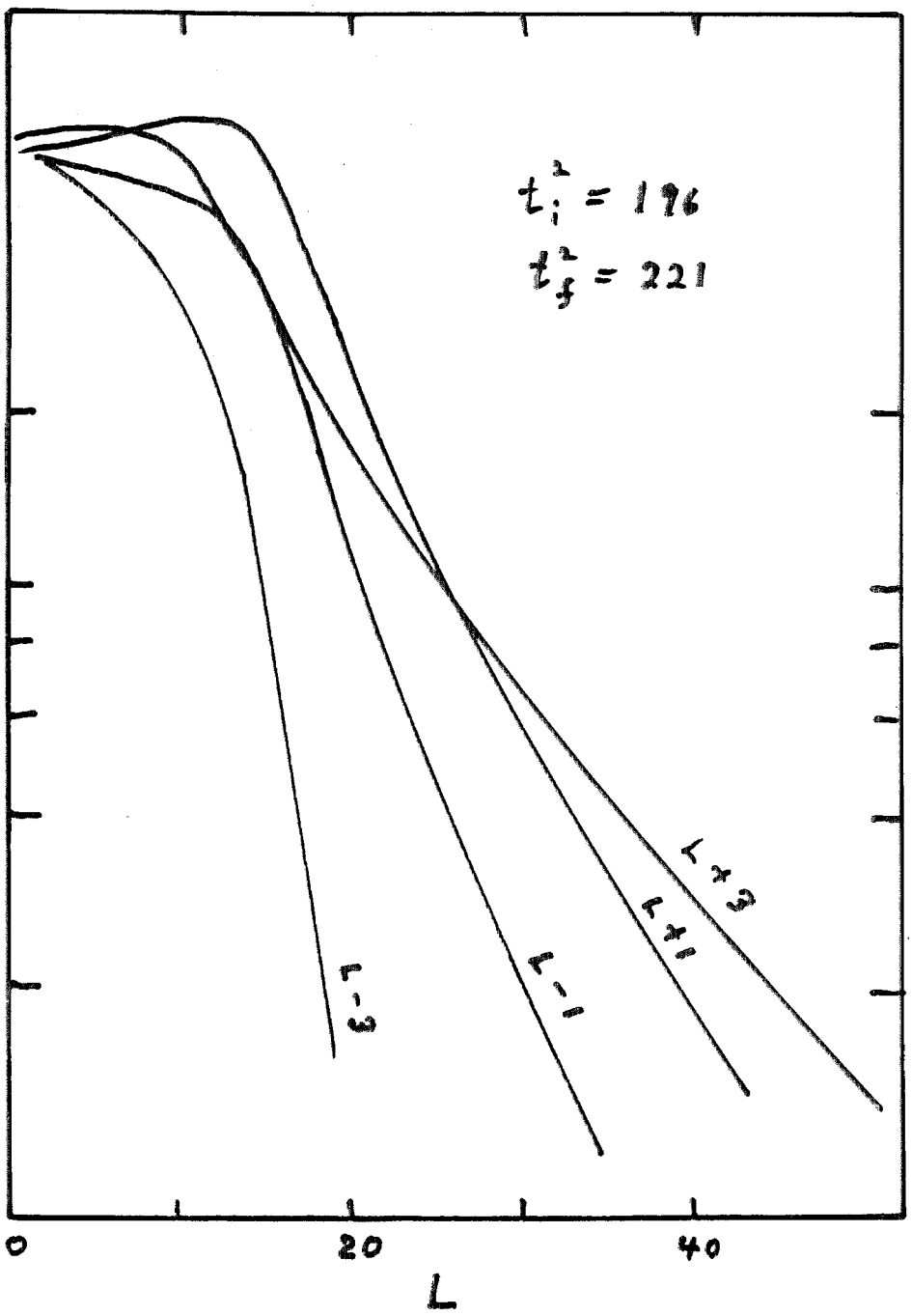


FIG. 11

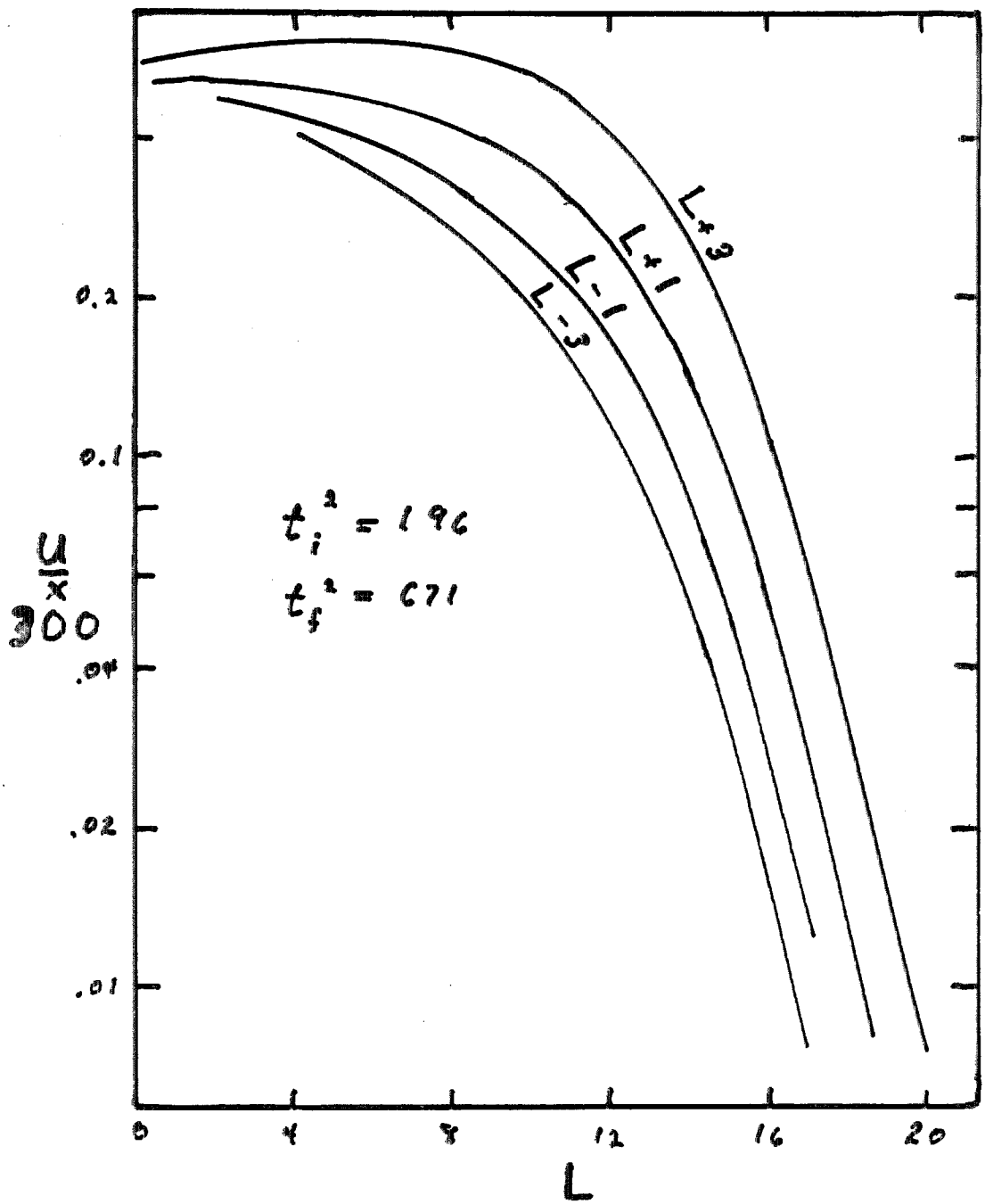


Fig. 12

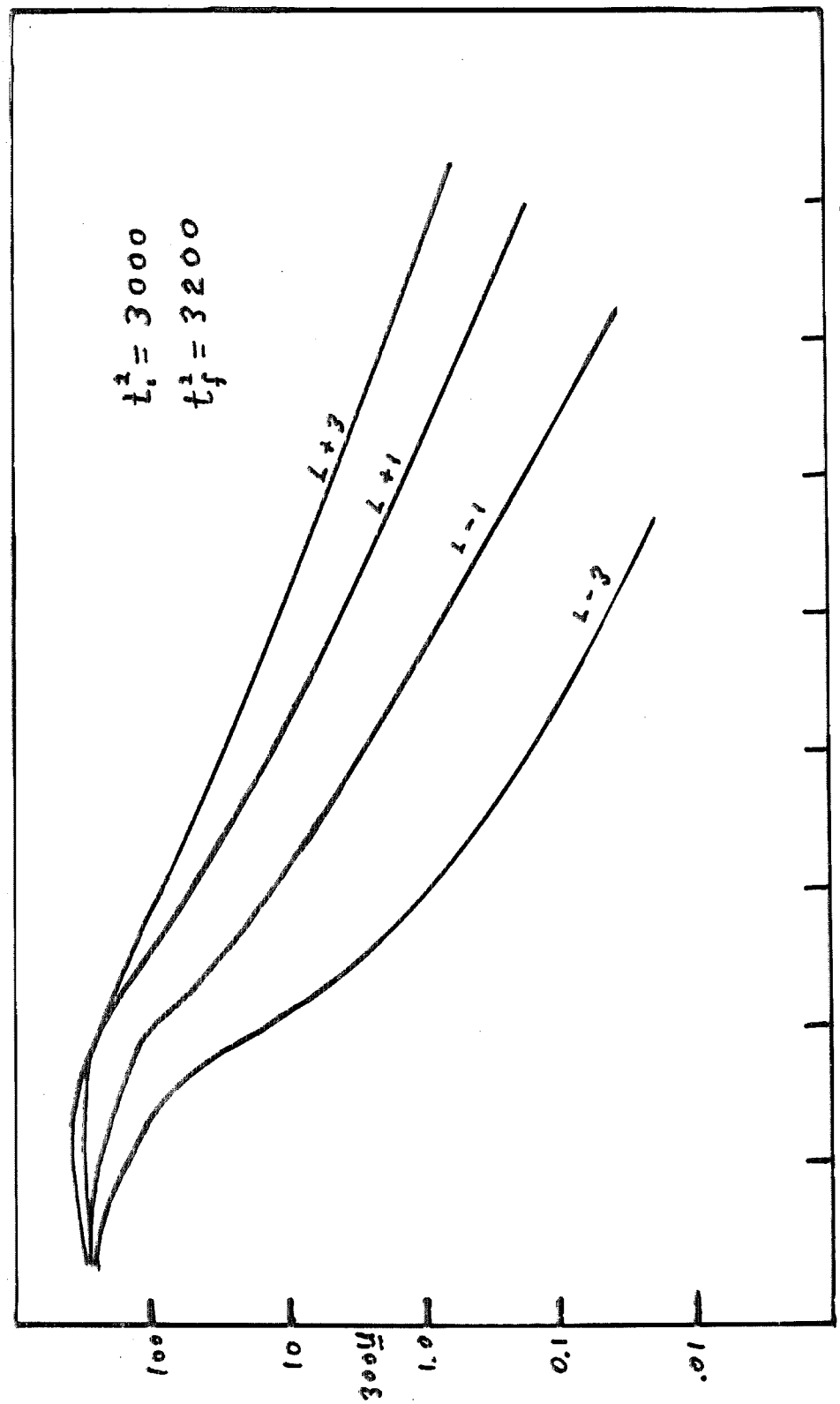
$t_i^2 = 3000$
$t_f^2 = 3200$
L+3
L+1
L-1
L-3
100
10
3000/L
1.0
0.1
.01
50
100
150
200
L

FiG. 13

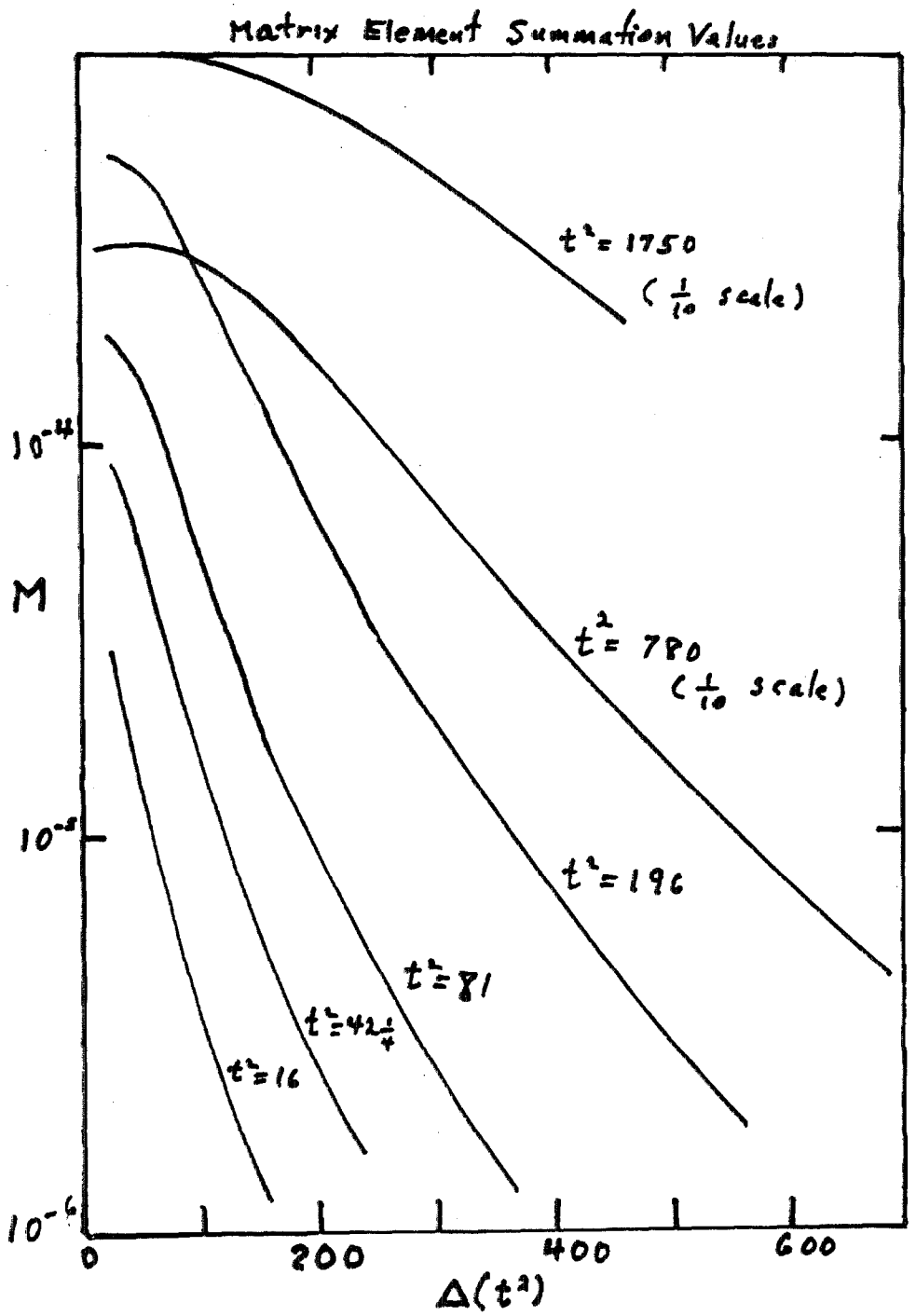
Matrix Element Summation Values
$t^2 = 1750$
($\frac{1}{10}$ scale)
$t^2 = 780$
($\frac{1}{10}$ scale)
$t^2 = 196$
$t^2 = 81$
$t^2 = 42\frac{1}{4}$
$t^2 = 16$
$10^{-4}$
M
$10^{-5}$
$10^{-6}$
0
200
400
600
$\Delta(t^2)$

Fig. 14

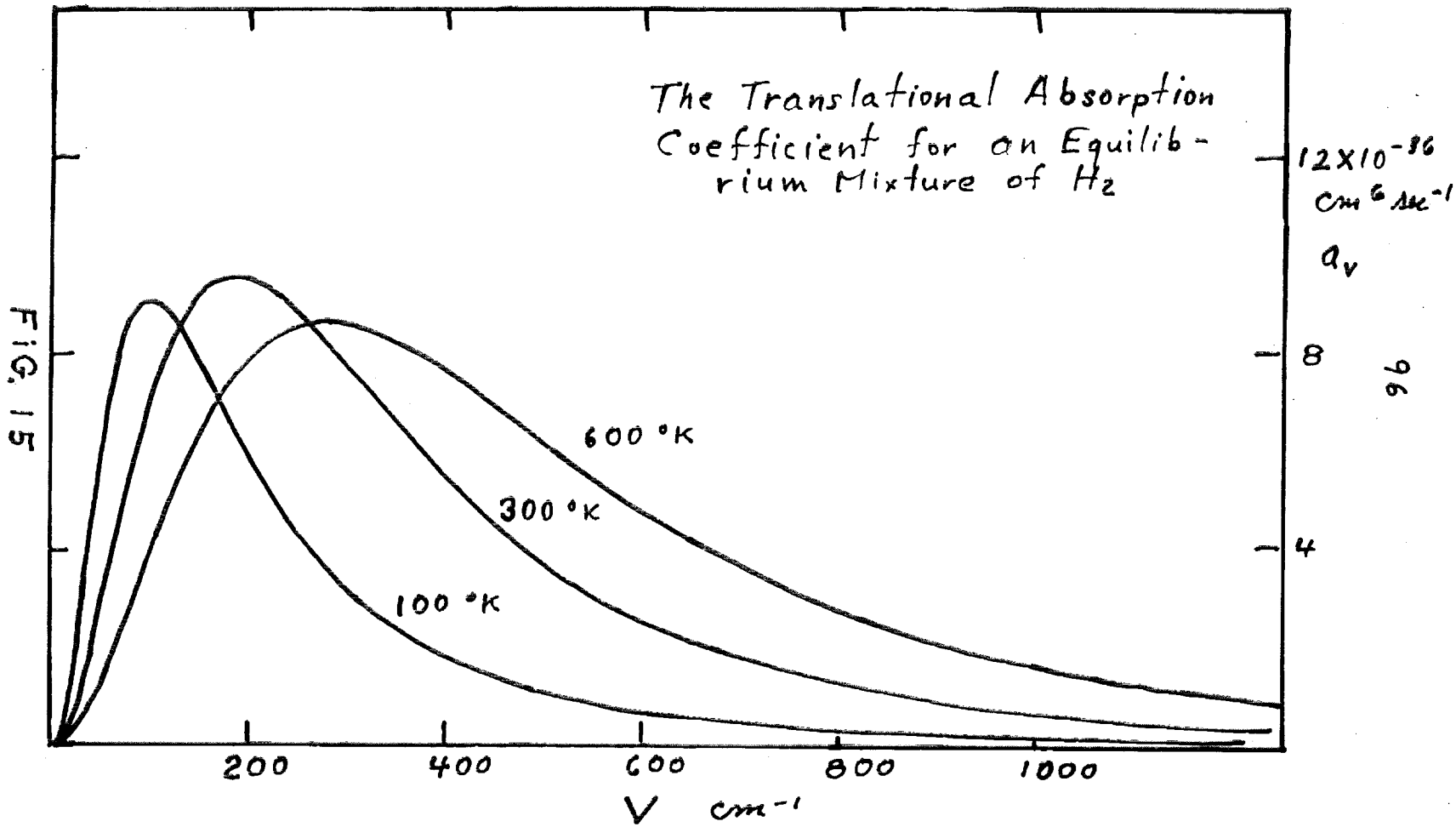
The Translational Absorption Coefficient for an Equilibrium Mixture of $H_2$
$12 \times 10^{-36}$ cm$^6$ sec$^{-1}$
$a_v$
8
4
96
600 °K
300 °K
100 °K
200
400
600
800
1000
V cm$^{-1}$

FIG. 15

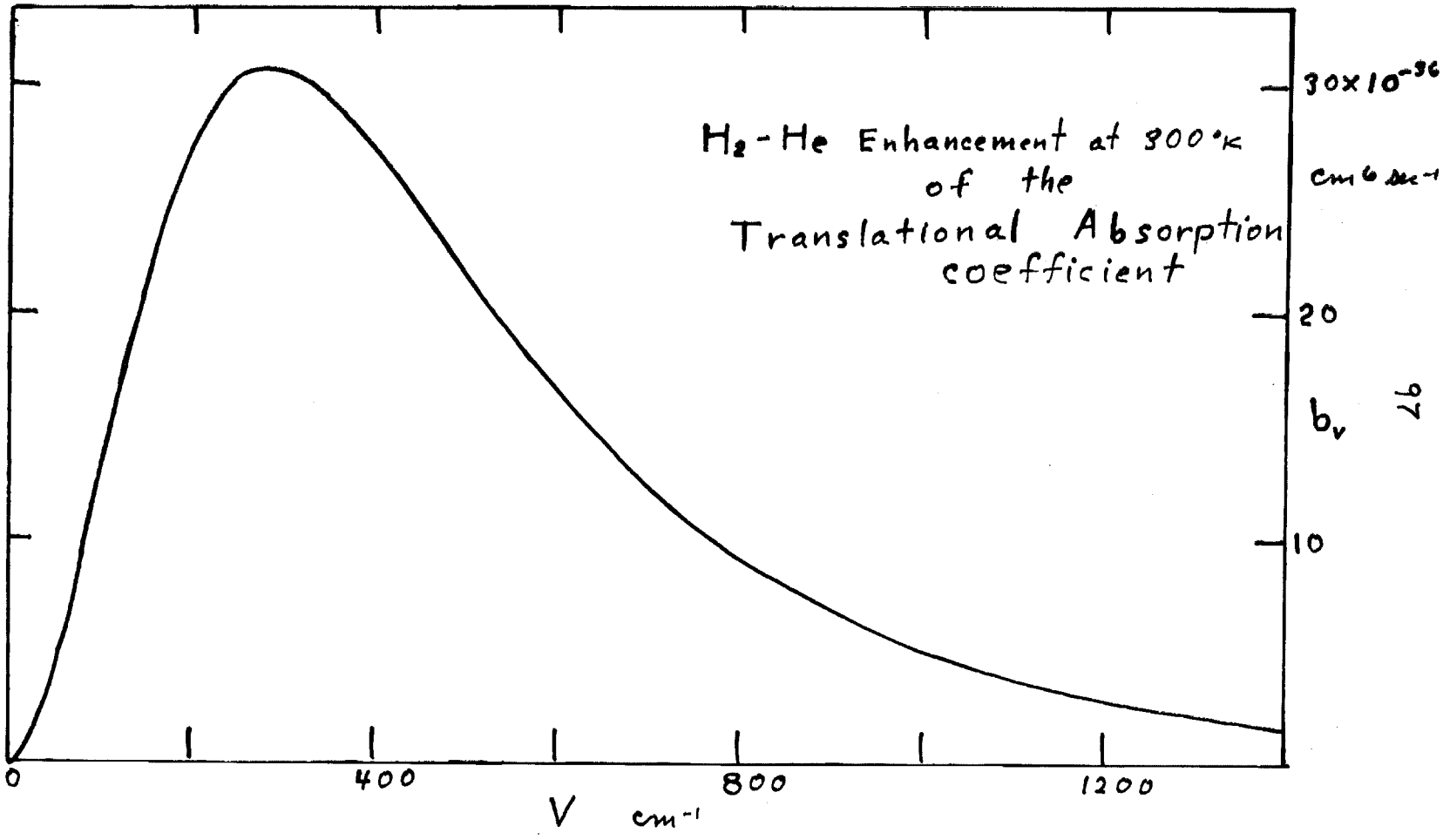
$H_2$-He Enhancement at 300°K
of the
Translational Absorption
coefficient
$30 \times 10^{-36}$
cm⁶ sec⁻¹
20
10
$b_\nu$
97
0
400
800
1200
V cm⁻¹

FIG. 16

If we interpolate among these values to get the sums at other frequencies and t-values, those sums will be less accurate due to the truncation error of the interpolating process. Final checks by comparing the integrated absorption from interpolated values with the formulae of section I-4 for different temperatures, indicate an overall accuracy of 1 per cent or better, as far as the numerical process is concerned(1). The actual error may be greater due to uncertainties in the values of the physical constants of the problem, particularly those for the $H_2$-He collisions. In addition, certain physical assumptions have been made along the way in obtaining a formula for the translational absorption. These will also affect the accuracy of the results.

We mention that in the $H_2$-He case, we computed the summations for only the angle independent term (which is 98 per cent of the entire absorption). Therefore, only the overlap matrix elements were computed in this case. It was unnecessary to use any process other than Simpson's rule for the matrix element integration because the induced moment dies off quite rapidly with increasing x. However, the same program was used to compute these quantities but the constants were changed and only two final states were necessary for each initial state.

(1) In the $H_2$-$H_2$ case, the tail was extrapolated and the profiles were integrated over frequency. The results at 600 $^{o}$K, 300 $^{o}$K and 100 $^{o}$K were compared with those obtained from equation (I-27). The relative errors were 0.5, 1.2 and 3 per cent, respectively. This agreement is an independent check on the calculations of sections I-6 and I-7. We expect the error to increase as the temperature decreases because equation (I-27) was computed using only the first quantum correction term. Therefore, we may rest assured that no significant computational error has been made in the calculation of the translational absorption coefficient.

The sums given by equation (I-106) and the temperature-independent part of equation (I-109) are tabulated in Appendix G for the $H_2$-$H_2$ and $H_2$-He cases, respectively. Note that for a fixed frequency, the higher-t values are approximately proportional to a power of t. The frequency dependence for various values of t is illustrated by Figure 14. Figures 15 and 16 give the resulting translational absorption profiles.

## I-8. THE THERMAL OPACITY OF $NH_3$

Laboratory measurements of the 10 μ band of $NH_3$ (Mould, Price and Wilkinson 1959), the 10 μ and 16 μ bands (Garing, Nielsen and Rao 1959) and the rotational lines (Loewenstein 1960; Hadni 1957; McCubbin and Sinton 1950; Foley and Randall 1941; Barnes 1935; Wright and Randall 1933; and Cartwright 1929) show that the $NH_3$ spectrum is scattered throughout the thermal region of the spectrum. They also show that the self-absorption is quite strong in the centers of the individual lines. That is, the lines become saturated in path lengths on the order of several cm through pure $NH_3$ at STP. As we observe about 700 cm of $NH_3$ at STP in the Jovian atmosphere (Kuiper 1952), we should make an estimate of the importance of $NH_3$ in governing the thermal equilibrium. In this connection, we consider the mean transmission of a sample of $NH_3$ over a frequency interval containing many lines but for which the planck function does not change very much. Even though the sample becomes opaque at frequencies in the centers of the lines, the mean transmission can still be quite high due to the fact that most of the radiation is being transmitted between the lines. However, as the pressure is raised and the path length is increased, even the absorption between the

lines becomes strong because of the fact that each line has a frequency tail of indefinite extent. The transmission of an $NH_3$ band is therefore quite sensitive to the shape of the line profiles in the extreme wings, the variation of this shape with temperature and pressure, and the relative positions of the lines. The fact is, that insufficient experimental data is available to give a reliable curve of growth for a band of $NH_3$ lines. We can proceed only by making certain dubious assumptions. One of these assumptions is that the shape of the wings is given by the Lorentz profile (the Doppler broadening being negligible). Goody (1964) points out that we are completely reliant on the observations for the shape of the wings since the theory indicates that this shape depends somewhat delicately on the statistics and the actual type of molecular interaction involved. For example, the R(0) wing of HC1 is found to vary as $(\nu-\nu_o)^{-1.73}$ whereas the self-broadened lines of the 4.3 $\mu$ $CO_2$ band are damped out exponentially in the wings according to

$$a_\nu = \frac{\alpha \exp(-0.135\,|\nu - \nu_o|^{0.7})}{\pi\,[(\nu-\nu_o)^2 + \alpha^2]} \qquad \text{(I-182)}$$

where $\nu_o$ is the central frequency of the line. On the other hand, the half-width $2\alpha$ is consistently found to vary directly as the pressure. Since the mean transmission varies exponentially on quantities which we are calculating on the basis of observations combined with crude assumptions, the results at best are very approximate. A better course of action would be to measure these mean transmissions experimentally as a function of temperature and pressure by means of a low-resolution infrared spectro-

meter. In addition to yielding information for our purposes, such a series of measurements would yield information on the line shapes in the extreme wings and consequently on the statistics and form of the intermolecular potential between $NH_3$ and other molecules or atoms.

Lacking adequate observations, we proceed with the approximate calculation of the mean intensities. We make the approximation that the lines of the 10 μ and 16 μ bands fall at random within local frequency intervals.

The monochromatic transmission is given by Lamberts's law

$$t_\nu = \exp(-\tau_\nu) = \exp(-\int a_\nu n dL) \qquad \text{(I-183)}$$

where $\tau_\nu$ is the monochromatic optical depth at frequency V, $a_\nu$ the molecular absorption coefficient, n the number density of absorber and dL the increment of path length through the absorber. The mean transmission over a frequency interval Δ for a band containing $\bar{N}$ lines falling at random in Δ is given by

$$\bar{t} = \exp(-\bar{W}/\delta) \qquad \text{(I-184)}$$

where $\bar{W}$ is the mean equivalent width of these lines and δ is the mean separation, $\Delta/\bar{N}$. The equivalent width for a single line is defined by

$$W = \int_0^\infty (1 - t_\nu) d\nu \, . \qquad \text{(I-185)}$$

By analogy with equation (I-183), we use equation (I-184) to define a mean optical depth of the band over this frequency interval by

$$\bar{\tau} = \bar{W}/\delta \qquad \text{(I-186)}$$

so that the mean transmission is given by $\exp(-\bar{\tau})$. $\bar{\tau}$ is computed for the $NH_3$ band by making the frequency intervals $\Delta$ small enough so that the absorption or the Planck function can be taken constant throughout each interval and by using high-resolution laboratory data to obtain $\bar{W}$ for each of these intervals.

Neglecting the influence of Doppler broadening, the $NH_3$ line absorption coefficient is approximated by

$$a_v = S\, h(x) \qquad \text{(I-187)}$$

where we assume the Lorentz profile for h(x):

$$h(x) = \frac{\alpha}{\pi(x^2 + \alpha^2)} \qquad \text{(I-188)}$$

and $x = V - V_o$, where $V_o$ is the central frequency of the line in wave-numbers, S is the line strength, which depends on the temperature through the Boltzmann factor, and $\alpha$ is given by

$$\alpha(J, K) = \alpha_o(J, K) \frac{P}{P_o} \sqrt{\frac{T_o}{T}} \qquad \text{(I-189)}$$

where J and K are quantum numbers, and $P_o$ and $T_o$ are the pressure and temperature at standard conditions. For the $NH_3$

inversion lines, Townes and Schawlow (1955) give for self-broadening at room temperature

$$\alpha(J,K) = 0.38 \frac{P}{P_o} \sqrt{\frac{K^2}{J(J+1)}} \text{ cm}^{-1} \qquad \text{(I-190)}$$

which gives values in the neighborhood of 0.2 $\text{cm}^{-1}$ at atmospheric pressure, in good agreement with the values of $\alpha$ for the 6 $\mu$ $NH_3$ band, which vary between about 0.08 and 0.3 $\text{cm}^{-1}$ (U.S. National Bureau of Standards 1958). We therefore assume that this formula approximates the values of $\alpha$ for the 10 $\mu$ and 16 $\mu$ $NH_3$ bands for the purpose of computing the mean line strengths. The finite instrumental slit width makes the direct evaluation of $\alpha$ for these bands inconvenient. We always have K less than or equal to J for a given J transition. If we further approximate the mean value of K by J/2, equation (I-190) becomes essentially independent of J so that the average value of $\alpha$ over this region of the band is simply

$$\bar{\alpha} = 0.19 \, P/P_o \text{ cm}^{-1} . \qquad \text{(I-191)}$$

Generalizing to include the temperature dependence and expressing $\bar{\alpha}$ in terms of the number density n instead of the pressure, we obtain

$$\bar{\alpha} = 0.19 \frac{n}{L_o} \sqrt{\frac{T}{293}} \text{ cm}^{-1} \qquad \text{(I-192)}$$

for self-broadening of $NH_3$ (where $L_o$ is Loschmidt's number).

To include the contribution of $H_2$ and He to $\alpha$, we make use of the results of Howard and Smith (1950) for a mixture of $NH_3$ and a foreign gas:

$$\alpha = n\sqrt{2}\,\bar{v}\,b^2 + n'\bar{v}''b''^2 \qquad \text{(I-193)}$$

where $\bar{v}$ is the mean velocity of $NH_3$, b and b'' are the effective collision diameters for self and mixed collisions, respectively, $\bar{v}''$ is given by

$$\bar{v}'' = [\bar{v}^2 + \bar{v}'^2]^{1/2} \qquad \text{(I-194)}$$

and the primed variables denote the corresponding quantities for the foreign molecule. Their values are given in Table I-2. The first column under b(A)· c

TABLE I-2

Line Broadening Parameters of Mixtures of $NH_3$, $H_2$ and He(For the 3, 3 line)

| Perturbing Gas | b(A)· c | $\alpha(cm^{-1})$for 1 mm Hg of perturber |
|---|---|---|
| $NH_3$ | 13.8 | $9 \times 10^{-4}$ |
| $H_2$ | (2.95, 3.1) | $1.0 \times 10^{-4}$ |
| He | (2.00, 2.4) | $0.4 \times 10^{-4}$ |

contains the values of Howard and Smith (1950) and the second contains those averaged from various sources by Townes and Schawlow (1955). The values of α correspond to the $NH_3$ (3, 3) line at STP. According to Table I-2, $H_2$ is only 11 per cent and He 5 per cent as efficient as $NH_3$ in broadening the $NH_3$ lines.

Equations (I-12 and 13) indicate that $\alpha$ is the sum of terms varying like

$$c \frac{n}{L_o} \sqrt{\frac{T}{\mu T_o}} \qquad \text{(I-195)}$$

where $\mu$ is the reduced mass of the colliding components. Therefore, the $\alpha$ for combined self and foreign broadening is

$$\alpha = 0.19 \left[ f(T) + (0.11\ \alpha_1 + 0.045\ \alpha_2) N/L_o \right] \ T/273 \qquad \text{(I-196)}$$

where the first term corresponds to the self-broadening of $NH_3$, the second to the $H_2$ enhancement and the third to the He enhancement. $\alpha_1$ and $\alpha_2$ are respective ratios of $H_2$ and He number densities to the total number density N. f(T) is the number density of $NH_3$ divided by $L_o$ and for saturation, is given by

$$\log f(T) = 1.01 + 3(\log T) - 1550/T - 8 \times 10^{-5}\ T^{1.8}. \qquad \text{(I-197)}$$

When unsaturated, f(T) presumably is proportional to the total density, as we assume complete mixing for the unsaturated components of the atmospheres.

We notice that the $NH_3$ lines will be broadened mainly by $H_2$ and He rather than by self-broadening in the upper atmosphere since f(T) goes rapidly to zero at temperatures below about 180 $^{o}$K. The self-broadening becomes important when the partial pressure of $NH_3$ becomes as large as about 10 per cent of the total pressure. $NH_3$ is at most a minor constituent in the atmospheres of the major planets. Each $NH_3$ molecule is perturbed more frequently by $H_2$

and He than by other $NH_3$ molecules. Below about 180 $^{o}K$, we may neglect self-broadening.

We now turn to the problem of computing the curve of growth for the 10 and 16 $\mu$ bands of $NH_3$ for isobaric and isothermal paths. We will then generalize to paths along which the pressure and temperature vary.

Since the laboratory data are for self-broadening, we will develop the formula for $\bar{\tau}$ generally so that we may reduce to either case. In our case,

$$\int a_\nu n \, dL = a_\nu n \, L \tag{I-198}$$

and the expression for the equivalent width becomes

$$W = \int_{-\infty}^{\infty} (1 - \exp(-nLSh(x))dx \, . \tag{I-199}$$

This expression may be evaluated analytically for the h(x) given by equation (I-188) to give

$$W = 2\pi \, \alpha \, \mathcal{L}(nLS/2\pi\alpha) \tag{I-200}$$

for

$$\mathcal{L}(u) = u \exp(-u) \, (I_o(u) + I_1(u)) \tag{I-201}$$

where the I are Bessel functions of the first kind with imaginary arguments. The asymptotic forms of equation (I-201) are

$$W \to nLS \qquad \text{when } nLS/2\pi\alpha \text{ is small}$$
$$W \to 2\sqrt{nLS\alpha} \qquad \text{when } nLS/2\pi\alpha \text{ is large} \tag{I-202}$$

The typical laboratory lines are found to be saturated, so that we take

$$\bar{W} = 2(nL\alpha)^{1/2}\,\overline{S^{1/2}} \tag{I-203}$$

with sufficient accuracy for our purposes. Inserting the value of $\alpha$ for self-broadening, we obtain

$$\bar{W} = (n/L_o)(L_o L\, 0.76\sqrt{T/273})\,\overline{S^{1/2}}\,. \tag{I-204}$$

It turns out that even in the unsaturated case, the error in assuming the saturated case formula is negligible for our purposes. We are referring to individual lines when we mention saturation in this discussion. The expression for the mean optical depth then becomes, in the general case,

$$\bar{\tau} = (\sqrt{0.76L_o}\,\bar{N}/\Delta\,\overline{S^{1/2}})\sqrt{L\, f(T)(T/273)^{1/4}}\,[1 + (0.1\alpha_1 + 0.05\alpha_2)N/L_o/f(T)]^{1/2} \tag{I-205}$$

which is proportional to the square root of the path length.

From the experimental data of Garing, Nielsen and Rao (1959), we measure the equivalent widths of typical $NH_3$ lines in

frequency intervals chosen according to the strength and density of the individual lines. This is done by a triangle approximation and is valid since the instrumental slit width will not appreciably affect the equivalent width of the lines. By this means, $\overline{S^{1/2}}$ is obtained and the results are given in Table I-3. These values are then inserted in equation (I-205) to obtain the mean optical depth for each interval. The value of the constant 0.76 in equation (I-205) is not critical since the value of $\overline{S^{1/2}}$ derived from the comparison with the lab data will be compensated accordingly. That is, it is the quantity $0.76\ L_o \bar{N}/\Delta\ \overline{S^{1/2}}$ which is experimentally derived. The main error in $\bar{\tau}$ is due to the non-randomness of line positions and the derivation of h(x) from the Lorentz curve in the wings.

We now generalize the results to actual paths along which the self-broadening is negligible. Define C by

$$C = (\ 0.76\ L_o\ \bar{N}/\Delta\ \overline{S^{1/2}}) \qquad \text{(I-206)}$$

and let

$$C' = C \cdot (0.1\alpha_1 + 0.05\alpha_2)^{1/2} \qquad \text{(I-207)}$$

and

$$H = \sqrt{T/273}\ N(T)/L_o\ . \qquad \text{(I-208)}$$

Then, we find

TABLE I-3

Absorption Properties of the 10 μ and 16 μ $NH_3$ Bands

| Frequency Interval | Δ | $\bar{N}$ | $\overline{S^{1/2}}$ | $0.76L_o(N/\Delta)S^{1/2}$ | $V_o$ |
|---|---|---|---|---|---|
| 500 - 620 $cm^{-1}$ | 120 $cm^{-1}$ | 32 lines | $3.7_4 \times 10^{-11} cm^{1/2}$ | .045 $cm^{-1/2}$ | 560 $cm^{-1}$ |
| 620 - 650 | 30 | 46 | $2.2_6$ | .016 | 635 |
| 650 - 715 | 65 | 58 | $2.0_8$ | .084 | 683 |
| 715 - 800 | 85 | 94(1) | 7.4 to 15.5 | .33 to .69 | 758 |
| 800 - 910 | 110 | 46(2) | 35.8 | .59 | 855 |
| 910 - 970 | 60 | 108 | 73.5 | 6.00 | 940 |
| 970-1060 | 90 | 22 | 83.6 | .92 | 1015 |
| 1060-1260 | 200 | 99 | 53.5 to 3.2 | 1.2 to .07 | 1160 |

$V_o$ is the mean frequency of the corresponding interval

(1) 84 lines, effectively, due to clustering and non-random overlapping.

(2) 40 lines, effectively, due to clustering and non-random overlapping.

$$\bar{\tau} = C' \left[ \int f \, H \, dL \right]^{1/2} . \qquad \text{(I-209)}$$

The number of cm-atm of $NH_3$ in the path is found by

$$N'(L) = \int_0^L f(T) dL . \qquad \text{(I-210)}$$

In the case of the rotational lines, we must modify the above treatment in order to account for the gaps between the bands of given J state. The rotational lines are conspicuous in the interval 20 $cm^{-1}$ to 320 $cm^{-1}$. Each group of lines arising from the same J state is separated from the neighboring groups by about 20 $cm^{-1}$. The number of lines in each group is about 2J and the width of each group is proportional to J. Within each group, we may approximate the transmission as that due to a random band. The transmission in the gaps between the lines must be treated differently or the absorption will be grossly overestimated. We give an approximate treatment below, based on the Lorentz line shape:

Let the gap be of width $2\Delta'$ and be large enough so that a Lorentz line is essentially proportional to $V^{-2}$ for V greater than $\Delta'$ from the line center. Also, let the gap be surrounded by a random array of equally strong lines of mean separation $\delta$. Goody (1964) gives the expression for the expected transmission at the center of the gap for a path at constant temperature and pressure:

$$t = \exp\left[ -2nLk_{\Delta'} - 2/\delta \int_{\Delta'}^{\infty} dV(1 - \exp(-nLk_V)) \right] \qquad \text{(I-211)}$$

With our approximations, the corresponding optical depth becomes

$$\bar{\tau} = 2z - 2\Delta'/\delta \left[ (1 - \exp(-z) - \sqrt{\pi z}\ \mathrm{erf}(\sqrt{z}) \right] \qquad \text{(I-212)}$$

for which the limiting cases are

$$\begin{array}{ll} 2(1 + \Delta'/\delta)\, z & \text{small } z \\ 2z + (2\Delta'/\delta)(\sqrt{\pi z} - 1) & \text{large } z \end{array} \qquad \text{(I-213)}$$

where $z = nLS\alpha/\pi\Delta'^2$. We use the small z approximation until it exceeds the large z approximation. For the rotational bands of $NH_3$, $\Delta' \sim 5\ cm^{-1}$ and $\delta$ is about $0.3\ cm^{-1}$. This implies that $2\pi\Delta'/\delta$ is about 100. If we define

$$y = (2/\delta)\sqrt{nLS\alpha} \qquad \text{(I-214)}$$

then in the center of the gap,

$$\bar{\tau} \approx (\delta/\Delta')y^2/2\pi \qquad \text{(I-215)}$$

for y less than 65, and in the band,

$$\bar{\tau} \approx y\ . \qquad \text{(I-216)}$$

We now assume that the gaps constitute half of the band interval and average the transmissions in the band and in the gaps according to

$$t = (\exp(-y) + \exp(-(\delta/\Delta')y^2/2\pi))/2 \ . \qquad \text{(I-217)}$$

We fit equation (I-217) to the laboratory data. This is done by measuring the integrated equivalent widths of each rotational band for given initial J and dividing by 20 $cm^{-1}$ (the separation of these bands) to approximate the mean optical depth in an interval including the band and gap. The corresponding transmission is equated to that of equation (I-217) and y is solved for as a function of frequency. Next, equation (I-214) is used to reduce y to 1 cm-atm of $NH_3$. In this way the constant of proportionality is determined. If this constant is denoted by $C_v$, then $C_v$ is given analytically by equation (I-206) and we find

$$y = C_v f(T)\sqrt{L}\,[1+(0.11\alpha_1+0.045\alpha_2)N(T)/(f(T)L_o)]^{1/2}(T/273)^{1/4}. \qquad \text{(I-218)}$$

This equation is for isothermal and isobaric paths. We find the mean optical depth to be:

$$\bar{\tau} = -\ln[(\exp(-y) + \exp(-y^2/100))/2] \qquad \text{(I-219)}$$

$$\bar{\tau} \to y/2 \ \text{ as } \ y \to \text{zero} \qquad \text{(I-220)}$$

$$\bar{\tau} \to \ln 2 + y^2/100 \text{ for intermediate y} \qquad \text{(I-221)}$$

We are not interested in the large y approximation (y greater than 65) since equation (I-215) does not hold in this case. Also, this

would correspond to more $NH_3$ than we find on Jupiter. Intermediate y is defined to be from about 1.4 to 65. The small y case may be taken from zero to 1.4. The value of $\alpha$ becomes equal to $\Delta'$ at 25 Amagats of $NH_3$. As this density exceeds that found in the portions of planetary atmospheres which are under study, the assumption that $\Delta'$ be large enough so that the lines vary as $V^{-2}$ in the center of the gap is valid if the Lorentz shape is valid.

The values of $C_v$ are plotted in Figure 17 for the 10 $\mu$, 16 $\mu$ and rotational bands. The rotational values were reduced 25 per cent to roughly account for the fact that we have ignored the remaining gaps in the computation of the transmission in the gap in question. In addition, the values have been corrected from room temperature to 130 $^{o}K$ by altering the Boltzmann factors of each of the 16 rotational bands and estimating the change in the normalization factor (partition function). While not intended to be accurate, this should approximately account for the temperature difference. For the highest energy band (320 $cm^{-1}$), the correction amounted to a reduction by only two-thirds.

The errors in this approximate treatment are such that the opacity tends to be overestimated. For example, the 10 $\mu$ and 16 $\mu$ $NH_3$ bands are not actually "random". This means that there will be more gaps than predicted by the random band model. Therefore, the actual light transmitted is greater. In addition, the half-widths of a line depend on both the quantum numbers J and K. The high-K lines are broader and are more apt to control the opacity in the gaps.

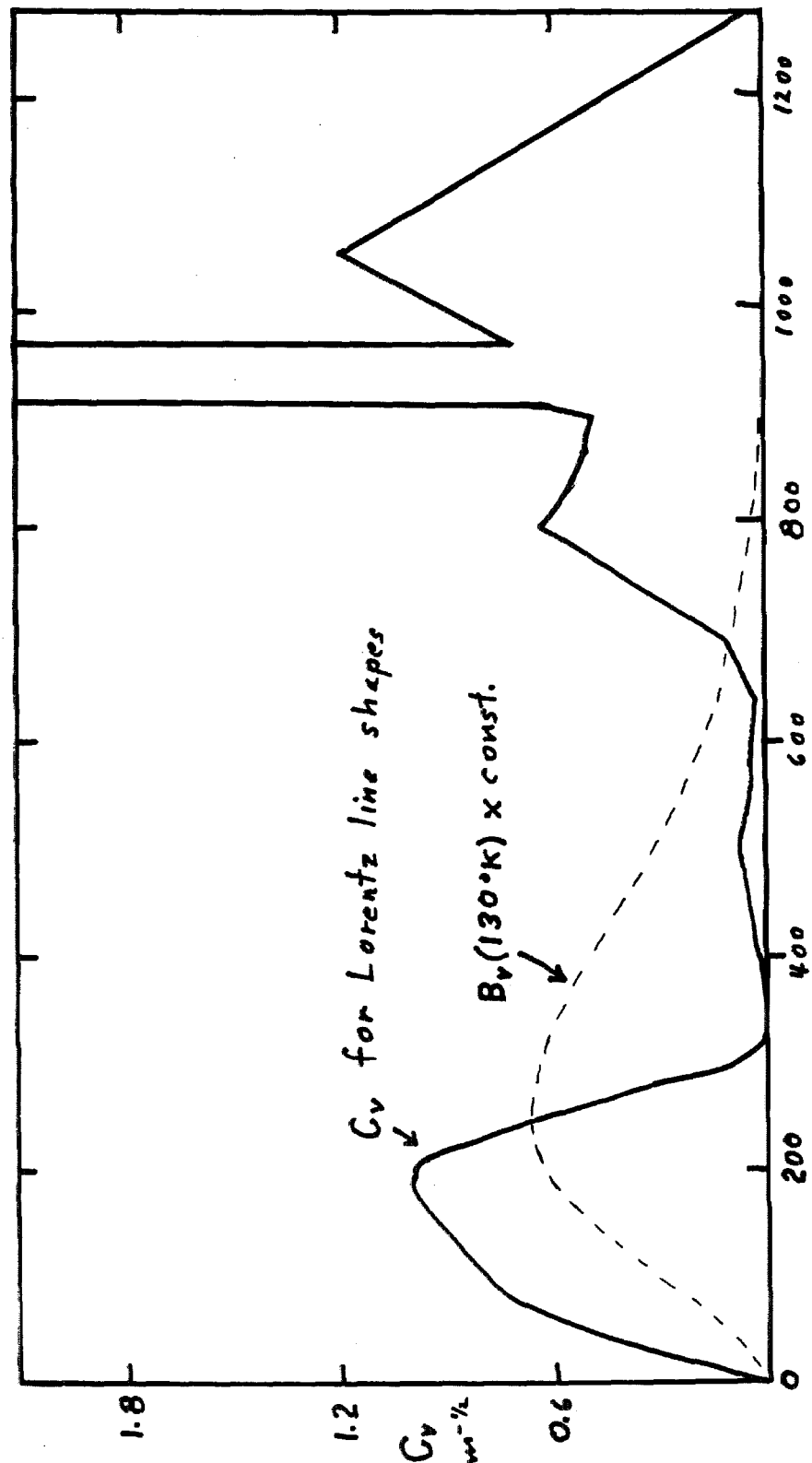
1.8
1.2
0.6
$C_\nu$ $cm^{-1/2}$
0
200
400
600
800
1000
1200
$\nu$ $cm^{-1}$
$C_\nu$ for Lorentz line shapes
$B_\nu(130°K)$ x const.

FIG. 17

On the other hand, if the actual wing decreases more slowly than the Lorentzian wing, then the absorption could be underestimated by this treatment. We must rely upon experimental determinations of the transmission for meaningful band models of $NH_3$. In this connection, we note that because of the square root dependence on the path length, the $\bar{\tau}$'s do not have the property of being additive. The implications of this on the construction of radiative equilibrium models are given in section II-4.

# PART II

# THE CALCULATION OF THE NON-GRAY MODEL ATMOSPHERES FOR THE MAJOR PLANETS

## II-1. ASSUMPTIONS

The non-gray models for the atmospheres of the major planets were calculated using the following assumptions:

a. $H_2$, He and possibly $NH_3$ are the chief thermal opacity sources in the atmospheres of the major planets.

b. Scattering is negligible in the thermal region so that the source function is approximated by the Planck function $B_\nu(T)$.

c. The atmospheres are optically thick at thermal frequencies in layers where the solar radiation is absorbed and converted to thermal radiation. This requires that the overlap between the diluted solar and thermal spectra must be negligible. This is indeed the case for the major planets.

d. The heat capacity of the atmospheres is high enough and the rotation is fast enough so that the effective temperature at a given latitude is independent of longitude. The value of this effective temperature, which is a measure of the thermal flux, will depend on the planet's albedo to solar light, its distance from the sun, the latitude and the inclination of the pole to the ecliptic.

e. The plane-parallel atmosphere approximation holds and the surface gravity is constant throughout the depth of the atmosphere. That is, the thickness of the atmosphere is negligible with respect to the radius of the planet.

f. The atmospheres are in hydrostatic equilibrium.

g. Complete mixing obtains for the unsaturated components.

h. The atmospheres are in a state of radiative equilibrium. We thus ignore convection, thereby restricting the range of applicability of the models to the upper atmospheres. If the convective zones lie deep enough, the solutions in the radiative zones will be valid.

i. The electron and radiation pressures are negligible.

j. The populations of the energy levels are given by LTE (local thermodynamic equilibrium).

As a consequence of these assumptions, the planetary thermal flux is constant above a certain layer at a given latitude. Above this layer, the planetary atmosphere behaves like a stellar atmosphere in which the energy is supplied from below, except that this energy varies with latitude in a way which can be approximated by varying the effective temperature of the model. Our approach is to construct planetary atmospheres according to the above assumptions and to check the self-consistency of the resulting models and obtain the regions in the planetary atmospheres where the solutions are valid. Then we complete our evaluation of the above assumptions by comparing the models with observations.

## II-2. THE EQUATIONS AND METHOD OF SOLUTION

The problem is to obtain the run of physical variables with depth in each of the atmospheres of the major planets according to the above assumptions. To this end, it is convenient to choose the monochromatic optical depth (Aller, 1953) at a particular frequency

$\tau_s$ as the independent variable. The advantages of this procedure over using a mean optical depth $\bar{\tau}$ are three-fold: Firstly, there is no unique $T(\bar{\tau})$ relationship in the non-gray case where the absorption coefficient varies with frequency. Secondly, the computation of $\bar{\tau}$ involves an integration over frequency which is unnecessary when $\tau_s$ is used. Thirdly, one retains the option of adding additional minor constituent opacities to the model without altering the solution to the hydrostatic equation, provided they do not lie at the standard frequency for which $\tau_s$ is defined. Of course, the temperature distribution may be significantly altered in the latter case.

Our goal is to first obtain $T(\tau_s)$ in each atmosphere. Then, we make use of the equations of state for the perfect gas and the saturated gas, liquid and solid to help obtain the remaining physical variables of interest. $T(\tau_s)$ is obtained by iterating an initial assumed $T(\tau_s)$ distribution for 50 prescribed and fixed values of $\tau_s$ given in Table II-1 until flux constancy has been obtained. At each iteration cycle, the physical variables, opacities and fluxes are computed at 30 frequencies covering the thermal spectrum using the current $T(\tau_s)$ distribution by means of a version of Dr. Mihalas' program for model stellar atmospheres (Mihalas 1964) modified by us to treat the major planets. Mihalas' modification of the Krook-Averett technique is used to correct the temperature and optical depth and obtain a new $T(\tau_s)$ distribution. The iterations are continued until the desired degree of convergence to flux constancy is obtained. The condition of radiative equilibrium is then fulfilled.

## TABLE II-1

The Grid of Depths and Frequencies Used in the Planetary Atmospheres Program

| $\tau_s$ | | $V(cm^{-1})$ | |
|---|---|---|---|
| 0 | 0.6 | 32 | 520 |
| 0.001 | 0.7 | 64 | 553 |
| 0.002 | 0.8 | 96 | 587 |
| 0.003 | 1.0 | 128 | 638 |
| 0.004 | 1.2 | 161 | 690 |
| 0.006 | 1.4 | 193 | 741 |
| 0.008 | 1.6 | 225 | 793 |
| 0.010 | 1.8 | 257 | 845 |
| 0.015 | 2.0 | 289 | 896 |
| 0.020 | 2.5 | 322 | 948 |
| 0.025 | 3.0 | 354 | 1000 |
| 0.030 | 3.5 | 387 | 1125 |
| 0.035 | 4.0 | 420 | 1250 |
| 0.040 | 5.0 | 454 | 1375 |
| 0.060 | 6.0 | 487 | 1500 |
| 0.080 | 8.0 | | |
| 0.100 | 10 | | |
| 0.125 | 14 | | |
| 0.15 | 18 | | |
| 0.20 | 22 | | |
| 0.25 | 26 | | |
| 0.30 | 30 | | |
| 0.35 | 40 | | |
| 0.40 | 50 | | |
| 0.5 | 60 | | |

The underlined frequencies are the standard frequencies at which $\tau_s$ are defined for various models.

In the case where molecular hydrogen and helium are the major constituents of the atmosphere, the monochromatic optical depth at the wave number V is related to the opacity by

$$\tau_V - \tau_{VO} = \int_{x_o}^{x} (n^2 A_V(T) + nn' B_V(T))dx/c \qquad (II-1)$$

where the distance x is measured positive downwards, n is the number density of $H_2$, n' is that of He, c is the speed of light, and the pressure-induced binary absorption coefficients $A_V(T)$ and $B_V(T)$ correspond to pure $H_2$ absorption and enhancement in $H_2$-He mixtures, respectively. They depend only on the temperature, T. Each coefficient has been given in Part I as the sum of rotational and translational contributions. The rotational contribution is given by equations (I-5, 19 and 23). The translational contribution for our cases of interest are evaluated numerically in units of $sec^{-1}$ $cm^6$ by

$$a_V = 27,461 \times 10^{-33} T^{-3/2} 2\mathscr{L}(T)(1-\exp(-1.43880V/T))\sqrt{V} \qquad (II-2)$$

$$\times \int_{t_m}^{t_M} \frac{\exp(M-t^2/t_o^2)dt}{\sqrt{1+1.95052t^2/V}}$$

for pure $H_2$ and

$$b_v = 38,588 \times 10^{-33}\, T^{-3/2}\,(1-\exp(-1.43880V/T))\sqrt{V}$$

$$\times \int_{t_m}^{t_M} \frac{\exp(N - t^2/t_1^2)\, dt}{\sqrt{1 + 1.674t^2/V}} \qquad \text{(II-3)}$$

for $H_2$-He enhancement. $\mathcal{L}(T)$ is a partition over the rotational states for an equilibrium mixture of ortho and parahydrogen at the temperature T, given by equation (I-28). Also,

$$t_o^2 = 0.35633\ T$$

$$t_1^2 = 0.4151\ T\ . \qquad \text{(II-4)}$$

Analytically, $t_M$ is infinity but may be approximated by $2.35\sqrt{T}$ since the higher t contribution is negligible. Also, $t_m$ is analytically zero but we used $t_m$ about equal to 1 in the program. The M and N are pre-computed data which are a function of both V and t. Exp(M) and exp(N) are computed from equations (I-106 and 109), respectively. M and N are slowly varying when plotted against ln(t), so that they are computed only for the eleven values of ln(t) given in Table II-2. The numerical values of exp(M) and exp(N) are tabulated in Appendix G at the standard values of ln(t).

TABLE II-2

STANDARD VALUES OF ln(t)

| | |
|---|---|
| 0.54930614 | 2.9957323 |
| 1.3862944 | 3.3296470 |
| 1.6479184 | 3.7336856 |
| 1.8718022 | 4.0081590 |
| 2.1972246 | 4.1470249 |
| 2.6390573 | |

The interval $(t_m, t_M)$ is divided into $(t_m - t_M)/H$ intervals of length H. M and N are interpolated quadratically on this range using the independent variable, $\ln(t_n)$ where $t_n = nH$ for integral n. The quadrature of equations (II-2 and 3) is then effected by Simpson's rule for each V less than 700 $cm^{-1}$. The translational absorption at higher frequencies is negligible with respect to the rotational absorption.

Using the fixed $\tau_S$ grid, the numerical calculation of the $\tau_V$ is effected by

$$\tau_V(\tau_S) = \int_0^{\tau_S} k_V/k_S \, d\tau_S \qquad \text{(II-5)}$$

where $k_V$ is the absorption coefficient per gram given by

$$k_V = \rho^{-1} d\tau_V/dx \qquad \text{(II-6)}$$

where

$$\rho = \mu m_p P/kT \qquad \text{(II-7)}$$

is the mass density, $\mu$ the mean molecular weight in units of $m_p$, $m_p$ is the mass of the proton, P is the total pressure, k is Boltzmann's constant and $\tau_v$ is given by equation (II-1).

The equation of hydrostatic equilibrium is

$$dP = \rho\, g\, dx \qquad \text{(II-8)}$$

where g is the surface gravity. Now taking advantage of the fact that the explicit density and frequency dependence of the opacity is separable, we reduce the equation of hydrostatic equilibrium to an integral depending only on the temperature and optical depth at the standard frequency. From equation (II-1), we find

$$d\tau_s = (n^2 A_s + nn' B_s)\, dx/c \ . \qquad \text{(II-9)}$$

Letting

$$\alpha_1 = n/N$$
$$\alpha_2 = n'/N \qquad \text{(II-10)}$$

where N is the total number density and dividing equation (II-8) by equation (II-9), we obtain

$$dP/d\tau_s = \frac{\rho\, gc}{N^2\, \alpha_1(\alpha_1 A_s + \alpha_2 B_s)} \quad . \qquad (II\text{-}11)$$

Using the relations $\rho = \mu m_p N$ and $N = P/kT$ for perfect gases, this becomes

$$d(P^2)/d\tau_s = 2\mu m_p\, gckT/\alpha_1^2(A_s + B_s\alpha_2/\alpha_1) \qquad (II\text{-}12)$$

where $\mu$, g, $\alpha_1$ and $\alpha_2$ are essentially constant, by assumption. Therefore, we finally obtain the expression

$$P^2(\tau_s) = \frac{2\mu m_p gck}{\alpha_1^2} \int_o^{\tau_s} \frac{T(t)\, dt}{A_s[T(t)] + B_s[T(t)]\,\alpha_2/\alpha_1} \qquad (II\text{-}13)$$

which has a well-behaved integrand and may be integrated by Simpson's rule. Note that $P^2$ is proportional to $\tau_s$ for smaller $\tau_s$.

The physical depth is evaluated by

$$x = x_o + \frac{2.3025851}{g} \int_{\log p_o}^{\log p} \frac{P}{\rho}\, d\log P \qquad (II\text{-}14)$$

using the trapezoidal rule and taking $x_o = 0$ at $\tau_s = .0005$. The equivalent number of Km of $H_2$ at STP overlying a given depth is given by

$$K = \frac{\alpha_1 P}{\mu(H_2)g} \frac{10^{-5}}{m_p L_o} = \frac{\alpha_1 P}{g\ 8.98} \qquad (II\text{-}15)$$

where $\mu(H_2)$ is the mean molecular weight of $H_2$ in units of $m_p$ and $L_o$ is Loschmidt's number.

According to our assumptions, the equation of transfer may be written

$$\mu \frac{\partial I_\nu(\mu, \tau_\nu)}{\partial \tau_\nu} = I_\nu - B_\nu(\tau_\nu) \qquad \text{(II-16)}$$

where $I_\nu$ is the specific intensity in frequency units, $\mu$ now is the cosine of the angle between the pencil of radiation and the vertical and $B_\nu$ is the Planck function for unit frequency interval

$$B_\nu(\tau_\nu) = \frac{2h\nu^3}{c^2} \frac{1}{\exp(h\nu/kT)-1} . \qquad \text{(II-17)}$$

When radiative equilibrium holds, it is convenient to apply equation (II-16) in its integral form:

$$F_\nu(\tau_\nu) = 2\pi \left[ \int_{\tau_\nu}^{\infty} B_\nu(t_\nu) E_2(t_\nu - \tau_\nu) dt_\nu - \int_o^{\tau_\nu} B_\nu(t_\nu) E_2(\tau_\nu - t_\nu) dt_\nu \right] \qquad \text{(II-18)}$$

where $E_2$ is the second exponential integral (Aller 1953) and $F_\nu$ is the monochromatic net flux at frequency $\nu$. It is related to the total flux F by

$$F = \sigma T_e^4 = \int_o^{\infty} F_\nu d\nu \qquad \text{(II-19)}$$

which is a constant given by the effective temperature, $T_e$, and $\sigma$ is the Stefan-Boltzmann constant.

For the emergent specific intensity, we have the expression

$$I_\nu(0,\mu) = \int_0^\infty B_\nu(t_\nu)\ \exp(-t_\nu/\mu)dt_\nu/\mu \qquad \text{(II-20)}$$

and for the mean intensity we have

$$J_\nu(\tau_\nu) = \frac{1}{2}\ \int_0^\infty B_\nu(t_\nu)E_1(|t_\nu - \tau_\nu|)dt_\nu \qquad \text{(II-21)}$$

where $E_1$ is the first exponential integral. These equations are evaluated by fitting polynomials to $B_\nu(t_\nu)$ over short $t_\nu$ intervals and doing the integrations analytically.

Mihalas (1964) gives for the temperature-optical depth correction formulae:

$$\tau_1' = -\tau_1\left[\frac{\int_0^\infty H_\nu^0 n_\nu'/n_\nu d\nu}{H^0}\right] + (1 - H/H^0) \qquad \text{(II-22)}$$

$$T_1 = \frac{1}{\int_0^\infty n_\nu \dot{B}_\nu(T^0)d\nu}\ \Big[(1+\tau_1')dH^0/dt - \sqrt{3}\,(1 - H/H^0(0))\int_0^\infty n_\nu H_\nu^0(0)d\nu \qquad \text{(II-23)}$$

$$+\ \tau_1\int_0^\infty (J_\nu^0 - B_\nu^0)n_\nu' d\nu\Big]$$

where $\tau_1$ and $T_1$ are the corrections, equation (II-22) is solved subject to $\tau_1(0) = 0$, $H_\nu = F_\nu/4\pi$, H is the frequency integral over $H_\nu$, $n_\nu$ is $k_\nu/k_s$, the primes denote differentiation with respect to $\tau_s$, the dot denotes differentiation with respect to temperature and the quantities with zero superscripts are the uncorrected values.

The radiative gradient is computed according to

$$\left.\frac{d\ln T}{d\ln P}\right|_{rad} = \frac{2P^2}{T}\left(\frac{dT}{d\tau_s}\right)\left(\frac{d\tau_s}{dP^2}\right) \qquad \text{(II-24)}$$

where $dT/d\tau_s$ is obtained by low order numerical differentiation and $d\tau_s/dP^2$ from equation (II-12). Therefore,

$$\left.\frac{d\ln T}{d\ln P}\right|_{rad} = \frac{dT}{d\tau_s}\left(\frac{P\alpha_1}{T}\right)^2 \frac{A_s + B_s\alpha_2/\alpha_1}{\mu g m_p c k} \qquad \text{(II-25)}$$

where $\mu$ is the mean molecular weight of the atmosphere in units of $m_p$.

To check the assumption of radiative equilibrium, the wet adiabatic gradient must be computed assuming phase equilibrium on the time scale of the adiabatic processes (or less) between the solid, liquid and gaseous states of the condensable components in the atmosphere. To this end, four constituents, $H_2$, He, $NH_3$ and $CH_4$ are considered. When $NH_3$ or $CH_4$ is saturated, there will be a heat of transformation released during an adiabatic expansion

opposing the decrease of temperature and resulting in a shallower adiabatic gradient.

We follow Lasker's technique (1963) in computing the wet adiabat for a multicomponent system containing two saturated components, denoted by subscripts n and c. The adiabatic change in such a system is given by

$$dQ = dU + PdV + Ldn_n + Mdn_c = 0 \qquad \text{(II-26)}$$

where

$$dU = (n_u \bar{C}_{v,u} + n_n C_{v,n} + n_c C_{v,c} + n'_n C_{v,n'} + n'_c C_{v,c'})dT \qquad \text{(II-27)}$$

where the subscript u denotes the uncondensable components, L and M are the heats of transformation per mole of constituents n and c, respectively, and are given by the Clausius-Clapeyron equation for perfect gases by

$$L = T \frac{v}{n_n} \frac{dP_n}{dT} = \alpha RT$$

$$M = T \frac{v}{n_c} \frac{dP_c}{dT} = \beta RT \qquad \text{(II-28)}$$

where the specific volumes of the condensed components are neglected, R is the gas constant and

$$P_n = A \exp(-\alpha)$$

$$P_c = B \exp(-\beta) \tag{II-29}$$

are fitted to experimental saturation vapor pressure curves. For a given molecule, these curves are a function of the temperature only. $n_i$ is the number of moles of component i, $C_{v,i}$ is the specific heat at constant volume (per mole) of species i, $\bar{C}_{v,u}$ is the mole-average of $C_{v,i}$ for the uncondensable components, $C_{v,i'}$ is for the $i^{th}$ condensed component and $n_i'$ is the number of moles of the $i^{th}$ condensed component.

Noting that the number of moles of uncondensable components remains the same during an adiabatic expansion, algebraic manipulation reveals that

$$\left.\frac{d\ln P}{d\ln T}\right|_{ad} = \frac{P_u}{P}\frac{d\ln P_u}{d\ln T} + \frac{P_n}{P}\alpha + \frac{P_c}{P}\beta \tag{II-30}$$

where

$$\frac{d\ln P_u}{d\ln T} = \left[\frac{P_u}{P}\frac{\bar{C}_{p,u}}{R} + \frac{P_n}{P}\frac{C_{p,n}}{R} + \frac{P_c}{P}\frac{C_{p,c}}{R} + \frac{n_n' C_{v,n'}}{n_u+n_n+n_c} + \frac{n_c' C_{v,c'}}{n_u+n_n+n_c} + \frac{P_n}{P}\alpha^2 + \frac{P_c}{P}\beta^2\right]\left[1 + \frac{P_n}{P}\alpha + \frac{P_c}{P}\beta\right]^{-1} \tag{II-31}$$

and where $C_{p,i}$ are the corresponding specific heats at constant pressure. It should be mentioned at this point that when this expression is reduced to the case of one saturated component and compared with Lasker's result (1963), a relatively small

term, $(C_{p,n}/R - C_{v,n'}/R)P_n/P$, obtained and later neglected by Lasker, is not obtained in the above derivation. Its physical significance is not clear to us, either.

Our particular application of the above equation is to the case where n corresponds to $NH_3$ and c to $CH_4$. Note that $P_u = P - P_c$ and that if either or both of $NH_3$ or $CH_4$ is unsaturated at a given level, the corresponding adiabat is obtained by setting the corresponding partial pressure equal to zero in equation (II-31). This is valid when both $NH_3$ and $CH_4$ are minor constituents. Neglecting the specific heat terms of the condensable components with respect to their $\alpha$ and $\beta$ terms, we may finally write

$$\frac{d\ln P_u}{d\ln T} \simeq \frac{\bar{C}_{p,u}/R + P_n \alpha^2/P + P_c \beta^2/P}{1 + P_n \alpha/P + P_c \beta/P} \qquad \text{(II-32)}$$

where

$$\bar{C}_{p,u} = \frac{\sum_i n_i C_{p,i}}{\sum_i n_i} \qquad \text{(II-33)}$$

the summations being carried out over the uncondensable constituents.

We find from the International Critical Tables (1928) that the saturation vapor pressures, when fitted to equations (II-29), give

$$
\begin{array}{lllll}
146^{\circ} \text{ to } 195^{\circ} & A = 1.325 \times 10^{13} & \alpha = 3753.6/T & & \\
79^{\circ} \text{ to } 89^{\circ} & B = 5.966 \times 10^{10} & \beta = 1190.1/T & & \text{(II-34)} \\
99^{\circ} \text{ to } 110^{\circ} & B = 9.714 \times 10^{9} & \beta = 1024.2/T & &
\end{array}
$$

where the units of A and B are dynes/cm$^2$ (c.f. Figure 18).

We must now evaluate equation (II-33). Since $NH_3$ and $CH_4$ are being neglected as they are minor constituents, we consider only the specific heats at constant pressure for helium and hydrogen. The value for helium is simply 2.500 R at all temperatures. For molecular hydrogen, we must distinguish between the ortho and para components and treat them as two separate gases.

During the adiabatic processes taking place in the atmospheres of the major planets, we expect the ratio of ortho to para hydrogen to remain constant in a given mole of $H_2$ because the half-life of ortho-para equilibrium is much longer than the duration of the adiabatic process. As a result, the specific heat of the mixture is an average of those for the pure ortho and pure para components weighted by their fractional abundance in moles. This abundance ratio is assumed to be given by the equilibrium mixture of ortho and para hydrogen at the local temperature. Table II-3 gives the values of $\bar{C}_p/R$ for $H_2$.

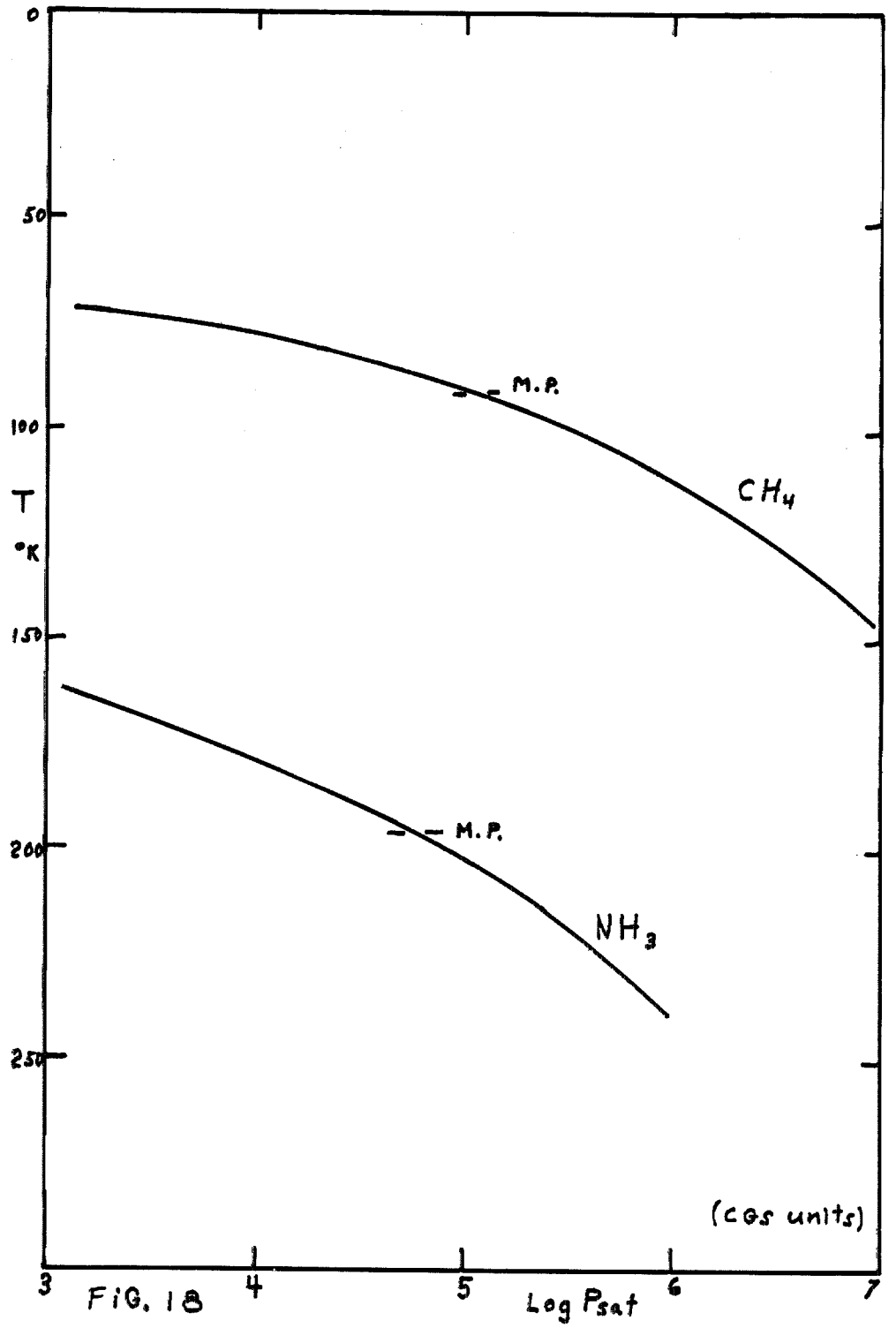


FIG. 18

TABLE II-3

EQUILIBRIUM VALUES OF $\bar{C}_p/R$ FOR $H_2$

| T | $C_p/R$ | T | $C_p/R$ |
|---|---|---|---|
| 0 | 2.5000 | 125 | 2.9708 |
| 15 | 2.5000 | 150 | 3.0976 |
| 20 | 2.5000 | 175 | 3.2037 |
| 25 | 2.5000 | 200 | 3.2899 |
| 30 | 2.5000 | 225 | 3.3577 |
| 40 | 2.5022 | 250 | 3.4085 |
| 50 | 2.5154 | 273.1 | 3.4424 |
| 75 | 2.6369 | 298.1 | 3.4679 |
| 100 | 2.8138 | | |

At about 10 $^{o}$K below the saturation temperature, the wet and dry adiabats approach each other.

## II-3. NUMERICAL TESTS OF THE PROGRAM

The program's solution to the equation of hydrostatic equilibrium was checked by doing a couple of integration cycles by hand and comparing the results with those of the program. The temperature-depth correction procedure was then checked by running the entire program for a gray opacity, for which the solution is known, and examining the final $T(\tau_s)$, flux, variation of flux with depth and degree of convergence. The flux was constant to within 0.03 per cent for $\tau_s$ less than twenty in the $T_e$ = 110 $^{o}$K gray model.

The frequency grid was chosen to trace out the opacity profile adequately. The frequency integrations were tested by running the same model twice; first, using a Simpson's rule and second, using a Weddle's rule for the integration. The results were virtually identical. The low frequency flux tail was approximated by Rayleigh's law and the upper limit of the integration was taken at 1500 $cm^{-1}$ instead of at infinity. The $H_2$-He opacity is weak here, but a strong methane absorption begins at frequencies greater than about 1250 $cm^{-1}$ so that we are justified in neglecting the flux above the upper limit of integration. The only case where it makes a difference is for the planet Jupiter. Finally, radiative equilibrium was also checked by examining the degree of validity of

$$\int_0^\infty k_\nu J_\nu d\nu = \int_0^\infty k_\nu B_\nu d\nu \qquad \text{(II-35)}$$

at each depth for each model. The results were quite satisfactory.

## II-4. ADDING $NH_3$

The $NH_3$ opacity depends on the amount of $NH_3$ along the absorbing path in gaseous form. Because of the low saturation vapor pressure of $NH_3$ at low temperatures, we may neglect the opacity due to $NH_3$ in the upper atmospheres of Saturn, Uranus and Neptune. In the case of Jupiter, use is made of the rough band model constructed in section I-8. If instead, we were to use equations (II-18, 20 and 21) directly, too many frequency points would be required due to the extremely rapid variation of the

absorption coefficient in the band and the computing time would therefore be prohibitive. Consequently, it is desirable to work with some kind of an average over the rotational structure, where $B_v$ varies much less rapidly than $k_v$. However, as Castor (1965) has pointed out, the mean "optical depth" for an $NH_3$ band, defined by the mean transmission of this band over a given frequency interval (c.f. section I-8), is not additive. For example, it may vary as the square root of the path length so that we cannot express the optical depth between two layers by the difference in the optical depths of the layers. For this reason, the term "optical depth" is perhaps bad terminology. It would be better to consider the "mean transmission", where it is understood that this quantity depends on the depths of the layers bounding the zone in question.

Because of this non-additivity, it is necessary to perform the proper frequency averages of equations (II-18, 20 and 21) over the $NH_3$ bands before the effect on radiative equilibrium of these bands can be quantitatively ascertained. We have not yet extended the formalism to this case and can therefore make only qualitative deductions. This is done in section III-4. d.

# PART III

# THE PROPERTIES OF THE MODELS

## III-1. COMPUTATIONAL RESULTS

Using the IBM 7040-7094 electronic computer, several non-grey models in radiative equilibrium were constructed for the major planets; Jupiter, Saturn, Uranus and Neptune. These models are tabulated in Appendix A. Table III-1 lists the models constructed for each major planet, their parameters and their major characteristics.

Models including helium were computed only for the extreme cases of Jupiter and Neptune. In these cases the helium number density was taken equal to that of the molecular hydrogen in the model. We note that helium cannot play a role in the thermal opacity when hydrogen is absent (neglecting the translational absorption resulting from collisions of He and other atmospheric constituents, such as methane). Models taking into account the contribution of ammonia to the thermal opacity were considered only in the case of Jupiter because this contribution is negligible in the radiative portions of the atmospheres of the other major planets due to the low saturation vapor pressure of ammonia at low temperatures. In the Jovian atmosphere, the ammonia concentration was taken to be that given by the saturation vapor pressure. Figure 18 shows the saturation vapor pressure of ammonia and methane as a function of temperature (International Critical Tables, 1928). As was mentioned previously, methane contributes negligibly to the thermal opacity.

TABLE III-1

The Models, Their Parameters and Their Characteristics

| | Model | $T_e$ | $T_o$ | $T_o/T_{og}$ | $\bar{\tau}(T_e)$ | $\bar{\tau}_c$ | $T_c$ | $K_c$ km-atm $H_2$ | $\Delta F/F$ |
|---|---|---|---|---|---|---|---|---|---|
| Jupiter | $H_2$ | 130 °K | 100.5 °K | .95 | .97 | 2.7 | 149 °K | 28 | 0.26 per cent |
| $T_B$=121 °K | $H_2$ | 120 | 93.6 | .96 | .99 | 2.9 | 139 | 30 | 0.6 |
| g = 2597 cgs | $H_2$ + He | 120 | 95.5 | .98 | .84 | 4.5 | 158 | 38 | 1.6 |
| | $H_2$ | 110 | 85.3 | .96 | 1.0 | 3.4 | 131 | 32 | 0.9 |
| Saturn | $H_2$ | 100 | 76.8 | .95 | 1.2 | 3.5 | 118 | 52 | 1.3 |
| $T_B$=89 °K | $H_2$ | 90 | 68.3 | .94 | 1.3 | 3.5 | 105 | 52 | 1.8 |
| g = 1063 cgs | $H_2$ | 80 | 60.0 | .93 | 1.4 | 3.7 | 91 | 55 | 1.8 |
| Uranus $T_B$ = 64 °K g = 1025 cgs | $H_2$ | 64 | 47.5 | .92 | 1.6 | 2.3[1] | 67 | 53 | 2.4 |

TABLE III-1 continued

| | Model | $T_e$ | $T_o$ | $T_o/T_{og}$ | $\bar{\tau}(T_e)$ | $\bar{\tau}_c$ | $T_c$ | $K_c$ km-atm $H_2$ | $\Delta F/F$ |
|---|---|---|---|---|---|---|---|---|---|
| Neptune | $H_2$ | 50 | 37.4 | .92 | 1.5 | 2.25 | 52 | 65 | 1.3 |
| $T_B$=50 $^oK$ | $H_2$ + He | 50 | 40.3 | .99 | .69 | 2.7(2) | 61 | 41 | 1.3 |
| g = 1373 cgs | | | | | | | | | |

(1) $\bar{\tau}_c$ = 4.0 if $CH_4$ were not present

(2) $\bar{\tau}_c$ = 3.2 if $CH_4$ were not present

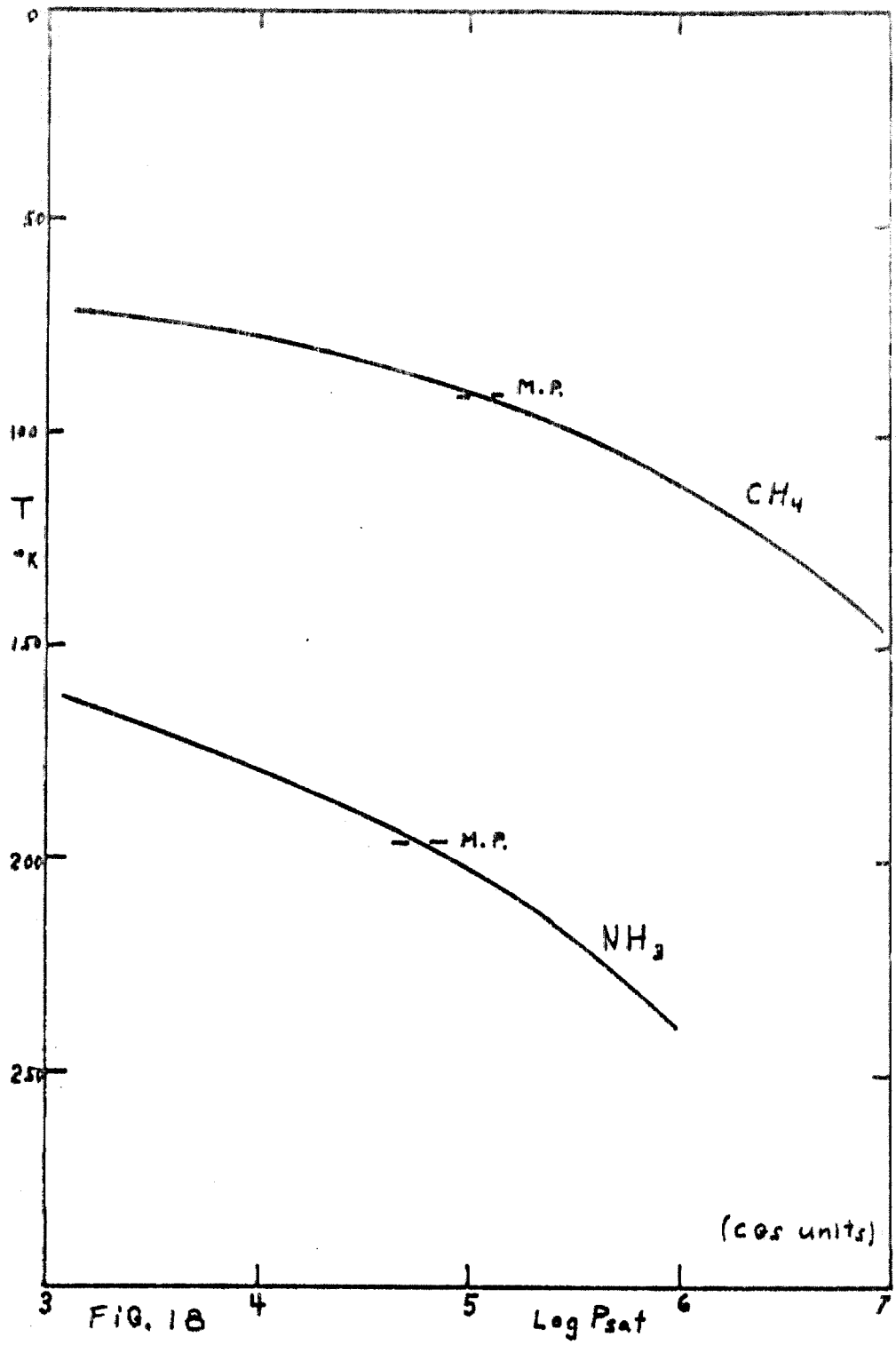


FIG. 18

The surface gravity for Jupiter was taken from Kuiper (1952) and for the remaining major planets was computed from the masses and radii using the data of Brower and Clemence (1961). Because of the uncertainties in the radii, the values for the surface gravities of the major planets are uncertain to the point where it is not worth while to correct for the planetary rotation. The error increases as the apparent size of the planet decreases. In section III-2 we shall see that the models are homologous with respect to changes in the surface gravity so that they may be easily corrected as better values of this quantity are obtained.

The effective temperature $T_e$ is a measure of the thermal flux according to equation (II-19). Where possible, the effective temperatures for these models were chosen to bracket the likely value at a representative latitude for each planet. Further discussion of this point is postponed to section III-4.

In column one of Table III-1 the surface gravity g is expressed in cgs units and $T_B$ is the corresponding rotating black body temperature (see section III-4). $T_o$ is the boundary temperature and $T_o/T_{og}$ is the ratio of the boundary temperature to the corresponding gray value. In columns six and seven, $\bar{\tau}$ is the Planck mean at the depth for which the temperature is equal to $T_e$ and at the depth where convection begins, respectively. $T_c$ is the temperature at the top of the convective zone and $K_c$ is the number of km-atm of $H_2$ (the equivalent number of km of $H_2$ at STP) overlying the depth at which convection begins. In the last column, $\Delta F/F$ is the percentage maximum relative deviation of the flux from the value given by $T_e$, in the layers of the atmosphere

for which the standard optical depth $\tau$ is less than twenty. For Jupiter and Saturn, $\tau$ was taken at 520 $cm^{-1}$ and for Uranus and Neptune, it was taken at 289 $cm^{-1}$. The rest of Table III-1 is self-explanatory.

## III-2. HOMOLOGY INVESTIGATION

The equation of hydrostatic equilibrium and the equations relating the physical variables are given by (II-7, 13, 14, 15, 25, 30 and 32). We attempt to reduce these equations to a homologous form by the following transformation of variables:

$$
\begin{aligned}
P &= g^{1/2}\,\mu^{1/2}\,T_o^{1/2}\,\alpha_1^{-1}\;\underline{P} \\
\rho &= g^{1/2}\,\mu^{3/2}\,T_o^{-1/2}\,\alpha_1^{-1}\;\underline{\rho} \\
x &= g^{-1}\,\mu^{-1}\,T_o\;\underline{x} \\
K &= g^{-1/2}\,\mu^{1/2}\,T_o^{1/2}\;\underline{P}/8.98 \\
T &= \underline{T}\;\;T_o \\
\tau &= \underline{\tau}\ .
\end{aligned}
\qquad \text{(III-1)}
$$

These equations define the underlined variables. We have used $T_o$ instead of $T_e$ in order to improve the degree of homology. When equations (III-1) are substituted in equations (II-1, 7, 13, 14, 15 and 25), we find

$$\underline{P} = \left[ 2m_p ck \int_o^{\underline{\tau}_s} \frac{\underline{T}\, d\tau_s}{A_s + B_s \alpha_2/\alpha_1} \right]^{1/2}$$

$$\rho = m_p \underline{P}/k\underline{T}$$

$$\underline{x} = 2.3025851 \int_{\underline{P}_o}^{\underline{P}} \frac{\underline{P}}{\underline{\rho}}\, d\log\underline{P}$$

$$\underline{T} = T/T_o \qquad \text{(III-2)}$$

$$\underline{\tau}_s = \underline{\tau}_o + \frac{1}{ck^2} \int_{\underline{x}_o}^{\underline{x}} \frac{(A_s + B_s \alpha_2/\alpha_1)}{\underline{T}^2}\, \underline{P}^2 d\underline{x}$$

$$\left.\frac{d\ln T}{d\ln P}\right|_{rad} = \frac{d\underline{T}}{d\underline{\tau}_s} \left(\frac{\underline{P}}{\underline{T}}\right)^2 \frac{(A_s + B_s \alpha_2/\alpha_1)}{6.92 \times 10^6} \quad .$$

The models are homologous if the underlined variables are the same from model to model. These equations show that a homology can exist only for a fixed helium-hydrogen ratio, $\alpha_2/\alpha_1$ and only if $\underline{T}$ is the same function of $\underline{\tau}_s$ for all the planets considered and $A_s$ and $B_s$ are insensitive to the temperature. If these conditions are satisfied, the first two of the equations (III-2) show that $\underline{P}(\underline{\tau}_s)$ and $\underline{\rho}(\underline{\tau}_s)$ will each be independent of g, $\mu$ and $T_o$. It then follows that $\underline{x}(\underline{P})$, $\underline{\tau}_s(\underline{x})$ and $d\ln T/d\ln P \Big|_{rad}$ will be independent of the model. However, the adiabatic lapse rate $d\ln T/d\ln P \Big|_{ad}$ depends on the absolute value of the temperature when saturation is

important so that the height of the convection zone is not homologous in this case.

Our models show that $\underline{T}$ is not a unique function of $\underline{\tau}_s$ in the non-gray case and varies as much as 27 per cent in the deeper layers. $T/T_e$ as a function of $\underline{\tau}_s$ deviates even more at the surface. Figure 19 shows the deviation from grayness and degree of homology of the $\underline{T}(\underline{\tau}_s)$ relation. In this connection we note that only the Jovian models neglecting $NH_3$ appear to have a fairly unique $\underline{T}(\underline{\tau}_s)$ relation. The dispersion in the other planets increases as the effective temperature is lowered. At $V_s = 520$ $cm^{-1}$, $A_s$ is quite insensitive to the temperature, while $B_s$ is somewhat sensitive. At $V_s = 289$ $cm^{-1}$, both $A_s$ and $B_s$ are somewhat sensitive to the temperature, explaining the increased dispersion for Uranus and Neptune in Figure 19.

We note from equations (III-2) that if $\alpha_2/\alpha_1$ and $T_e$ are fixed, the underlined variables are not affected by changes in g, $\mu$ or $\alpha_1$ provided that the changes in $\mu$ and $\alpha_1$ reflect the addition or subtraction of atmospheric constituents which play no role in the thermal opacity. Under this condition, the temperature distribution will not be altered during this change. In this way, the models are indeed homologous with respect to g, $\mu$ and $\alpha_1$, except for the height of the convection zone.

Plots of log $\underline{P}(\underline{T})$ for the various models show a significant dispersion except for the case of the Jovian models. Plots of log $\underline{P}(\log \underline{\tau}_s)$ are well defined for Jupiter and Saturn pure $H_2$ models but not for Uranus or Neptune models. For each model, however, the pressure was found to vary quite accurately as the square root of $\tau_s$ in the region where radiative equilibrium is valid so that the curves could be superimposed by an appropriate scale change of $\tau_s$.

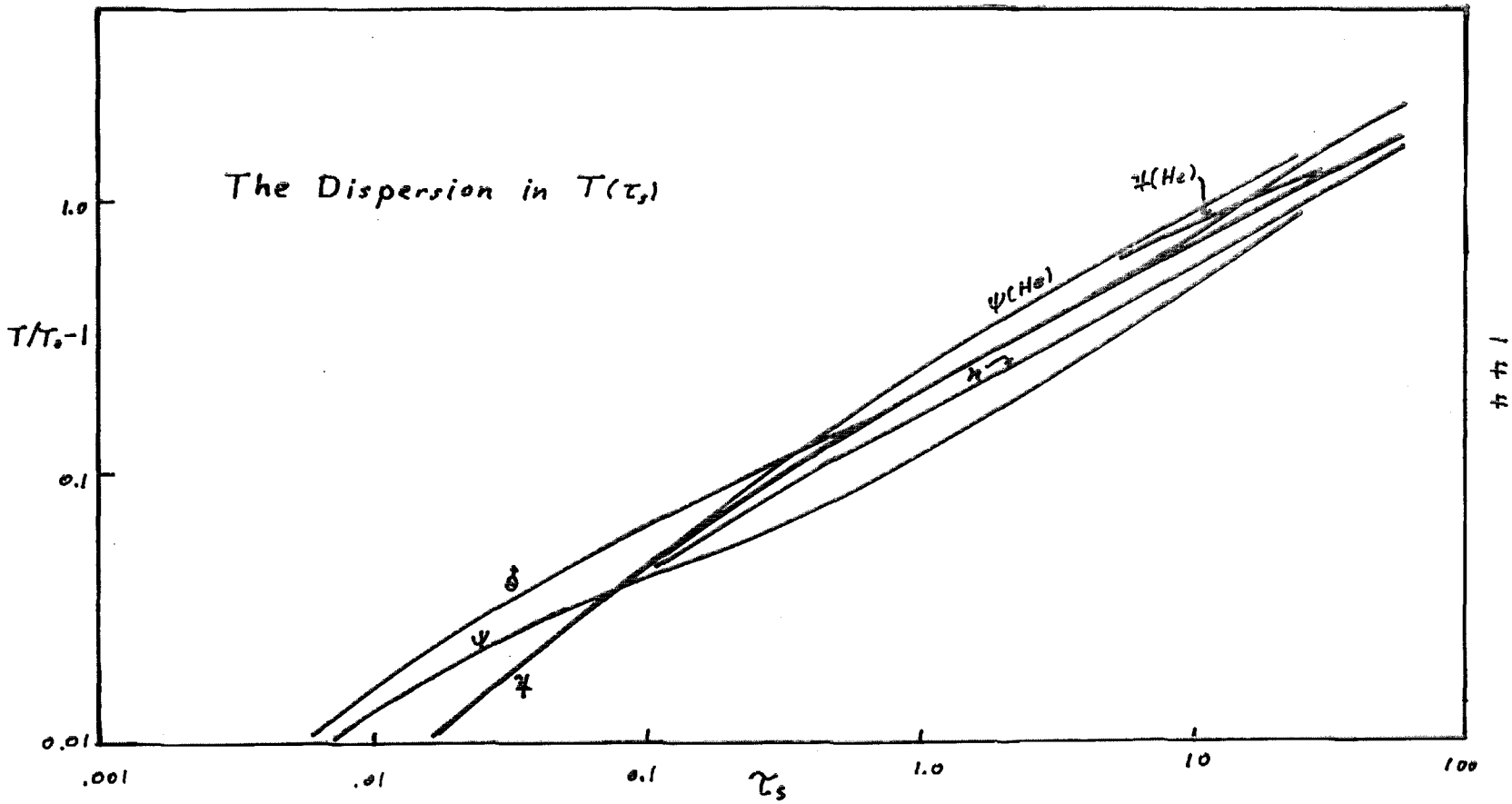
The Dispersion in T(τs)
T/T₀-1
1.0
0.1
0.01
.001
.01
0.1
1.0
10
100
τs
ψ(He)
ψ(He)
δ
ψ
χ

FIG. 19

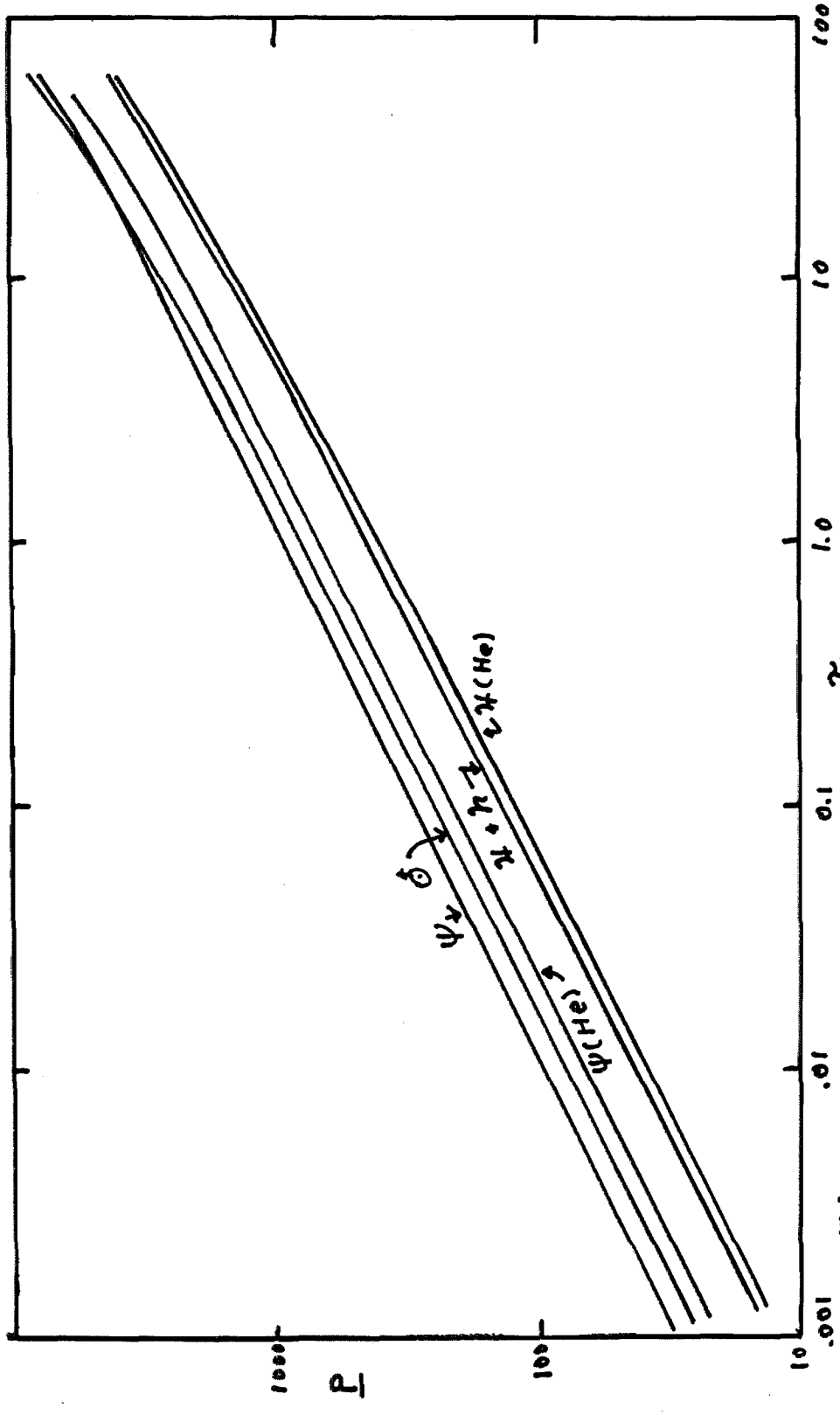
100
10
1.0
0.1
.01
.001
$\tau_5$
1000
100
10
$P_1$
$\psi_{H(He)}$
$\psi_H + \psi_{He} + \psi_{2H(He)}$
$\psi_H$
$\phi$

FIG. 20

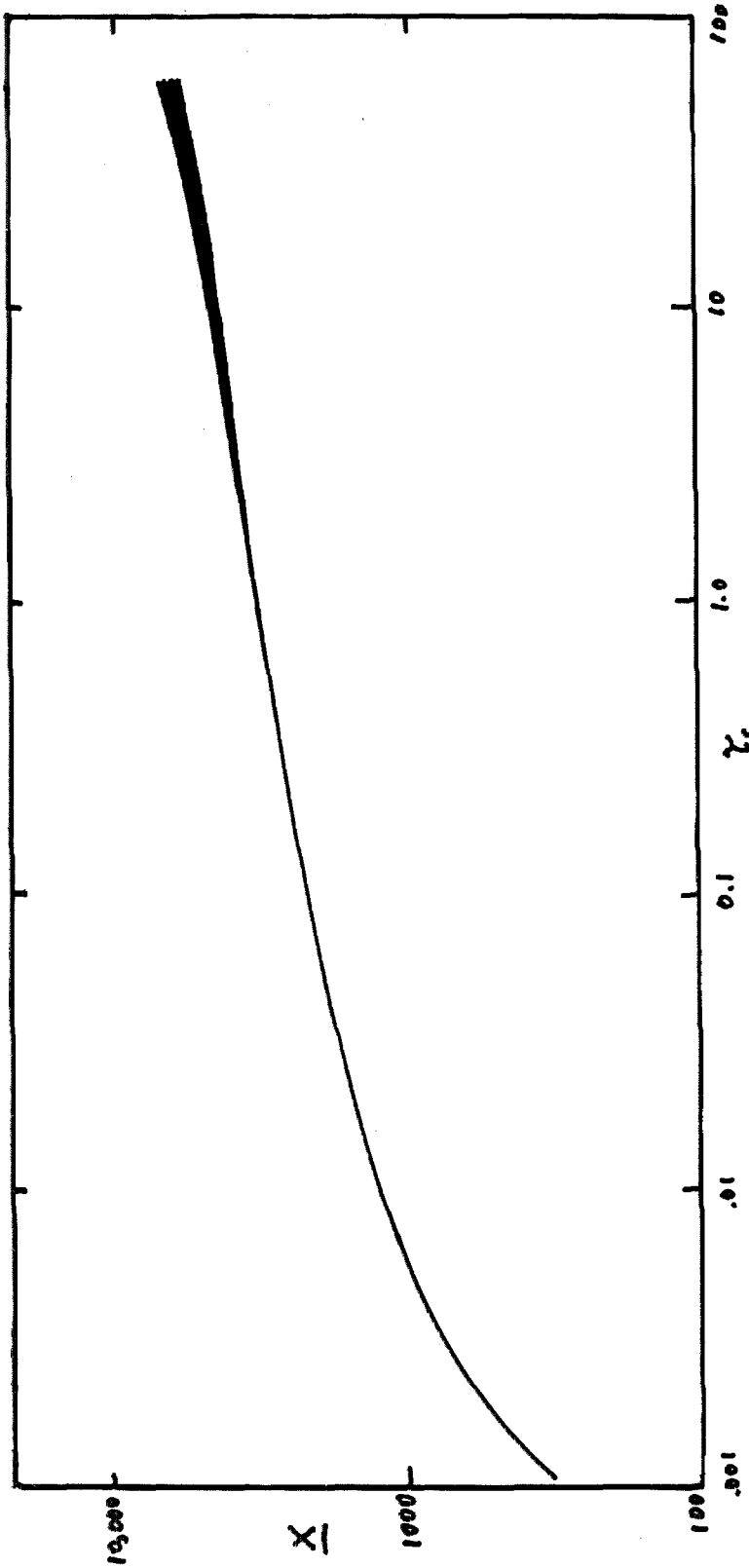


Fig. 21, The Dispersion in $\chi(\tau_s)$

Figure 21 shows that $\underline{x}(\underline{\tau}_s)$ is remarkably well defined for all of the models, with only a small dispersion at the deeper layers. The agreement between the models using different standard frequencies is explained by the fact that in a given model, $d\underline{x}(\underline{\tau}_v)/d\underline{\tau}_v$ is the same for constant value of $\tau_v$ at all frequencies where the absorption coefficient varies negligibly with frequency or temperature. Such is the case for the two standard frequencies, 289 and 520 $cm^{-1}$.

We summarize by pointing out that except for the wet adiabat, the variables of the $H_2$-He models are homologous with respect to changes in g, $\mu$ and $\alpha_1$ under the conditions noted above but are not homologous with respect to changes in $T_e$ (in contrast with the gray case), $T_o$ or $\alpha_2/\alpha_1$. Exceptions are that the Jovian models for $\alpha_2/\alpha_1 = 0$ appear to be homologous in $T_e$ as well and the variable $x(\tau_s)$ appears to be universally homologous at either of the two standard frequencies used.

## III-3. THE SELF-CONSISTENCY OF THE MODELS

We are now in a position to check the self-consistency of the models by evaluating some of the assumptions listed in section II-1.

Scattering was assumed to be negligible with respect to absorption in the thermal spectrum. Vardya (1962) gives

$$\sigma = \frac{8\pi^3}{3\lambda^4} \left[\frac{\mu^2 - 1}{n}\right]^2 \qquad \text{(III-3)}$$

for the Rayleigh scattering cross section. For molecular hydrogen, this becomes

$$\sigma = 8.49 \times 10^{-45}/\lambda^4 \ \text{cm}^2 \qquad \text{(III-4)}$$

where $\lambda$ is in cm. Dalgarno and Williams (1962) point out that this is correct in the long wavelength limit or for $\lambda$ greater than 5500 Angstroms. They also give the Planck mean for Rayleigh scattering by $H_2$ as

$$\sigma_p(T) = 1.48 \times 10^{-42} T^4 + 8.12 \times 10^{-51} T^6 + \ldots \qquad \text{(III-5)}$$

At 200 $^{o}$K, this becomes $2.37 \times 10^{-33}$ cm$^2$/molecule. For a path length equivalent to 100 km-atm, the corresponding mean optical depth is $6.38 \times 10^{-7}$, which is negligible. At 1000 wave numbers, the monochromatic optical depth for 100 km-atm $H_2$ is $2.1 \times 10^{-6}$. Since the absorption increases with wavelength in this region, it is quite clear that scattering due to $H_2$ is negligible in the thermal spectrum. Also, since the index of refraction of He is less than that for $H_2$, the Rayleigh scattering due to He is negligible in the thermal spectrum. This is also the case for $CH_4$ and $NH_3$.

The Mie scattering for solid crystals of $NH_3$ and condensed particles of $CH_4$ may be important if the size of the particles is on the order of the thermal wavelengths and the particle density is high enough. We may neglect Mie scattering at thermal frequencies in the radiative portions of the atmosphere if the particles of about 50 $\mu$ are either too heavy to remain suspended in a convectionless zone or are otherwise too rare in these zones to be important. Perhaps this problem can be made the target of future observations.

Reference to the models shows that the Planck mean optical depth at the 160 $^{o}$K level, where the $NH_3$ bands in the visible spectral region become strong, varies from 4 to 10 in the Jovian models and is greater than 15 in the Saturnian models. This justifies assumption II-1. c for Jupiter and Saturn. In Neptune, Uranus and possibly Saturn, $CH_4$ is frozen out in the upper atmosphere. There, the $CH_4$ concentration is at most given by the saturation vapor pressure (see Figure 18). If the absorption of solar light through the resulting paths of $CH_4$ is negligible with respect to the net absorption at thermal frequencies, we are justified in making the assumption that the atmospheres of all the major planets are optically thick at thermal frequencies in the layers where the solar radiation is absorbed and converted to thermal radiation. Both Uranus and Neptune exhibit very strong $CH_4$ absorption in the visible spectrum, but this absorption must arise in the deeper, warmer layers where the saturation vapor pressure is high enough to produce it. The assumption therefore seems justified.

We now consider the effect of longitude on the mean temperature of a 100 km-atm radial column of $H_2$ 1 $cm^2$ in cross-section in the Jovian atmosphere. This column contains about 4 moles of $H_2$ and has a thermal capacity $C_p$ about $10^8$ ergs/mole/$^{o}$K. The upward flux in this column is supplied from below and is represented by the effective temperature. If $T_e$ = 120 $^{o}$K on the average, this flux is 1.17 x $10^4$ ergs/sec/$cm^2$. The Jovian period is about 10 hours so that this column spends five hours in darkness. If we stop the energy supply of this column and let it radiate through its top surface, it will radiate about 2.1 x $10^8$ ergs. When

equated to the change in internal energy of the column, this amounts to a change in the mean temperatures of only one-half degree in going from the evening to the morning limb. Thus, the heat capacity of the atmosphere is great enough so that the temperature distribution is essentially independent of the longitude on Jupiter. This result, first pointed out by Urey (1959), is insensitive to the numbers used to obtain it. The rotation periods of Saturn and Uranus are also about 10 hours and that for Neptune is about 16 hours. The values of $C_p$ are about the same as for Jupiter. The effective temperatures are all lower so that the above calculation is representative of the other major planets, as well. The main difference is that their poles are less perpendicular to the ecliptic plane so that elements passing through the subsolar point spend less than half of their time in darkness. As a result, the time average over a rotation period of the effective temperature of points on the "summer" side of the equator are higher (and lower on the "winter" side) than would otherwise be the case. Again, there will be a latitudinal, but hardly a longitudinal temperature dependence. The seasonal variations for Uranus are particularly extreme, since its pole lies nearly in the ecliptic plane. At times, its equatorial plane passes through the sun and at times, its pole points in the direction of the sun. The sun thus alternately back-warms first one pole and then the other with a period of 84 years. When a pole is pointed towards the sun, Uranus radiates from a surface $2\pi R^2$. This is in contrast with the case where the sun is at an equinox and Uranus radiates from a surface $4\pi R^2$. Therefore, the warmest weather on Uranus is found near the pole during midsummer.

Table III-1 shows the values of $\bar{\tau}_c$ (Planck mean) where the models become unstable toward convection. Strictly speaking, the presence of the convective zone affects the solution not only in this zone but also in the radiative zone above it so that the radiative equilibrium models are only approximations to the idealized situation. Since convection occurs where the radiative gradient d1nT/d1nP exceeds the adiabatic gradient, the temperature at a given level in the convective zone will be less than that given by radiative equilibrium. Section III-4 investigates the error made by assuming the radiative solution in the convective zone. The temperature at a given level in the radiative zone is affected by the temperature distribution in the convective zone by an amount depending on the difference in optical depth between the respective layers in the convective and radiative zones according to equation (II-18) in which $\tau_v$ is taken to lie in the radiative zone. As a result of this coupling, the actual top of the convective zone may differ from that given by Table III-1, where the Schwarzschild criterion was used. The point we wish to emphasize is that if the top of the convective zone is optically deep, the temperature distribution in the upper radiative zone will be unaffected by the presence of the convective layer and the radiative solution will be valid. In this sense, we see that the radiative solutions for the Saturnian models and the Jovian models where He was added are most valid because their convective zones lie deepest ($\bar{\tau}_c$ from 3.5 to 4.5). On the other hand, the pure $H_2$ models for Uranus and Neptune are least valid because they have the shallowest radiative zones ($\bar{\tau}_c$ = 2.3). Adding $H_e$ has the effect of increasing the value of $\bar{\tau}_c$ defined in III-1. In all cases, the temperature distribution

in the radiative zone is a somewhat insensitive function of the convective details of a model and the radiative equilibrium models will suffice for our purposes.

Figure 22 shows that in all cases, the extent of the atmosphere between x = 0 and the convective zones is negligible with respect to the radius of the planet. We are therefore justified in making the plane-parallel atmosphere assumption and assuming the surface gravity constant throughout the atmosphere.

The electron pressure is negligible at planetary temperatures and pressures because no substance is degenerate in the upper atmosphere or ionized except in the sunlit portion of the extreme upper atmosphere where the density is very low (Gross and Rasool 1964).

The radiation pressure varies like $aT^4/3$ where $a = 7.57 \times 10^{-15}$ ergs/cm$^3$/$^o$K$^4$. At T = 300 $^o$K, the radiation pressure is $2.0 \times 10^{-6}$ dynes/cm$^2$, which is quite negligible.

The assumption of LTE was checked by checking the validity of Kirchoff's law:

$$j_\nu = k_\nu B_\nu \qquad \text{(III-6)}$$

where $j_\nu$ is the thermal emission coefficient per gram, $k_\nu$ is the absorption coefficient per gram and $B_\nu$ is the Planck function. This was accomplished by computing, at each level of the model, the ratio between the number of absorptions per gram of material per second (equation III-7)

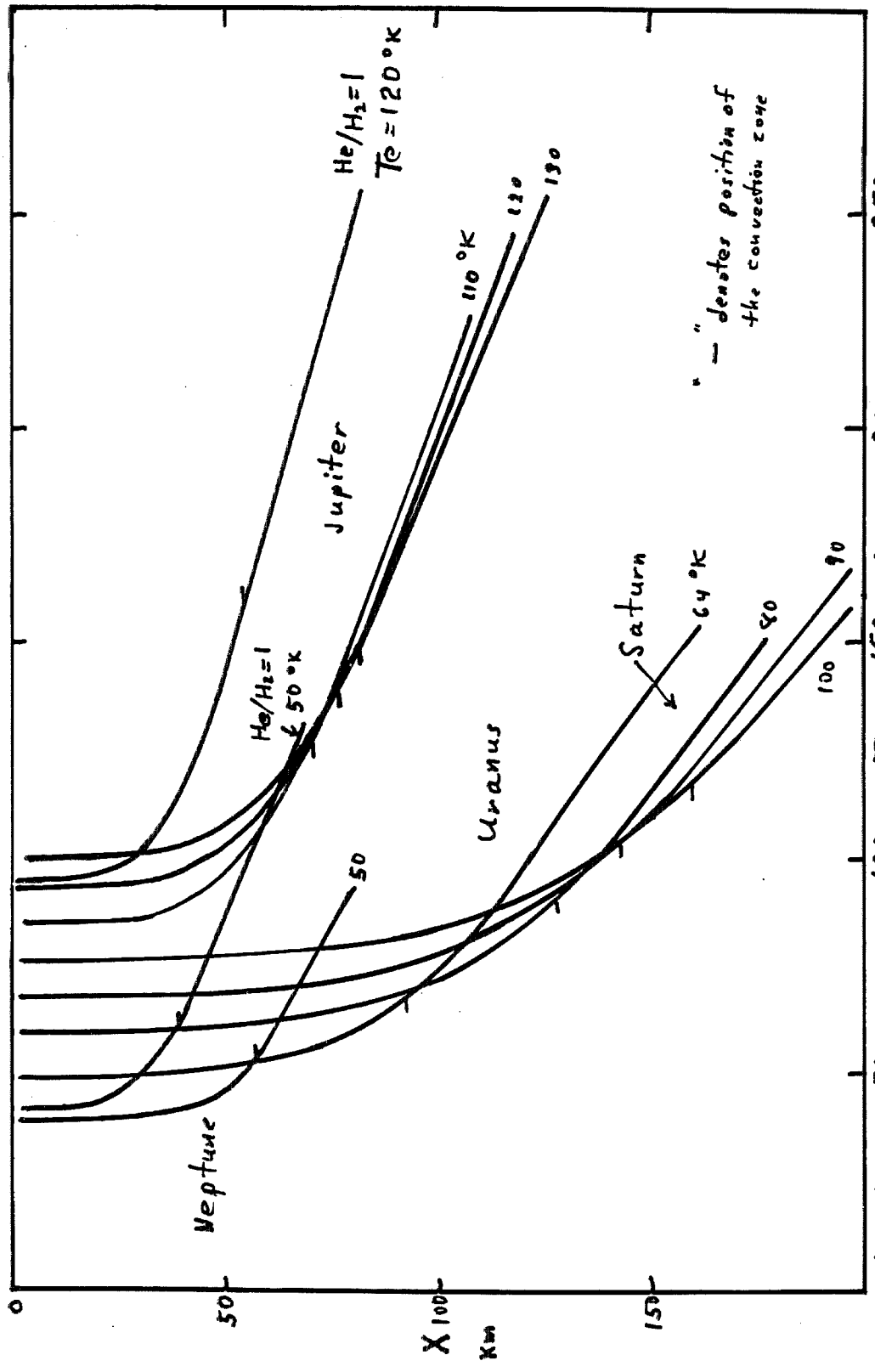
He/H₂=1
Te=120°K
110°K
120
130
"—" denotes position of the convection zone
Jupiter
He/H₂=1
150°K
Saturn
64°K
Uranus
50
90
100
Neptune
0
50
100
150
X
Km
50
100
150
200
250
T °K

FIG. 22

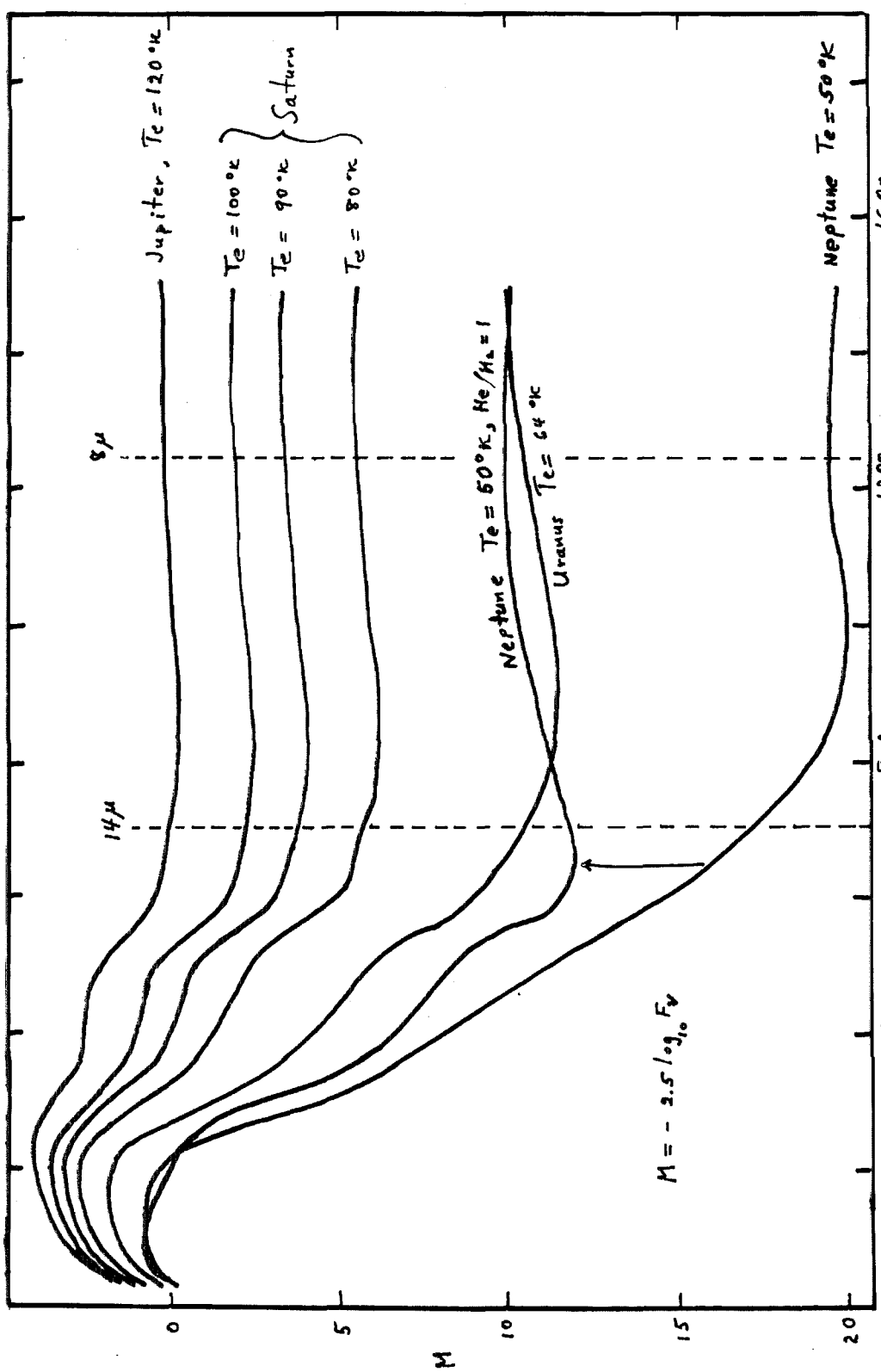
Jupiter, Te = 120°K
Te = 100°K
Te = 90°K
Te = 80°K
Saturn
8μ
14μ
Neptune Te = 60°K, He/H2 = 1
Uranus Te = 54°K
Neptune Te = 50°K
M = - 2.5 log10 Fν
M
0
5
10
15
20
400
800
1200
1600
ν cm⁻¹

FIG. 23

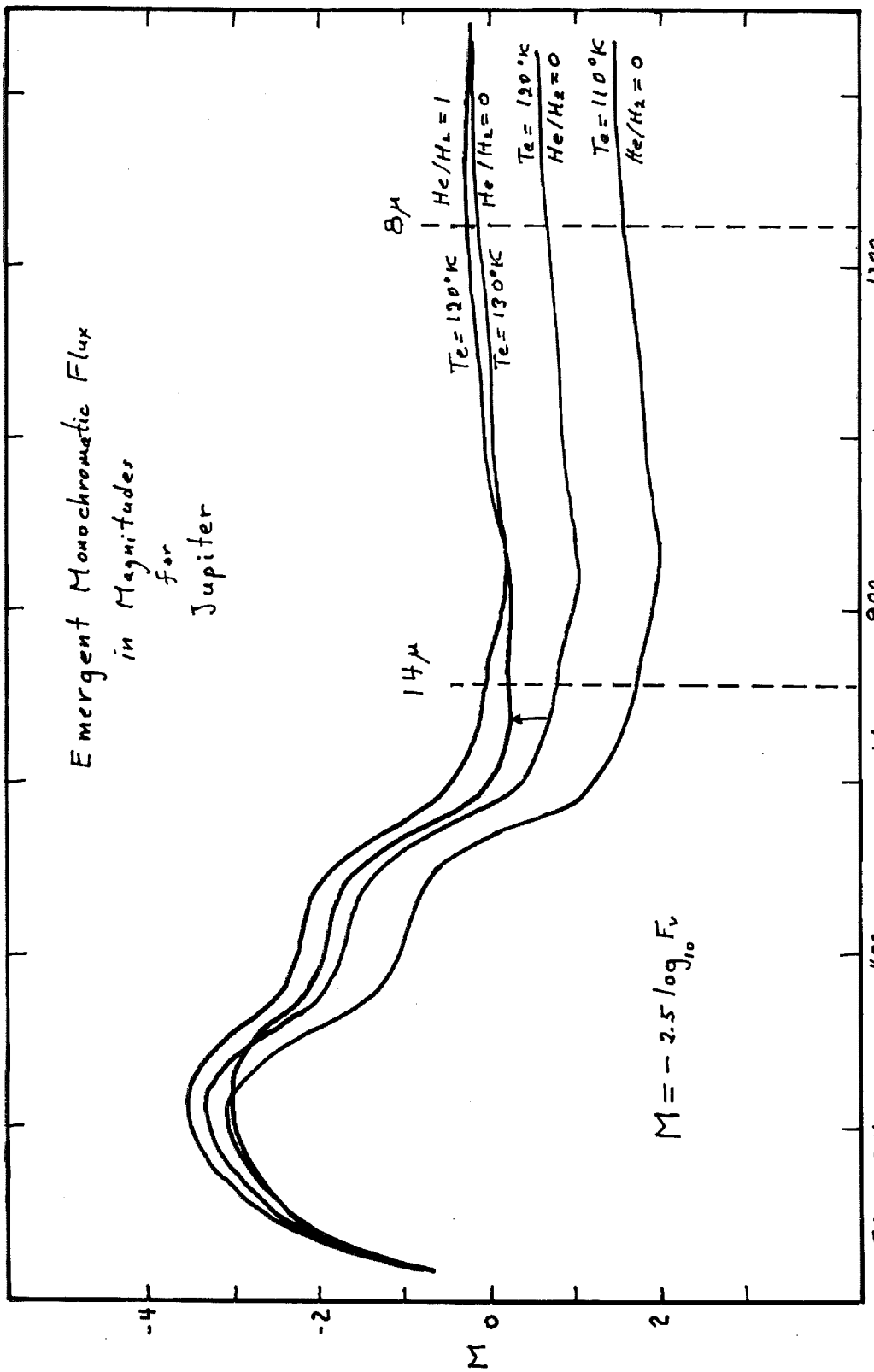
Emergent Monochromatic Flux
in Magnitudes
for
Jupiter
8μ
14μ
He/H₂ = 1
He/H₂ = 0
He/H₂ = 0
He/H₂ = 0
Te = 120°K
Te = 130°K
Te = 120°K
Te = 110°K
M = − 2.5 log₁₀ Fν
M
ν
cm⁻¹
-4
-2
0
2
400
800
1200

FIG. 24

$$4\pi \int_0^\infty \frac{k_\nu J_\nu}{h\nu} \, d\nu \qquad \text{(III-7)}$$

and the number of thermal emissions per gram per second (equation III-8) assuming Kirchoff's law.

$$4\pi \int_0^\infty \frac{k_\nu B_\nu}{h\nu} \, d\nu \ . \qquad \text{(III-8)}$$

This ratio should be unity when LTE holds. The models show that LTE indeed holds in the deeper atmospheres of all the major planets, but deviates toward the surface so that the above ratios become as low as 0.98, 0.98, 0.96, and 0.93, respectively; for Jupiter, Saturn, Uranus and Neptune pure $H_2$ models. For the $H_2$-He Jovian and Neptunian models, the ratios with the maximum deviation are respectively, 0.93 and 0.91. We see that the deviation is worse for the models with He. This is because He provides an effective block for radiation leaving the surface of the planet at low frequencies so that at these frequencies, $J_\nu$ falls further below $B_\nu$.

By and large, the deviations from LTE are not serious. The populations of the rotational levels and the relative velocity distribution of $H_2$-$H_2$ and $H_2$-He collisions will be affected in the upper atmosphere as well as the equilibrium mixture of ortho and para hydrogen. However, the validity of the assumption that the ortho-para ratio is given by the equilibrium mixture at the local temperature is itself open to doubt as there is sure to be some mixing in the atmosphere and the half-life of this equilibrium

process is very long at low pressures in the absence of paramagnetic catalysts (Farkas 1935). With such catalysts present, equilibrium could be achieved in a few hours. In the absence of catalysts, equilibrium could be achieved in a week or so deeper in the atmosphere where the pressure is higher. The upper atmosphere is apt to contain a "normal" mixture of hydrogen, where the ortho-para ratio is a cross-sampling of equilibrium mixtures at temperatures characteristic of the deepest regions of the atmosphere. The affect of this uncertainty on the opacity may be more pronounced than those resulting from deviations from LTE near the surface. Figure 4 shows the temperature dependence of the factor which depends on the ortho-para ratio in the translational opacity for $H_2$-$H_2$ collisions (the $H_2$-He translational case is quite insensitive to the ortho-para ratio). This figure shows the case corresponding to an equilibrium mixture. For temperatures above 200 $^{o}$K, the equilibrium ortho-para ratio is essentially 3 : 1. Therefore, if equilibrium was achieved deep in the atmosphere, where the temperature was greater than 200 $^{o}$K, the error in the translational opacity at 100 $^{o}$K would be several per cent too low. That is, the actual back-warming would be even greater. In this sense, our equilibrium $H_2$ models represent a lower limit to the actual greenhouse effect. The ortho-para dependence of the rotational absorption is such that the error in taking an equilibrium mixture above 112 $^{o}$K, when the ortho-para ratio is essentially 3 : 1, is less than 4 per cent. This holds for both the $H_2$-$H_2$ and the $H_2$-He cases.

## III-4. PHYSICAL INTERPRETATION

### III-4. a. The Effective Temperature

The effective temperature is a measure of the thermal flux in the case of the major planets, where the thermal and diluted solar spectra are separate. We cannot measure this flux from the earth's surface because of the strong $CO_2$, $H_2O$ and $O_3$ absorption in the earth's atmosphere at thermal frequencies. There is a "window" in the 8 - 14 $\mu$ region and a small weather-sensitive window at 26 $\mu$ through which light may pass with relatively little absorption. This is insufficient for measuring the thermal flux but may be used to measure fluxes in certain frequency intervals. This information could then be used to narrow the range of possible models satisfying the observations, thereby bracketing the effective temperature. In the case of the major planets, however, the emission from the earth's atmosphere masks the light received from Uranus, Neptune and Saturn so that we cannot get very reliable measurements in their cases. One solution to the problem would be to measure the planetary fluxes from outside the earth's atmosphere. This may soon be feasible from an orbiting observatory.

For the present, we consider the indirect evaluation of the effective temperature. If the Bond albedo to sunlight A of each planet were known, then the thermal flux could be derived since it is (1 - A) times the diluted solar flux at the planet. The Bond albedo is defined to be the ratio of the total integrated flux reflected in all directions to the total incident integrated flux and is given by

$$A = \frac{j(0)}{F} \; 2 \int_0^{\pi} \Phi(a) \sin a \, da \qquad \text{(III-9)}$$

where F is the incident flux, j(0) is the reflected flux at opposition, $\Phi$ is the phase function and "a" is the phase angle. This equation is usually applied only to visible light. The incident solar flux which is not scattered must be absorbed and converted to infrared frequencies by thermodynamic processes and be manifested by the thermal spectrum. However, the Bond albedo depends on the scattering phase function which, in turn, depends on the nature of the scattering particles in the planetary atmosphere. The phase angle is the angle at the planet between the sun and the direction of the scattered ray. An earth-bound observer cannot measure rays singly scattered in the atmospheres of the major planets for which the phase angle exceeds 12 degrees. Therefore, he cannot measure the Bond albedo directly and thereby obtain the effective temperature.

In order to estimate the Bond albedo, one must make assumptions about the nature of the scattering particles. It would be better to derive the Bond albedo by fitting the models to the observations, if possible, and thereby obtain information on the nature of the scattering particles. With this philosophy in mind, models were computed at various likely effective temperatures.

To get an idea of the effective temperature, we computed the equilibrium temperature of a rapidly rotating black body located at the same distance from the sun as the planet in question. This is denoted by $T_B$ in Table III-1 and is given by

$$T_B = 276/\sqrt{r}\ ^{o}K \qquad \text{(III-10)}$$

where r is the semi-major axis of the planet's orbit in astronomical units. When the sun is at an equinox, the body absorbs solar light over an area $\pi R^2$ where R is its radius and radiates uniformly from a surface area $4\pi R^2$. The resulting equilibrium temperature is $T_B$. This is also equal to the effective temperature of the body and is an upper limit on the mean effective temperature of the corresponding planet, averaged over latitude. That is, $T_B$ is also an upper limit to the effective temperature of the corresponding planet when there is thorough latitudinal mixing. In this case, the mean effective temperature is given by

$$T_e = T_B \sqrt[4]{1 - A} \qquad \text{(III-11)}$$

where the black-body case corresponds to zero Bond albedo. The Jovian atmosphere is rotating differentially parallel to the equator with the shortest period near the equator and the longest at the poles. The atmosphere exhibits little latitudinal mixing. We estimate the effect of latitude on the effective temperature in the case that the latitudinal heat flow is negligible. However, we should point out that the absence of latitudinal mixing does not necessarily preclude a strong latitudinal flow of heat. For example, local convective zones could support such a flow. We proceed by substituting a rapidly rotating body of Bond albedo A for the black body and compute the effective temperature at each latitude $T_e(\Phi)$ by assuming that the flux absorbed at a given latitude $\Phi$ is also radiated at that latitude. The result is

$$T_e(\Phi) = T_e \sqrt[4]{\frac{4}{\pi} \cos \Phi} \, . \qquad \text{(III-12)}$$

This equation shows that the maximum temperature at equinox is 1.06 $T_e$ at the equator. During the solstices, this temperature is greater, depending on the inclination of the axis of rotation to the orbital plane. In the case of a specific model for Saturn, the presence and inclination of the rings must be taken into account. In our models, we have computed $T_e$ from equation (III-10) and used equation (III-12) to set an upper limit on the grid of effective temperatures for which models were computed.

III-4. b. The Interpretation of Prominent Features

All of the models of the major planets exhibit a pronounced increase of temperature with depth. In the absence of internal heat sources, this must be true down to a level where sunlight can no longer penetrate. In the overlying layers, sunlight is absorbed and converted to thermal radiation. That which is not absorbed is scattered into space. However, the presence of a strong opacity at thermal frequencies in the upper layers inhibits the free radiation into space of the thermal radiation. Above the layers where the sunlight is absorbed, such molecules absorb a fraction of the outgoing thermal flux and, upon emission in all directions, cause some of this flux to be directed inwards. Conservation of energy requires that the net flux be constant with depth (in the plane-parallel atmosphere approximation). Therefore, the stronger this "backwarming" is at a given level, the stronger the outward flux is. The energy density, and therefore the temperature,

is proportional to this outward flux. This is the basis for the "greenhouse effect".

The efficiency of the opacity in backwarming the atmosphere will govern the extent to which the atmosphere is heated. In each model, this efficiency may be compared with that for a gray opacity source. To this end, the ratio of the boundary temperature to that for a gray atmosphere of the same effective temperature $T_o/T_{og}$ is tabulated in Table III-1 for each model. In addition, $\bar{\tau}(T_e)$, the Planck mean optical depth at which the temperature equals the effective temperature, is tabulated. Examination of these quantities shows that in all of the $H_2$ or $H_2$-He models the backwarming is less efficient than in the gray case. This is due to the fact that the monochromatic absorption near the flux maxima is less than the mean absorption. Consequently, not as much flux is trapped and the energy density is less than that in the corresponding gray case. This causes smaller boundary temperatures and deeper mean optical depths where the temperature equals the effective temperature.

Table III-1 shows that the most efficient models are those containing He. For these models, the gray values are the most closely approximated. This is due to the fact that the $H_2$-He translational absorption coefficient is stronger than that for the $H_2$-$H_2$ case (see Figures 15 and 16) and is shifted to larger frequencies, thereby filling the gap between the rotational and translational $H_2$-$H_2$ profiles. Therefore, adding He increases the backwarming relative to the gray case. Table III-1 shows that, on the whole, the $H_2$-$H_2$ models become progressively less efficient as the effective temperature is lowered. This is indicated by both

$T_o/T_{og}$ and $\bar{\tau}(T_e)$. This is due to the fact that as the temperature is lowered, the maximum of the Planck curve is shifted into a frequency region where the absorption is progressively less than the mean. This reflects the weakness of the translational absorption coefficient with respect to the rotational case. The least efficient case is given by the Uranus model for which $\bar{\tau}(T_e) = 1.6$, compared to the 0.64 for the gray case. Neptune is slightly more efficient, giving $\bar{\tau}(T_e) = 1.5$. As we have not yet run a model including $NH_3$ to convergence, we cannot give the corresponding numbers for this case. However, the presence of the rotational band in the 20 $cm^{-1}$ to 300 $cm^{-1}$ region means that the effect of adding $NH_3$ will be to increase the backwarming efficiency of the model with respect to the gray case.

Figures 23 and 24 give the emergent monochromatic flux for each model. The dips at 355 $cm^{-1}$ and 590 $cm^{-1}$ are due to the S(0) and S(1) transitions in $H_2$. The relatively large opacity at these frequencies causes the emergent flux to be smaller near these frequencies. Since the total flux must be constant, this causes the flux to be higher at other frequencies. In all the models excluding $NH_3$, the flux appears to have a minimum near 900 $cm^{-1}$. The increase longwards of 900 $cm^{-1}$ eventually reaches a maximum and then declines. It is due to the fact that the opacity in the high-frequency tail of the pressure-induced rotational transition is decreasing faster than the emission from the high-frequency tail of the Planck curves in the lower layers of the atmosphere.

The flux maxima occur near 200 $cm^{-1}$ between the rotational and translational maxima where the absorption is weak and the Planck emission is strong. The effect of adding He is to strengthen

the translational absorption and dilute the rotational absorption. This depresses the maximum and raises the rest of the curve. This is particularly apparent in the case of Neptune. The 9.5 magnitude increase of the flux at 1000 $cm^{-1}$ with the addition of He is due to the fraction of a magnitude decrease at 200 $cm^{-1}$. This is possible quantitatively because the flux at 200 $cm^{-1}$ is 20.5 magnitudes stronger than that at 1000 $cm^{-1}$.

We have seen that the pressure is proportional to the square root of $\tau_s$. This is a consequence of the fact that the pressure-induced absorption is proportional to the square of the density. Another consequence is the presence of a marked stratosphere on each major planet. That is, each model is approximately isothermal up to about one-tenth of an atmosphere pressure or a density of $3 \times 10^{-5}$ $gm/cm^3$. In this region there is a transition zone, below which the temperature increases linearly with physical depth. Therefore, the scale height ($kT/\mu m_p g$) also increases linearly with depth below the transition zone. Increasing the effective temperature has the effect of decreasing the derivative of the scale height with respect to depth. That is, since the pressure at a given mass-level is fixed by the surface gravity, increasing the temperature causes the density to decrease and the atmosphere to swell.

The effect of sublimation equilibrium is to lower the adiabat, thereby raising the altitude of the convection zone. This particularly is apparent in the cases of Uranus and Neptune where the presence of $CH_4$ moves the top of the convective zones from $\overline{\tau}_c = 4$ to 2.3 and from 3.2 to 2.7, respectively.

Figure 25 shows several limb-darkening curves. In the 8 - 14 $\mu$ region, the darkening is very pronounced in the $H_2$ and

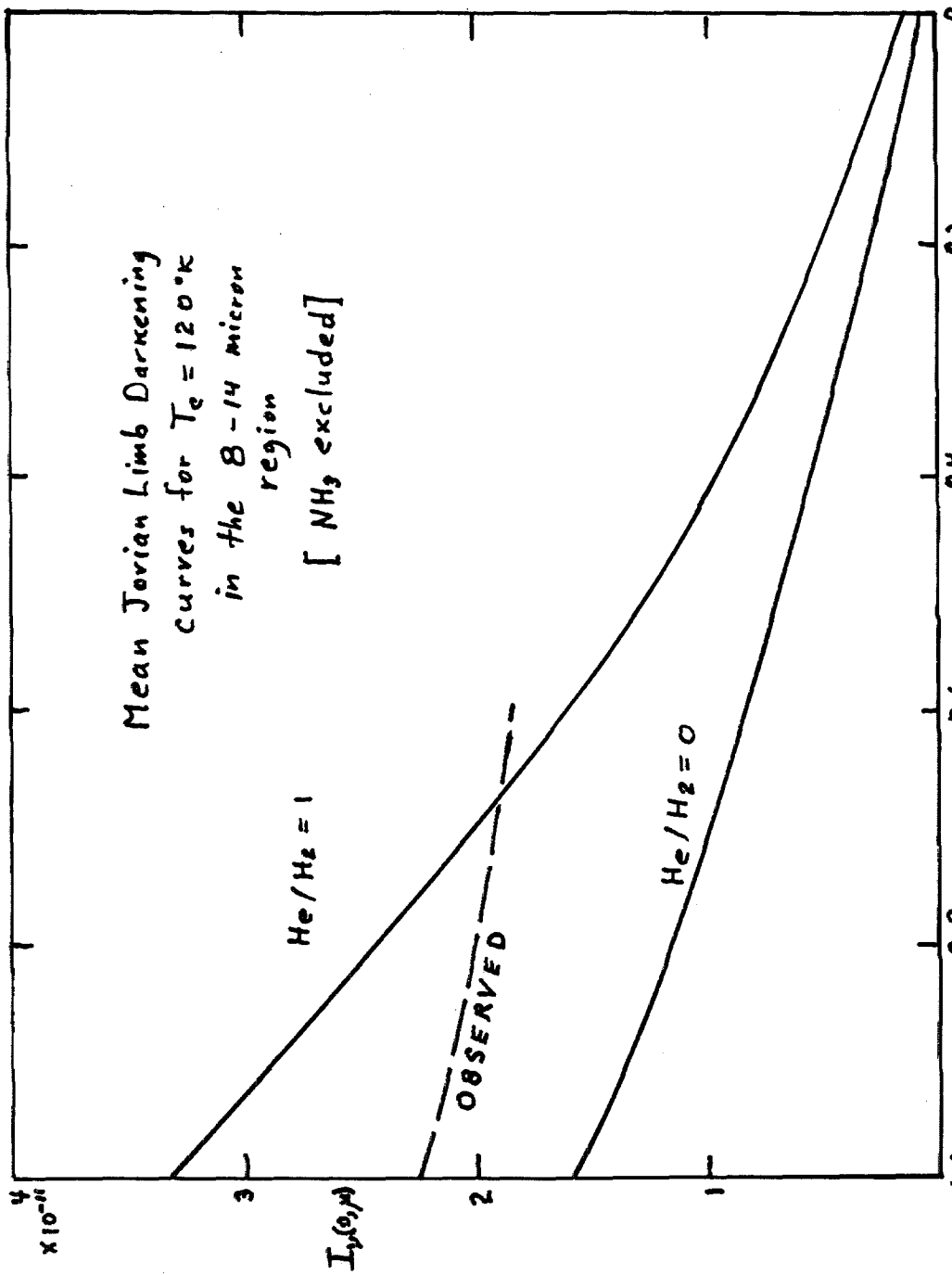
Mean Jovian Limb Darkening
Curves for $T_e = 120°K$
in the 8-14 micron
region
[ $NH_3$ excluded]
$He/H_2 = 1$
OBSERVED
$He/H_2 = 0$
$I_\nu(\theta,\mu)$
$\times 10^{-11}$
4
3
2
1
0
0.2
0.4
0.6
0.8
1.0
$\mu = \cos\theta$

FIG. 25

$H_2$-He models. This reflects the increase of the Planck function with $\tau_V$ for V in this region. In addition, light in this region is coming from the high-frequency tails of the Planck curves. These tails diminish exponentially with increasing frequency and decreasing temperature. The steepness of the limb-darkening curves in this frequency region is due to the fact that the increasing temperature at greater depths causes the Planck function at that depth to "shift" to higher frequencies causing a rapid $B_V(\tau_V)$ variation. The addition of $NH_3$ results in shallower limb-darkening curves because $NH_3$ masks the deeper layers giving a slower $B_V(\tau_V)$ variation in this frequency region.

III-4. c. The Convection Zone

By equating the work done by the bouyancy forces on a rising element of gas to the mean kinetic energy of this element, one obtains (DeMarque 1960)

$$\sqrt{\overline{v^2}} = \sqrt{gH(\nabla - \nabla_A)Q}(\ell/H)/(2\sqrt{2}) \qquad \text{(III-13)}$$

$$F_c = \rho C_p T \bar{v} (\ell/H)(\nabla - \nabla_A)/(2\mu) \, . \qquad \text{(III-14)}$$

In these equations, $\overline{v^2}$ is the mean square velocity of the rising element of gas, $F_c$ is the flux transported by this convective element, H is the scale height, $\ell$ is the length of a typical convective column, $\nabla = d\ln T/d\ln P$ and $\nabla_A$ is the corresponding quantity for the adiabatic lapse rate, g is the surface gravity, $\rho$ is the density, $C_p$ is the specific heat capacity per gm-mole at constant pressure, T is the temperature and Q is given by

$$Q = 1 - \partial \ln \mu / \partial \ln T \Big|_p \qquad \text{(III-15)}$$

where $\mu$ is the mean molecular weight. If we approximate $\bar{v}$ by $\sqrt{\overline{v^2}}$ and insert equation (III-13) into (III-14), we find that

$$\nabla - \nabla_A = \frac{\mu}{T}\left[\frac{32 m_p}{k} \frac{F_c^2}{C_p^2 Q \rho^2} \left(\frac{H}{\ell}\right)^4\right]^{1/3} . \qquad \text{(III-16)}$$

In the models, we neglect the rate of change of the mean molecular weight with respect to T at constant pressure so that Q is on the order of unity. In addition, we assume that the turbulence parameter $\ell$ is on the order of the scale height. We note that the total flux F emitted by the planet must be an upper limit on the convective flux, $F_c$. If we substitute F for $F_c$ and insert values of the physical variables which are typical for planetary atmospheres in equation (III-16); we obtain, for these values, an upper limit for $\nabla - \nabla_A$. In all cases of the major planets, this upper limit is quite small, being about $10^{-4}$. Therefore, we conclude that within the convection zones of the atmospheres of the major planets, we may safely make the approximation that

$$\frac{d\ln T}{d\ln P} = \frac{d\ln T}{d\ln P}\Big|_{ad} . \qquad \text{(III-17)}$$

This result is in contrast with that for stellar atmospheres, where the radiative rather than the adiabatic gradient approximates d1nT/d1nP. The difference is due to the much smaller fluxes in

planetary atmospheres and the larger densities in their convection zones. Equation (III-17) is therefore valid for all planetary atmospheres provided that $\rho$ or Q is not too small within the convection zone.

If equation (III-16) is inserted into equation (III-13), one obtains

$$\sqrt{\overline{v^2}} = \left[\frac{k}{4m_p}\ \frac{F_c Q}{\rho C_p}\ \frac{\ell}{H}\right]^{1/3} . \qquad \text{(III-18)}$$

Again, if $F_c$ is replaced by F and typical values are inserted for the physical variables, equation (III-18) gives an upper limit to the rms velocity for the turbulent element corresponding to these variables. For the same reasons, we find that this velocity also must be small in planetary atmospheres. For example, near the top of the convective zone in the $T_e$ = 120 $^{o}$K Jovian model, the upper limit to the rms convective velocity is 2.0 meters per second (4.5 miles per hour) and becomes smaller at greater depths. The corresponding velocity near the bottom of the earth's atmosphere is, according to equation (III-18), about 6 miles an hour. This is in good agreement with the observed velocities. Equation (III-18) and our models lead us to predict that the turbulent motion in the atmospheres of the major planets should decrease in the progression from Jupiter to Neptune at least as fast as the four-thirds power of the effective temperature. It may be possible to use equation (III-18) with the models of this thesis to determine lower limits on the effective temperatures of the major planets by

observationally studying the turbulent velocities. Since the absorption in the visible region of the spectrum is weak near the top of the convective zone and since the extinction at this level is apt to be due primarily to scattering by solid particles tossed about in the convective zone, such observations may be feasible.

We are now in a position to check the validity of the models in the convective regions. Equation (III-17) can be reduced to quadrature:

$$\log P = \log P_c + 0.4343 \int_{T_c}^{T} \frac{dT}{T \nabla_A} \qquad \text{(III-19)}$$

where $\nabla_A$ is given by equations (II-30) and (II-32). $P_c$ and $T_c$ are the values at the top of the convection zone. Inverting the equation of hydrostatic equilibrium, we obtain

$$\tau_s = \tau_c + \frac{\alpha_1^2}{\mu g m_p c k} \int_{T_c}^{T} \left(\frac{P}{T}\right)^2 \frac{(A_s + B_s \alpha_2/\alpha_1)}{\nabla_A} dT \qquad \text{(III-20)}$$

where $\tau_c$ is the value at the top of the convective zone. Obtaining P/T from the solution of equation (III-19), the integrand of equation (III-20) is known as a function of temperature and can be integrated numerically to give $\tau_s(T)$ in the convective region. The other physical variables follow directly from these solutions. The correction to logP(T) for the four planets, together with the radiative equilibrium solutions, are plotted in Figures 26 and 27.

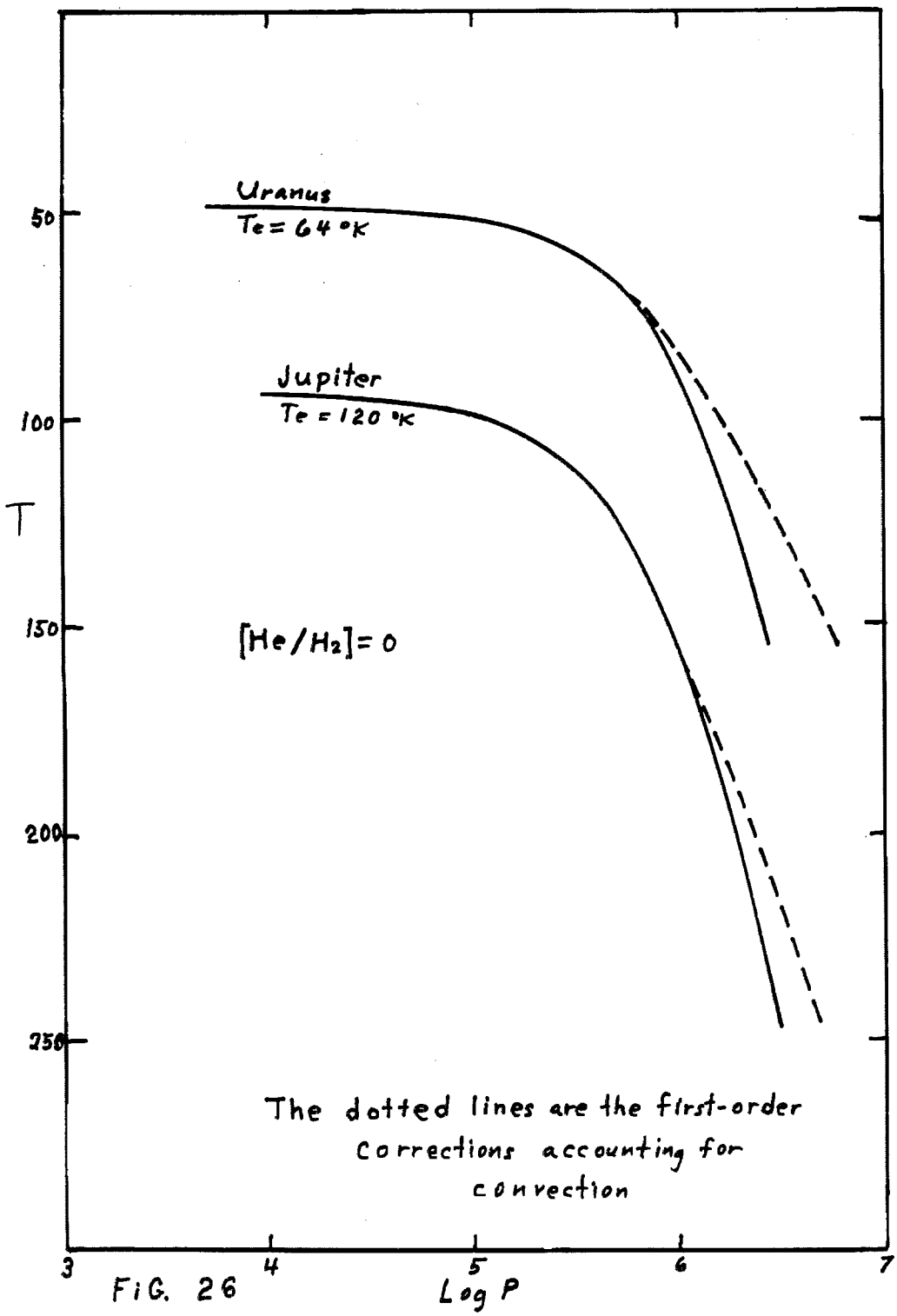
Uranus
Te = 64 °K
Jupiter
Te = 120 °K
[He/H2] = 0
T
50
100
150
200
250
3
4
5
6
7
Log P
The dotted lines are the first-order corrections accounting for convection

FIG. 26

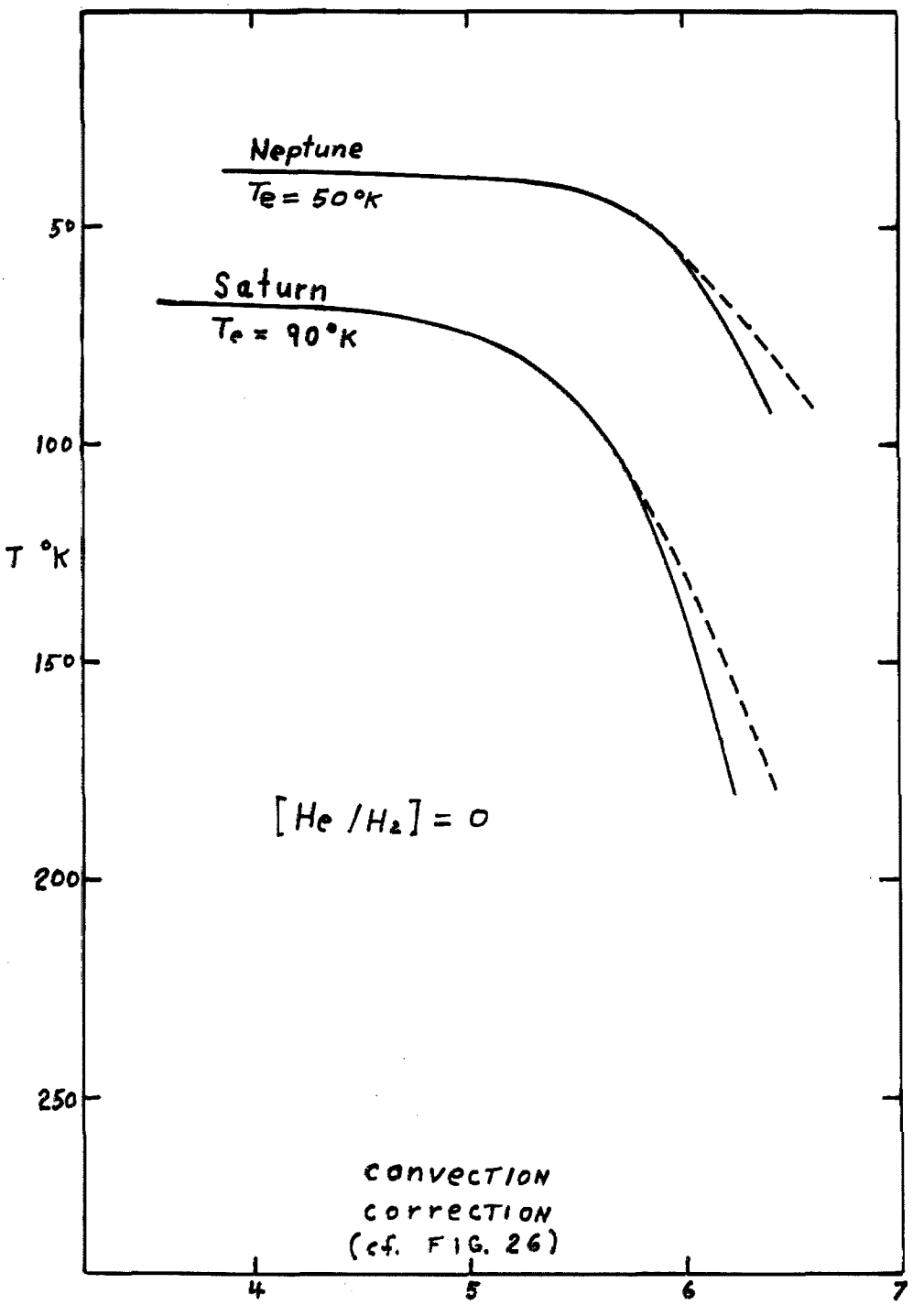
Neptune
$T_e = 50°K$
Saturn
$T_e = 90°K$
50
100
150
200
250
T °K
$[He/H_2] = 0$
convection
correction
(cf. FIG. 26)
4
5
6
7
log P

FIG. 27

As these figures show, the correction deep in the atmosphere can be quite large.

The tops of the convection zones depend on the $NH_3$ and $CH_4$ relative abundances by number. The upper limits of these abundances are given for each model in Table III-2. If the gas is

TABLE III-2

The Adopted Values of the Relative Abundances of $NH_3$ and $CH_4$

| Planet | $NH_3/H_2$ | $CH_4/H_2$ |
|---|---|---|
| Jupiter | 0.0002 | 0.003 |
| Saturn | 0.0002 | 0.006 |
| Uranus | 0 | 0.01 |
| Neptune | 0 | 0.01 |

saturated, then its saturation vapor pressure instead of the value in Table III-2 determines its relative abundance. The values in this table fix the level at which saturation ends. The models in Figures 26 and 27 were computed using the values in this table.

In the above fashion, we have accounted for convection. However, the correction is still a "first order" one because it is evident that the solution in the radiative equilibrium zone will be affected by the correction in the convective zone. A given layer in the radiative zone will receive a smaller contribution from the source function in the convective zone. Therefore, our correction has the effect of destroying radiative equilibrium in the radiative

zone and we must alter the temperature distribution in this zone until radiative equilibrium is again achieved. In general, the top of the convection zone will occur at a different level after this correction, so that we must also alter the solution in the convection zone. We repeat this process until it converges to the final temperature distribution before getting models which are valid in both the radiative and convective zones. We have not extended the calculations to this point. However, we point out that in all of the models, the top of the convection zone lies below a Planck mean optical depth of 2.2 and lies below 3.4 for five of the models. Therefore, the actual solutions in the upper radiative zones must be approximated reasonably well by the present radiative solutions.

III-4.d. The Effect of $NH_3$ on the Jovian Thermal Opacity

The effect of adding $NH_3$ to the thermal opacity is to increase the efficiency of the backwarming process. As a result, the temperature and radiative gradient of a given zone will increase. Also, the top of the convection zone will rise. Table III-1 shows the temperatures and Planck mean optical depths at the top of this zone in the models. The height of this zone was computed on the basis of an adiabatic gradient which included saturated $NH_3$ (in the Jovian and Saturnian models) but for a radiative gradient which excluded the opacity due to this $NH_3$. The result therefore gives a lower limit on this height.

We assume that the Jovian $NH_3$ is saturated until the temperature is high enough so that the $NH_3/H_2$ ratio is 0.0002. At deeper levels, we assume the mixing ratio of $NH_3$ to be a constant. Because of the low saturation vapor pressure of $NH_3$ at low temperatures, the partial pressure of $NH_3$ in the upper part of the

Jovian atmosphere (above the 115 $^{o}$K level) may be neglected. Therefore, it is not necessary for $NH_3$ to be saturated above this region. As a consequence, we side-step the question of whether the $NH_3$ crystals go high enough into the radiative portion of the atmosphere to maintain saturation there. If $NH_3$ were saturated throughout all of the layers of the $T_e$ = 120 $^{o}$K $H_2$ model, 7 meter-atm of $NH_3$ would be traversed by the time the 160 $^{o}$K level was penetrated. Our adopted upper limit to the $NH_3/H_2$ ratio causes saturation to end at the 148 $^{o}$K level, which underlies 100 cm-atm of $NH_3$, and lowers the level underlying 7 meter-atm of $NH_3$ to the 230 $^{o}$K level, which underlies 73 km-atm of $H_2$. To refine the 0.0002 figure, it is necessary to know the effective depth of penetration of light from the $\lambda$6470 band of $NH_3$ and whether the 7 meter-atm figure for the $NH_3$ abundance, which was obtained from the strength of this band, is itself reliable.

In the $T_e$ = 120 $^{o}$K model under consideration, the top of the convection zone occurs at a temperature of 140 $^{o}$K, a mean optical depth due to $H_2$ of 2.9 and at the bottom of a 17 cm-atm column of $NH_3$. Only 0.2 cm-atm of $NH_3$ overlies the 120 $^{o}$K level so that most of the $NH_3$ in the radiative portion of this model occurs in the zone between the 120 and 140 $^{o}$K levels. At the 120 $^{o}$K level, the Planck mean optical depth due to $H_2$ is about 0.94. According to section I-8, the mean optical depths, due only to $NH_3$, of the 140 $^{o}$K and 120 $^{o}$K layers are approximately given by $\bar{\tau}$ = 0.65 C and 0.05 C, respectively, where C is plotted in Figure 17 as a function of frequency. These values are overestimates since the temperature of the bottom layer was assumed constant throughout the path in their calculation. Very approximately, the corresponding Planck

means of these $NH_3$ optical depths are 0.3 and 0.02, respectively. When compared with the corresponding Planck means for $H_2$ alone (2.9 and 0.9, respectively), we see that the opacity due to $NH_3$ plays only a minor role in the radiative portion of the $T_e = 120\ ^oK$ $H_2$ Jovian model. If the effective temperature is lowered, this role becomes vanishingly small. If He is added, this role increases, because the convective zone is lowered.

The opacity of $NH_3$ in the convective zone cannot be ignored, because it may be important in determining the frequency distribution of the flux emerging from this zone. If the $NH_3$ were saturated right down to the 160 $^oK$ level (corresponding to a 7 meter-atm path length), the Planck mean optical depth of this layer due to $NH_3$ would be about 0.8, according to our rough band model, and this is still quite smaller than the value of 5.5 due to $H_2$ alone. However, the monochromatic $H_2$ absorption is weak at frequencies near the maximum of the Planck curve, varying from 1 to 5 between 200 $cm^{-1}$ and 300 $cm^{-1}$ at this level. On the other hand, the monochromatic $NH_3$ absorption in this region is stronger than the mean, being about 1.7 near its maximum. Consequently, the presence of $NH_3$ can alter the emergent flux, change the depth of the convection zone and alter the temperature in the radiative zone even though it may be operating only in the convective zone. However, because of the relative weakness of the $NH_3$ mean opacity compared to that of $H_2$, the most noticeable change would probably be in the redistribution of the emergent flux.

### III-4. e. Phase Equilibrium, Mist Levels, Cloud Levels and Precipitation Zones

When $NH_3$ or $CH_4$ is in equilibrium with either the solid or liquid phase, the vapor pressure is a function only of the local temperature. We refer to this situation as phase equilibrium. Under this circumstance, the vapor pressure cannot exceed its saturation value.

It is likely that either $NH_3$ or $CH_4$ is saturated in the upper atmospheres of the major planets, at least in the zones where its density may not be neglected. In these cases, the partial pressure depends only on the temperature (provided mixing is negligible). This temperature dependence is not necessarily that given by the solution of the hydrostatic equilibrium equation. Therefore, one cannot, in general, have phase equilibrium and hydrostatic equilibrium simultaneously. For this reason, if $NH_3$ or $CH_4$ is initially distributed in the atmosphere according to the saturation vapor pressure, it will not be in hydrostatic equilibrium. Because the pressure increases more slowly with temperature in the case of hydrostatic equilibrium than it does in the case of phase equilibrium (below the isothermal stratosphere), this distribution will tend toward hydrostatic equilibrium. In the process, elements of the saturated gas will rise to higher levels where they become super-saturated and unstable towards phase equilibrium. As a result, the gas will condense and fall to deeper, warmer and unsaturated layers where it will vaporize and replenish the supply of the gas at the lower levels. Thus, a cyclic process occurs in the upper troposphere whereby continuous $NH_3$ or $CH_4$ "rain" or "snow" precipitation may occur, even above the "convection zone" referred

to in the previous sections. This process also transfers heat, not only by the mass movement of the saturated gas, but also by the fact that as the gas condenses in the upper levels, it releases its "heat of condensation" and as the precipitate vaporizes in the lower levels, it acquires the "heat of vaporization". Again, the total flux transported must be less than that emitted by the planet. This sets an upper limit to the activity in the precipitation areas which becomes progressively more restrictive as the effective temperature is lowered. In addition to heat transport, this cyclic process could help to mix the atmospheric constituents in the radiative zone.

In the convection zone, there tends to be strong mixing of the $CH_4$ and $NH_3$ with the $H_2$ and He because changes are too fast to allow phase or hydrostatic equilibrium to take place. Therefore, in the absence of saturation, their mixing ratios in this zone should be constant with depth. At the level where saturation begins, the strong upward currents will cause condensation and precipitation. From this level to the top of the convection zone, there should be solid or liquid precipitation so that this zone should define the cloud layers. The precipitation will extend into the unsaturated zone to a depth where vaporization occurs (cf. Figure 28).

The storm activity in the convective zone should be stronger than that in the cyclic cells of the radiative zone because of the strong turbulence and greater saturation vapor pressure. On the other hand, because of the relatively long time scale of the equilibrium process in the radiative zone, the activity in the cyclic cells is comparatively weak. Therefore, the convection zone is probably responsible for the observed clouds and storm activity

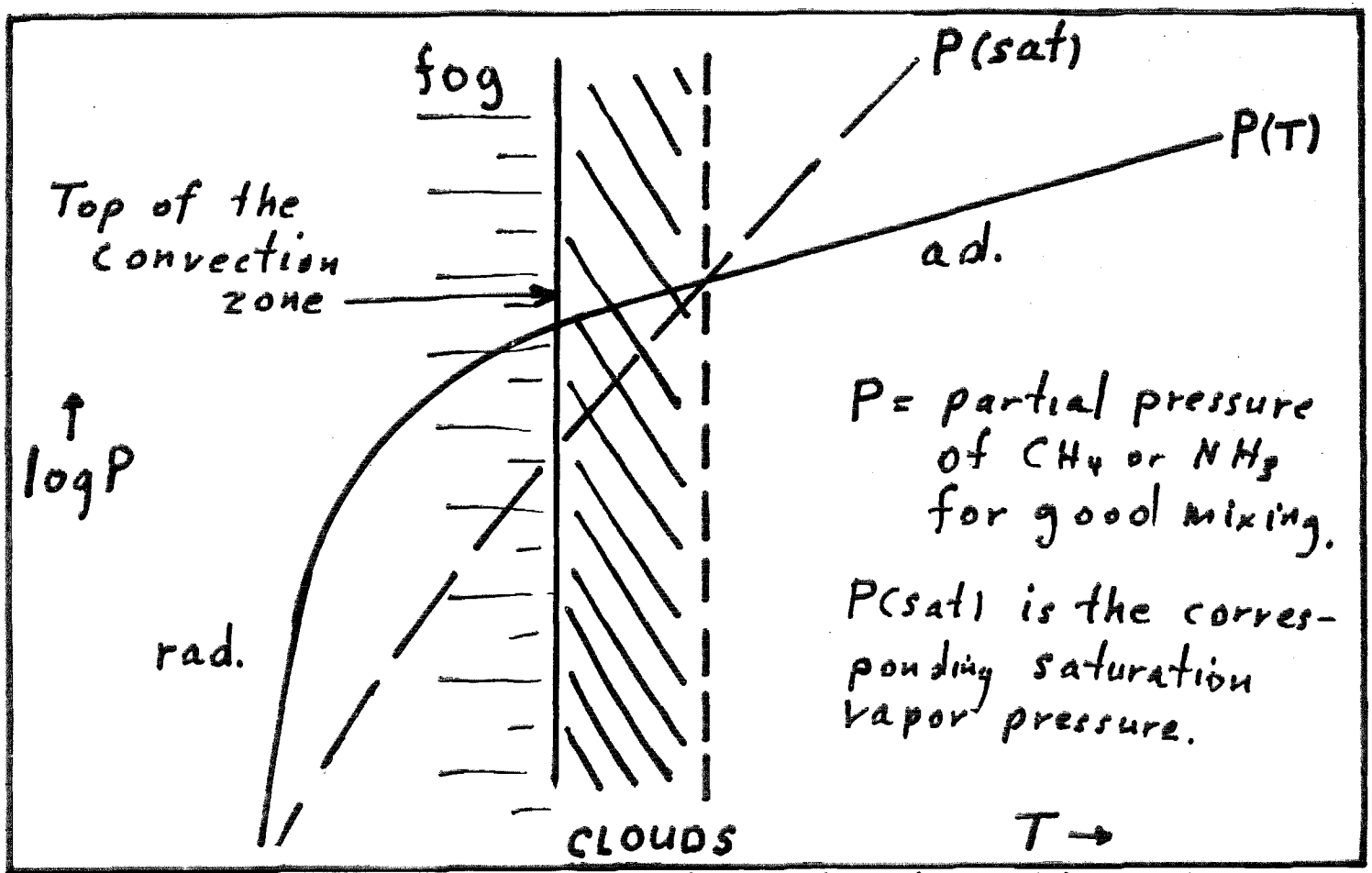


FIG. 28 Schematic Planetary Atmosphere

whereas the cyclic cells probably give rise to a relatively thin ice mist of the frozen vapor or a tenuous fog of the liquified vapor. Both $NH_3$ and $CH_4$ are crystalline substances in the solid state and should give rise to weather phenomena with much the same physics as occurs with $H_2O$ in the Earth's atmosphere. In cases where the convection zone is unsaturated, violent storm activity should be absent, but there still may be a visible mist zone if the density in the saturated region is high enough. Table III-3 gives the positions of the mist or cloud layers for the adopted

TABLE III-3

| | | | | $NH_3$ | | $CH_4$ | | Con- |
|---|---|---|---|---|---|---|---|---|
| Planet | $T_e$ | $He/H_2$ | $T_c$ | $T_{sat}$ | $\log P_{sat}$ | $T_{sat}$ | $\log P_{sat}$ | vective Clouds? |
| Jupiter | 130 | 0 | 149 | 143 | 2.07 | - | - | none |
| | 120 | 0 | 139 | 146 | 2.21 | - | - | $NH_3$ |
| | 120 | 1 | 158 | 145 | 2.15 | - | - | none |
| | 110 | 0 | 131 | 148 | 2.33 | - | - | $NH_3$ |
| Saturn | 100 | 0 | 118 | (146) | (2.23) | - | - | ($NH_3$) |
| | 90 | 0 | 105 | (149) | (2.35) | marginal | | ($NH_3$) |
| | 80 | 0 | 91 | (151) | (2.48) | 71 | 3.04 | ($NH_3$) |
| Uranus | 64 | 0 | 76 | - | - | 76 | 3.91 | $CH_4$ |
| Neptune | 50 | 0 | 52 | - | - | 82 | 4.46 | $CH_4$ |
| | 50 | 1 | 61 | - | - | about same | | $CH_4$ |

$NH_3$ and $CH_4$ densities of the models. As there is doubt whether $NH_3$ exists on Saturn, the $NH_3$ values in this case are enclosed in parentheses. These $NH_3$ values for Saturn were computed neglecting the correction for convection. In the other cases, this correction was taken into account, if it mattered. The last column indicates whether the model contains a saturated region in the convection zone.

Note that the Saturnian models have no $CH_4$ cloud zone but will have a deep $NH_3$ cloud zone if $NH_3$ is sufficiently abundant. The $T_e = 80\ ^{o}K$ model shows the presence of a high $CH_4$ mist zone. If the rings are sufficiently tilted, the effective temperature might be low enough so that such a mist could extend to low latitudes. If this is the case, then it might be possible to detect this mist by polarization measurements or satellite eclipse observations. Detection of the mist would yield information on the effective temperature of Saturn. In the $T_e = 80\ ^{o}K$ model, this mist level lies about 35 km above the top of the convection zone and about 75 km above the $NH_3$ mist and cloud zone, if the latter exists.

Note that the Uranus and Neptune models all have a $CH_4$ cloud zone. Also, note that the existence of an $NH_3$ cloud zone in the Jovian models depends on the $He/H_2$ ratio and the effective temperature. In these models, the thermal opacity of $NH_3$ was ignored. However, we recall that one effect of adding the $NH_3$ thermal opacity is to raise the convection zone. This may cause even the $T_e = 120\ ^{o}K$ $H_2$-He model to have a cloud zone.

# PART IV

## COMPARISON WITH THE OBSERVATIONS

The existing observations indicate the presence of a significant amount of backwarming in the atmosphere of each major planet. For example, Jupiter exhibits limb darkening in the radiometric (8 to 14 μ) region (Murray, Wildey and Westphal 1964). In the 8 to 14 μ region, Low (1964) obtains a brightness temperature of $93 \pm 3$ $^{o}$K for Saturn. Kellermann (1965) finds unpolarized radiation with greater brightness temperatures in the 6 to 20 cm region. Due to the lack of polarization, he interprets the radiation as being of thermal origin (It should be noted, however, that Rose, Bologna and Slonaker (1963) reported that the 10 cm radiation from Saturn was observed to be polarized). The differences in the brightness temperatures can be explained by the existence of a thermal opacity which varies with frequency so that at different frequencies, one sees contributions from layers of different temperatures. The very presence of strong $CH_4$ bands on Uranus and Neptune is evidence that there is an efficient backwarming process in operation. This conclusion is due to the fact that $CH_4$ solidifies at 90 $^{o}$K and its saturation vapor pressure decreases very rapidly below this temperature. Kuiper (1952) finds 2.3 and 3.7 km-atm of $CH_4$ on Uranus and Neptune, respectively. To support such columns of $CH_4$, the partial pressure of this gas at the base would have to be greater than the saturation vapor pressure of $CH_4$ at 95 $^{o}$K. This temperature significantly exceeds the rotating blackbody temperatures of Uranus and Neptune, which are 64 $^{o}$K and 50 $^{o}$K, respectively. Therefore, in the absence of the backwarming

of planetary radiation (regardless of origin), the base of this column cannot be in phase equilibrium and will freeze out leaving a $CH_4$ abundance which is significantly less than that observed.

In addition, the observation of the presence of $CH_4$ in the atmospheres of all the major planets indicates that in each of these planets, convection cannot occur to very great depths. This puts a restriction on either the magnitude of the thermal flux which may be due to any internal heat source or the depth of the atmosphere. Wildt (1958) pointed out that "An adiabatic temperature gradient persisting over any large depth below the cloud level is clearly impossible because high temperatures would be reached very soon. Methane would then be destroyed irreversibly, and convective exchange with the atmosphere above the clouds would long ago have deprived it of all methane, which is so prominent a spectroscopic feature of all the giant planets. There remains the possibility of a sub-adiabatic temperature gradient extending to great depths". Our models show that backwarming is indeed important in the atmospheres of all the major planets and that convection is indeed attained in the upper portion of the atmospheres. However, at depths below the layers where solar light penetrates, we expect, in the absence of an internal heat source, convection to cease and the temperature to tend to a constant value. This is compatible with the observation of $CH_4$. If there is an internal heat source, then the observations require it to be sufficiently weak so that convection does not occur in the high temperature regions, making exchange with the upper atmosphere efficient. If convection occurs, then the atmosphere must not be so deep that high temperatures are reached. A solid surface must then exist below the atmosphere and lie at a relatively shallow depth.

The presence of $H_2$ in the atmospheres of the major planets has been detected by the observation of the vibrational overtones of the quadrupole and pressure-induced dipole lines. The S(0), S(1), S(2) and Q(1) quadrupole lines of the (3-0) band and the S(0) and S(1) quadrupole lines of the (4-0) band have been observed on Jupiter by Kiess, Corliss and Kiess (1960) and Spinrad and Trafton (1963). Münch and Spinrad (1963) have detected the S(0) and S(1) quadrupole lines of the (4-0) band in the Saturnian spectrum and Spinrad and Trafton (1963) have detected the corresponding S(0) line on Uranus. Herzberg (1952) has detected the pressure-induced S(0) line of the (3-0) transition and Spinrad (1963) has observed the corresponding (4-0) line in the atmosphere of Uranus and Neptune. Contamination of the spectral region with $CH_4$ absorption makes the detection of the other rotational transitions of the pressure-induced spectrum, including the double transitions, rather difficult.

In an attempt to obtain quantitative data on the pressure-induced lines for the purpose of evaluating some of the free parameters of our models, such as the $He/H_2$ ratio, we have investigated the (3-0) and (4-0) regions of the spectrum observationally for all of the major planets. However, these data must wait for laboratory comparisons of absorption in $H_2$-He mixtures at low temperatures in the λ6420 region. The (3-0) region at λ8270 is contaminated with $CH_4$ making the results of such a comparison less accurate. We describe, briefly, the manner in which the observations were obtained.

We used high contrast-fine grain IV-N Eastman Kodak spectroscopic plates and the medium-dispersion B spectrograph

with the 1.5" (solid block) and 3" schmidt cameras. Observations were made from the Newtonian foci of the 100" and 60" telescopes of the Mount Wilson Observatory. The OG or K2 filter was used to remove the higher order spectra. In the cases of Jupiter and Saturn, the Whitford screens were used to reduce the intensity without the loss of definition which occurs when screens are used in the collimated beam of the spectrograph. The low dispersion was necessary in order to make the pressure-induced features visible (their half-width is about 40 Angstroms).

To offset the long exposure times needed for the λ5500-λ8800 sensitive IV-N plates, these plates were ammoniated prior to exposure. This process decreased the exposure time required by about a factor of 15. After exposure, the plates were developed for 8 minutes in D-19 with continual agitation. If the plates were developed soon after exposure, there was no problem with fogging. Figures 30, 31 and 32 show representative spectra of the major planets in the (4-0) region.

At a dispersion of 700Å/mm, the λ6420 line (S(0)) of the (4-0) pressure-induced line was easily detectable on the Uranus and Neptune plates. On Jupiter, the presence of the λ6470 $NH_3$ band prevents us from seeing this line in the Jovian spectrum. We examined a high-dispersion Coude plate of this region, but the $NH_3$ lines are so numerous, that the continuous pressure-induced feature could not be seen, even on a compressed wavelength scale. The presence of $CH_4$ bands prevents us from identifying neighboring pressure-induced lines. In Saturn, there is some question about the presence of $NH_3$ above the cloud level. Dunham (1934) observed a "trace" of $NH_3$ on Saturn, but the stronger λ7900 band

was photometrically examined and found to be absent (Münch 1965).

Several Saturnian spectra show the presence of an absorption near λ6420 which is stronger than that of the spectra of Titan (see Figure 31). If this is not due to $NH_3$, then it must be due to $H_2$ as the Titan spectra show that $H_2O$ vapor absorption in the Earth's atmosphere cannot be responsible. At any rate, the Saturn feature is weaker than either the Uranus or Neptune features. The half-width of the pressure-induced line varies as the square root of the temperature so that the line would be more difficult to detect at higher temperatures. However, the weakness of this line may also be due to an abundance rather than a temperature effect. It would suggest that the path length of $H_2$ was shorter on Saturn than on Uranus or Neptune (due possibly to the presence of a higher cloud layer). As the theory of line strengths for the higher vibrational overtones is at present inadequate for obtaining quantitative estimates of the amount of $H_2$ above the cloud layers of the planets, we must resort to laboratory comparisons. Herzberg (1952) found that 120 meters of a 3 : 1 mixture of He and $H_2$ at 100 atm pressure and 78 $^{o}$K best fitted the (3-0) absorption in the spectra of Uranus and Neptune. The temperature is based on the observed half-width of the S(0) line at λ8270. To compare with Herzberg's results, we examine the 78 $^{o}$K levels of our Uranus and Neptune models. We square the local pressure and multiply it by the number of km-atm of $H_2$ and compare the result with 75, which is the laboratory value corresponding to the absorption due only to $H_2$ if that due to He can be neglected in comparison (if not, then 75 is an upper limit). On this basis, the pure $H_2$ Neptune model can be ruled out since it

gives a product equal to 325, far in excess of the value, 75. The 1 : 1 He-$H_2$ model gives a product equal to 46, and therefore cannot be ruled out. Also, the $H_2$ Uranus model gives a value equal to 39 and cannot be ruled out. The only basis thus far for ruling out the $H_2$ Uranus model is the observed 3 : 1 He-$H_2$ ratio. We have not computed such a model but it seems likely that it will give a product less than 75. Herzberg claims that the temperature 78 $^{o}$K may be an underestimate, but he does not believe it to be an overestimate. Increasing this temperature will have the effect of improving the agreement between our models and the observations. Because of the blending due to neighboring $CH_4$ bands, it does not seem very wise to put much emphasis on this laboratory comparison, except to note the general overall compatibility between the $H_2$-He models of Uranus and Neptune and the observations. However, we note that the lowest visible layer in the frequency of the S(0) line of the (3-0) band of $H_2$ is below the top of the convection zone in all of the computed models. Adding He to the models has the observed effect of lowering the top of the convection zone. This may be another argument for a He/$H_2$ ratio greater than unity since we expect the top of the cloud layer to be associated with the top of the convection zone. Since laboratory data for the (4-0) pressure-induced band do not yet exist, we cannot make a comparison of this band with the laboratory spectra.

Spinrad and Trafton (1963) estimate that 27 km-atm of $H_2$ exists above the Jovian cloud level on the basis of the strengths of the S(0) and S(1) quadrupole lines of the (3-0) band, assuming that these lines are not saturated. Foltz and Rank (1963) claim that this figure could be as high as 270 km-atm if the lines are

saturated. Field (1965) has reviewed the problem and shown that all data are consistent with 30 to 80 km-atm of $H_2$ but that the absence of strong Rayleigh scattering at 0.4 μ indicates that 30 km-atm is the most likely value for Jupiter. This is in excellent agreement with the amount of $H_2$ found above the convection zone in our $H_2$ and $H_2$-He models (see Table III-1). It would appear that the amounts of $H_2$ required to cause convection in the atmospheres of the major planets, as evidenced by our models, is quite compatible with the amounts of $H_2$ observed above their cloud layers. It thus appears that the top of the cloud layer and the top of the convection zone are correlated in the atmospheres of the major planets. As it is well known, this is indeed the case in the Earth's atmosphere.

The cloud layer on Uranus and Neptune is presumably due to the convective movement of saturated $CH_4$ while the Jovian cloud layer is due to the convective movement of saturated $NH_3$. The cloud layer of Saturn is more of a mystery since $NH_3$ is not observed and $CH_4$ is likely to condense only in the upper part of the radiative portion of its atmosphere. The $CH_4/H_2$ ratios used in the models were computed using Kuiper's observed $CH_4$ abundances (1952) and estimates of the amount of $H_2$ above the cloud layer. These ratios were applicable only where $CH_4$ was not saturated. In the saturated layers, the equilibrium vapor pressure determined the value of this ratio.

Baum and Code (1953) determined the scale height of the Jovian stratosphere by means of observing the differential refraction during the occultation of σ-Arietis. They find that it is unlikely that this scale height is greater than 12.5 km or less than

8.3 km. It appears that a value around 9.5 km would be close to the actual value. They assume that the region of the atmosphere responsible for the diminution is isothermal. As the extinction is small in this region, our models indicate that this is likely to be true. The range of mean molecular weights and boundary temperatures compatible with the occultation observations are presented in Figure 29 along with the points corresponding to our models. Right away, it is apparent that the $H_2$ models with boundary temperature $T_0$ greater than about 80 $^{o}$K can be ruled out. This corresponds to $H_2$ models for which $T_e$ is greater than about 102 $^{o}$K.

We now attempt to fix a likely range for the effective temperature on the basis of a rough consideration of the Bond albedo and the observed geometric albedo, assuming no internal heat source.

The Bond albedo (equation III-9) depends on the value of the phase integral. This phase integral, in turn, depends on the particle phase function, $\Phi$. If this phase function varies as

$$\Phi = \bar{\omega}_0(1 + bf(a)) \qquad \text{(IV-1)}$$

where f(a) is antisymmetric about $a = \pi/2$, then the phase integral does not depend upon the value of b. It then equals $2\bar{\omega}_0$. Various forms of $\Phi$ have been investigated from the limb darkening observations in the visual region of the spectrum (Horak 1950; Anderson 1965). A common form is one in which $f(a) = \cos a$ and $\bar{\omega}_0$ is the particle albedo. The particle albedo is observed to vary considerably with wavelength in the visual region, as does the geometric albedo. The resulting Bond albedo must be averaged over wavelength with the

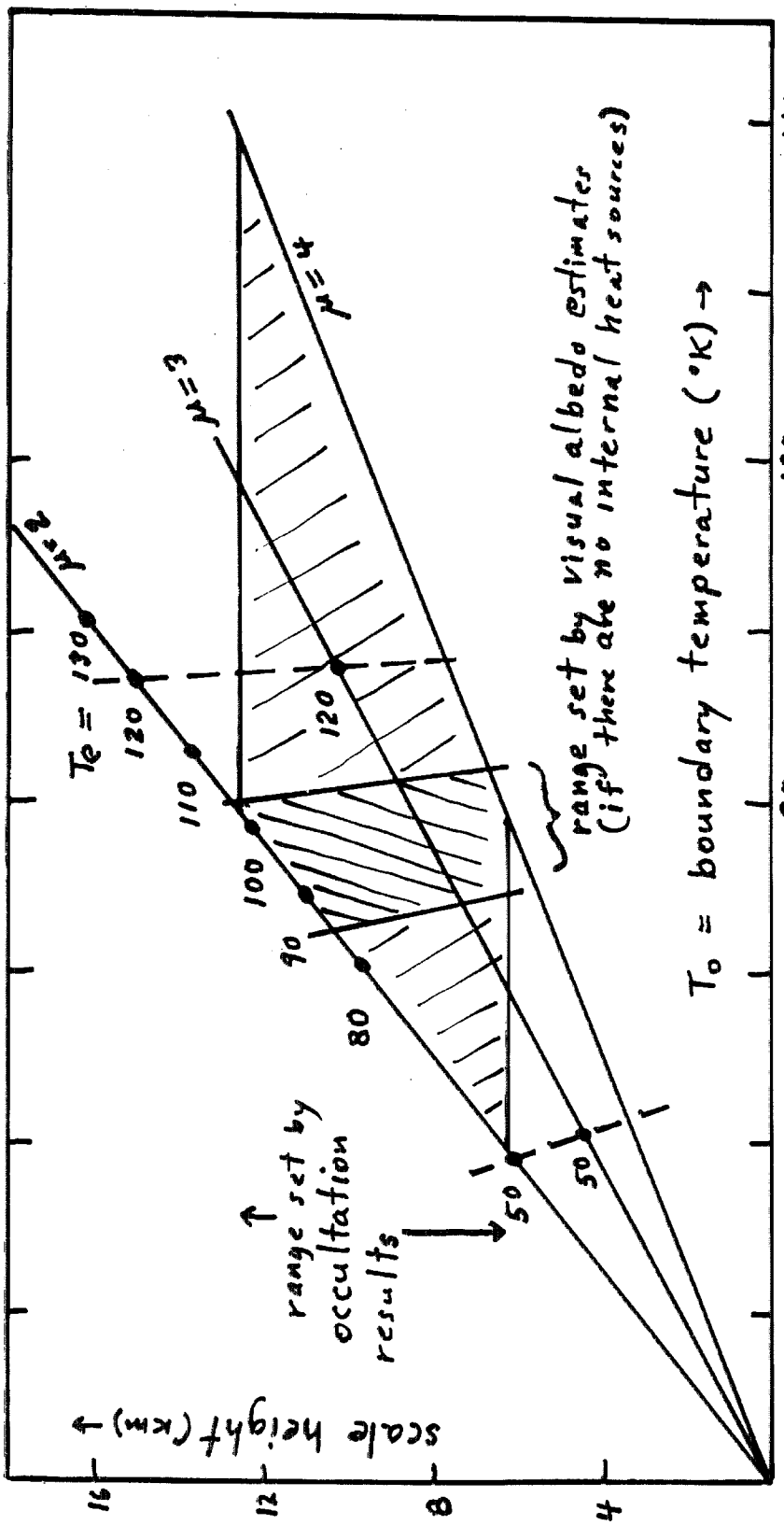


FIG. 29 The Models vs. the Observations

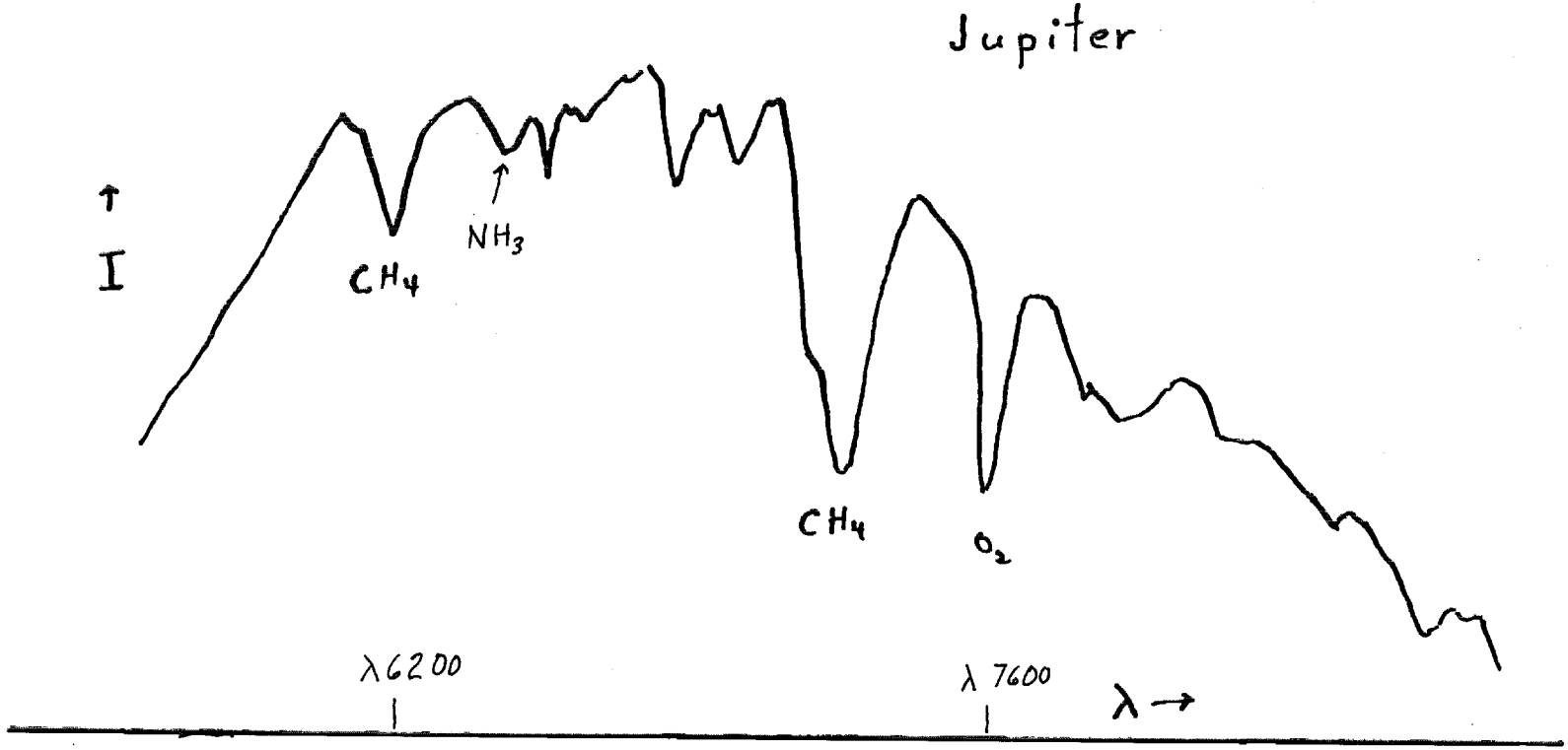


FIG. 30

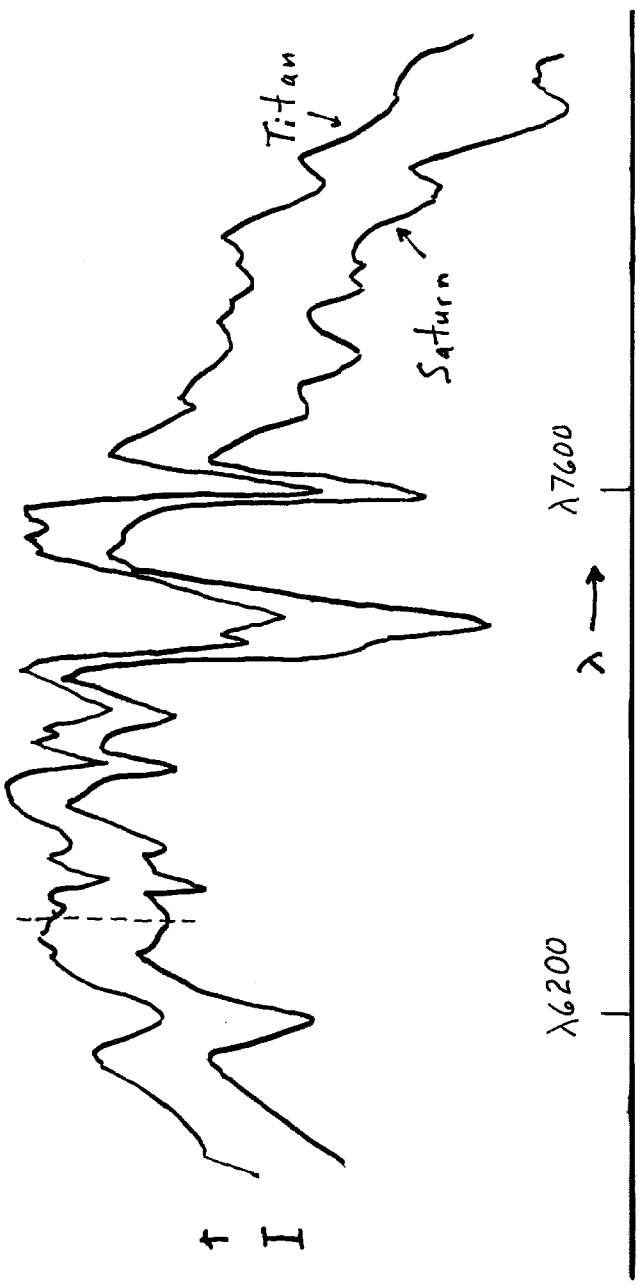


FIG. 31

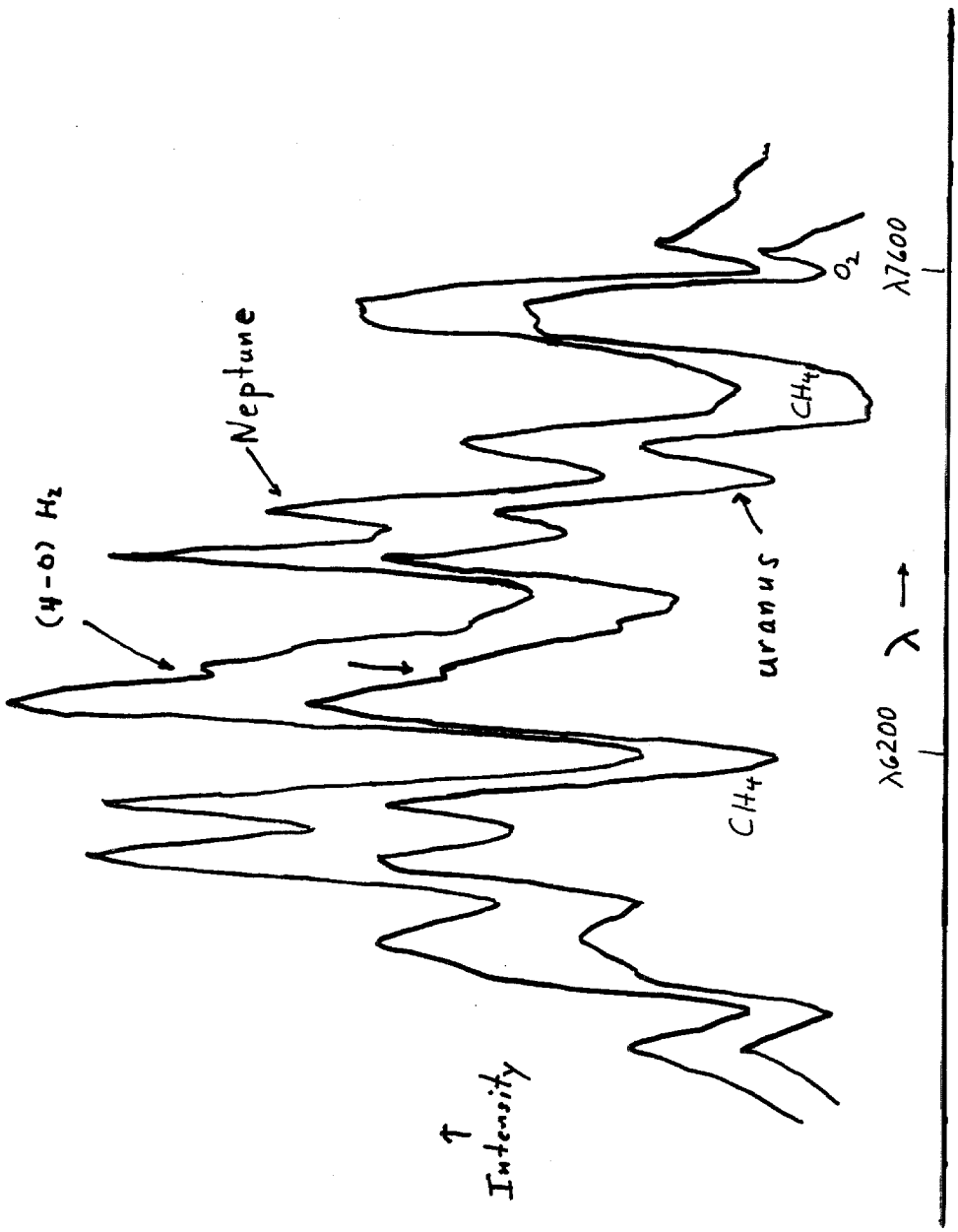


Fig. 32

solar spectrum as the weighting function in order to yield the effective temperature. This average is not well known, but it appears likely that it is less than the Jovian visual Bond albedo obtained by Harris (1961) of 0.73. As a result, the Jovian effective temperature is probably greater than the 85 $^{o}$K value implied by this albedo. If $\bar{\omega}_o$ is greater than 0.65 and the mean geometric albedo is greater than 0.35 (which seems quite likely), then an upper limit to the Jovian effective temperature is 104 $^{o}$K. When converted to $T_o$, this region is shown on Figure 29.

We now consider the Jovian limb darkening in the 8 to 14 $\mu$ region. Figure 25 shows several limb darkening curves for the $H_2$ and $H_2$-He models along with the observed limb darkening. These models always give a limb darkening which is too steep. We conclude that the limb darkening is due to another molecule. Methane is excluded because its absorption at frequencies less than 1200 $cm^{-1}$ is negligible. On the other hand, $NH_3$ has a strong absorption band in the 9 to 13 $\mu$ region. As we will see, this band is responsible for the shallowness of the observed limb darkening profile.

From the analysis of section I-8, we found that the mean "optical depth" of an $NH_3$ band, averaged over the rotational structure, varied as the square root of the path length. If we perform the corresponding average of $I_\nu(0,\mu)$, defined by equation (II-20), we obtain

$$\bar{I}_\nu(0,\mu) = \int_0^\infty B_\nu(\bar{\tau}) \exp(-\bar{\tau}/\sqrt{\mu}) d\bar{\tau}/\sqrt{\mu} \qquad \text{(IV-2)}$$

for the limb darkening due to $NH_3$ alone. Using the temperature and pressure distributions of the $T_e = 120\ ^{o}K$, $H_2$ and $H_2$-He models, several limb darkening curves in the 10 to 13 $\mu$ region were computed neglecting the contribution of $H_2$ and He and normalizing so that $\bar{I}_\nu(0, 1)$ equaled the observed value. It was found that in all cases, the slopes of these curves were even shallower than the observed slope. Since the slopes in the models excluding $NH_3$ are all significantly steeper than the observed slope (when normalized as above), we conclude that the observed slope can be represented by a model containing the proper ratios of $H_2$, He and $NH_3$. Since the form of the absorption due to He in this frequency region is like that for $H_2$, the main effect of varying the $He/H_2$ ratio is to alter the importance of the role played by $NH_3$ in determining the slope of the limb darkening curve in the 8 to 14 $\mu$ region.

Because of the approximations often required in making analytical estimates, it is sometimes more convincing to make a more exact, but numerical, estimate. This is the case when we attempt to estimate the $He/H_2$ ratio and $T_o$ from the observed limb darkening and other data. It would be better to compute a finer grid of Jovian models about the most likely values in order to make the fullest use of the observations. However, this requires more computing funds so that for the purposes of this thesis, we must be temporarily satisfied with a rough analytical estimate.

Wildey (1964) has approximated the Jovian mean limb darkening curve observed in the 8-14 micron region by an analytical expression. However, the observations exist only in the range of $\mu = \cos\theta$ from 0.6 to 1.0. As Wildey points out, the extrapolation to smaller $\mu$

values may be inaccurate. This expression predicts a value of $T_o$ of about 140 $^oK$, which is unlikely in view of the observations unless a strong internal heat source is present. As the values of this $T_o$ is quite sensitive to the observations when they are restricted to a range of $\mu$ greater than 0.6, it seems probable that the actual value of $T_o$ is lower and the Jovian limb darkening curve decreases rapidly for $\mu$ less than 0.6. We interpret the flatness of the observed profile in the 0.6 to 1.0 region as being due to the 10 micron band of $NH_3$. When $\mu$ is greater than 0.6, the $NH_3$ opacity causes the temperature of the influential levels to change slowly with optical depth. For $\mu$ less than 0.6, one sees a dominant contribution from higher levels where $NH_3$ is weak due to the temperature dependence of its saturation vapor pressure. Therefore, $NH_3$ should be more influential in determining the shape of the limb darkening curve for the larger $\mu$ values and $H_2$ - He should be more influential for the smaller values of $\mu$. In this way, compatibility may be obtained between the models and the observations.

When $B_\nu$ is a linear function of $\tau_\nu$, the theory of steller atmospheres predicts (Aller 1953) that the form of the limb darkening curve near the center of the disk ($\mu \approx 1$) is determined by the layers for which the total optical depth at the frequency in question is about unity. We find $B_\nu$ to approximately vary linearly with $\tau_\nu$ near $\tau_\nu = 1$. On this basis, we will try to deduce information on the $He/H_2$ ratio and $T_o$ values in the Jovian atmosphere. Let $\tau_N$ be the optical depth of a given layer due to absorption by $NH_3$ and let $\tau_H$ be the optical depth of this layer due to absorption by $H_2$ and He. We are concerned with layers for which $\tau_N + \tau_H \approx 1$

in the 8 to 14 micron range. The ratio $\tau_N/\tau_H$ will then give an indication of the relative importance of $NH_3$ and $H_2$-He mixtures in determining the shape of the limb darkening curve. The $T_e = 120\ ^oK$ model with $He/H_2 = 1$ suggests that $\tau_N/\tau_H \approx 3$ will reproduce the observed slope. Equations (II-9), (I-209), Table I-1 and $\tau_N + \tau_H = 1$ imply that

$$\left(\frac{T}{T_o}\right)^4 + C\left[\frac{0.1\alpha_1 + 0.05\alpha_2}{\sqrt{(2\alpha_1 + 4\alpha_2)(\alpha_1^2 + 0.09\,\alpha_1\alpha_2)}}\right]^{1/2}$$

$$\left[\frac{1}{T_o^2}\int_{T_o}^{T} T^{2.5} f(T)dT\right]^{1/2} \approx 1 \qquad \text{(IV-3)}$$

where C is a constant and the latter term is the dominant contribution.

From this equation, we see that if $T_o$ is decreased, T must be slightly lowered since the integral is a rapidly varying function of T and is insensitive to $T_o$. This implies that $T/T_o$ is raised and $\tau_N/\tau_H$ is lowered. Decreasing $\alpha_1$ corresponds to increasing the $He/H_2$ ratio. To preserve the equality, T must be lowered (when $\alpha_1$ is small enough). This means $T/T_o$ is lowered and thus, $\tau_N/\tau_H$ is raised. Therefore, we can compute models where the limb darkening is flatter by increasing the effective temperature, including the thermal opacity of $NH_3$ or by increasing the $He/H_2$ ratio. For example, we find that a model for which $T_o$ is 105 or 110 $^oK$ and $He/H_2 = 1$ may yield the observed slope of the limb darkening curve when it is normalized at $\mu = 1$. However, the

slope may also be duplicated by models of lower $T_o$ and higher $He/H_2$ ratios. When $\alpha_1$ is small, the explicit $\alpha$ dependence of equation (IV-3) becomes $\alpha_1^{-1/4}$. The value of T must be reduced to compensate for the change in $\alpha_1$. Thus, $\tau_H$ decreases while $\tau_N$ increases.

Our models indicate that for $He/H_2 = 0$, a value of $T_o$ equal to 94 $^oK$ ($T_e = 120\ ^oK$) is not sufficient to explain the flatness of the observed limb darkening profile. Equation (IV-3) shows that the limb darkening of all such $H_2$ models at lower boundary temperatures will depart even further from the observations when the effect of $NH_3$ on the thermal opacity is neglected. Taking this opacity into account, we can hardly expect the value of $T_o$ to decline. This is because the thermal absorption of $NH_3$ occurs in the gap between the maxima of the translational and rotational profiles thereby restricting the flow of radiation into space. Because of the gaps in the rotational bands of $NH_3$, the transmission at these frequencies is less than at the 10 micron region. We have found that the Planck mean optical depth due $NH_3$ absorption is significantly less than that due to $H_2$ in the case of the $T_e = 120\ ^oK$ model. Furthermore, it becomes less quite rapidly in the lower temperature regions due to the upper limit on the concentration set by the saturation vapor pressure. The absorption of $NH_3$ in the thermal spectrum is insignificant above the layers responsible for the observed limb darkening curve. The $NH_3$ will affect the temperature distribution in this region by altering the frequency distribution of the flux entering this region from the deeper layers (where the thermal absorption of $NH_3$ is not insignificant). In all of our models, as well as those of Mihalas (1964), the boundary

temperature is less than that for the gray case of the same effective temperature. It appears that the effect of a non-gray opacity is to permit freer radiation into space. Therefore, the effect of adding $NH_3$ may raise the boundary temperature by several degrees. However, in order to raise the value of $\tau_N/\tau_H$ significantly, the increase in temperature of the region responsible for the limb darkening must more than compensate for this rise in $T_o$. In the layers responsible for the limb darkening, a model for which the $NH_3$ thermal opacity is taken into account would have to mimic the temperature distribution of the corresponding layers of a $H_2$ model with a value of $T_e = 120\ ^oK$, while exhibiting a value of $T_o$ which is more than $20\ ^oK$ lower than that for the $T_e \leq 120\ ^oK$ models. It appears highly unlikely that the presence of the thermal opacity of $NH_3$ could bring about such a change in these layers merely by altering the frequency dependence of the flux emerging from deep within the atmosphere.

Since the models for which $He/H_2 = 0$ and $T_e$ is greater than $102\ ^oK$ have been ruled out due to the fact that they cannot explain the occultation results, it follows that all the models for which $He/H_2 = 0$ must be ruled out, even if an internal heat source is considered.

We now consider Jovian models which contain He. For the $He/H_2 = 1$ models, the boundary temperature is close to the gray value. Neglecting the thermal opacity of $NH_3$ for the above reasons, we find that the limb darkening of the models is still too steep at $T_o = 96\ ^oK$. Therefore, the cooler models are ruled out. However, the $He/H_2 = 1$ models between $T_o = 105$ and $115\ ^oK$ may be permitted, but it is necessary to incorporate an internal heat

source for these models since their effective temperature exceeds 130 $^{o}$K and the rotating black body temperature is 120 $^{o}$K. By increasing the $He/H_2$ ratio, we may obtain models which satisfy the albedo estimates and therefore do not require an internal heat source, but then it is necessary that the $He/H_2$ ratio be large. The Rayleigh scattering of He is 13 times as weak as that for $H_2$. If a very large $He/H_2$ ratio existed, the Rayleigh scattering would be important. As it is, the frequency dependence of the Jovian radiation in the blue is not characteristic of Rayleigh scattering except perhaps between the clouds (Münch 1965). It is probably due to particle scattering near the top of the cloud layer. The models imply that convection takes place from 30 to 60 km-atm of $H_2$ below the surface of Jupiter. The Rayleigh scattering of this column of $H_2$ at 0.4 microns is from 0.24 to 0.48. It is difficult to see how a large $He/H_2$ can exist on this basis.

In addition, Spinrad and Trafton (1963) have found that the half-widths of the $CH_4$ lines indicate that the total pressure at the Jovian cloud level is such that a 2 : 1 mixture of He and $H_2$ is indicated. It is difficult to see how an effective temperature less than 130 $^{o}$K could satisfy this observation. Possibly, problems may arise, due to the variation of temperature and pressure along the absorbing path, that make interpretation of the observed widths difficult and the deduction of the bottom of the absorbing layer uncertain. However, the observations, taken as a whole, indicate a preference for the existence of an internal heat source yielding a flux greater than $4 \times 10^3$ ergs/sec/cm$^2$, somewhat less than the incident solar flux. At the same time, they set an upper limit to the $He/H_2$ ratio, complementing the lower limit obtained above.

In conclusion, we observe that the models are flexible enough to account for the observations made thus far. However, when compared with these observations they predict various phenomena. It would seem profitable to make future observations that would verify or negate these predictions in order to obtain a better understanding of the major planets.

# APPENDIX A

## NON-GRAY MODEL ATMOSPHERES FOR THE MAJOR PLANETS

In the models tabulated below, $\tau$ stands for the optical depth at the standard frequency. This frequency is underlined in column seven, which contains the grid of frequencies (in wave number units) used in the computation of the models. T is the temperature in degrees Kelvin, P is the total pressure, K is the number of km-atm of $H_2$ overlying the layer in question, and x is the geometric depth in km. The zero-point of x is taken at $\tau = 0.0005$. S is the value of $(A_s + B_s\alpha_2/\alpha_1) \times 10^{36}$ in cgs units, where $A_s$ and $B_s$ are the binary absorption coefficients for $H_2$-$H_2$ and $H_2$-He collisions at the standard frequency. $F_\nu$ is the monochromatic flux in frequency units, ergs $cm^{-2}$ sec $(cps)^{-1}$. To obtain the monochromatic flux per unit wave number interval, $F_\nu$ should be multiplied by c.

Convection occurs for the values below the horizontal line. Since these values were computed for radiative equilibrium, their error increases with depth. See section III-4. c for a discussion of the corrections to be applied in the convection zone. The relative $CH_4$ and $NH_3$ abundances are used only for computing the position of the convection zone; the opacity of $NH_3$ has not been included in these models (see section III-4. d). An inequality sign indicates that the ratio is an upper limit. This ratio fixes the level where saturation begins. Models including He have been computed only for the limiting cases of Jupiter and Neptune.

JUPITER $T_e = 130\ ^{o}K$ $g = 2597$ cgs

$CH_4/H_2 \leq .003$ $NH_3/H_2 \leq .0002$ $He/H_2 = 0$

| $\tau$ | T | logP | K | x | S | V | $F_\nu/\pi$ |
|---|---|---|---|---|---|---|---|
| 0. | 101.6 | 3.824 | 0.29 | - | 82.2 | 32 $cm^{-1}$ | 0.52 - 10 |
| 0.002 | 101.8 | 4.125 | 0.57 | 11.2 | 82.3 | 64 | 1.37 - 10 |
| 0.004 | 101.9 | 4.276 | 0.81 | 16.8 | 82.3 | 96 | 2.41 - 10 |
| 0.006 | 102.1 | 4.364 | 0.99 | 20.1 | 82.3 | 128 | 3.53 - 10 |
| 0.010 | 102.3 | 4.475 | 1.28 | 24.3 | 82.4 | 161 | 4.61 - 10 |
| 0.020 | 102.9 | 4.626 | 1.81 | 29.9 | 82.6 | 193 | 5.48 - 10 |
| 0.030 | 103.4 | 4.714 | 2.22 | 33.2 | 82.7 | 225 | 5.84 - 10 |
| 0.040 | 103.8 | 4.777 | 2.56 | 35.6 | 82.9 | 257 | 5.36 - 10 |
| 0.060 | 104.7 | 4.866 | 3.14 | 39.0 | 83.1 | 289 | 4.17 - 10 |
| 0.100 | 106.1 | 4.978 | 4.07 | 43.3 | 83.6 | 322 | 2.92 - 10 |
| 0.150 | 107.6 | 5.067 | 5.00 | 46.8 | 84.1 | 354 | 2.07 - 10 |
| 0.250 | 110.3 | 5.180 | 6.49 | 51.3 | 84.9 | 387 | 1.82 - 10 |
| 0.350 | 112.6 | 5.254 | 7.70 | 54.3 | 85.6 | 420 | 1.70 - 10 |
| 0.400 | 113.5 | 5.284 | 8.25 | 55.6 | 85.9 | 454 | 1.59 - 10 |
| 0.500 | 115.3 | 5.334 | 9.25 | 57.7 | 86.5 | 487 | 1.35 - 10 |
| 0.600 | 117.0 | 5.375 | 10.2 | 59.4 | 86.9 | 520 | 9.56 - 11 |
| 0.700 | 118.5 | 5.409 | 11.0 | 60.9 | 87.4 | 553 | 5.87 - 11 |
| 0.800 | 120.0 | 5.440 | 11.8 | 62.2 | 87.8 | 587 | 3.62 - 11 |
| 1.00 | 122.6 | 5.490 | 13.3 | 64.4 | 88.4 | 638 | 2.68 - 11 |
| 1.20 | 125.0 | 5.531 | 14.6 | 66.3 | 89.0 | 690 | 2.36 - 11 |
| 1.40 | 127.2 | 5.567 | 15.8 | 89.5 | 67.9 | 741 | 2.21 - 11 |
| 1.60 | 129.2 | 5.597 | 17.0 | 90.0 | 69.4 | 793 | 1.97 - 11 |
| 1.80 | 131.1 | 5.624 | 18.0 | 90.2 | 70.6 | 845 | 1.84 - 11 |
| 2.00 | 132.9 | 5.649 | 19.1 | 90.6 | 71.8 | 896 | 1.93 - 11 |
| 2.50 | 137.2 | 5.700 | 21.5 | 91.5 | 74.4 | 948 | 2.06 - 11 |
| 3.00 | 140.8 | 5.743 | 23.7 | 76.5 | 92.3 | 1000 | 2.10 - 11 |
| 3.50 | 144.3 | 5.779 | 25.8 | 78.4 | 93.1 | 1125 | 2.20 - 11 |
| 4.00 | 147.5 | 5.810 | 27.7 | 80.1 | 93.7 | 1250 | 2.48 - 11 |
| 5.00 | 153.4 | 5.863 | 31.3 | 83.0 | 95.1 | 1375 | 2.64 - 11 |
| 6.00 | 158.5 | 5.906 | 34.6 | 85.5 | 96.1 | 1500 | 2.68 - 11 |

cont'd

| τ | T | logP | K | x | S |
|---|---|---|---|---|---|
| 8.00 | 167.8 | 5.975 | 40.5 | 89.6 | 97.6 |
| 10.0 | 175.8 | 6.029 | 45.9 | 93.0 | 98.8 |
| 14.0 | 189.3 | 6.112 | 55.4 | 98.5 | 99.7 |
| 18.0 | 200.6 | 6.175 | 64.1 | 103 | 99.9 |
| 22.0 | 210.2 | 6.226 | 72.1 | 107 | 99.8 |
| 26.0 | 218.8 | 6.269 | 79.6 | 110 | 99.6 |
| 30.0 | 226.5 | 6.306 | 86.7 | 113 | 99.2 |
| 40.0 | 242.9 | 6.382 | 103.3 | 120 | 98.3 |
| 50.0 | 256.7 | 6.442 | 118.5 | 125 | 97.2 |
| 60.0 | 268.5 | 6.491 | 132.8 | 130 | 96.0 |

JUPITER $T_e = 120\ ^oK$ $g = 2597$ cgs

$CH_4/H_2 \leq .003$ $NH_3/H_2 \leq .0002$ $He/H_2 = 0$

| $\tau$ | T | logP | K | x | S | V | $F_\nu/\pi$ |
|---|---|---|---|---|---|---|---|
| 0. | 93.6 | 3.812 | 0.28 | - | 80.0 | 32 $cm^{-1}$ | 0.46 - 10 |
| 0.002 | 93.8 | 4.113 | 0.56 | 10.3 | 80.0 | 64 | 1.20 - 10 |
| 0.004 | 93.9 | 4.264 | 0.79 | 15.5 | 80.1 | 96 | 2.08 - 10 |
| 0.006 | 94.0 | 4.352 | 0.96 | 18.5 | 80.1 | 128 | 3.01 - 10 |
| 0.010 | 94.3 | 4.463 | 1.25 | 22.3 | 80.2 | 161 | 3.88 - 10 |
| 0.020 | 94.8 | 4.614 | 1.76 | 27.6 | 80.3 | 193 | 4.55 - 10 |
| 0.030 | 95.2 | 4.702 | 2.16 | 30.6 | 80.4 | 225 | 4.73 - 10 |
| 0.040 | 95.6 | 4.765 | 2.50 | 32.8 | 80.5 | 257 | 4.16 - 10 |
| 0.060 | 96.4 | 4.854 | 3.06 | 35.9 | 80.7 | 289 | 3.03 - 10 |
| 0.100 | 97.7 | 4.966 | 3.97 | 39.9 | 81.1 | 322 | 1.97 - 10 |
| 0.150 | 99.1 | 5.055 | 4.87 | 43.1 | 81.5 | 354 | 1.32 - 10 |
| 0.250 | 101.5 | 5.168 | 6.32 | 47.3 | 82.2 | 387 | 1.12 - 10 |
| 0.350 | 103.5 | 5.243 | 7.51 | 50.1 | 82.8 | 420 | 1.02 - 10 |
| 0.400 | 104.3 | 5.273 | 8.04 | 51.2 | 83.0 | 454 | 9.40 - 11 |
| 0.500 | 106.0 | 5.323 | 9.02 | 53.1 | 83.6 | 487 | 7.91 - 11 |
| 0.600 | 107.4 | 5.364 | 9.91 | 54.7 | 84.0 | 520 | 5.47 - 11 |
| 0.700 | 108.8 | 5.398 | 10.7 | 56.1 | 84.5 | 553 | 3.17 - 11 |
| 0.800 | 110.1 | 5.428 | 11.5 | 57.3 | 84.9 | 587 | 1.84 - 11 |
| 1.00 | 112.4 | 5.479 | 12.9 | 59.3 | 85.6 | 638 | 1.30 - 11 |
| 1.20 | 114.6 | 5.520 | 14.2 | 61.1 | 86.2 | 690 | 1.13 - 11 |
| 1.40 | 116.5 | 5.555 | 15.4 | 62.5 | 86.8 | 741 | 1.04 - 11 |
| 1.60 | 118.3 | 5.586 | 16.5 | 63.8 | 87.3 | 793 | 9.30 - 12 |
| 1.80 | 120.0 | 5.612 | 17.6 | 65.0 | 87.8 | 845 | 8.67 - 12 |
| 2.00 | 121.6 | 5.637 | 18.6 | 66.1 | 88.2 | 896 | 9.14 - 12 |
| 2.50 | 125.3 | 5.688 | 20.9 | 68.4 | 89.1 | 948 | 9.86 - 12 |
| 3.00 | 128.6 | 5.730 | 23.0 | 70.4 | 89.9 | 1000 | 1.02 - 11 |
| 3.50 | 131.7 | 5.766 | 25.0 | 72.1 | 90.3 | 1125 | 1.10 - 11 |
| 4.00 | 134.5 | 5.797 | 26.9 | 73.6 | 90.9 | 1250 | 1.26 - 11 |
| 5.00 | 139.9 | 5.850 | 30.4 | 76.2 | 92.1 | 1375 | 1.34 - 11 |
| 6.00 | 144.5 | 5.893 | 33.5 | 78.5 | 93.1 | 1500 | 1.36 - 11 |

cont'd

| τ | T | logP | K | x | S |
|---|---|---|---|---|---|
| 8.00 | 153.0 | 5.962 | 39.3 | 82.2 | 95.1 |
| 10.0 | 160.3 | 6.016 | 44.4 | 85.3 | 96.4 |
| 14.0 | 172.9 | 6.097 | 53.7 | 90.3 | 98.5 |
| 18.0 | 183.4 | 6.159 | 61.9 | 94.3 | 99.5 |
| 22.0 | 192.5 | 6.210 | 69.5 | 97.8 | 99.7 |
| 26.0 | 200.5 | 6.252 | 76.6 | 101 | 99.9 |
| 30.0 | 207.7 | 6.289 | 83.4 | 104 | 99.8 |
| 40.0 | 223.2 | 6.364 | 99.1 | 109 | 99.4 |
| 50.0 | 236.1 | 6.423 | 113 | 114 | 98.7 |
| 60.0 | 247.3 | 6.472 | 127 | 119 | 98.0 |

JUPITER $T_e = 120\ ^{o}K$ $g = 2597$ cgs

$CH_4/H_2 \leq .003$ $NH_3/H_2 \leq .0002$ $He/H_2 = 1$

| $\tau$ | T | logP | K | x | S | V | $F_\nu/\pi$ |
|---|---|---|---|---|---|---|---|
| | | | | | | $32\ cm^{-1}$ | |
| 0. | 95.5 | 4.17 | .31 | - | 96.1 | | 0.41 - 10 |
| 0.002 | 95.7 | 4.467 | .63 | 7.2 | 96.1 | 64 | 1.08 - 10 |
| 0.004 | 95.8 | 4.617 | .89 | 10.5 | 96.2 | 96 | 1.80 - 10 |
| 0.006 | 96.0 | 4.706 | 1.09 | 12.6 | 96.2 | 128 | 2.46 - 10 |
| 0.010 | 96.2 | 4.817 | 1.41 | 15.2 | 96.3 | 161 | 3.00 - 10 |
| 0.020 | 96.7 | 4.968 | 1.99 | 18.7 | 96.5 | 193 | 3.39 - 10 |
| 0.030 | 97.2 | 5.056 | 2.44 | 20.8 | 96.7 | 225 | 3.58 - 10 |
| 0.040 | 97.7 | 5.119 | 2.82 | 22.3 | 96.9 | 257 | 3.49 - 10 |
| 0.060 | 98.5 | 5.208 | 3.46 | 24.5 | 97.2 | 289 | 3.00 - 10 |
| 0.100 | 99.9 | 5.320 | 4.47 | 27.2 | 97.8 | 322 | 2.23 - 10 |
| 0.150 | 101.4 | 5.409 | 5.50 | 29.3 | 98.5 | 354 | 1.56 - 10 |
| 0.250 | 104.2 | 5.522 | 7.13 | 32.2 | 99.6 | 387 | 1.36 - 10 |
| 0.350 | 106.4 | 5.596 | 8.46 | 34.1 | 101 | 420 | 1.27 - 10 |
| 0.400 | 107.5 | 5.626 | 9.06 | 34.9 | 101 | 454 | 1.19 - 10 |
| 0.500 | 109.5 | 5.676 | 10.2 | 36.2 | 102 | 487 | 1.03 - 10 |
| 0.600 | 111.2 | 5.717 | 11.2 | 37.3 | 103 | 520 | 7.22 - 11 |
| 0.700 | 112.9 | 5.751 | 12.1 | 38.2 | 103 | 553 | 4.20 - 11 |
| 0.800 | 114.5 | 5.781 | 13.0 | 39.1 | 104 | 587 | 2.40 - 11 |
| 1.00 | 117.4 | 5.832 | 14.6 | 40.5 | 105 | 638 | 1.82 - 11 |
| 1.20 | 120.1 | 5.873 | 16.0 | 41.7 | 106 | 690 | 1.74 - 11 |
| 1.40 | 122.5 | 5.908 | 17.4 | 42.7 | 107 | 741 | 1.79 - 11 |
| 1.60 | 124.8 | 5.939 | 18.6 | 43.6 | 108 | 793 | 1.73 - 11 |
| 1.80 | 127.0 | 5.966 | 19.8 | 44.5 | 108 | 845 | 1.75 - 11 |
| 2.00 | 129.1 | 5.990 | 21.0 | 45.2 | 109 | 896 | 1.98 - 11 |
| 2.50 | 134.0 | 6.042 | 23.6 | 46.9 | 111 | 948 | 2.23 - 11 |
| 3.00 | 138.1 | 6.085 | 26.0 | 48.3 | 113 | 1000 | 2.34 - 11 |
| 3.50 | 142.1 | 6.121 | 28.3 | 49.5 | 114 | 1125 | 2.51 - 11 |
| 4.00 | 145.7 | 6.152 | 30.4 | 50.6 | 115 | 1250 | 2.77 - 11 |
| 5.00 | 152.4 | 6.205 | 34.4 | 52.6 | 118 | 1375 | 2.84 - 11 |
| 6.00 | 157.8 | 6.248 | 37.9 | 54.2 | 119 | 1500 | 2.74 - 11 |

cont'd

| τ | T | logP | K | x | S |
|---|---|---|---|---|---|
| 8.00 | 167.2 | 6.316 | 44.4 | 56.9 | 122 |
| 10.0 | 175.1 | 6.370 | 50.2 | 59.1 | 124 |
| 14.0 | 187.7 | 6.451 | 60.6 | 62.7 | 127 |
| 18.0 | 197.9 | 6.513 | 69.8 | 65.6 | 128 |
| 22.0 | 206.3 | 6.562 | 78.2 | 68.1 | 129 |
| 26.0 | 213.8 | 6.604 | 86.1 | 70.2 | 130 |
| 30.0 | 220.5 | 6.639 | 93.4 | 72.1 | 130 |
| 40.0 | 234.6 | 6.712 | 110 | 76.1 | 131 |
| 50.0 | 246.3 | 6.768 | 126 | 79.4 | 132 |
| 60.0 | 256.4 | 6.815 | 140 | 82.2 | 132 |

JUPITER $T_e = 110\ ^oK$ g - 2597

$CH_4/H_2 \leq .003$ $NH_3/H_2 \leq .0002$ $He/H_2 = 0$

| $\tau$ | T | logP | K | x | S | V | $F_\nu/\pi$ |
|---|---|---|---|---|---|---|---|
| 0. | 85.3 | 3.798 | .27 | - | 77.6 | 32 $cm^{-1}$ | 0.40 - 10 |
| 0.002 | 85.5 | 4.100 | .54 | 9.4 | 77.7 | 64 | 1.03 - 10 |
| 0.004 | 85.6 | 4.250 | .76 | 14.1 | 77.7 | 96 | 1.77 - 10 |
| 0.006 | 85.7 | 4.338 | .94 | 16.9 | 77.7 | 128 | 2.51 - 10 |
| 0.010 | 85.9 | 4.450 | 1.21 | 20.4 | 77.8 | 161 | 3.20 - 10 |
| 0.020 | 86.4 | 4.600 | 1.71 | 25.1 | 77.9 | 193 | 3.68 - 10 |
| 0.030 | 86.8 | 4.684 | 2.10 | 27.9 | 78.0 | 225 | 3.72 - 10 |
| 0.040 | 87.2 | 4.752 | 2.42 | 29.9 | 78.1 | 257 | 3.09 - 10 |
| 0.060 | 87.9 | 4.840 | 2.97 | 32.8 | 78.3 | 289 | 2.07 - 10 |
| 0.100 | 89.1 | 4.953 | 3.85 | 36.4 | 78.7 | 322 | 1.22 - 10 |
| 0.150 | 90.3 | 5.042 | 4.72 | 39.3 | 79.1 | 354 | 7.59 - 11 |
| 0.250 | 92.5 | 5.155 | 6.13 | 43.1 | 79.7 | 387 | 6.16 - 11 |
| 0.350 | 94.2 | 5.230 | 7.28 | 45.6 | 80.2 | 420 | 5.44 - 11 |
| 0.400 | 95.0 | 5.260 | 7.79 | 48.2 | 80.4 | 454 | 4.94 - 11 |
| 0.500 | 96.5 | 5.309 | 8.74 | 48.4 | 80.7 | 487 | 4.13 - 11 |
| 0.600 | 97.7 | 5.350 | 9.61 | 49.9 | 81.1 | 520 | 2.79- 11 |
| 0.700 | 99.0 | 5.385 | 10.4 | 51.1 | 81.4 | 553 | 1.51 - 11 |
| 0.800 | 100.1 | 5.415 | 11.1 | 52.2 | 81.8 | 587 | 8.03 - 12 |
| 1.00 | 102.2 | 5.466 | 12.5 | 54.1 | 82.4 | 638 | 5.43 - 12 |
| 1.20 | 104.1 | 5.507 | 13.8 | 55.7 | 82.9 | 690 | 4.59 - 12 |
| 1.40 | 105.8 | 5.542 | 14.9 | 57.0 | 83.5 | 741 | 4.18 - 12 |
| 1.60 | 107.4 | 5.573 | 16.0 | 58.2 | 84.0 | 793 | 3.80 - 12 |
| 1.80 | 108.9 | 5.600 | 17.1 | 59.3 | 84.5 | 845 | 3.53 - 12 |
| 2.00 | 110.3 | 5.624 | 18.0 | 60.2 | 84.9 | 896 | 3.70 - 12 |
| 2.50 | 113.7 | 5.675 | 20.3 | 62.3 | 85.9 | 948 | 3.99 - 12 |
| 3.00 | 116.6 | 5.717 | 22.4 | 64.1 | 86.8 | 1000 | 4.18 - 12 |
| 3.50 | 119.3 | 5.753 | 24.3 | 65.6 | 87.6 | 1125 | 4.61 - 12 |
| 4.00 | 121.8 | 5.784 | 26.1 | 67.0 | 88.3 | 1250 | 5.28 - 12 |
| 5.00 | 126.6 | 5.836 | 29.4 | 69.4 | 89.4 | 1375 | 5.64 - 12 |
| 6.00 | 130.7 | 5.879 | 32.5 | 71.4 | 90.1 | 1500 | 5.71 - 12 |

cont'd

| τ | T | logP | K | x | S |
|---|---|---|---|---|---|
| 8.00 | 138.2 | 5.948 | 38.0 | 74.8 | 91.7 |
| 10.0 | 144.8 | 6.001 | 43.0 | 77.5 | 93.1 |
| 14.0 | 156.2 | 6.083 | 51.9 | 82.0 | 95.7 |
| 18.0 | 165.9 | 6.144 | 59.8 | 85.7 | 97.3 |
| 22.0 | 174.4 | 6.194 | 67.0 | 88.7 | 98.7 |
| 26.0 | 181.9 | 6.236 | 73.8 | 91.5 | 99.3 |
| 30.0 | 188.6 | 6.272 | 80.2 | 93.9 | 99.7 |
| 40.0 | 203.2 | 6.346 | 95.0 | 99.2 | 99.9 |
| 50.0 | 215.3 | 6.404 | 109 | 103.6 | 99.7 |
| 60.0 | 225.8 | 6.452 | 121 | 107.5 | 99.3 |

SATURN $T_e = 100\ ^{o}K$ $g = 1063$ cgs

$CH_4/H_2 \leq .006$ $NH_3/H_2 \leq .0002$ $He/H_2 = 0$

| $\tau$ | T | logP | K | x | S | V | $F_\nu/\pi$ |
|---|---|---|---|---|---|---|---|
| | | | | | | 32 $cm^{-1}$ | |
| 0. | 76.8 | 3.589 | 0.41 | - | 75.1 | | 3.34 - 11 |
| 0.002 | 76.9 | 3.890 | 0.81 | 20.7 | 75.2 | 64 | 8.54 - 11 |
| 0.004 | 77.0 | 4.040 | 1.15 | 31.0 | 75.2 | 96 | 1.44 - 10 |
| 0.006 | 77.2 | 4.129 | 1.41 | 37.1 | 75.2 | 128 | 2.00 - 10 |
| 0.010 | 77.4 | 4.240 | 1.82 | 44.8 | 75.3 | 161 | 2.49 - 10 |
| 0.020 | 77.8 | 4.391 | 2.58 | 55.2 | 75.4 | 193 | 2.80 - 10 |
| 0.030 | 78.2 | 4.479 | 3.16 | 61.4 | 75.5 | 225 | 2.72 - 10 |
| 0.040 | 78.5 | 4.542 | 3.65 | 65.8 | 75.7 | 257 | 2.10 - 10 |
| 0.060 | 79.1 | 4.631 | 4.48 | 72.1 | 75.8 | 289 | 1.26 - 10 |
| 0.100 | 80.2 | 4.743 | 5.80 | 80.0 | 76.1 | 322 | 6.67 - 11 |
| 0.150 | 81.3 | 4.832 | 7.12 | 86.5 | 76.5 | 354 | 3.81 - 11 |
| 0.250 | 83.2 | 4.945 | 9.24 | 94.8 | 77.0 | 387 | 2.92 - 11 |
| 0.350 | 84.6 | 5.020 | 11.0 | 100.4 | 77.4 | 420 | 2.45 - 11 |
| 0.400 | 85.3 | 5.050 | 11.8 | 102.6 | 77.6 | 454 | 2.14 - 11 |
| 0.500 | 86.6 | 5.100 | 13.2 | 106.5 | 78.0 | 487 | 1.76 - 11 |
| 0.600 | 87.7 | 5.141 | 14.5 | 109.7 | 78.3 | 520 | 1.17 - 11 |
| 0.700 | 88.7 | 5.175 | 15.7 | 112.4 | 78.6 | 553 | 5.91 - 12 |
| 0.800 | 89.7 | 5.205 | 16.8 | 114.8 | 78.8 | 587 | 2.85 - 12 |
| 1.00 | 91.4 | 5.256 | 18.9 | 118.9 | 79.4 | 638 | 1.82 - 12 |
| 1.20 | 93.0 | 5.297 | 20.8 | 122.3 | 79.8 | 690 | 1.48 - 12 |
| 1.40 | 94.4 | 5.332 | 22.5 | 125.2 | 80.2 | 741 | 1.30 - 12 |
| 1.60 | 95.7 | 5.363 | 24.2 | 127.8 | 80.5 | 793 | 1.20 - 12 |
| 1.80 | 97.0 | 5.390 | 25.7 | 130.1 | 80.9 | 845 | 1.11 - 12 |
| 2.00 | 98.2 | 5.414 | 27.2 | 132.2 | 81.2 | 896 | 1.16 - 12 |
| 2.50 | 101.0 | 5.465 | 30.6 | 136.8 | 82.0 | 948 | 1.25 - 12 |
| 3.00 | 103.5 | 5.507 | 33.7 | 140.6 | 82.8 | 1000 | 1.33 - 12 |
| 3.50 | 105.8 | 5.543 | 36.6 | 144.0 | 83.5 | 1125 | 1.55 - 12 |
| 4.00 | 107.9 | 5.574 | 39.3 | 146.9 | 84.2 | 1250 | 1.77 - 12 |
| 5.00 | 112.0 | 5.626 | 44.3 | 152.1 | 85.4 | 1375 | 1.80 - 12 |
| 6.00 | 115.5 | 5.669 | 48.9 | 156.4 | 86.5 | 1500 | 1.85 - 12 |

cont'd

| τ | T | logP | K | x | S |
|---|---|---|---|---|---|
| 8.00 | 122.0 | 5.737 | 57.2 | 163.6 | 88.3 |
| 10.0 | 127.8 | 5.790 | 64.6 | 169.5 | 89.7 |
| 14.0 | 138.0 | 5.871 | 77.9 | 179.2 | 91.7 |
| 18.0 | 146.7 | 5.933 | 89.8 | 187.0 | 93.5 |
| 22.0 | 154.4 | 5.982 | 100.6 | 193.7 | 95.3 |
| 26.0 | 161.2 | 6.024 | 110.6 | 199.5 | 96.6 |
| 30.0 | 167.4 | 6.059 | 120.1 | 204.7 | 97.6 |
| 40.0 | 180.6 | 6.132 | 141.9 | 216.0 | 99.3 |
| 50.0 | 191.7 | 6.189 | 161.8 | 225.5 | 99.6 |
| 60.0 | 201.2 | 6.236 | 180.4 | 233.8 | 99.9 |

SATURN $T_e = 90\ ^{o}K$ $g = 1063$ cgs

$CH_4/H_2 \leq .006$ $NH_3/H_2 \leq .0002$ $He/H_2 = 0$

| $\tau$ | T | log P | K | x | S | V | $F_\nu/\pi$ |
|---|---|---|---|---|---|---|---|
| 0. | 68.3 | 3.571 | 0.39 | - | 72.7 | 32 $cm^{-1}$ | 2.76 - 11 |
| 0.002 | 68.5 | 3.872 | 0.78 | 18.4 | 72.7 | 64 | 6.92 - 11 |
| 0.004 | 68.6 | 4.022 | 1.10 | 27.6 | 72.7 | 96 | 1.13 - 10 |
| 0.006 | 68.7 | 4.111 | 1.35 | 33.0 | 72.8 | 128 | 1.53 - 10 |
| 0.010 | 68.9 | 4.222 | 1.75 | 39.9 | 72.8 | 161 | 1.86 - 10 |
| 0.020 | 69.3 | 4.373 | 2.47 | 49.2 | 72.9 | 193 | 2.03 - 10 |
| 0.030 | 69.6 | 4.461 | 3.03 | 54.7 | 73.0 | 225 | 1.88 - 10 |
| 0.040 | 69.9 | 4.524 | 3.50 | 58.6 | 73.1 | 257 | 1.31 - 10 |
| 0.060 | 70.5 | 4.613 | 4.30 | 64.2 | 73.3 | 289 | 6.77 - 11 |
| 0.100 | 71.4 | 4.725 | 5.56 | 71.3 | 73.5 | 322 | 3.15 - 11 |
| 0.150 | 72.3 | 4.815 | 6.84 | 77.0 | 73.8 | 354 | 1.63 - 11 |
| 0.250 | 73.9 | 4.928 | 8.87 | 84.4 | 74.2 | 387 | 1.16 - 11 |
| 0.350 | 75.1 | 5.002 | 10.5 | 89.4 | 74.6 | 420 | 9.09 - 12 |
| 0.400 | 75.7 | 5.032 | 11.3 | 91.4 | 74.8 | 454 | 7.49 - 12 |
| 0.500 | 76.7 | 5.082 | 12.7 | 94.8 | 75.1 | 487 | 5.99 - 12 |
| 0.600 | 77.6 | 5.123 | 13.9 | 97.6 | 75.4 | 520 | 3.92 - 12 |
| 0.700 | 78.4 | 5.157 | 15.1 | 100.0 | 75.6 | 553 | 1.85 - 12 |
| 0.800 | 79.2 | 5.187 | 16.1 | 102.1 | 75.9 | 587 | 7.97 - 13 |
| 1.00 | 80.6 | 5.238 | 18.1 | 105.7 | 76.3 | 638 | 4.69 - 13 |
| 1.20 | 81.9 | 5.279 | 19.9 | 108.7 | 76.7 | 690 | 3.62 - 13 |
| 1.40 | 83.1 | 5.314 | 21.6 | 111.3 | 77.0 | 741 | 3.01 - 13 |
| 1.60 | 84.2 | 5.344 | 23.2 | 113.5 | 77.3 | 793 | 2.75 - 13 |
| 1.80 | 85.2 | 5.371 | 24.6 | 115.6 | 77.6 | 845 | 2.54 - 13 |
| 2.00 | 86.2 | 5.395 | 26.0 | 117.4 | 77.9 | 896 | 2.65 - 13 |
| 2.50 | 88.5 | 5.447 | 29.3 | 121.4 | 78.5 | 948 | 2.88 - 13 |
| 3.00 | 90.5 | 5.484 | 32.3 | 124.8 | 79.1 | 1000 | 3.14 - 13 |
| 3.50 | 92.4 | 5.524 | 35.0 | 127.7 | 79.7 | 1125 | 3.88 - 13 |
| 4.00 | 94.1 | 5.555 | 37.6 | 130.3 | 80.1 | 1250 | 4.75 - 13 |
| 5.00 | 97.5 | 5.607 | 42.4 | 134.7 | 81.0 | 1375 | 5.18 - 13 |
| 6.00 | 100.5 | 5.650 | 46.8 | 138.5 | 81.9 | 1500 | 4.92 - 13 |

cont'd

| τ | T | logP | K | x | S |
|---|---|---|---|---|---|
| 8.00 | 106.0 | 5.718 | 54.8 | 144.8 | 83.6 |
| 10.0 | 111.1 | 5.771 | 61.9 | 149.9 | 85.2 |
| 14.0 | 120.0 | 5.852 | 74.5 | 158.3 | 87.8 |
| 18.0 | 127.9 | 5.913 | 85.8 | 165.0 | 89.7 |
| 22.0 | 134.9 | 5.963 | 96.1 | 170.8 | 91.0 |
| 26.0 | 141.3 | 6.004 | 106 | 176.0 | 92.4 |
| 30.0 | 147.1 | 6.040 | 115 | 180.6 | 93.6 |
| 40.0 | 159.4 | 6.112 | 136 | 190.5 | 96.3 |
| 50.0 | 169.8 | 6.112 | 155 | 198.8 | 97.9 |
| 60.0 | 178.8 | 6.215 | 172 | 206.1 | 99.1 |

SATURN $T_e = 80\ ^{o}K$ $g = 1063$ cgs

$CH_4/H_2 \leq .006$ $NH_3/H_2 \leq .0002$ $He/H_2 = 0$

| $\tau$ | T | log P | K | x | S | V | $F_\nu/\pi$ |
|---|---|---|---|---|---|---|---|
| 0. | 60.0 | 3.547 | 0.37 | - | 71.2 | 32 $cm^{-1}$ | 2.18 - 11 |
| 0.002 | 60.1 | 3.848 | 0.74 | 16.2 | 71.2 | 64 | 5.33 - 11 |
| 0.004 | 60.2 | 3.998 | 1.04 | 24.3 | 71.3 | 96 | 8.40 - 11 |
| 0.006 | 60.3 | 4.087 | 1.28 | 29.0 | 71.3 | 128 | 1.09 - 10 |
| 0.010 | 60.4 | 4.198 | 1.65 | 35.0 | 71.3 | 161 | 1.28 - 10 |
| 0.020 | 60.8 | 4.349 | 2.34 | 43.2 | 71.3 | 193 | 1.34 - 10 |
| 0.030 | 61.1 | 4.438 | 2.87 | 48.0 | 71.4 | 225 | 1.15 - 10 |
| 0.040 | 61.3 | 4.501 | 3.32 | 51.4 | 71.4 | 257 | 6.99 - 11 |
| 0.060 | 61.8 | 4.589 | 4.07 | 56.3 | 71.5 | 289 | 2.99 - 11 |
| 0.100 | 62.5 | 4.702 | 5.27 | 62.6 | 71.6 | 322 | 1.20 - 11 |
| 0.150 | 63.3 | 4.791 | 6.48 | 67.6 | 71.7 | 354 | 5.53 - 12 |
| 0.250 | 64.5 | 4.905 | 8.41 | 74.1 | 71.9 | 387 | 3.57 - 12 |
| 0.350 | 65.5 | 4.980 | 10.0 | 78.4 | 72.1 | 420 | 2.54 - 12 |
| 0.400 | 65.9 | 5.009 | 10.7 | 80.2 | 72.2 | 454 | 1.90 - 12 |
| 0.500 | 66.7 | 5.059 | 12.0 | 83.1 | 72.3 | 487 | 1.42 - 12 |
| 0.600 | 67.4 | 5.100 | 13.2 | 85.6 | 72.5 | 520 | 9.11 - 13 |
| 0.700 | 68.0 | 5.135 | 14.3 | 87.7 | 72.6 | 553 | 4.10 - 13 |
| 0.800 | 68.6 | 5.165 | 15.3 | 89.5 | 72.7 | 587 | 1.55 - 13 |
| 1.00 | 69.7 | 5.215 | 17.2 | 92.6 | 73.0 | 638 | 8.22 - 14 |
| 1.20 | 70.6 | 5.257 | 18.9 | 95.2 | 73.3 | 690 | 5.75 - 14 |
| 1.40 | 71.5 | 5.292 | 20.5 | 97.4 | 73.5 | 741 | 4.33 - 14 |
| 1.60 | 72.3 | 5.322 | 22.0 | 99.4 | 73.8 | 793 | 3.70 - 14 |
| 1.80 | 73.1 | 5.349 | 23.4 | 101.1 | 74.0 | 845 | 3.33 - 14 |
| 2.00 | 73.8 | 5.373 | 24.7 | 102.7 | 74.2 | 896 | 3.43 - 14 |
| 2.50 | 75.6 | 5.424 | 27.8 | 106.1 | 74.8 | 948 | 3.80 - 14 |
| 3.00 | 77.1 | 5.466 | 30.6 | 109.0 | 75.2 | 1000 | 4.23 - 14 |
| 3.50 | 78.6 | 5.501 | 33.2 | 111.4 | 75.7 | 1125 | 5.59 - 14 |
| 4.00 | 79.9 | 5.532 | 35.7 | 113.6 | 76.1 | 1250 | 6.91 - 14 |
| 5.00 | 82.5 | 5.584 | 40.2 | 117.4 | 76.8 | 1375 | 7.33 - 14 |
| 6.00 | 84.9 | 5.627 | 44.3 | 120.6 | 77.5 | 1500 | 6.28 - 14 |

cont'd

| τ | T | logP | K | x | S |
|---|---|---|---|---|---|
| 8.00 | 89.3 | 5.694 | 51.8 | 125.8 | 78.7 |
| 10.0 | 93.3 | 5.747 | 58.6 | 130.2 | 79.9 |
| 14.0 | 100.6 | 5.828 | 70.6 | 137.2 | 81.9 |
| 18.0 | 107.3 | 5.890 | 81.2 | 142.9 | 84.0 |
| 22.0 | 113.4 | 5.939 | 91.0 | 147.7 | 85.8 |
| 26.0 | 119.1 | 5.980 | 100 | 152.0 | 87.5 |
| 30.0 | 124.1 | 6.016 | 109 | 155.9 | 88.8 |
| 40.0 | 135.0 | 6.088 | 128 | 164.2 | 91.0 |
| 50.0 | 144.1 | 6.144 | 146 | 171.3 | 93.0 |
| 60.0 | 152.0 | 6.191 | 163 | 177.4 | 94.9 |

URANUS $T_e = 64\ ^{o}K$ $g = 1025$ cgs

$CH_4/H_2 \leq .01$ $NH_3/H_2 = 0$ $He/H_2 = 0$

| $\tau$ | T | logP | K | x | S | V | $F_\nu/\pi$ |
|---|---|---|---|---|---|---|---|
| 0. | 47.5 | 3.739 | 0.60 | - | 22.5 | 32 $cm^{-1}$ | 1.39 - 11 |
| 0.002 | 47.8 | 4.040 | 1.19 | 13.3 | 22.6 | 64 | 3.19 - 11 |
| 0.004 | 47.9 | 4.190 | 1.68 | 20.0 | 22.7 | 96 | 4.54 - 11 |
| 0.006 | 48.1 | 4.278 | 2.06 | 23.9 | 22.8 | 128 | 5.31 - 11 |
| 0.010 | 48.3 | 4.389 | 2.66 | 28.8 | 22.9 | 161 | 5.65 - 11 |
| 0.020 | 48.7 | 4.539 | 3.76 | 35.5 | 23.2 | 193 | 5.37 - 11 |
| 0.030 | 49.1 | 4.627 | 4.60 | 39.5 | 23.4 | 225 | 3.95 - 11 |
| 0.040 | 49.4 | 4.689 | 5.31 | 42.4 | 23.6 | 257 | 1.71 - 11 |
| 0.060 | 49.9 | 4.777 | 6.50 | 46.4 | 23.8 | 289 | 4.77 - 12 |
| 0.100 | 50.6 | 4.887 | 8.38 | 51.5 | 24.3 | 322 | 1.45 - 12 |
| 0.150 | 51.2 | 4.975 | 10.2 | 55.7 | 24.6 | 354 | 5.46 - 13 |
| 0.250 | 52.2 | 5.085 | 13.2 | 61.0 | 25.1 | 387 | 2.84 - 13 |
| 0.350 | 53.0 | 5.158 | 15.6 | 64.5 | 25.5 | 420 | 1.60 - 13 |
| 0.400 | 53.3 | 5.187 | 16.7 | 65.9 | 25.6 | 454 | 9.31 - 14 |
| 0.500 | 54.0 | 5.235 | 18.7 | 68.3 | 25.9 | 487 | 5.51 - 14 |
| 0.600 | 54.5 | 5.275 | 20.5 | 70.3 | 26.1 | 520 | 3.12 - 14 |
| 0.700 | 55.0 | 5.309 | 22.1 | 72.0 | 26.2 | 553 | 1.34 - 14 |
| 0.800 | 55.5 | 5.338 | 23.6 | 73.5 | 26.4 | 587 | 4.25 - 15 |
| 1.00 | 56.5 | 5.387 | 26.5 | 76.1 | 26.8 | 638 | 1.69 - 15 |
| 1.20 | 57.4 | 5.427 | 29.0 | 78.2 | 27.1 | 690 | 8.73 - 16 |
| 1.40 | 58.2 | 5.461 | 31.4 | 80.0 | 27.3 | 741 | 5.35 - 16 |
| 1.60 | 58.9 | 5.490 | 33.6 | 81.6 | 27.5 | 793 | 3.68 - 16 |
| 1.80 | 59.7 | 5.516 | 35.7 | 83.0 | 27.8 | 845 | 2.85 - 16 |
| 2.00 | 60.5 | 5.540 | 37.6 | 84.3 | 28.0 | 896 | 2.58 - 16 |
| 2.50 | 62.2 | 5.589 | 42.2 | 87.2 | 28.4 | 948 | 2.54 - 16 |
| 3.00 | 63.8 | 5.630 | 46.4 | 89.6 | 28.7 | 1000 | 3.05 - 16 |
| 3.50 | 65.3 | 5.665 | 50.3 | 91.6 | 29.0 | 1125 | 4.58 - 16 |
| 4.00 | 66.8 | 5.696 | 53.9 | 93.5 | 29.2 | 1250 | 7.00 - 16 |
| 5.00 | 69.6 | 5.747 | 60.7 | 96.8 | 29.4 | 1375 | 9.48 - 16 |
| 6.00 | 72.1 | 5.790 | 66.9 | 99.6 | 29.8 | 1500 | 1.11 - 15 |

cont'd

| τ | T | logP | K | x | S |
|---|---|---|---|---|---|
| 8.00 | 77.0 | 5.858 | 78.4 | 104.3 | 30.2 |
| 10.0 | 81.7 | 5.913 | 88.9 | 108.3 | 30.2 |
| 14.0 | 90.5 | 5.999 | 108 | 115.2 | 30.0 |
| 18.0 | 98.9 | 6.066 | 126 | 121.1 | 29.6 |
| 22.0 | 106.6 | 6.122 | 144 | 126.4 | 29.2 |
| 26.0 | 114.2 | 6.170 | 161 | 131.3 | 28.8 |
| 30.0 | 120.4 | 6.212 | 177 | 135.8 | 28.5 |
| 40.0 | 133.9 | 6.297 | 215 | 145.9 | 27.8 |
| 50.0 | 145.0 | 6.365 | 252 | 154.7 | 27.3 |
| 60.0 | 154.5 | 6.421 | 286 | 162.4 | 27.0 |

NEPTUNE $T_e = 50\ ^{o}K$ $g = 1373$ cgs

$CH_4/H_2 \leq .01$ $NH_3/H_2 = 0$ $He/H_2 = 0$

| τ | T | logP | K | x | S | V | $F_\nu/\pi$ |
|---|---|---|---|---|---|---|---|
| 0. | 37.4 | 3.842 | 0.56 | - | 14.7 | 32 $cm^{-1}$ | 0.86 - 11 |
| 0.002 | 37.6 | 4.143 | 1.13 | 7.8 | 14.8 | 64 | 1.72 - 11 |
| 0.004 | 37.7 | 4.293 | 1.59 | 11.7 | 14.9 | 96 | 2.09 - 11 |
| 0.006 | 37.7 | 4.380 | 1.95 | 14.0 | 15.0 | 128 | 2.10 - 11 |
| 0.010 | 37.9 | 4.491 | 2.51 | 16.9 | 15.3 | 161 | 1.95 - 11 |
| 0.020 | 38.1 | 4.640 | 3.54 | 20.8 | 15.3 | 193 | 1.63 - 11 |
| 0.030 | 38.3 | 4.727 | 4.33 | 23.1 | 15.5 | 225 | 9.63 - 12 |
| 0.040 | 38.4 | 4.789 | 4.99 | 24.7 | 15.6 | 257 | 2.43 - 12 |
| 0.060 | 38.6 | 4.876 | 6.10 | 27.1 | 15.8 | 289 | 3.57 - 13 |
| 0.100 | 38.9 | 4.986 | 7.85 | 30.0 | 16.0 | 322 | 8.40 - 14 |
| 0.150 | 39.2 | 5.073 | 9.59 | 32.3 | 16.2 | 354 | 2.61 - 14 |
| 0.250 | 39.6 | 5.182 | 12.3 | 35.3 | 16.6 | 387 | 1.01 - 14 |
| 0.350 | 39.9 | 5.254 | 14.5 | 37.3 | 16.8 | 420 | 4.05 - 15 |
| 0.400 | 40.1 | 5.282 | 15.5 | 38.1 | 17.0 | 454 | 1.64 - 15 |
| 0.500 | 40.4 | 5.329 | 17.3 | 39.4 | 17.2 | 487 | 6.63 - 16 |
| 0.600 | 40.6 | 5.368 | 18.9 | 40.5 | 17.4 | 520 | 2.67 - 16 |
| 0.700 | 40.9 | 5.401 | 20.4 | 41.4 | 17.6 | 553 | 9.92 - 17 |
| 0.800 | 41.1 | 5.429 | 21.8 | 42.2 | 17.8 | 587 | 2.86 - 17 |
| 1.00 | 41.6 | 5.476 | 24.3 | 43.5 | 18.2 | 638 | 6.89 - 18 |
| 1.20 | 42.1 | 5.514 | 26.5 | 44.7 | 18.6 | 690 | 1.96 - 18 |
| 1.40 | 42.5 | 5.547 | 28.6 | 45.6 | 18.9 | 741 | 6.8 - 19 |
| 1.60 | 42.9 | 5.575 | 30.5 | 46.4 | 19.3 | 793 | 2.9 - 19 |
| 1.80 | 43.3 | 5.599 | 32.2 | 47.2 | 19.6 | 845 | 1.6 - 19 |
| 2.00 | 43.7 | 5.621 | 33.9 | 47.8 | 19.8 | 896 | 1.2 - 19 |
| 2.50 | 44.7 | 5.668 | 37.7 | 49.2 | 20.5 | 948 | 1.0 - 19 |
| 3.00 | 45.5 | 5.705 | 41.1 | 50.4 | 21.2 | 1000 | 9.5 - 20 |
| 3.50 | 46.4 | 5.737 | 44.3 | 51.4 | 21.7 | 1125 | 1.2 - 19 |
| 4.00 | 47.2 | 5.765 | 47.2 | 52.3 | 22.2 | 1250 | 1.7 - 19 |
| 5.00 | 48.7 | 5.811 | 52.5 | 53.9 | 23.2 | 1375 | 1.6 - 19 |
| 6.00 | 50.1 | 5.845 | 57.3 | 55.2 | 24.0 | 1500 | 1.4 - 19 |

cont'd

| τ | T | log P | K | x | S |
|---|---|---|---|---|---|
| 8.00 | 52.7 | 5.909 | 65.7 | 57.3 | 25.4 |
| 10.0 | 55.2 | 5.956 | 73.2 | 59.0 | 26.3 |
| 14.0 | 59.6 | 6.028 | 86.5 | 61.9 | 27.7 |
| 18.0 | 63.8 | 6.084 | 98.4 | 64.3 | 28.7 |
| 22.0 | 68.0 | 6.130 | 109 | 66.4 | 29.4 |
| 26.0 | 71.4 | 6.169 | 120 | 68.3 | 29.8 |
| 30.0 | 74.5 | 6.203 | 129 | 70.0 | 30.0 |
| 40.0 | 81.4 | 6.274 | 152 | 73.8 | 30.2 |
| 50.0 | 87.1 | 6.331 | 174 | 77.1 | 30.1 |
| 60.0 | 92.0 | 6.379 | 194 | 80.1 | 29.9 |

NEPTUNE $T_e = 50\ ^{o}K$ $g = 1373$ cgs

$CH_4/H_2 \leq .01$ $NH_3/H_2 = 0$ $He/H_2 = 1$

| $\tau$ | T | logP | K | x | S | V | $F_\nu/\pi$ |
|---|---|---|---|---|---|---|---|
| | | | | | | $32\ cm^{-1}$ | |
| 0. | 40.3 | 4.084 | 0.49 | - | 31.2 | | 1.02-11 |
| 0.002 | 40.4 | 4.385 | 0.98 | 5.6 | 31.3 | 64 | 1.96-11 |
| 0.004 | 40.4 | 4.535 | 1.39 | 8.4 | 31.4 | 96 | 2.21-11 |
| 0.006 | 40.5 | 4.623 | 1.70 | 10.0 | 31.4 | 128 | 1.99-11 |
| 0.010 | 40.6 | 4.734 | 2.20 | 12.1 | 31.7 | 161 | 1.60-11 |
| 0.020 | 40.8 | 4.885 | 3.11 | 14.9 | 31.8 | 193 | 1.21-11 |
| 0.030 | 41.1 | 4.972 | 3.81 | 16.6 | 32.0 | 225 | 8.63-12 |
| 0.040 | 41.2 | 5.035 | 4.39 | 17.8 | 32.2 | 257 | 5.19-12 |
| 0.060 | 41.6 | 5.122 | 5.38 | 19.5 | 32.5 | 289 | 1.73-12 |
| 0.100 | 42.2 | 5.233 | 6.93 | 21.6 | 33.1 | 322 | 2.97-13 |
| 0.150 | 42.9 | 5.320 | 8.48 | 23.3 | 33.7 | 354 | 7.41-14 |
| 0.250 | 44.0 | 5.431 | 10.9 | 25.5 | 34.8 | 387 | 3.27-14 |
| 0.350 | 45.0 | 5.503 | 12.9 | 27.0 | 36.2 | 420 | 1.67-14 |
| 0.400 | 45.5 | 5.532 | 13.8 | 27.6 | 36.2 | 454 | 9.80-15 |
| 0.500 | 46.3 | 5.580 | 15.4 | 28.6 | 36.9 | 487 | 6.48-15 |
| 0.600 | 47.1 | 5.619 | 16.9 | 29.5 | 37.6 | 520 | 4.33-15 |
| 0.700 | 47.9 | 5.652 | 18.2 | 30.2 | 38.2 | 553 | 1.78-15 |
| 0.800 | 48.6 | 5.681 | 19.5 | 30.8 | 38.7 | 587 | 3.2 -16 |
| 1.00 | 49.8 | 5.729 | 21.7 | 31.9 | 39.7 | 638 | 1.8 -16 |
| 1.20 | 51.0 | 5.769 | 23.8 | 32.8 | 40.7 | 690 | 1.9 -16 |
| 1.40 | 52.1 | 5.802 | 25.7 | 33.6 | 41.4 | 741 | 2.5 -16 |
| 1.60 | 53.1 | 5.831 | 27.5 | 34.3 | 42.0 | 793 | 3.1 -16 |
| 1.80 | 54.1 | 5.857 | 29.2 | 35.0 | 42.6 | 845 | 3.9 -16 |
| 2.00 | 55.0 | 5.880 | 30.8 | 35.6 | 43.1 | 896 | 4.8 -16 |
| 2.50 | 57.2 | 5.929 | 34.5 | 36.8 | 44.2 | 948 | 5.9 -16 |
| 3.00 | 59.0 | 5.970 | 37.8 | 37.9 | 45.1 | 1000 | 7.1 -16 |
| 3.50 | 60.9 | 6.004 | 40.9 | 38.9 | 45.9 | 1125 | 9.9 -16 |
| 4.00 | 62.5 | 6.035 | 43.9 | 39.7 | 46.6 | 1250 | 1.17-15 |
| 5.00 | 65.6 | 6.085 | 49.4 | 41.2 | 47.7 | 1375 | 1.16-15 |
| 6.00 | 68.2 | 6.128 | 54.4 | 42.5 | 48.5 | 1500 | 9.8 -16 |

cont'd

| τ | T | logP | K | x | S |
|---|---|---|---|---|---|
| 8.00 | 73.2 | 6.195 | 63.5 | 44.7 | 49.8 |
| 10.0 | 77.4 | 6.248 | 71.8 | 46.6 | 50.7 |
| 14.0 | 84.9 | 6.331 | 86.8 | 49.7 | 51.9 |
| 18.0 | 91.2 | 6.393 | 100 | 52.2 | 52.6 |
| 22.0 | 96.7 | 6.444 | 113 | 54.4 | 53.0 |
| 26.0 | 101.7 | 6.488 | 125 | 56.4 | 53.4 |
| 30.0 | 106.0 | 6.525 | 136 | 58.2 | 53.8 |
| 40.0 | 115.5 | 6.600 | 162 | 62.0 | 54.6 |
| 50.0 | 123.3 | 6.659 | 185 | 65.3 | 55.2 |
| 60.0 | 130.0 | 6.708 | 207 | 68.1 | 55.6 |

# APPENDIX B

## THE DERIVATION OF THE PAIR DISTRIBUTION FUNCTION INCLUDING THE FIRST QUANTUM CORRECTION TERM

Letting g(x) be the pair distribution function, we have

$$g(x) = g^{o}(x) + g^{1}(x) + \ldots \tag{B-1}$$

where $g^{o}(x)$ is the classical expression,

$$g^{o}(x) = \exp\left[-U(x)/kT\right] \tag{B-2}$$

and $g^{1}(x)$ is the first quantum correction term in the expansion in powers of $\hbar^2$. Letting $\mu$ be the reduced mass and $\beta = 1/kT$, Uhlenbeck and Beth (1936) give the expression

$$\frac{g(x)}{g^{o}(x)} = 1 + \frac{\hbar^2\beta^2}{12\mu}\left[-\nabla^2 U + (\nabla U)^2\beta/2\right] + \ldots \tag{B-3}$$

where $x = r/\sigma$. In our application, $U = 4\epsilon\,(x^{-12} - x^{-6})$ so that

$$-\nabla^2 U + (\nabla U)^2 = \left[-(x^2U')'/x^2 + U'^2\beta/2\right]\sigma^{-2}. \tag{B-4}$$

Differentiating U(x), we find

$$\begin{aligned} -(x^2U')'/x^2 &= 24\,\epsilon\,(-22x^{-14} + 5x^{-8}) \\ U'^2\beta/2 &= 8\beta\,\epsilon^2\,(144x^{-26} - 144x^{-20} + 36x^{-14}). \end{aligned} \tag{B-5}$$

Defining the dimensionless quantity $\Lambda^2 = h^2/2\mu\epsilon\sigma^2$, we obtain

$$\frac{g(x)}{g^o(x)} = 1 + \Lambda^2\left(\frac{\beta\epsilon}{\pi}\right)^2\left[-\frac{22}{x^{14}} + \frac{5}{x^8} + 12\beta\epsilon\left(\frac{4}{x^{26}} - \frac{4}{x^{20}} + \frac{1}{x^{14}}\right)\right] + \cdots \tag{B-6}$$

Inserting the values for the $H_2$-$H_2$ case, namely $\Lambda^2 = 3.0$ and $\epsilon/k = 37.0\ ^oK$, we obtain equation (I-16). The corresponding values for the $H_2$-He case are $\Lambda^2 = 4.92$ and $\epsilon/k = 19.4\ ^oK$. Insertion of these values leads to equation (I-21).

# APPENDIX C

## THE DERIVATION OF THE TRACE FORM OF THE ABSORPTION COEFFICIENT

Equation (I-34) may be written

$$a\, v/k = \sum_{i<f} P_i |\underline{u}_{if}|^2 hcV_{if} - \sum_{i<f} P_f |\underline{u}_{if}|^2 hcV_{if} \qquad (C-1)$$

$$= \sum_{i<f} P_i |\underline{u}_{if}|^2 hcV_{if} + \sum_{i<f} P_f |\underline{u}_{fi}|^2 hcV_{fi}\,, \qquad (C-2)$$

where we have made use of the Hermitian property of $\underline{u}_{if}$, namely, $\underline{u}_{if} = \underline{u}^*_{fi}$. The energy of a level labeled i is $E_i$. We define $hcV_{if} = E_f - E_i$ so that the plus sign arises from the interchange of the subscripts. We now re-define the labels in the second summation so that the old index i becomes the new index f and the old index f becomes the new index i. We can do this because both i and f are dummy indices. This gives us

$$a\, v/k = \sum_{i<f} P_i |\underline{u}_{if}|^2 hcV_{if} + \sum_{i>f} P_i |\underline{u}_{if}|^2 hcV_{if} \qquad (C-3)$$

$$= \sum_{i,f} P_i |\underline{u}_{if}|^2 hcV_{if}\,, \qquad (C-4)$$

where the summation now extends over all initial and all final states. This expression becomes

$$a\ v/k = \sum_{i,f} P_i \underline{u}_{if} \underline{u}_{fi} (E_f - E_i) \tag{C-5}$$

$$= \sum_{i,f} P_i \underline{u}_{if} [\langle f|\underline{u}|i\rangle E_f - \langle f|\underline{u}|i\rangle E_i] \tag{C-6}$$

where i and f are the energy eigenstates in the Dirac notation. Therefore, if H denotes the Hamiltonian operator,

$$a\ v/k = \sum_{i,f} P_i \langle i|\underline{u}|f\rangle [\langle f|H\,\underline{u}|i\rangle - \langle f|\underline{u}\,H|i\rangle] \tag{C-7}$$

$$= \sum_{i,f} P_i \langle i|\underline{u}|f\rangle\langle f|H\,\underline{u} - \underline{u}\,H|i\rangle \tag{C-8}$$

$$= \sum_{i} P_i \langle i|\underline{u}\cdot(H\,\underline{u} - \underline{u}\,H)|i\rangle \tag{C-9}$$

$$= \sum_{i} \langle i|\overline{P}\,\underline{u}\cdot[H, \underline{u}]|i\rangle \tag{C-10}$$

$$= \mathrm{Tr}\left\{\overline{P}\,\underline{u}\cdot[H, \underline{u}]\right\} \tag{C-11}$$

where Tr denotes the trace operation, defined by the last two equations, and $\overline{P}$ denotes the operator, which when acting on i, gives rise to the normalized Boltzmann factor, $P_i$. That is

$$\bar{P}|i> = P_i|i> \tag{C-12}$$

where

$$P_i = \exp(-\beta E_i)/\sum_j \exp(-\beta E_j) \tag{C-13}$$

and the summation extends over all energy states. Finally,

$$a = k v^{-1} \mathrm{Tr}\left\{\bar{P}\, \underline{u} \cdot [H, \underline{u}]\right\} \tag{C-14}$$

in agreement with equation (I-35), where $[H, \underline{u}]$ denotes the commutator of H and $\underline{u}$. Equation (C-14) is invariant with respect to the states in which it is represented, provided these states are a complete set which span the space in question.

Equation (C-1) can be derived from (C-11) by proceeding in reverse order, provided that $|i>$ and $|f>$ are the energy eigenstates.

# APPENDIX D

## PROPERTIES OF THE CLEBSCH-GORDON COEFFICIENTS

The notation is the same as that used by Rose (1957). In the vector addition of angular momenta, the representation where $\underline{J}^2$ and $J_z$, as well as $\underline{J}_1^2$ and $\underline{J}_2^2$, are diagonal with eigenvalues j(j+1) and m, respectively, is given by $\psi(j\ m)$, where

$$\psi(j\ m) = \sum_{m_1, m_2} C(j_1\ j_2\ j;\ m_1\ m_2\ m)\psi(j_1 m_1)\psi(j_2 m_2) \qquad \text{(D-1)}$$

and where the C are the Clebsch-Gordon, or C-coefficients. The inverse transformation is

$$\psi(j_1 m_1)\,\psi(j_2 m_2) = \sum_{j,\,m} \psi(j\ m)C(j_1\ j_2\ j;\ m_1\ m_2\ m)\ . \qquad \text{(D-2)}$$

The orthogonality relations are

$$\sum_{m_1, m_2} C(j_1\ j_2\ j;\ m_1\ m_2\ m)C(j_1\ j_2\ j';\ m_1\ m_2\ m') = \delta(j, j')\delta(m, m'), \qquad \text{(D-3)}$$

$$\sum_{j} C(j_1\ j_2\ j;\ m_1, m-m_1, m)C(j_1\ j_2\ j;\ m_1', m-m_1', m) = \delta(m, m_1') \qquad \text{(D-4)}$$

or

$$\sum_{j} C(j_1\ j_2\ j;\ m_1\ m_2\ m)C(j_1\ j_2\ j;\ m_1'\ m_2'\ m) = \delta(m_1 \cdot m_1') \cdot \delta(m_2, m-m_1)\delta(m_2, m_2'). \qquad \text{(D-5)}$$

Note that in the notation of the C-coefficient of equation (D-1), the Clebsch-Gordon coefficient vanishes unless $m = m_1 + m_2$ and the triangle relation $\Delta(j_1\ j_2\ j)$ holds. This triangle relation means that unless

$$j = j_1 + j_2,\ j_1 + j_2 - 1,\ \ldots\ ,\ |j_1 - j_2|\ , \qquad \text{(D-6)}$$

the corresponding Clebsch-Gordon coefficient vanishes. For explicit values of these coefficients, see texts such as Condon and Shortley (1951).

# APPENDIX E

## THE SUMMATION OVER THE ANGULAR MOMENTUM STATES

Using equations (I-59, 63 and 64), we find that the expression for the matrix element is

$$R\langle f|u_v|i\rangle = \sqrt{64\pi^3/3}\int \sum_{y_1 y_2 W L''} \psi^*(J_1' J_2' L' J_{12}' J' M')\langle A\rangle \tag{E-1}$$

$$\psi(y_1 y_2 L'' W 1 v)\ \psi(J_1 J_2 L J_{12} J M)\ d\underline{\Omega}$$

where the singly primed variables denote the final states. Making use of equation (I-61), the above equation becomes (neglecting exchange symmetry)

$$R\langle f|u_v|i\rangle = \sqrt{64\pi^3/3} \sum_{y_1 y_2 W L''} \langle A\rangle \sum_{\substack{m_1 m_2 m_L M_{12} \\ m_1' m_2' m_L' M_{12}' \\ m_1'' m_2'' m_L'' M_{12}''}} \int_1 Y_1^*(J_1' m_1') Y_1(y_1 m_1'') Y_1(J_1 m_1) d1$$

$$\cdot \int_2 Y_2^*(J_2' m_2') Y_2(y_2 m_2'') Y_2(J_2 m_2) d2 \int_3 Y_3^*(L' m_L') Y_3(L'' m_L'') Y_3(L m_L) d3$$

$$\cdot C(J_1 J_2 J_{12}; m_1 m_2 M_{12})$$

$$C(J_1' J_2' J_{12}'; m_1' m_2' M_{12}')$$

$$C(J_{12}\ L\ J;\ M_{12}\ m_L\ M)$$
$$C(J'_{12}\ L'\ J';\ M'_{12}\ m'_L\ M')$$
$$C(y_1\ y_2\ W;\ m''_1\ m''_2\ M''_{12})$$
$$C(W\ L''\ 1;\ M''_{12}\ m''_L\ v) \qquad \text{(E-2)}$$

where the C's are the Clebsch-Gordon coefficients (described in Appendix D), $Y_i(j\ m)$ is the spherical harmonic of the $i^{th}$ set of angular variables and di is the differential for integration over these variables. Let

$$\langle j'\ m' | y\ M\ j\ m\rangle = \int_{4\pi} Y^*(j'\ m')Y(y\ M)Y(j\ m)d\underline{\Omega} \qquad \text{(E-3)}$$

then

$$\sum_{m,\,m'} \langle j'\ m' | y M\ j\ m\rangle\langle y'\ M'\ j\ m | j'\ m'\rangle = L_y(j', j)\delta(y, y')\delta(M, M')/4\pi \qquad \text{(E-4)}$$

where $L_y(j', j)$ is given by equation (I-66) and vanishes unless $\Delta(j\ y\ j')$ and $j + y + j'$ is even.

Now square equation (E-2) and start summing:

$$\sum_{k'L'} |R\ \underline{u}_{k\ L}|^2 P = \sum_{\substack{L\ L'v \\ J_1J'_1 \\ J_2J'_2 \\ M\ M' \\ J_{12}J'_{12} \\ J\ J'}} P(J_1)P(J_2) \sum_{\substack{y_1y_2WL'' \\ \underline{y}_1\underline{y}_2\underline{WL}''}} (64\pi^3/3)\langle A\rangle\langle \underline{A}\rangle \sum_{\substack{m_1m_2m_LM_{12} \\ m'_1m'_2m'_LM'_{12} \\ m''_1m''_2m''_LM''_{12}}}$$

$$
\begin{aligned}
&\cdot \sum_{\substack{m_1 m_2 m_L M_{12} \\ \underline{m}_1 \underline{m}_2 \underline{m}_L \underline{M}_{12} \\ m'_1 m'_2 m'_L M'_{12} \\ \underline{m}'_1 \underline{m}'_2 \underline{m}'_L \underline{M}'_{12} \\ m''_1 m''_2 m''_L M''_{12}}} \langle J'_1\, m'_1 | y_1\, m''_1\, J_1\, m_1 \rangle \langle \underline{y}_1\, \underline{m}''_1\, J_1\, \underline{m}_1 | J'_1\, \underline{m}'_1 \rangle \\
&\quad \cdot \langle J'_2\, m'_2 | y_2\, m''_2\, J_2\, m_2 \rangle \langle \underline{y}_2\, \underline{m}''_2\, J_2\, \underline{m}_2 | J'_2\, \underline{m}'_1 \rangle \\
&\quad \cdot \langle L'\, m'_L | L''\, m''_L\, L\, m_L \rangle \langle \underline{L}''\, \underline{m}''_L\, L\, \underline{m}_L | L'\, \underline{m}'_L \rangle \qquad \text{(E-5)} \\
&\quad \cdot C(J_1\, J_2\, J_{12}; m_1\, m_2\, M_{12}) C(J_1\, J_2\, J_{12}; \underline{m}_1\, \underline{m}_2\, \underline{M}_{12}) \\
&\quad C(J'_1\, J'_2\, J'_{12}; m'_1\, m'_2\, M'_{12}) C(J'_1\, J'_2\, J'_{12}; \underline{m}'_1\, \underline{m}'_2\, \underline{M}'_{12}) \\
&\quad C(J_{12}\, L\, J\; ; M_{12}\, m_L\, M) C(J_{12}\, L\, J\; ; \underline{M}_{12}\, \underline{m}_L\, M) \\
&\quad C(J'_{12}\, L'\, J'; M'_{12}\, m'_L\, M') C(J'_{12}\, L'\, J'; \underline{M}'_{12}\, \underline{m}'_L\, M') \\
&\quad C(y_1\, y_2\; W; m''_1\, m''_2\, M''_{12}) C(\underline{y}_1\, \underline{y}_2\; \underline{W}; \underline{m}''_1\, \underline{m}''_2\, \underline{M}''_{12}) \\
&\quad C(W\, L''\; 1; M''_{12}\, m''_L\, v\;) C(\underline{W}\, \underline{L}''\; 1; \underline{M}''_{12}\, \underline{m}''_L\, v\;) .
\end{aligned}
$$

The P(J) is the Boltzmann factor for the $J^{th}$ rotational state and is normalized such that

$$\sum_J (2J + 1)P(J) = 1 \; . \qquad \text{(E-6)}$$

We now effect the summation over J and then J'. Referring to the orthogonality relations of the C-coefficients in Appendix D, we see that this results in the replacing of the C-coefficients containing these variables by the factor, $\delta(M_{12}, \underline{M}_{12})\delta(m_L, \underline{m}_L)$ $\delta(m_L, M - M_{12})\delta(M'_{12}, \underline{M}'_{12})\delta(m'_L, \underline{m}'_L)\delta(m'_L, M' - M'_{12})$, where $\delta(i, j)$ is the Kronecker delta.

Since M and M' appear only in these $\delta$-functions, summing over M and M' merely has the effect of removing the factors

$\delta(m_L, M-M_{12})\delta(m'_L, M-M'_{12})$. Summing over $\underline{M}_{12}$, $\underline{m}_L$, $\underline{M}'_{12}$ and $\underline{m}'_L$ results in the elimination of the remaining delta functions and the setting of $\underline{M}_{12} = M_{12}$, $\underline{m}_L = m_L$, $\underline{M}'_{12} = M'_{12}$ and $\underline{m}'_L = m'_L$. It is then possible to apply an orthogonality relation to each of the two pairs of C-coefficients containing $J_{12}$ and $J'_{12}$, respectively. Summation over $J_{12}$ and $J'_{12}$ results in the factors $\delta(m_1, \underline{m}_1)\delta(m_2, \underline{m}_2)\delta(m_2, M_{12}-m_1)\delta(m'_1, \underline{m}'_1)\delta(m'_2, \underline{m}'_2)$ $\delta(m'_2, M'_{12}-m'_1)$. We then sum over $\underline{m}_1$, $\underline{m}_2$, $\underline{m}'_1$, $\underline{m}'_2$, $M_{12}$ and $M'_{12}$ to obtain

$$\sum_{\substack{L\,L'\,v \\ J_1 J'_1 \\ J_2 J'_2}} P(J_1)P(J_2) \sum_{y_1 y_2 W L''} <A><\underline{A}> 64\pi^3/3 \sum_{\substack{m_1 m_2 m_L \\ m'_1 m'_2 m'_L \\ m''_1 m''_2 m''_L M''_{12}}} \sum_{\substack{m''_1 m''_2 \\ \underline{m}''_L \underline{M}''_{12}}} \qquad \text{(E-7)}$$

$$\cdot <J'_1\ m'_1 | y_1\ m''_1\ J_1\ m_1><\underline{y}_1\ \underline{m}''_1\ J_1\ m_1 | J'_1\ m'_1>$$

$$<J'_2\ m'_2 | y_2\ m''_2\ J_2\ m_2><\underline{y}_2\ \underline{m}''_2\ J_2\ \underline{m}_2 | J'_2\ \underline{m}'_2>$$

$$<L'\ m'_L | L''\ m''_L\ L\ m_L><\underline{L}''\ \underline{m}''_L\ L\ m_L | L'\ m'_L>$$

$$C(y_1\ y_2\ W; m''_1\ m''_2\ M''_{12}) C(\underline{y}_1\ \underline{y}_2\ \underline{W}; \underline{m}''_1\ \underline{m}''_2\ \underline{M}''_{12})$$

$$C(W\ L''\ 1\ ; M''_{12}\ m''_L\ v\ ) C(\underline{W}\ \underline{L}''\ 1\ ; \underline{M}''_{12}\ \underline{m}''_L\ v)\ .$$

This may be written in terms of the Racah coefficients as

$$\sum_{\substack{L\,L'\,v\\ J_1J_1'\\ J_2J_2'}} P(J_1)P(J_2) \sum_{\substack{y_1y_2WL''\\ \underline{y}_1\underline{y}_2\underline{W}\underline{L}''}} \langle A \rangle\langle \underline{A} \rangle / 3 \sum_{\substack{m_1''m_2''\\ m_L''M_{12}''}} \sum_{\substack{\underline{m}_1''\underline{m}_2''\\ \underline{m}_L''\underline{M}_{12}''}} L_{y_1}(J_1', J_1)\, \delta(y_1,\underline{y}_1)\delta(m_1'',\underline{m}_1'')$$

$$\cdot\, L_{y_2}(J_2', J_2)\, \delta(y_2,\underline{y}_2)\delta(m_2'',\underline{m}_2'')\, L_{L''}(L', L)\, \delta(L'',\underline{L}'')\delta(m_L'',\underline{m}_L'') \tag{E-8}$$

$$C(y_1\, y_2\, W\, ; m_1''\, m_2''\, M_{12}'')C(\underline{y}_1\, \underline{y}_2\, \underline{W}\, ; \underline{m}_1''\, \underline{m}_2''\, \underline{M}_{12}'')$$

$$C(W\, L''\, 1\, ; M_{12}''\, m_L''\, v\,)C(\underline{W}\, \underline{L}''\, 1\, ; \underline{M}_{12}''\, \underline{m}_L''\, v\,)\,.$$

Summing over $y_1$, $\underline{y}_2$, $\underline{m}_1''$, $\underline{m}_2''$, $\underline{L}''$ and $\underline{m}_L$ now gives

$$\sum_{\substack{L\,L'\,v\\ J_1J_1'\\ J_2J_2'}} P(J_1)P(J_2) \sum_{\substack{y_1y_2WL''\\ \underline{W}}} \langle A \rangle\langle \underline{A} \rangle / 3\, L_{y_1}(J_1', J_1)L_{y_2}(J_2', J_2)L_{L''}(L', L) \tag{E-9}$$

$$\cdot \sum_{\substack{m_1''m_2''\\ m_L''M_{12}''\underline{M}_{12}''}} C(y_1\, y_2\, W\, ; m_1''\, m_2''\, M_{12}'')C(y_1\, y_2\, \underline{W}; m_1''\, m_2''\underline{M}_{12}'')$$

$$\cdot C(W\, L''\, 1\, ; M_{12}''\, m_L''\, v\,)C(\underline{W}\, L''\, 1; \underline{M}_{12}''\, m_L''\, v\,)\,.$$

Summing over $m_1''$ and $m_2''$ replaces the first two C-coefficients by $\delta(W, \underline{W})\delta(M_{12}'', \underline{M}_{12}'')$. Summing over $\underline{M}_{12}''$ and $\underline{W}$ results in setting $\underline{M}_{12}'' = M_{12}''$ and $\underline{W} = W$ in all remaining expressions. Then we sum over $m_L''$ and $M_{12}''$ to get rid of the last two C-coefficients. The resulting expression is independent of v so summing over v introduces a factor of three. We finally obtain

$$\sum_{\substack{y_1 y_2 W L'' \\ L\ L'}} L_{L''}(L', L)\,|\langle A\rangle|^2 \sum_{\substack{J_1\ J_1' \\ J_2\ J_2'}} P(J_1)P(J_2)L_{y_1}(J_1', J_1)L_{y_2}(J_2', J_2)\,, \tag{E-10}$$

which is the same as given in equation (I-98).

# APPENDIX F

## A FAST ASYMTOTIC EXPANSION FOR $\int_x^\infty x^{-s} \cos(ax + b)\, dx$

We use a technique similar to that of G. Blanch (1946) in computing a rapidly convergent asymptotic expansion for the exponential integrals: Let

$$A = \int_x^\infty x^{-s} \cos(ax + b)\, dx \tag{F-1}$$

then

$$A = \mathrm{Re}\left\{ \exp(ib)\, B \right\} \tag{F-2}$$

where

$$B = \int_x^\infty x^{-s} \exp(iax)dx = \int_x^\infty \exp(iax - s\ 1n\ x)dx. \tag{F-3}$$

Letting

$$G = iax - s\ 1n\ x \tag{F-4}$$

we find

$$dG/dx = (iax - s)/x \tag{F-5}$$

so that

$$B = \int_x^\infty (\exp(G)dG)dx/dG\ . \tag{F-6}$$

We integrate equation (F-6) by parts. This is accomplished by integrating the factor exp(G)dG and differentiating the factor dx/dG. The result is

$$B = -\exp(iax)/[x^{s-1}(iax - s)] + \int_x^\infty (\exp(G)dG)xs/(iax - s)^3. \tag{F-7}$$

This process is repeated several times to yield the result,

$$\begin{aligned} A = \mathrm{Re}\{&\exp[i(ax + b)]/[x^{s-1}(s - iax)]\cdot[1 + s/(s - iax)^2 \\ &+ s(s + 2iax)/(s - iax)^4 + s(s^2 + 8iaxs - 6a^2x^2)/(s - iax)^6 \\ &+ s(s^3 + 22iaxs^2 - 58a^2x^2s - 24ia^3x^3)/(s - iax)^8] \\ &+ \text{remainder}\}. \end{aligned} \tag{F-8}$$

When $x_o = -iax$, $n = s$ and $x = 1$, equation (F-8) reduces to G. Blanch's expression and agrees with it. We evaluate equation (F-8) using complex arithmetic in the IBM 7090-7094 high-speed electronic computer, and then take the real part of the numerical answer.

# APPENDIX G

## NUMERICAL VALUES OF THE MATRIX ELEMENT SUMMATIONS

The first part of this appendix presents the numerical values of equation (I-106) exclusive of the factor $2\mathcal{L}(T)$, evaluated for the $H_2$-$H_2$ case. The column labeled A gives the value of the final minus the initial value of the square of t. The paragraph of equation (I-112) defines t. Column B gives the initial value of $t^2$ and column C gives the corresponding evaluation, which is the value of exp(M) used in equation (II-2) for computing the frequency profile of the translational absorption coefficient due to $H_2$-$H_2$ collisions.

The second part presents the numerical evaluation of equation (I-109) for the $H_2$-He case, exclusive of the term containing the factor $\mathcal{L}(T)$. This omitted term is only 2 per cent of the total contribution. Columns D, E and F correspond to columns A, B and C, respectively, except that column F contains the results for the $H_2$-He enhancement. This column gives the value of exp(N) used in equation (II-3) to compute the frequency profile of the translational absorption coefficient due to $H_2$-He collisions. (The values in columns C and F are interpolated logarithmically in the $t^2$ - $\Delta(t^2)$ plane before actually evaluating equations (II-2) or (II-3) ).

The accuracy declines for large values of $\Delta(t^2)/t^2$ (where the values are small). However, the bulk of this table should be accurate to within a 0. 1 per cent relative error as far as the numerical approximations warrant.

| A | B | C |
|---|---|---|
| 7.500E 01 | 4.000E 03 | 3.056E-02 |
| 1.250E 02 | 4.000E 03 | 3.044E-02 |
| 1.750E 02 | 4.000E 03 | 2.968E-02 |
| 2.250E 02 | 4.000E 03 | 2.818E-02 |
| 3.750E 02 | 4.000E 03 | 2.054E-02 |
| 4.750E 02 | 4.000E 03 | 1.515E-02 |
| | | |
| 2.500E 01 | 3.030E 03 | 2.081E-02 |
| 7.500E 01 | 3.030E 03 | 2.095E-02 |
| 1.250E 02 | 3.030E 03 | 2.071E-02 |
| 1.750E 02 | 3.030E 03 | 1.984E-02 |
| 2.250E 02 | 3.030E 03 | 1.826E-02 |
| 2.750E 02 | 3.030E 03 | 1.620E-02 |
| 3.750E 02 | 3.030E 03 | 1.173E-02 |
| 4.750E 02 | 3.030E 03 | 7.969E-03 |
| | | |
| 2.500E 01 | 1.750E 03 | 9.884E-03 |
| 7.500E 01 | 1.750E 03 | 9.959E-03 |
| 1.250E 02 | 1.750E 03 | 9.548E-03 |
| 1.750E 02 | 1.750E 03 | 8.524E-03 |
| 2.250E 02 | 1.750E 03 | 7.109E-03 |
| 2.750E 02 | 1.750E 03 | 5.677E-03 |
| 3.750E 02 | 1.750E 03 | 3.377E-03 |
| 4.750E 02 | 1.750E 03 | 1.926E-03 |
| 1.250E 01 | 7.800E 02 | 3.332E-03 |
| 2.500E 01 | 7.800E 02 | 3.363E-03 |
| 5.000E 01 | 7.800E 02 | 3.390E-03 |
| 7.500E 01 | 7.800E 02 | 3.310E-03 |
| 1.000E 02 | 7.800E 02 | 3.094E-03 |
| 1.250E 02 | 7.800E 02 | 2.743E-03 |
| 1.500E 02 | 7.800E 02 | 2.396E-03 |
| 1.750E 02 | 7.800E 02 | 2.021E-03 |
| 2.250E 02 | 7.800E 02 | 1.371E-03 |
| 2.750E 02 | 7.800E 02 | 9.052E-04 |
| 3.750E 02 | 7.800E 02 | 3.991E-04 |
| 4.750E 02 | 7.800E 02 | 1.864E-04 |
| 7.500E 02 | 7.800E 02 | 3.156E-05 |
| | | |
| 1.250E 01 | 4.000E 02 | 1.387E-03 |
| 2.500E 01 | 4.000E 02 | 1.410E-03 |
| 3.750E 01 | 4.000E 02 | 1.419E-03 |
| 5.000E 01 | 4.000E 02 | 1.402E-03 |
| 6.250E 01 | 4.000E 02 | 1.351E-03 |
| 7.500E 01 | 4.000E 02 | 1.275E-03 |
| 1.000E 02 | 4.000E 02 | 1.070E-03 |
| 1.250E 02 | 4.000E 02 | 8.480E-04 |
| 1.500E 02 | 4.000E 02 | 6.538E-04 |
| 1.750E 02 | 4.000E 02 | 4.941E-04 |
| 2.000E 02 | 4.000E 02 | 3.719E-04 |
| 2.250E 02 | 4.000E 02 | 2.806E-04 |
| 2.500E 02 | 4.000E 02 | 2.129E-04 |
| 2.750E 02 | 4.000E 02 | 1.630E-04 |
| 3.750E 02 | 4.000E 02 | 6.141E-05 |
| 4.750E 02 | 4.000E 02 | 2.631E-05 |

| A | B | C |
|---|---|---|
| 1.250E 01 | 1.960E 02 | 5.581E-04 |
| 2.500E 01 | 1.960E 02 | 5.728E-04 |
| 3.750E 01 | 1.960E 02 | 5.661E-04 |
| 5.000E 01 | 1.960E 02 | 5.331E-04 |
| 6.250E 01 | 1.960E 02 | 4.801E-04 |
| 7.500E 01 | 1.960E 02 | 4.177E-04 |
| 1.000E 02 | 1.960E 02 | 2.962E-04 |
| 1.250E 02 | 1.960E 02 | 2.024E-04 |
| 1.500E 02 | 1.960E 02 | 1.381E-04 |
| 1.750E 02 | 1.960E 02 | 9.534E-05 |
| 2.000E 02 | 1.960E 02 | 6.708E-05 |
| 2.250E 02 | 1.960E 02 | 4.794E-05 |
| 2.750E 02 | 1.960E 02 | 2.611E-05 |
| 3.250E 02 | 1.960E 02 | 1.511E-05 |
| 3.750E 02 | 1.960E 02 | 9.164E-06 |
| 4.750E 02 | 1.960E 02 | 3.744E-06 |
| 7.500E 02 | 1.960E 02 | 5.047E-07 |
| | | |
| 1.250E 01 | 8.100E 01 | 1.912E-04 |
| 2.500E 01 | 8.100E 01 | 1.953E-04 |
| 3.750E 01 | 8.100E 01 | 1.780E-04 |
| 5.000E 01 | 8.100E 01 | 1.475E-04 |
| 6.250E 01 | 8.100E 01 | 1.168E-04 |
| 7.500E 01 | 8.100E 01 | 8.979E-05 |
| 1.000E 02 | 8.100E 01 | 5.268E-05 |
| 1.250E 02 | 8.100E 01 | 3.191E-05 |
| 1.500E 02 | 8.100E 01 | 2.030E-05 |
| 1.750E 02 | 8.100E 01 | 1.344E-05 |
| 2.000E 02 | 8.100E 01 | 9.210E-06 |
| 2.250E 02 | 8.100E 01 | 6.509E-06 |
| 2.750E 02 | 8.100E 01 | 3.473E-06 |
| 3.750E 02 | 8.100E 01 | 1.188E-06 |
| 4.750E 02 | 8.100E 01 | 4.735E-07 |
| | | |
| 1.250E 01 | 4.225E 01 | 9.164E-05 |
| 2.500E 01 | 4.225E 01 | 9.035E-05 |
| 3.750E 01 | 4.250E 01 | 7.463E-05 |
| 5.000E 01 | 4.225E 01 | 5.499E-05 |
| 6.250E 01 | 4.250E 01 | 3.994E-05 |
| 7.500E 01 | 4.225E 01 | 2.851E-05 |
| 1.000E 02 | 4.225E 01 | 1.564E-05 |
| 1.250E 02 | 4.225E 01 | 9.280E-06 |
| 1.500E 02 | 4.225E 01 | 5.862E-06 |
| 1.750E 02 | 4.225E 01 | 3.892E-06 |
| 2.250E 02 | 4.225E 01 | 1.893E-06 |
| | | |
| 1.250E 01 | 2.700E 01 | 5.711E-05 |
| 2.500E 01 | 2.700E 01 | 5.385E-05 |
| 3.750E 01 | 2.700E 01 | 4.053E-05 |
| 5.000E 01 | 2.700E 01 | 2.812E-05 |
| 6.250E 01 | 2.700E 01 | 1.939E-05 |
| 7.500E 01 | 2.700E 01 | 1.373E-05 |
| 1.000E 02 | 2.700E 01 | 7.446E-06 |
| 1.250E 02 | 2.700E 01 | 4.437E-06 |
| 1.500E 02 | 2.700E 01 | 2.817E-06 |
| 1.750E 02 | 2.700E 01 | 1.876E-06 |

| A | B | C |
|---|---|---|
| 1.250E 01 | 1.600E 01 | 3.419E-05 |
| 2.500E 01 | 1.600E 01 | 3.011E-05 |
| 3.750E 01 | 1.600E 01 | 2.060E-05 |
| 5.000E 01 | 1.600E 01 | 1.348E-05 |
| 6.250E 01 | 1.600E 01 | 9.119E-06 |
| 7.500E 01 | 1.600E 01 | 6.412E-06 |
| 1.000E 02 | 1.600E 01 | 3.510E-06 |
| 1.250E 02 | 1.600E 01 | 2.111E-06 |
| 1.500E 02 | 1.600E 01 | 1.352E-06 |
| 1.750E 02 | 1.600E 01 | 9.041E-07 |
| | | |
| 1.250E 01 | 3.000E 00 | 9.312E-06 |
| 2.500E 01 | 3.000E 00 | 6.354E-06 |
| 3.750E 01 | 3.000E 00 | 3.694E-06 |
| 5.000E 01 | 3.000E 00 | 2.359E-06 |
| 6.250E 01 | 3.000E 00 | 1.617E-06 |
| 7.500E 01 | 3.000E 00 | 1.162E-06 |
| 1.000E 02 | 3.000E 00 | 6.596E-07 |

| D | E | F |
|---|---|---|
| 7.500E 01 | 4.000E 03 | 8.855E-02 |
| 1.250E 02 | 4.000E 03 | 8.638E-02 |
| 1.750E 02 | 4.000E 03 | 8.281E-02 |
| 2.250E 02 | 4.000E 03 | 7.829E-02 |
| 3.750E 02 | 4.000E 03 | 6.079E-02 |
| 4.750E 02 | 4.000E 03 | 4.866E-02 |
| | | |
| 2.500E 01 | 3.030E 03 | 5.524E-02 |
| 7.500E 01 | 3.030E 03 | 5.472E-02 |
| 1.250E 02 | 3.030E 03 | 5.285E-02 |
| 1.750E 02 | 3.030E 03 | 5.018E-02 |
| 2.250E 02 | 3.030E 03 | 4.661E-02 |
| 2.750E 02 | 3.030E 03 | 4.253E-02 |
| 3.750E 02 | 3.030E 03 | 3.380E-02 |
| 4.750E 02 | 3.030E 03 | 2.576E-02 |
| | | |
| 2.500E 01 | 1.750E 03 | 2.126E-02 |
| 7.500E 01 | 1.750E 03 | 2.091E-02 |
| 1.250E 02 | 1.750E 03 | 1.979E-02 |
| 1.750E 02 | 1.750E 03 | 1.809E-02 |
| 2.250E 02 | 1.750E 03 | 1.595E-02 |
| 2.750E 02 | 1.750E 03 | 1.381E-02 |
| 3.750E 02 | 1.750E 03 | 9.857E-03 |
| 4.750E 02 | 1.750E 03 | 6.686E-03 |
| | | |
| 1.250E 01 | 7.800E 02 | 5.112E-03 |
| 2.500E 01 | 7.800E 02 | 5.138E-03 |
| 5.000E 01 | 7.800E 02 | 5.102E-03 |
| 7.500E 01 | 7.800E 02 | 4.958E-03 |
| 1.000E 02 | 7.800E 02 | 4.724E-03 |
| 1.250E 02 | 7.800E 02 | 4.424E-03 |
| 1.500E 02 | 7.800E 02 | 4.079E-03 |
| 1.750E 02 | 7.800E 02 | 3.711E-03 |
| 2.250E 02 | 7.800E 02 | 2.978E-03 |
| 2.750E 02 | 7.800E 02 | 2.320E-03 |
| 3.750E 02 | 7.800E 02 | 1.345E-03 |
| 4.750E 02 | 7.800E 02 | 7.687E-04 |
| 7.500E 02 | 7.800E 02 | 1.782E-04 |
| | | |
| 1.250E 01 | 4.000E 02 | 1.586E-03 |
| 2.500E 01 | 4.000E 02 | 1.602E-03 |
| 3.750E 01 | 4.000E 02 | 1.583E-03 |
| 5.000E 01 | 4.000E 02 | 1.565E-03 |
| 6.250E 01 | 4.000E 02 | 1.531E-03 |
| 7.500E 01 | 4.000E 02 | 1.497E-03 |
| 1.000E 02 | 4.000E 02 | 1.375E-03 |
| 1.250E 02 | 4.000E 02 | 1.231E-03 |
| 1.500E 02 | 4.000E 02 | 1.079E-03 |
| 1.750E 02 | 4.000E 02 | 9.317E-04 |
| 2.000E 02 | 4.000E 02 | 7.958E-04 |
| 2.250E 02 | 4.000E 02 | 6.745E-04 |
| 2.500E 02 | 4.000E 02 | 5.690E-04 |
| 2.750E 02 | 4.000E 02 | 4.787E-04 |
| 3.750E 02 | 4.000E 02 | 2.390E-04 |
| 4.750E 02 | 4.000E 02 | 1.223E-04 |

| D | E | F |
|---|---|---|
| 1.250E 01 | 1.960E 02 | 4.553E-04 |
| 2.500E 01 | 1.960E 02 | 4.638E-04 |
| 3.750E 01 | 1.960E 02 | 4.621E-04 |
| 5.000E 01 | 1.960E 02 | 4.517E-04 |
| 6.250E 01 | 1.960E 02 | 4.342E-04 |
| 7.500E 01 | 1.960E 02 | 4.115E-04 |
| 1.000E 02 | 1.960E 02 | 3.576E-04 |
| 1.250E 02 | 1.960E 02 | 3.010E-04 |
| 1.500E 02 | 1.960E 02 | 2.483E-04 |
| 1.750E 02 | 1.960E 02 | 2.026E-04 |
| 2.000E 02 | 1.960E 02 | 1.642E-04 |
| 2.250E 02 | 1.960E 02 | 1.330E-04 |
| 2.750E 02 | 1.960E 02 | 8.734E-05 |
| 3.250E 02 | 1.960E 02 | 5.799E-05 |
| 3.750E 02 | 1.960E 02 | 3.907E-05 |
| 4.750E 02 | 1.960E 02 | 1.854E-05 |
| 7.500E 02 | 1.960E 02 | 3.098E-06 |
| | | |
| 1.250E 01 | 8.100E 01 | 1.014E-04 |
| 2.500E 01 | 8.100E 01 | 1.052E-04 |
| 3.750E 01 | 8.100E 01 | 1.042E-04 |
| 5.000E 01 | 8.100E 01 | 9.958E-05 |
| 6.250E 01 | 8.100E 01 | 9.274E-05 |
| 7.500E 01 | 8.100E 01 | 8.476E-05 |
| 1.000E 02 | 8.100E 01 | 6.833E-05 |
| 1.250E 02 | 8.100E 01 | 5.372E-05 |
| 1.500E 02 | 8.100E 01 | 4.182E-05 |
| 1.750E 02 | 8.100E 01 | 3.252E-05 |
| 2.000E 02 | 8.100E 01 | 2.535E-05 |
| 2.250E 02 | 8.100E 01 | 1.985E-05 |
| 2.750E 02 | 8.100E 01 | 1.238E-05 |
| 3.750E 02 | 8.100E 01 | 5.165E-06 |
| 4.750E 02 | 8.100E 01 | 2.341E-06 |
| | | |
| 1.250E 01 | 4.225E 01 | 3.573E-05 |
| 2.500E 01 | 4.225E 01 | 3.778E-05 |
| 3.750E 01 | 4.225E 01 | 3.709E-05 |
| 5.000E 01 | 4.225E 01 | 3.473E-05 |
| 6.250E 01 | 4.225E 01 | 3.158E-05 |
| 7.500E 01 | 4.225E 01 | 2.820E-05 |
| 1.000E 02 | 4.225E 01 | 2.185E-05 |
| 1.250E 02 | 4.225E 01 | 1.667E-05 |
| 1.500E 02 | 4.225E 01 | 1.269E-05 |
| 1.750E 02 | 4.225E 01 | 9.701E-06 |
| 2.250E 02 | 4.225E 01 | 5.781E-06 |
| | | |
| 1.250E 01 | 2.700E 01 | 1.830E-05 |
| 2.500E 01 | 2.700E 01 | 1.959E-05 |
| 3.750E 01 | 2.700E 01 | 1.908E-05 |
| 5.000E 01 | 2.700E 01 | 1.764E-05 |
| 6.250E 01 | 2.700E 01 | 1.584E-05 |
| 7.500E 01 | 2.700E 01 | 1.399E-05 |
| 1.000E 02 | 2.700E 01 | 1.066E-05 |
| 1.250E 02 | 2.700E 01 | 8.048E-06 |
| 1.500E 02 | 2.700E 01 | 6.082E-06 |
| 1.750E 02 | 2.700E 01 | 4.623E-06 |

| D | E | F |
|---|---|---|
| 1.250E 01 | 1.600E 01 | 8.903E-06 |
| 2.500E 01 | 1.600E 01 | 9.643E-06 |
| 3.750E 01 | 1.600E 01 | 9.308E-06 |
| 5.000E 01 | 1.600E 01 | 8.511E-06 |
| 6.250E 01 | 1.600E 01 | 7.572E-06 |
| 7.500E 01 | 1.600E 01 | 6.640E-06 |
| 1.000E 02 | 1.600E 01 | 5.011E-06 |
| 1.250E 02 | 1.600E 01 | 3.758E-06 |
| 1.500E 02 | 1.600E 01 | 2.828E-06 |
| 1.750E 02 | 1.600F 01 | 2.143E-06 |
| | | |
| 1.250E 01 | 3.000E 00 | 1.457E-06 |
| 2.500E 01 | 3.000E 00 | 1.592E-06 |
| 3.750E 01 | 3.000E 00 | 1.525E-06 |
| 5.000E 01 | 3.000E 00 | 1.385E-06 |
| 6.250E 01 | 3.000E 00 | 1.227E-06 |
| 7.500E 01 | 3.000E 00 | 1.073E-06 |
| 1.000E 02 | 3.000E 00 | 8.074E-07 |

## REFERENCES

Aller, L. H., 1953, The Atmospheres of the Sun and the Stars, (New York: Ronald Press).

Anderson, C. M., 1965, private communication.

Barnes, R. B., 1935, Phys. Rev., 47, 658.

Baum, W. A., and Code, A. D., 1953, A. J., 58, 108.

Beth, E., and Uhlenbeck, G. E., 1937, Physica 4, 915.

Blanch, G., 1946, The Functions $E_n(x)$ by G. Placzek, National Research Council of Canada, Division of Atomic Energy, Chalk River, Ontario.

Brower, D., and Clemence, G. M., 1961, Solar System, Vol. 3, ed. by G. P. Ruiper and B. M. Middlehurst, Chapter 3.

Cartwright, C. H., and Badger, R. M., 1929, Phys. Rev., 33, 692.

Castor, J. I., 1965, private communication.

Colpa, J. P., and Ketelaar, J. A. A., 1958, Mol. Phys., 1, 343.

Condon, E. U., and Shortley, G. H., 1951, The Theory of Atomic Spectra (Cambridge Press).

Dalgarno, A. and Williams, D. A., 1962, Ap. J., 136, 690.

De Boer, J., 1949, Repts. Progr. Phys., 12, 305.

Demargue, P., 1960, Ap. J., 132, 366.

Dunham, T., 1934, P. A. S. P., 46, 231.

Farkas, A., 1935, Orthohydrogen, Parahydrogen and Heavy Hydrogen (Cambridge: The University Press).

Field, G. B., 1965, Hydrogen Molecules and Astronomy: A Review by W. B. Somerville, G. B. Field, and K. Dressler (The Princeton University Observatory), page 32.

Foley, H. M., and Randall, H. M., 1941, Phys. Rev., 59, 171.

Foltz, J. V., and Rank, D. H., 1963, Ap. J., 138, 1319.

Garing, J. S., Nielsen, H. H., and Rao, K. N., 1959, J. Mol. Spectros., 3, 496.

Goody, R. M., 1964, Atmospheric Radiation I, (Oxford at the Clarendon Press).

Gross, S. H., and Rasool, S. I., 1964, Icarus, 3, 311.

Hadni, A., 1957, proc. of the Colloquium Spectroscopium Internationale VI (London: Pergamon Press), 632.

Harris, D. L., 1961, Solar System, vol. 3, ed. by G. P. Kuiper, and B. M. Middlehurst, Chapter 8 (Chicago: University of Chicago Press).

Heastie, R., and Martin, D. H., 1962, Can. J. Phys., 40, 122.

Herzberg, G., 1952, Ap. J., 115, 337.

Hildebrand, F. B., 1956, Introduction to Numerical Analysis (New-York: McGraw-Hill Book Co., Inc.).

Horak, H. C., 1950, Ap. J., 112, 445.

Howard, R., and Smith, W. V., 1950, Phys. Rev., 79, 132.

Hunt, J. L., and Welsh, H. L., 1964, Con. J. Phys. 42, 873.

International Critical Tables, 1928 (New York: McGraw-Hill Book Co., Inc.)

Kellermann, K. I., 1965, private communication.

Kiess, C. C., Corliss, C. H., and Kiess, H. K., 1960, Ap. J., 132, 221.

Kiss, Z. J., Gush, H. P., and Welsh, H. L., 1959, Con. J. Phys., 37, 362.

Kiss, Z. J., and Welsh, H. L., 1959, Con. J. Phys., 37, 1249.

Kuiper, G. P., 1952, The Atmospheres of the Earth and Planets (Chicago: The University of Chicago Press), Chapter 12.

Lasker, B. M., 1963, Ap. J., 138, 709.

Loewenstein, E. V., 1960, J. Opt. Soc. of Amer., 50, 1163.

Low, F. J., 1964, Abstracts of the 116th Meeting of the Amer. Astron. Soc.

McCubbin, T. K., Jr., and Sinton, W. M., 1950, J. Opt. Soc. of Amer., 40, 537.

Michels, A., and Wouters, H., 1941, Physica, 8, 923.

Mihalas, D. M., 1964, Thesis, California Institute of Technology.

Morse, P. M., and Feshbach, H., 1953, Methods of Theoretical Physics, vol. 1 (New York: McGraw-Hill Book Co., Inc.).

Mould, H. M., Price, W. C., and Wilkinson, G. R., 1959, Spectrochimica Acta, 15, 314.

Münch, G., 1965, private communication.

Münch, G., and Spinrad, H., 1963, Mem. Soc. Roy. Sci. Liege, Ser. 5, 7, 541.

Murray, B. C., Wildey, R. L., and Westphal, J. A., 1964, Ap. J., 139, 986.

Öpik, E. J., 1962, Icarus, 1, 200.

Poll, J. D., and Van Kranendonk, J., 1961, Can. J. Phys., 39, 189.

Rose, M. E., 1957, Elementary Theory of Angular Momentum (New York: John Wiley and Sons, Inc.).

Rose, W. K., Bologna, J. M., and Slonaker, R. M., 1963, A. J., 68, 78.

Spinrad, H., 1963, Ap. J., 138, 1242.

Spinrad, H., and Trafton, L. M., 1963, Icarus, 2, 25.

Stoicheff, B. P., 1957, Can. J. Phys., 35, 730.

Teddington, Eng. National Physical Laboratory, 1958, Modern Computing Methods (New York: Philosophical Library).

Townes, C. H., and Schawlow, A. L., 1955, Microwave Spectroscopy (New York: McGraw-Hill Book Co., Inc.).

Trafton, L. M., 1964, Ap. J., 140, 1340.

Uhlenbeck, G. E., and Beth, E., 1936, Physica, 3, 729.

Urey, H. C., 1959, Handbuch der Physik vol. 50, ed. by S. Flügge (Vienna: Springer Verlag Press), p. 363.

U. S. National Bureau of Standards 1958, 61, 141.

Van Kranendonk, J., and Kiss, Z. J., 1959, Can. J. Phys., 37, 1187.

Vardya, M. S., 1962, Ap. J., 135, 303.

Watson, G. N., 1944, A Treatise on the Theory of Bessel Functions (New York: The Macmillan Co.).

Wildey, R. L., 1964, Icarus, 3, 322.

Wildt, R., 1958, P. A. S. P., 70, 237.

Wright, N., and Randall, H. M., 1933, Phys. Rev., 44, 391.

Zabriskie, F., 1962, A. J., 67, 168.